HYDROGEN BONDED ANIONS

by

TERENCE ANTHONY O'SHEA

A dissertation submitted in part fulfilment
of the requirements for a Doctor of Philosophy
Degree at the University of Warwick.

March, 1969.

PREFACE.

The work described in this dissertation is original, except in those portions where it is specifically stated to the contrary. It has not been submitted, either wholly, or in part, for a degree at this, or at any other university.

J. A. O'Shea

A C K N O W L E D G E M E N T S

The author wishes to thank Professor T. C. Waddington for his constant help and encouragement throughout the course of the work. He is grateful to many other Members of the Department, Research Students and Technical Staff who have assisted in many ways, and in particular to Dr. J. A. S. Smith for providing the NQR facilities and to R. Lynch for recording the NQR Spectra. He is also indebted to many people outside this university for providing other facilities and to Miss R. Perry for some excellent typing.

Thanks are due to the University of Warwick for a maintenance grant.

C O N T E N T S

SUMMARY

The work recorded in this thesis can be divided into three sections. The first section (chapter three) is concerned with essentially weak H-bonded anions of the type $XH(O_2CR)^-$, where X^- is a group 7 halide ion, and R is H, CH_3, CF_3 or $CHCl_2$. The IR spectrum of each of these anions has been examined and complete assignments have been made in most cases. The relationships which exist in the series, which are a direct result of their chemical similarities, are discussed in terms of the pK_a values of the acid and base concerned.

The second section (chapter four) deals with Type B hydrogen dicarboxylate salts of acetic acid and its halogenated derivatives. Their IR spectra have been examined at the temperature of liquid nitrogen and assignments have been made. The importance of low isotopic shifts is discussed and used as evidence for asymmetry in the potential energy surface of the proton. Secondary evidence from other techniques, viz. NQR, inelastic neutron scattering, Raman and Far IR spectroscopy, has been obtained which parallels and confirms the results from IR spectroscopy.

Type A salts, which are thought to be examples of symmetric H-bonds, have been examined by the same techniques which were used for Type B salts. In particular their IR spectra have been examined and assigned for the first time. Attention is drawn to the low frequency of νOH and νOD, and to its high isotopic shift. The IR spectrum of Potassium hydrogen diaspirinate has been recorded,

but not analysed in detail, and it is clear that it is similar to the much simpler IR spectrum of the Type A salts prepared in this work. The latter example represents a case where very recent and accurate neutron diffraction data is available and where it was suggested that νOH is below 1000cm^{-1}. This evidence, together with work on Type A and B salts, has led to an idea of the shape of the potential energy well for the proton and deuterium in Type A salts which is based on a symmetric double minimum. A similar situation is suggested for the proposed symmetric cases of HCl_2^-, and the differences from the HF_2^- system is made apparent in the text.

CHAPTER ONE

INTRODUCTION

Chapter 1.

I N T R O D U C T I O N

1. Hydrogen Bonded Anions

Over the past decade an extensive amount of literature has appeared on all aspects of hydrogen (H-) bonding (1,2.) Recently Hamilton and Ibers have summarised the techniques available for H-bond studies (3). With this vast amount of data available it remains only for a general outline to be discussed here, with particular attention to the more recent controversies which still exist.

In general, an H-bond is formed between a proton donor, HX, and an electron donor, Y, where Y can be a negatively charged species. The X-Y distance is between a normal chemical bond and the Van der Waals radii of X and Y. If an electrostatic model is assumed then it is not surprising that the strongest H-bond exists in HF_2^-. However, it is now believed that considerable covalent character exists in HF_2^- and other H-bonds of this type (4, 5, 6.)

The HF_2^- ion is a member of a very large class of H-bonded anions which can be isolated as salts in a crystalline state. The enthalpy of formation (ΔH) of HF_2^- in solid KHF_2 is -27 Kcal/mole (7) and the calculated gas phase value is -57 Kcal/mole (8). The use of large cations, thereby lowering the lattice energy of the system, have made possible the isolation of much weaker anions. Many H-bonded anions have now been isolated which parallel salt hydrates in the water system. Table 1,1. shows a selection of those which have been prepared and characterised to date.

A large class of acid salts exist where a monobasic carboxylic acid is H-bonded to a carboxylate group. Salts of this type have been known for a long time and structural details were known as early as 1922 (24). A considerable amount of structural and spectroscopic information is now available on hydrogen dicarboxylate salts and will be a subject of a subsequent section.

TABLE 1.1

Cation (+)	Anion (-)	Ref.
Group 1	HF_2	(3)
Cs,Me_4N, etc.	HCl_2	(9, 10)
Me_4N,Ph_4As	HBr_2	(11,12)
n-Bu_4N	HI_2	(13)
Et_4N	HFCl	(14)
Et_4N	HFBr	(14)
n-Bu_4N	HFI	(14)
Cs,n-Bu_4N	HClBr	(9,15)
n-Bu_4N	HClI	(15)
n-Bu_4N	ClH(OAc)	(16)
n-Bu_4N	ClH(OFm)	(16)
n-Bu_4N	BrH(OAc)	(16)
n-Bu_4N	BrH(OFm)	(16)
Me_4N	$HClNO_3$	(15)
Ph_4As	$H(NO_3)_2$	(17)
Ph_4As	$H(NO_2)_2$	(18)
Ph_4As	$H(NCS)_2$	(19)
K	$H(OMe)_2$	(20)
n-Pr_4N	$H(CN)_2$	(21)
n-Bu_4N	HClCN	(22)
n-Bu_4N	HBrCN	(22)
Et_4N	$ClHCCl_3$	(23)
Et_4N	$BrHCCl_3$	(23)

Intramolecular H-bonded anions have also been the subject of much work, the classical example being potassium hydrogen maleate (25, 26). Potassium hydrogen malonate, on the other hand, is intermolecular in the solid phase (27) but is intramolecular in solution (28). This emphasises that crystal forces can modify the structure of H-bonded species, and that the solid state structure is not necessarily preserved in solution (28).

Although a considerable amount of work has gone into the isolation of H-bonded anions, the main body of the research has centred on structural determinations. This essentially reduces to determining the position of the hydrogen atom in relation to the groups bonded to it, and is, therefore, the subject of the next section (3).

2. Structure of Hydrogen Bonded Anions

The small size of a hydrogen atom renders structural determinations of H-bonded anions difficult. The advent of neutron diffraction has contributed a great deal in solving the problem for weak H-bonds, but it is inconclusive for strong H-bonded species (3). Ibers and McGaw have pointed out that only the coupled use of neutron diffraction and spectroscopic techniques can determine unambiguously the structure where a hydrogen atom is situated near to the mid point between two interacting groups (3, 29).

The most likely shapes of the potential energy well along the bond axis in linear H-bonded anions are shown in fig. 1,2 (30). Non linear species are also known, especially in weak H-bonds, but will only be discussed in specific cases (3). The groups X and Y are different in the diagrams, however, the same arguments are applicable when X and Y is the same group.

Case 1 represents an asymmetric H-bond with the hydrogen atom associated more closely with one of the groups, and is generally found in cases where X and Y have different chemical and physical properties (31). If two distinct minima occur in the well, 1(b), then two different compounds will exist. However, the compound with the hydrogen atom associated with Y

will be very unstable. Case 1 examples can be found in many crystalline hydrates and neutron diffraction alone can determine their structures unambiguously (3). For cases where X and Y are complex groups, such as $CH_3CO_2^-$, then an infrared (IR) spectrum will show a superposition of the acid and base spectrum, which in itself is strong evidence in favour of case 1 (30). For species such as $ClHBr^-$ all the bands in the IR spectrum above about $200cm^{-1}$ are associated with proton motion. This situation will be discussed in more detail in chapter three.

Case 2 represents an asymmetric H-bond with two equally possible equilibrium positions separated by a high energy barrier (30). Such a situation was suggested in $DCrO_2$, where it is quite clear that the deuterium bond is asymmetric (32). This case will be discussed in more detail at a later stage.

Cases 3 and 4 represent the most difficult cases to distinguish. In the former, the possibility of proton tunneling exists because of the low potential energy barrier (30). A neutron diffraction study on such a compound would indicate an elongated contour map representing the thermal motion of the hydrogen atom along the bond axis, and its centre would coincide with the mid point between groups X and Y (32). The latter cannot be distinguished unambiguously from an example of case 4 where a high thermal vibration of the proton occurs along the bond axis (29). Hadži and Novak suggested that IR spectroscopy can distinguish between such cases since proton tunneling will give rise to several bands corresponding to νXH (30). The IR spectrum of KH_2PO_4 was interpreted on the basis of proton tunneling (33) but has recently been reinterpreted (34). This compound will be discussed at a later stage. Ibers emphasised again that only the coupled use of neutron diffraction and spectroscopic techniques can differentiate unambiguously between cases 3 and 4 (35).

The spectroscopic techniques which have been used in H-bond studies are listed below, along with the type of information which can be obtained

Figure 1,2.

Potential Energy Wells

Fig.1.2

(1)

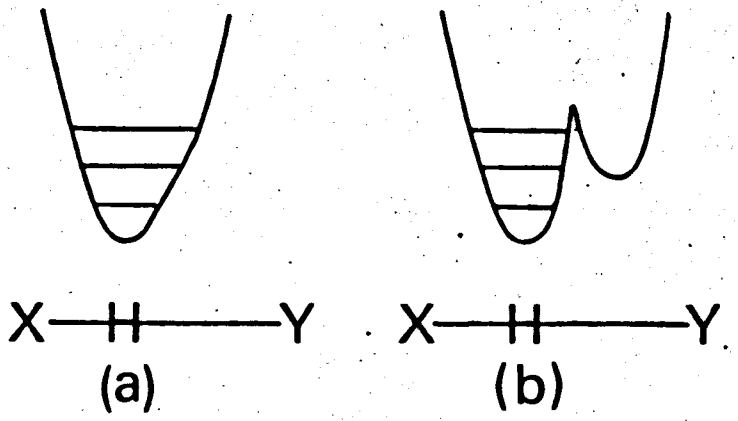

(2)

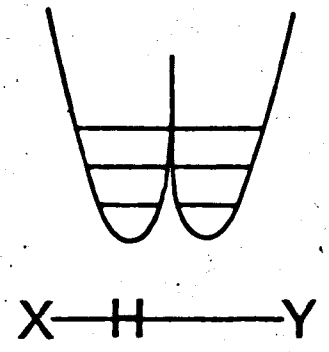

(3)

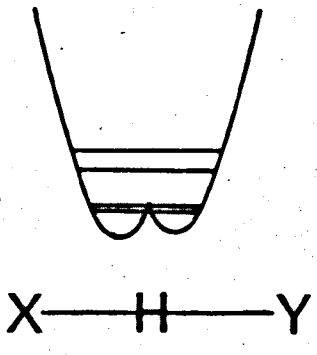

(4)

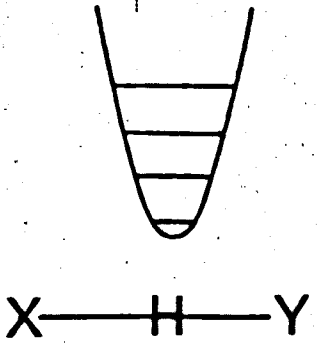

in the solid phase (1) (2) (3).

Infrared Spectroscopy ($4000cm^{-1}$-$200cm^{-1}$)	Energy levels of proton
Far Infrared Spectroscopy ($200cm^{-1}$-$20cm^{-1}$)	Low frequency H-bond vibrations
Raman Spectroscopy	Complementary to IR data in determining point groups
Polarised IR Spectroscopy	Type of vibration
Inelastic Neutron Scattering	Proton motion and energy levels of proton
Nuclear Magnetic Resonance (NMR)	Tunneling and Molecular Motion
Nuclear Quadrupole Resonance (NQR)	Electric Field Gradients

IR Spectroscopy has in the past contributed the main source of information on H-bonded anions and will be the subject of the next section. Far infrared and Raman spectroscopy has not been used extensively because of the experimental difficulties associated with the spectral region and with solids, respectively. However, now that some of the latter difficulties have been overcome these techniques have become more informative. Inelastic neutron scattering has only recently been used and can be treated as complementary to IR Spectroscopy (3). NMR techniques have been applied to proton and deuterium samples and are particularly sensitive to tunneling (3). NQR Spectroscopy is restricted to compounds which contain nuclei with a quadrupole moment but, at present, little information is available.

3. IR Spectra of H-bonded Species.

This subject has been discussed in detail by Sheppard (36) and others (5) (1) and, therefore, will not be discussed at length here. The normal modes of vibration are shown in fig. 1,3. (36). With increasing H-bond strength (thermochemical) in structurally related systems νXH is progressively (36):

(a) lowered in frequency

(b) broadened in contour

(c) enhanced in integrated intensity

Part (a) has been attributed to a lowering of the force constant of

FIGURE 1,3 (36)

Type of Vibration		Description	Notation
Free Molecule	H-bonded State		
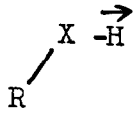	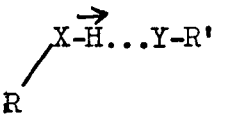	XH stretching	ν XH
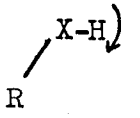	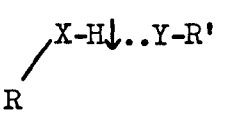	XH in-plane bending	δ XH
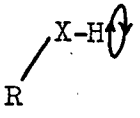	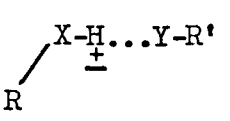	XH out-of-plane bending	γXH
Translation	$\overleftarrow{(RXH)}\ldots\overrightarrow{(Y-R')}$	H-bond stretching	ν(XH...Y)
Translation	$\downarrow(R\text{-}XH)\uparrow\ldots\uparrow(Y\text{-}R')\downarrow$	H-bond bending	δ (RXH...YR')
	$\downarrow(R\text{-}XH)\uparrow\ldots\downarrow(Y\text{-}R')\uparrow$		γ (RXH...YR')

the XH bond which is caused by an overal reduction in the X-H--Y bond length (36). Many early workers suggested correlations between the (X-H--Y) distance and νXH (37, 38, 39), but correlations are not good for short H-bonded species (40). More recently, Ratajczak and Thomas suggested that unique relations do not exist between the vibrational frequencies of the proton and bond lengths in O-H-O systems (41).

Parts (b) and (c) represent the most dramatic changes which occur on H-bond formation. The bending vibrations δXH and τXH, on the other hand, are much narrower and for most species the effect of H-bond formation is to reduce the band width (36, 41). The theories which have been suggested for the band width of νXH in O-H-O systems are listed below (41) and can be generalised to all systems:

(a) The superposition of peaks due to several different H-bonded species.

(b) Sum and difference combinations between νOH and ν(OH-O)

(c) Fermi resonance between νOH, overtones, and combination bands resulting in an enhancement of intensity of the later two.

(d) The effect of proton tunneling giving rise to multiple νOH structure

(e) Anharmonic coupling between νOH and low frequency H-bond vibrations.

Sheppard suggested that strong anharmonic interaction of νXH with ν(XH-Y) together with Fermi resonance of νXH with overtones and combination bands was the most effective mechanism in accounting for band breadth (36). Bratož, Hadži and Sheppard suggested this mechanism for νOH in carboxylic acids (42). The mechanism of interaction of νOH and ν(OH-O) was studied theoretically by Marechal and Witkowski in 1968 (43), and was based on Sheppard's modification of Stepanov's mechanism (36).

Stepanov and Bateuv independently suggested that νXH is anharmonically coupled to νXH-Y and will give rise to a range of sub-bands of frequency given by νXH $\pm n\,\nu$(XH-Y) (36). This theory, known as the frequency modulation theory, implies a considerable temperature dependency which will reduce the intensity of difference bands on cooling (36). Sheppard pointed out that

on absorption of $h\nu XH$ the potential energy curve for the first excited state will have its equilibrium position displaced relative to that of the ground state (36). This will give rise to temperature independent bands since the transitions occur from the ground state to sub-levels of the first excited state (36). Marechal and Witkowski proposed a mechanism of coupling of X-H-Y stretching modes with $\nu(X-H)$ and from the equations describing the coupling they reproduced stick diagrams of the spectrum of acetic acid and imidazole, which were in good agreement with experimental data (43). The isotopic behaviour was also studied and found to be in good agreement with the published spectra of D-acetic acid and imidazole-D. They did not, however, discuss the temperature behaviour of the spectra (43). The theoretical calculations on dimeric acetic acid were complicated by the presence of two hydrogen atoms which cannot be treated independently. They also emphasised that overtones and combination bands falling in the region of νOH would be enhanced in intensity by Fermi resonance with νOH. Marechal and Witkowski reported a calculation on imidazole and suggested a similar mechanism for the band breadth of νNH (43). This mechanism may account for the failure of earlier workers to find a simple relationship between νNH and low frequency H-bond vibrations in imidazole and purines (44, 45). Marechal and Witkowski emphasised again that overtone and combination bands will complicate the region of νNH in imidazole.

In many systems, particularly HF_2^-, the structure of νXH is smooth even at low temperature (36). Stepanov suggested a theory, called the Predissociated theory, where a continuum of energy levels were produced from overlap of different $\nu XH-Y$ energy levels of ground and first excited states of the proton (36). Whether such a mechanism operates, however, is still an open question (36).

Salthouse and Waddington have recently suggested a temperature independent mechanism which accounts for the smooth contour of νFH in KHF_2(46). Their mechanism is based on interactions of neighbouring HF_2^- units which

splits the energy levels. ~~in the same manner as dipole-dipole interactions causes energy level splitting and band broadening in solid state NMR signals~~. The splitting is dependent on the distance separating HF_2^- units and because of the large number of near neighbours the overal effect is a near continuum of energy levels. This theory was tested by isolating HF_2^- in alkali halide host lattices. Narrow bands were observed for νFH and δHF which sharpened further at -196°C. Sharp bands were also observed for DF_2^- and in the spectrum ofadilute isotopic mixture of HF_2^- (46, 61).

A mechanism for band broadening in n-decanol was suggested which was similar to the one proposed for HF_2^-(47). Low temperature polarised IR spectra of dilute isotopic mixtures of n-decanol indicated that νOH in the chain structure was composed of two bands, viz. in-phase and out-of-phase motions of the hydrogen atom. It was suggested that the in-phase motion was broader than the out-of-phase motion because of interactions of the hydrogen motion along the chain in the former. Isotopic dilution removed the coupling and hence sharp bands were observed for both vibrations (47).

Although neighbouring group interactions seems a plausible mechanism in HF_2^- and in n-decanol, it cannot be regarded, at present, as being the dominant mechanism in all systems (45). For example, the breadth of νNH in purines and imidazole does not sharpen appreciably with isotopic dilution (44, 45). However, the one thing that is clear is that all mechanisms can dominate but the precise mechanism operating will depend on the system and on the phase (36, 47). Anharmonicity also plays an important part and is incorporated into all mechanisms except in the mechanism suggested by Salthouse and Waddington where it is not implied (48).

4. Hydrogen Dihalides

The most thoroughly understood anionic H-bond is HF_2^-. Evidence based on the techniques tabulated below suggest that the proton is residing in a symmetric single potential energy well which has a small amount of quartic character (49).

Technique	Information obtained	ref.
IR spectrum		(50)
Polarised IR spectrum	Assignments consistent with $D_{\infty h}$	(51)
Raman Spectrum		(52)
Crystal Entropy	Zero entropy at 0^oK	(7)
NMR (solid phase)	Absence of proton tunneling (KHF_2)	(53)
Neutron Diffraction	Root mean square amplitude of vibrations of H and D	(29, 35)
Inelastic Neutron Scattering (cold)	Absence of transitions associated with double minimum in KHF_2	(54)

The distinction between cases 3 and 4 (fig. 1,2) was made on the basis of neutron diffraction and IR data (29). From neutron diffraction data the mean square amplitude of vibration of H and D alone was calculated and compared with the value obtained from IR data assuming a potential energy well similar to case 4, (fig. 1,2.) (29). Ibers and McGaw repeated the calculation assuming H and D were off centre in a symmetric double minimum potential energy well (29). It was concluded from a comparison of Δ for cases 3 and 4 with Δ from neutron diffraction that case 4 was more realistic (29). Ibers repeated the calculation for KHF_2 using the same equations as shown below, and arrived at a similar conclusion (35). Further details are shown in table 1,4.

$$\Delta = \langle u_n^2 \rangle_H - \langle u_n^2 \rangle_F = (h/16\pi^2 m_F) \left\{ (2m_F - m_H/m_H \nu_3) - (1/\nu_1) \right\}$$

where $\nu_3 = \nu$ FH

$\nu_1 = \nu$ (FH-F)

Δ = mean square amplitude of vibration of H or D alone

m_F, m_H = mass of F and H, respectively

$\langle U_n^2 \rangle_H$, $\langle U_n^2 \rangle_F$ = mean square amplitude of vibration of H and, F respectively

TABLE 1,4 (29, 35)

Atom	Parameter	$NaHF_2(A^{o2})$	$NaDF_2(A^{o2})$
F	$\langle U_{\perp}^2 \rangle$	0.0289(8)	0.0263(18)
	$\langle U_{\parallel}^2 \rangle$	0.0145(7)	0.0158(15)
H or D	$\langle U_{\perp}^2 \rangle$	0.0320(13)	0.0245(22)
	$\langle U_{\parallel}^2 \rangle$	0.0245(12)	0.0197(21)

$\Delta = 0.0100 A^{o2}$ for H

$\Delta = 0.0039 A^{o2}$ for D

Spectroscopic Value

$\nu_3(H) = 1577 cm^{-1}$

$\nu_3(D) = 1150 cm^{-1}$

$\nu_1(H) = {}_1(D) = 600 cm^{-1}$

$\Delta = 0.0097\ A^{o2}$ for H

$\Delta = 0.0062\ A^{o2}$ for D

Atom	Parameter	$KHF_2(A^{o2})$
F	$\langle U_{\parallel}^2 \rangle^{\frac{1}{2}}$	0.0207
H	$\langle U_{\parallel}^2 \rangle^{\frac{1}{2}}$	0.0289

$\Delta = 0.0082\ A^{o2}$

(spectroscopic)$\Delta = 0.0106\ A^{o2}$

The analogous compounds for the remainder of group 7 have only been prepared comparatively recently (see table 1.1). Waddington isolated Me_4NHCl_2 in 1958 and its IR spectrum was assigned by comparison with HF_2^- (10). However, Evans and Lo have more recently examined the IR spectrum of HCl_2^- with different cations and concluded that the symmetry of HCl_2^- was dependent on the cation used (55). NQR work on Me_4NHCl_2 and Et_4NHCl_2 suggested that HCl_2^- was asymmetric in the former and symmetric in the latter (56, 57), which agreed with their IR work (55). In 1967, Nibler and Pimentel suggested that in $CsHCl_2$, which is stable at -80°C, HCl_2^- possessed $C_{\infty v}$ symmetry (9). The HCl_2^- ion is still, therefore, a subject of controversy. A neutron diffraction study would contribute a great deal in determining its structure but, unfortunately, the hygroscopic nature of the compounds render diffraction and polarised IR work very difficult. Neutron diffraction data is, however, now available on a compound formulated as $CsCl_2\frac{1}{3}H_3O^+HCl_2^-$ which was thought to contain HCl_2^- (58-60). Schroeder and Ibers confirmed the presence of HCl_2^- and suggested that a mirror plane exists through the hydrogen atom which reflects one chlorine into the other (58). They were unable, however, to record an IR spectrum (58). Neutron inelastic scattering and further NQR experiments may, however, throw light on the controversy centred on HCl_2^- (61).

5. Acid Salts of Monobasic Acids

Acid salts of monobasic carboxylic acids have associated with them a short O--O bond length in the range 2.4A° - 2.5A° (table 1,5.). Coulson has suggested that in H-bonds shorter than 2.45A° the hydrogen atom will reside in a symmetric single potential energy well (62). Speakman classified salts of this kind, with short H-bonds, into type A and type B. Type A represent anions where there is an element of symmetry at the mid point between the two carboxylate groups. Usually this is a centre of inversion, though it can be a C_2 axis as in sodium hydrogen diacetate (63).

TABLE 1, 5.

Acid Salts of Monobasic Carboxylic Acids

Type A.

H-bond	Symmetry	O-OA°	ref.
KH Bisphenylacetate	C_i	2.445	(66, 67, 68)
KH Di-p-hydroxybenzoate hydrate	C_i	2.458±0.006	(85, 86)
KH Dibenzoate	C_i	2.51	(87)
NaH Diacetate	C_2	2.4333	(88)
RbHDi-o-nitrobenzoate	C_i	2.43±0.01	(64)
NH_4H Dicinamate	C_i	2.51±0.03	(89)
K(or NH_4, Rb) H Di-p-chlorobenzoate	C_i	2.457±0.013	(90)
KH Di-trifluoroacetate	C_i	2.435	(91)
CsH Di-trifluoroacetate	C_i	2.38±0.03	(91)
RbH Diaspirinate	C_i	2.48±0.02	(92)
KH Diaspirinate	C_i	2.455±0.005	(93)
KH Diaspirinate	C_i	2.448	(70)
KH Dianisate	C_2	2.476	(94)

Type B.

KH Di-p-nitrobenzoate	C_1	2.49	(64)
RbH Bisglycollate	C_s	2.53	(95)
KH Diformate	C_1	2.45	(65)
NH_4H Disalicylate hydrate		range from 2.76-2.53	(96)

Speakman suggested that in type A salts, where the carboxylate groups are crystallographically identical, the proton can be considered as being symmetrically placed between the two oxygens. Also, the $R\text{-}CO_2$ groups are intermediate in character between the carboxylate and carboxyl group, which is born out in the parameters determined from x-ray diffraction (63).

Type B salts, which also have short O--O distances, are representative of those anions where the two carboxylate groups are crystallographically distinct and also different in their dimensions (64). A recent example is potassium hydrogen diformate, but no details were available on the position of the hydrogen atom (65).

Hadži and Novak have pointed out that the distinction between a symmetric H-bond and a case where the hydrogen atom is evenly distributed between two positions of minimum potential energy cannot be made by diffraction techniques alone (30). Hadži suggested that spectroscopic data is much better suited for this purpose (30). However, in view of the work of Ibers et al on HF_2^- even spectroscopic data is not sufficient at present, though it is still probably the best guide (29).

A typical example of a type A salt is potassium hydrogen bisphenylacetate, KHP_2. X-ray diffraction (66) and neutron diffraction (67, 68) suggest that the hydrogen atom is situated midway between the two oxygen atoms and the symmetry of the anion, as implied by the space group $C2/_s$, is C_i. Its IR spectrum, characteristic of type A salts, has no band above $1800cm^{-1}$ which can be assigned to νOH(30). It also shows a very broad background absorption in the region $1500 - 600cm^{-1}$, which contracts on cooling and shifts to lower frequency on deuteration. Hadži and Novak also pointed out that because the two carboxylate groups are related by a centre of inversion through the hydrogen atom, the mutual exclusion principle will operate, viz. the out-of-phase motions of the two $\nu C{=}O$ will be IR active and Raman inactive, while the

in-phase motion will be IR inactive and Raman active. The effect of this will be that the spectrum will not be a superposition of the acid and base spectrum. The short H-bond length of 2.44A° (66) suggests, from frequency-bond length relationships, that νOH should be around 1700cm^{-1} (38). Since only one strong band, i.e. a very broad νC=O, was observed in this region Hadži and Novak suggested that νC=O and νOH are strongly coupled together (30). On deuteration νC=O shifted to 1650cm^{-1} and a new band appeared at 1320cm^{-1} which was assigned to an uncoupled νOD (30).

The location of the two bending vibrations presented a problem because of the extreme breadth and complexity in the region 1500 - 600cm^{-1} (30). However, Hadži and Novak assigned the in-plane bend to a band at 1270cm^{-1} which disappeared on deuteration, and the out-of-phase bend was associated with the extreme breadth in the region of 900cm^{-1}. They recognised the possibility that the potential energy surface in which the proton is residing may be an odd one, and in 1966 they suggested that νOH may be as low as 1000cm^{-1}, even though this contradicted their earlier assignments (69).

Recent neutron diffraction data on potassium hydrogen diaspirinate has indicated a very high root mean square amplitude of thermal vibration (0.19A°) along the H-bond axis (70). This is to be compared with the value of 0.1A° found in $NaHF_2$(29). Based on the same calculation as Ibers and McGaw used for HF_2^- (29), Hamilton and co-workers suggested that νOH may be less than 1000cm^{-1} (70). They also suggested that the thermal motion perpendicular to the bond axis was much smaller than along the bond axis and the values of 0.09A° and 0.03A° would give rise to a bending frequency in the region of 2000cm^{-1}. They concluded by saying that the potential energy well along the bond axis was essentially flat with the proton executing extremely anharmonic motion (70).

Additional evidence for the existence of a symmetric single minimum potential energy well in type A salts was obtained from solid state NMR spectroscopy (71). Blinc and Hadži observed that in KH_2PO_4, where there

is strong evidence for proton tunneling, a strong and narrow signal was observed, whereas in KHP_2 and potassium hydrogen maleate (KHM) a weak signal was observed which was very easily saturated (71, 72). From this Blinc and Hadži concluded that no proton tunneling exists in KHP_2 or KHM and that they were symmetric H-bonded species.

Although acid salts of type A hydrogen dicarboxylates are suspected as having a symmetric H-bond with the proton in a single potential energy well a full explanation of their IR spectrum is still required. Hadži has tackled the problem by examining the IR spectrum of a series of H-bonded adducts with different donor and acceptor strengths (69, 73, 74). The crystalline adducts examined were composed of phosphine, arsine and amine oxides and sulphoxides with strong acids such as HNO_3 and hydrogen halides (73). The liquid H-bonded adducts constituted halogenated acetic acids with sulphoxides, phosphine oxides and other bases (74). By varying the acid and base strength in the H-bonded adducts evidence of proton transfer to the base was found in some cases, eg. pyridine-n-oxide with hydrogen halides (73). Some crystalline adducts gave spectra similar to those observed for type A salts, eg. (α-picoline oxide)$_2$ HBr. In the liquid adducts they observed similar features with evidence for proton transfer in some cases and spectra similar to type A salts in others (74). It was noted that spectra similar to those for type A salts were obtained when the acid and base strengths of the donor and acceptor groups were approximately equal. It was suggested, therefore, that the broad absorption centred near 1300cm^{-1}, which was not sensitive to change of state, was associated with the asymmetric stretch of the hydrogen atom (74). Also, the low isotopic shift observed for this band in the liquid adducts is a clear argument against a genuine symmetric potential energy well (74). These results seem, therefore, to reflect the unlikelihood of the acid and base proton affinities being equal. In type A hydrogen dicarboxylate salts the short H-bond and the equivalence of the two carboxylate groups favour the formation of a symmetric H-bond. Crystal packing

can, however, distort the anion thereby rendering the H-bond asymmetric (40). An exception to this may be potassium hydrogen chloromaleate, which has a short intramolecular H-bond (2.38°A), where neutron diffraction data suggests that the hydrogen atom is midway between two non equivalent and chemically distinct carboxyl groups (76)

6. Potassium Dihydrogen Phosphate.

Proton tunneling was invoked to explain the IR spectrum of potassium dihydrogen phosphate (33). A neutron diffraction study was also interpreted in terms of a double minimum potential well (77, 78). Blinc and Hadži interpreted the doublet structure of νOH on the basis of a splitting of the ground and first excited states as a result of a low potential energy barrier:

Fig. 1,6

IR active bands (a) Raman active bands (b)

The existence of a low frequency band (100 cm^{-1}) was assigned to the 0-1 transition, indicated in diagram (a), and was suggested as evidence for a splitting of the ground state energy levels (79). However, Hill and Ichiki in 1968, on the basis of polarised IR studies, suggested that the two bands at 2700cm^{-1} (0-3) and 2300(1-2) cm^{-1} in KH_2PO_4 were due to coupled proton motions in the PO_4 units (34). They suggested that, although proton tunneling may occur in this compound, the type of spectrum obtained does not require the existence of tunneling. The explanation of Hill and Ichiki seems, therefore, to support the earlier view that if the ground state is split by 100cm^{-1}, as suggested by Hadži and Blinc, then clearly the IR spectrum should be temperature dependent (80). This point is worth emphasising as if the splitting is greater than 10cm^{-1} then cooling to liquid nitrogen temperature will cause a considerable depopulation of state1, as shown in diagram (a)

and in the table below. The result will be that transition 0-3 will give rise to the most intense band and the highest in frequency. The numbers in the columns represent the ratio N_o/N_1, where N_o, N_1 are the populations of state 0 and 1 respectively, and the population of each state is given by $N_o = \exp(-E_o/KT)$.

Splitting of ground state / Temperature	$100cm^{-1}$	$10cm^{-1}$	$1cm^{-1}$
300°K	1.62	1.49	1.05
100°K	4.26	1.56	1.14
10°K	1.8×10^6	4.26	1.56

7. Chromous Acid (3)

Neutron diffraction studies on $HCrO_2$ and $DCrO_2$ have revealed that the O-D-O bond in $DCrO_2$ is not centrosymmetric and that it is best represented as a symmetric double minimum potential case (3,32). In $HCrO_2$, on the other hand, the proton is essentially centred at the mid point between the two oxygen atoms (3,32). In $HCrO_2$ Hamilton and Ibers suggested that, although the symmetry of the O-H-O bond could not be determined unambiguously, the evidence in favour of a centrosymmetric H-bond was as good as in any of the type A salts (3). Another notable feature of this system was the increase in the O-H-O distance (0.06A°) on substituting deuterium for the hydrogen (3). From NMR data on $HCrO_2$ Ibers, Holm and Adams concluded that the vibrational amplitude of the hydrogen atom normal to the bond was greater than the vibrational amplitude along the bond (81). This point was also evident from the neutron diffraction study on $HCrO_2$. The thermal parameters of the deuterium atom in $DCrO_2$ were not significantly different from zero (3). From NMR data Ibers, Holm and Adams concluded that although they could not distinguish between a symmetric or asymmetric OHO bond in $HCrO_2$ they could eliminate a model based on rapid proton tunneling between two equilibrium positions (81)

The IR spectrum of the $HCrO_2$ system shows anomalous isotopic behaviour and the assignments are shown below (82):

	$HCrO_2$	isotopic shift	$DCrO_2$	
ν OH(D)	$1650cm^{-1}$		$1917cm^{-1}$ $1594cm^{-1}$	ν OD
δ OH(D)	$1202cm^{-1}$	1.44	$836cm^{-1}$	

Snyder and Ibers suggested that the IR data could not be accounted for on the basis of the same potential energy function in $HCrO_2$ and $DCrO_2$ (83). Recent inelastic neutron scattering experiments on $HCrO_2$ have shown the existence of low frequency bands which can not be explained on the basis of a symmetric hydrogen bond (84). More recent theoretical calculations on the the $HCrO_2$ system have shown that it is not necessary to invoke different potential energy wells in $HCrO_2$ and $DCrO_2$ in order to explain their IR spectrum (120). The alternative explanation advanced was based on a asymmetric double minimum potential energy well with the first excited state close to the top of the barrier (120). Such a model gives rise to low isotopic shifts, and will be discussed in more detail in chapter four.

The intention of the work recorded in this thesis was to examine spectroscopically a range of H-bonded anions built on acetic acid and its halogenated derivatives. The first class examined (chapter three) represent an extension of the number of XHY^- type anions where X^- is a halide ion and Y is a carboxylate group. Finally in chapters four and five type A and type B hydrogen dicarboxylate salts have been examined using a variety of spectroscopic techniques. The salts chosen represent a block of hydrogen dicarboxylates anions with alkali metal cations. The main purpose in the latter systems was to assign, as far as possible, their IR spectrum, which has so far not been reported in the literature.

CHAPTER TWO

EXPERIMENTAL TECHNIQUES

Chapter two

EXPERIMENTAL TECHNIQUES

2,1. The Vacuum System

The most elegant technique for preparations which involve a nonaqueous solvent is by the use of an efficient vacuum system. Furthermore, the use of a vacuum system minimises trace amounts of water vapour, a potential danger to the purity of hygroscopic compounds. The vacuum system employed is of the standard type used in this laboratory and is shown diagramatically in fig.2,1.

The vacuum system was constructed of pyrex glass and was assembled onto a metal framework by means of clamps and bosses. The system was evacuated with a two stage mercury diffusion pump which was backed by a rotary oil pump. A provision for preventing volatile waste material from contaminating the oil in the pump and also as a safeguard against suck back from the oil pump was maintained in the use of a "muck" trap cooled in liquid nitrogen.

Compounds were connected and removed from the system at various points on the line by apparatus fitted with standard "Quickfit" ground glass cones and sockets. When a compound was heated on an oil bath, tin foil was wrapped round the joints to prevent the grease from overheating and flowing onto the compound. All the taps were greased with Apiezon-N-grease and Picein wax was used to seal sections of the system. This enabled the system to be dismantled easily after breakages and also for general cleaning of the system.

Large flasks ranging from five litre to twenty litre were connected to a section of the line for storage of large quantities of volatile materials, e.g. hydrogen chloride and acetic acid. They were arranged so that their contents could be used at any time and that the amount of gas inside the flask could be replenished as its quantity diminished.

Low temperature materials contained in silvered Dewar flasks were of

Figure 2,1.

The Vacuum System.

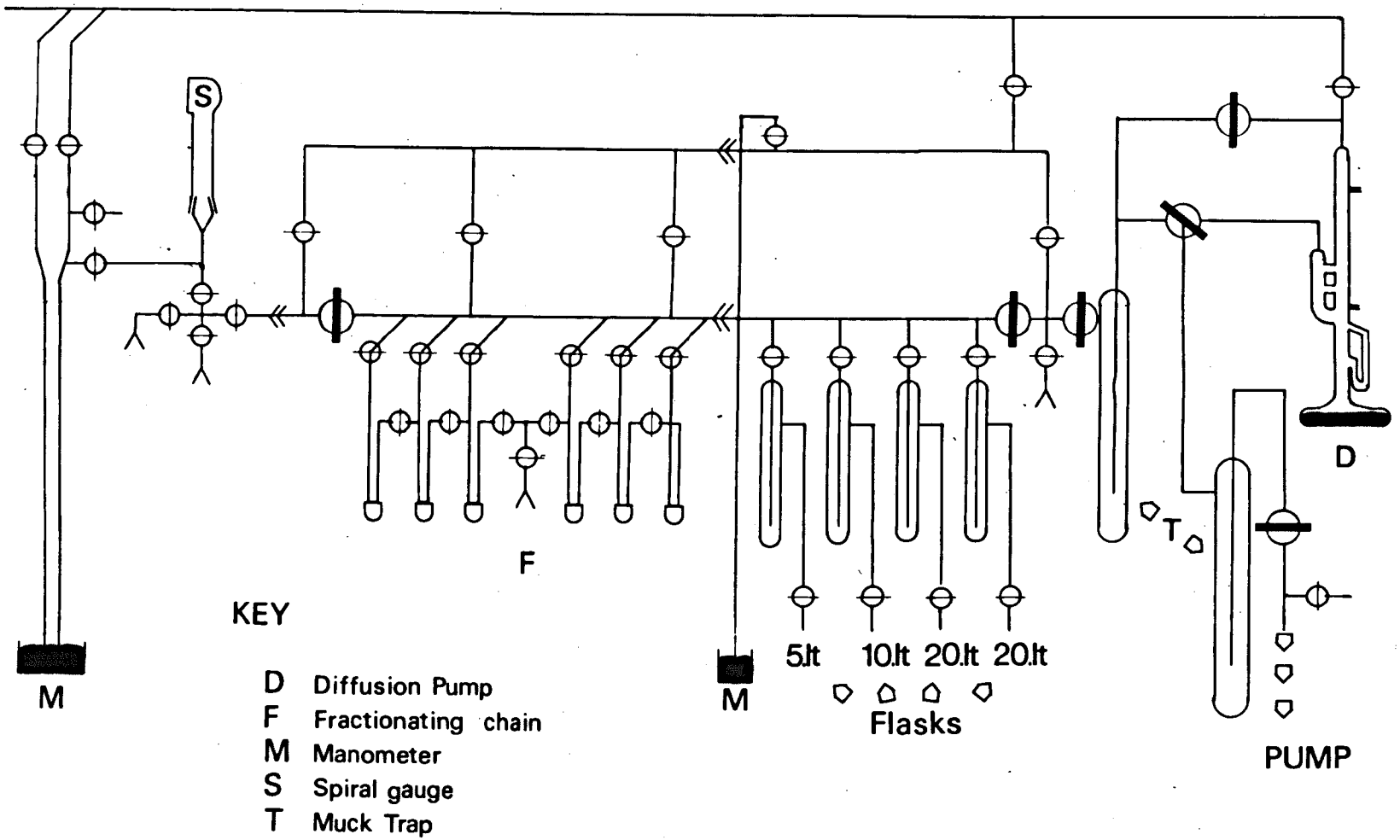
S
M
F
M
5lt
10lt
20lt
20lt
Flasks
T
D
PUMP
KEY
D Diffusion Pump
F Fractionating chain
M Manometer
S Spiral gauge
T Muck Trap

Fig. 2. 1

constant use during the course of the work and a selection is listed below:

Table 2.2

Cold Bath	Temperature (97)
Acetone-dryice-slurry	-84°C
Toluene slush	-95°C
Liquid nitrogen	-196°C

Volatile materials were condensed in traps using liquid nitrogen as the refrigerant. Cold baths were also used extensively for purifying volatile materials whereby the appropriate choice of cold bath served as a fractionating device. This process was carried out in a special part of the line with cold baths which were arranged so that any volatile material on passing through the trap would be condensed and maintained at the temperature of the refrigerant.

Pressure measurements were carried out by two systems: The first method was a mercury manometer which could measure the pressure throughout the system and was read by means of a travelling microscope. This manometer was also used as a safety valve in the preparation of large quantities of volatile materials and guarded against the pressure exceeding one atmosphere. The second method was a spiral gauge used in conjunction with two wide bore mercury manometers. The deflection of the mirror in the guage was about 45° per atmosphere pressure, and the pressure was measured by a null point operation using the wide bore mercury manometer.

The various parts of the line, in particular the large storage flasks and connecting tubes, were calibrated for volume by observing the pressure changes on expanding air into the system from a molecular weight bulb of known volume, fig. 2,3(a), and assuming ideal gas behaviour to apply.

2,2. The Dry Box

The hygroscopic nature of many of the compounds studies necessitated

the use of an efficient dry box. The dry box, which was of a standard type (Gallenkamp MA-150), was kept dry by means of two crystallising dishes containing P_2O_5. Moisture inside, resulting from small leaks, was reduced to a minimum by stirring the drying agent at the beginning of each day and also by replacing the drying agents periodically with a fresh supply. The air in the dry box was dried quickly by recycling the air through a column of silica gel mixed with molecular sieve. An air compresser connected to the dry box performed this operation. This method was particularly useful after volatile materials had been handled in the dry box.

2,3. Analytical Methods.

(a) Weight Analysis

A considerable number of the compounds used in this work were prepared in a reaction cell which is shown diagramatically in fig. 2,3 (b). A good guide to the stoichiometry of the compounds prepared was obtained by the technique of weight analysis (21). This entailed weighing out the evacuated reaction cell followed by reweighing the evacuated cell containing the dry starting material. An excess of the solvent was then condensed onto the compound in the reaction cell, care being taken to ensure that the solvent did not come into contact with the grease on the B.24 joint. After allowing the temperature to reach room temperature, the excess solvent was pumped away and the reaction cell was reweighed. The process of pumping and reweighing was continued until no further decrease in weight was observed or, in the case of weak H-bonded species, until the desired molar ratio was reached. It was important in all the above weighings that the grease on the B.14 joint was removed before each weighing. This was done by wiping the joint with a tissue which had been moistened with chloroform. The results of the weighings then provided sufficient data for an assessment of the stoichiometry of the compound isolated.

Figure 2,3.

(a) Molecular Weight Bulb

(b) Reaction Cell

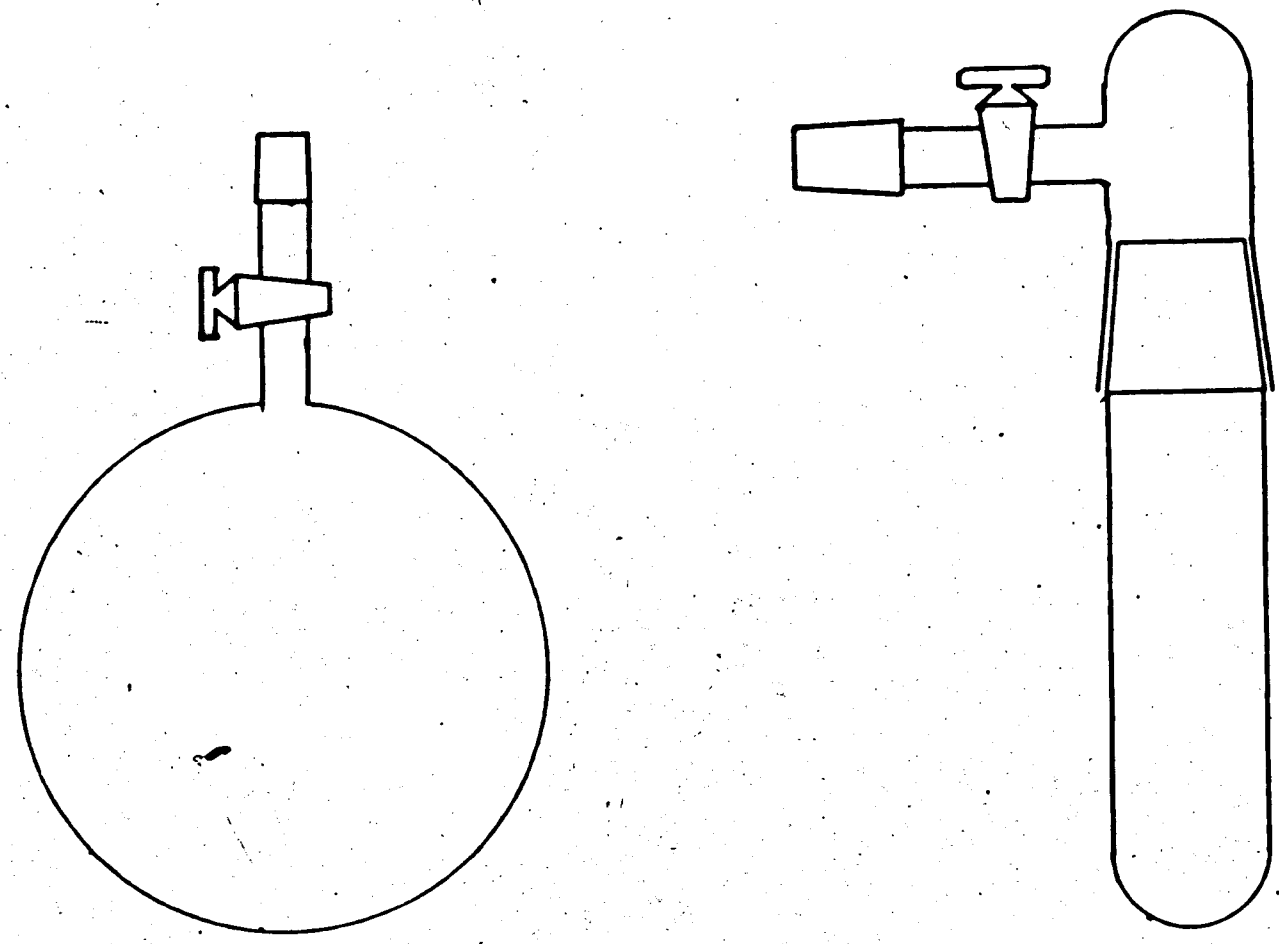

Fig. 2.3

(b) Chemical Analysis

Chemical methods of analysis were carried out on both the anion and the cation to determine the percentage by weight of each in the compound. Cations ranging from tetramethylammonium (Me_4N^+) to tetra-n-butylammonium ($n\text{-}Bu_4N^+$) were determined by gravimetric analysis using sodium tetraphenylborate as the precipitating reagent. All the compounds were dissolved in water and any halogen present was determined as halide ion by Volhards method (98). The percentage by weight of carboxylic acids were determined by acid-base titrations with standard sodium hydroxide.

(c) Elemental Analysis

Elemental analysis was not carried out on compounds which were likely to decompose appreciably with time or which were particularly sensitive to air. The compounds which were examined by this method were type A and type B hydrogen dicarboxylate salts. The cation determination was done spectrophotometrically and the anion elements by combustion techniques. These services were provided by Bernhadt Ltd. of Munich in Germany.

2,4. Preparation of Starting Materials.

(a) Tetra-n-butylammonium Chloride

Tetra-n-butylammonium iodide, obtained from British Drug Houses, was dissolved in a small volume of spectroscopic methanol and an excess of a freshly prepared silver chloride suspension in methanol was added. The solution was allowed to stand in the dark for about an hour in order that complete exchange had occurred. The silver iodide precipitate was then filtered off and the filtrate was evaporated down until an orange brown oil remained. The oil was dissolved in redistilled benzene. The benzene was distilled off, and the process of dissolution and distillation repeated twice more. The brownish solid was washed several times with dry ether and gradually the compound became white. The last traces of ether were removed by pumping on the vacuum line. An IR spectrum of the compound showed no

traces of water, methanol or ether and was similar to a spectrum of $n\text{-}Bu_4NI$.

(b) Carboxylic Acids

The carboxylic acids employed were Anala R grade where possible and those which were volatile enough were purified further by distillation on the vacuum line, followed by storing them in fractionating traps. Prior to this operation, the liquid carboxylic acids were dried over molecular sieve. The purity of the volatile acids were checked by gas and liquid phase IR spectra. The results were found to be in good agreement with published spectra. Those acids which were solid at room temperature were pumped dry on the vacuum line and their IR spectra were checked with the literature and found to be in agreement. The melting points were also found to be in agreement with the literature values.

(c) Deutero Carboxylic Acids

Acids were deuterated in the hydroxyl position by adding the stoichiometric quantity of deuterium oxide, obtained from Novsk and Hydro Elektrisch, to the anhydride of the acid. The process was carried out in a reaction cell which was warmed to accelerate the reaction. The deutero acid was then frozen down in liquid nitrogen and degassed on the vacuum line. They were finally stored in a section of the fractionating chain which was reserved for deutero acids. An IR spectrum was examined to determine the amount of deutero acid present. Deutero samples of acetic and trifluoroacetic acids were prepared by this method.

In the case of dichloromaleic acid, which exists as a solid, the deutero acid was prepared by adding an excess of D_2O to the anhydride followed by pumping to remove the excess D_2O. The anhydride was obtained from Ralph N. Emanual Ltd.

Deuteroformic acid was prepared in the apparatus shown in fig. 2.4. An excess of sodium formate, obtained from Hopkin and Williams, was thoroughly dried beforehand on the line and onto this D_3 Phosphoric acid was dropped very slowly. The D_3 Phosphoric acid was obtained from Ciba

Figure 2,4.

Preparation of Deutero Formic Acid.

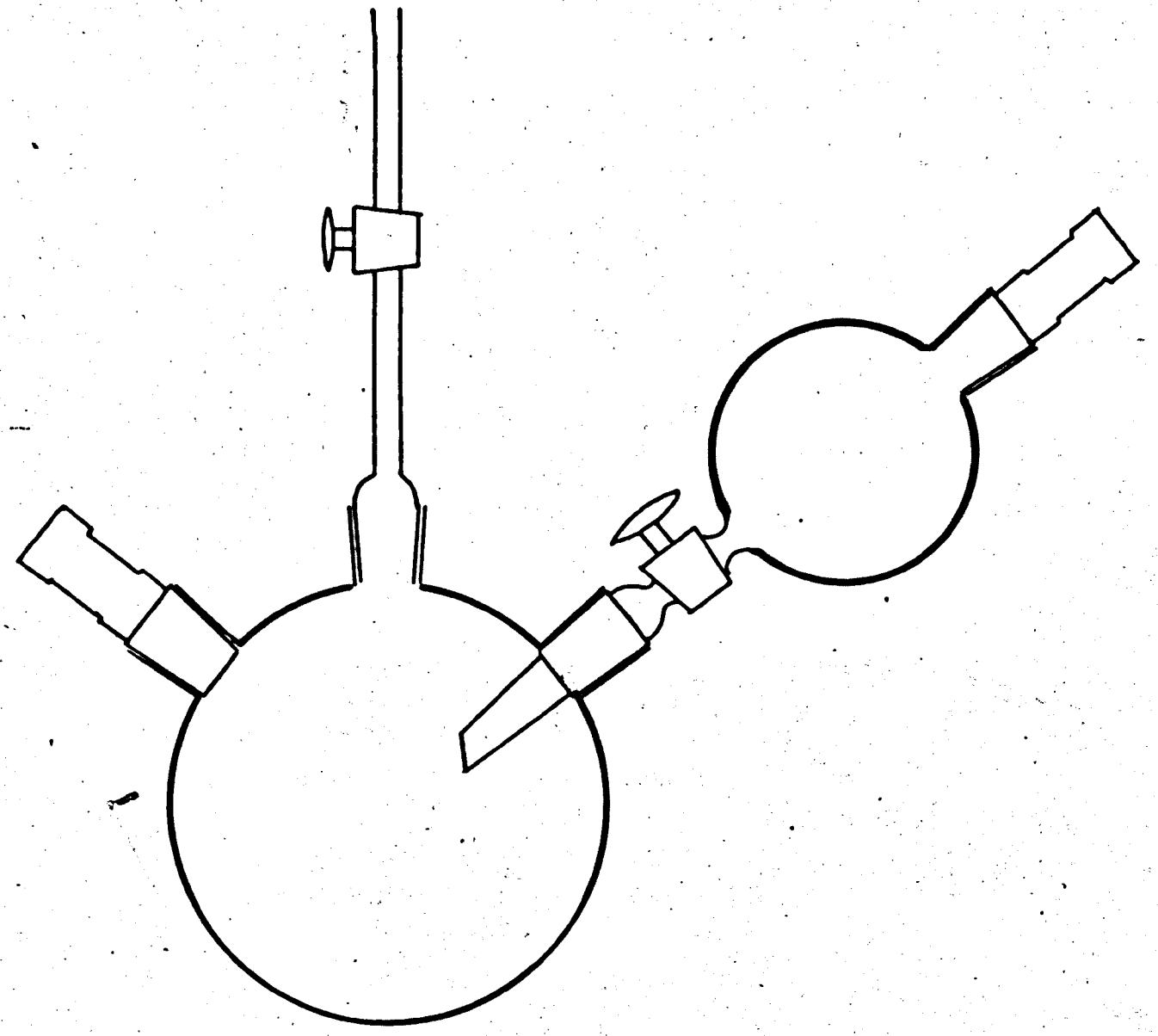

Fig. 2.4

and was an 85% solution in D_2O. The deuteroformic acid liberated was pumped away and collected in a liquid nitrogen trap. Heating was necessary to decompose any H-bonded species formed with sodium formate. The acid was dried by exposing it to anhydrous copper sulphate followed by vacuum distillation (99). Its IR spectrum was found to be in good agreement with published spectra.

(d) Simple Salts

Carboxylate salts of Group 1 metals were prepared by adding the stoichiometric amount of acid to the carbonate dissolved in a small amount of water. After effervescence had ceased the water was pumped away on the vacuum line. An IR spectrum was recorded to check the purity of the compound. In some cases, eg. halogenated carboxylates, prolonged pumping on an oil bath at 110°C was necessary to remove the last traces of water.

(e) Solvents

(i) Purification of Chloroform

Anala R grade chloroform, obtained from Hopkin and Williams, contains about 2% ethanol and was removed by the following procedure:

To Anala R chloroform (500ml) contained in a separating funnel (1000ml) a small quantity of concentrated sulphuric acid (10ml) was added. After shaking the solution for about ten minutes the heavier layer of sulphuric acid was separated off leaving the chloroform behind in the funnel. This process was repeated about five times by which time all the ethanol had been removed. Distilled water (250ml) was then added to the chloroform and the solution was shaken for about five minutes. The chloroform layer was separated off and the process was repeated with a fresh supply of water. The procedure was continued until the chloroform was neutral to phenolphthalein. The chloroform was finally stored in a dark bottle over molecular sieve. A PMR spectrum was recorded under high sensitivity and the complete absence of ethanol and water was confirmed.

(ii) Methylene Dibromide

This compound was obtained from Hopkin and Williams and was stored over molecular sieve to remove any water present.

2, 5. Low Temperature Infrared Cells

The IR spectrum of most of the species prepared in this work were recorded at both room and liquid nitrogen temperatures. Very late on in the course of the work one compound was examined at the temperature of liquid helium. Both these cells were constructed entirely in pyrex glass by Mr. K. Holden.

1 (a) Liquid Nitrogen Infrared Cell

A diagram of this cell is shown in fig. 2.5. The cell is made up of three sections. The first, part A, is essentially a silvered dewar with a pyrex-kovar seal at its base. A copper rod about three inches long inside the liquid nitrogen section of the dewar served to speed up the rate of cooling of the copper block, C. The bottom part of the cell, B, contained a pair of CsI plates piceined onto the flanged portholes in B. Part C is a copper block with a screw thread connecting it to the copper part of A. A pair of CsI plates were placed in C and contained the mull of the material under investigation. The cell was evacuated by means of an outlet in B which was connected to a tap by means of a cone and socket joint. Finally the copper block C was arranged so that its centre coincided with the centre of the windows on the outside of B.

(b) Method of Operation

Once the cell had been set up and all taps and joints had been greased, the cell was evacuated on the system shown in fig. 2.6. The pumping was continued until a dark vacuum was obtained, which usually took about fifteen minutes. Care was taken in testing the cell for leaks, especially in the regions of the caesium iodide plates, as pin holes were very easily

Figure 2, 5.

Liquid Nitrogen IR Cell.

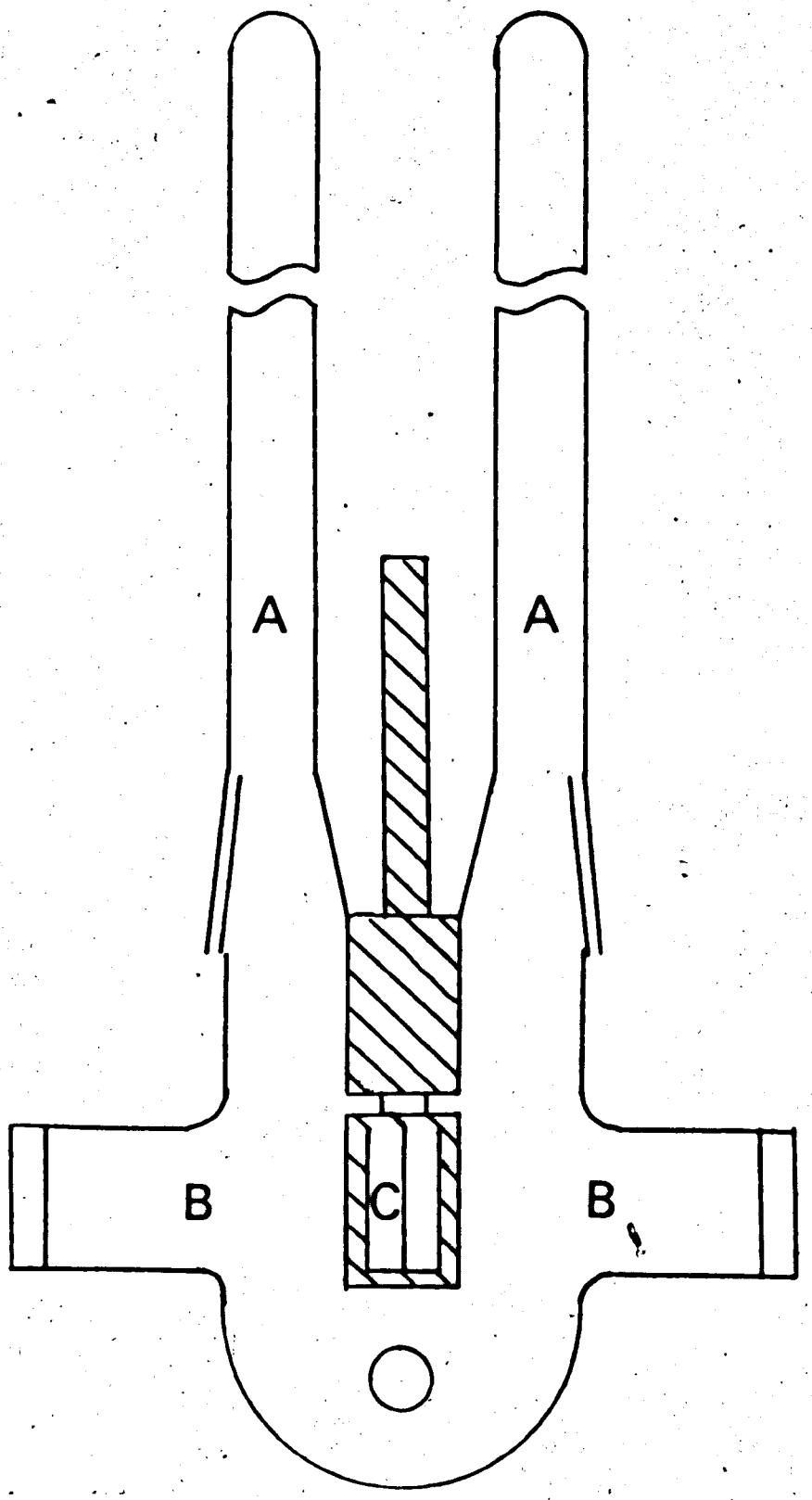

Fig. 2.5

Figure 2,6.

Vacuum System

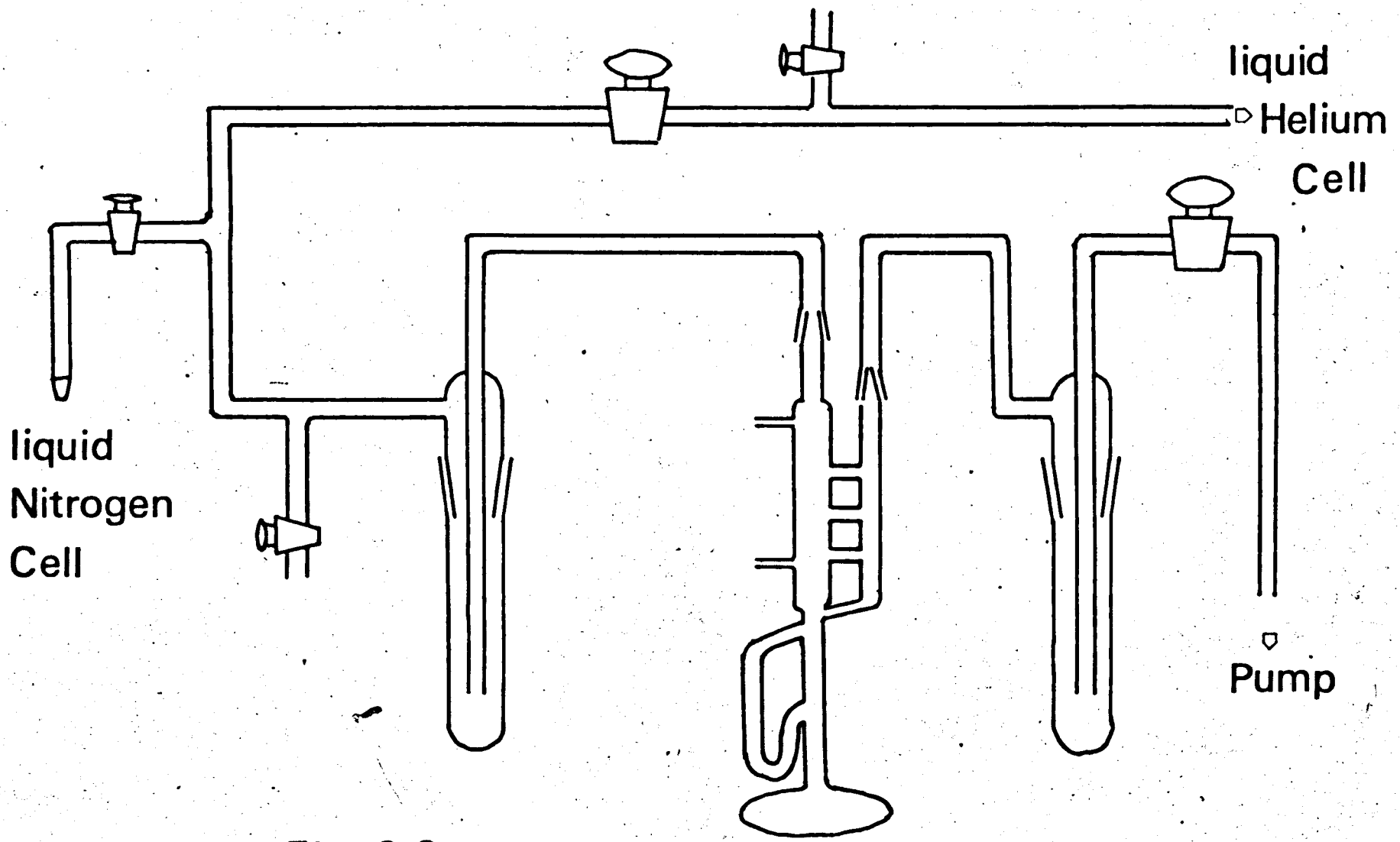

Fig. 2:6

produced by the high voltage discharge. Liquid nitrogen was then quickly poured in up to the top of the dewar. The initial boil off of nitrogen was high, consequently the contents of the dewar had to be topped up soon after the initial one. This was necessary to prevent the nitrogen level from falling too low and allowing ice to form in the region of the copper rod thus giving rise to bad thermal conductivity between the copper and the nitrogen. Once the boil off of nitrogen had reached a steady state, the system was left for about thirty minutes in order that the plates inside the block had reached thermal equilibrium. The dewar was topped up during this period whenever the level dropped too low. Measurement of the temperature of the plates by a thermocouple showed that the plates were at the temperature of liquid nitrogen (100).

Spectra were recorded by isolating the cell from the pumping system and clamping it in the region of the sample beam of the spectrometer. Accidents as a result of the cell slipping were prevented by resting the cell on a cork ring. Once the cell was in position, slight adjustments were made to ensure that the alignment of the cell gave maximum optical transparency. A polythene sheet was used to enclose the system from water vapour and the enclosure was finally purged with dry air. Slow scans were then necessary to obtain accurate pen response.

2(a) Liquid Helium Cell

The liquid helium cell is shown diagramatically in fig. 2,7. Working at the temperature of liquid helium demands precision work in the construction of the glassware. Also, in order that the helium remains liquid for any length of time, it was necessary to have the liquid helium dewar inside another dewar containing liquid nitrogen. These requirements, along with the minimum heat losses, required that the overall length of the cell was 118.5cm.

The cell was composed of three sections. The two main sections were silvered dewars which were separated by a vacuum jacket. The liquid

Figure 2, 7

Liquid Helium IR Cell

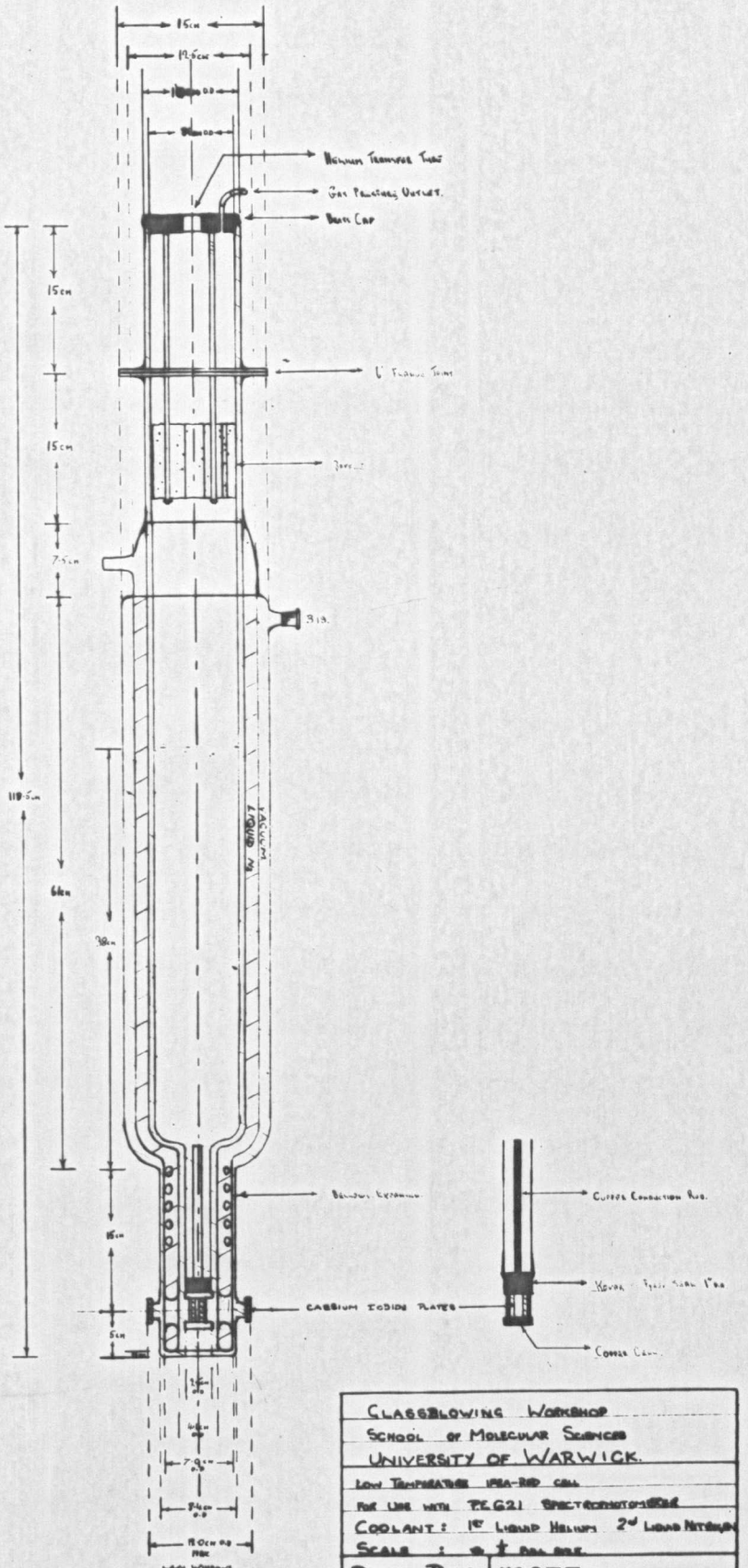

GLASSBLOWING WORKSHOP	
SCHOOL OF MOLECULAR SCIENCES	
UNIVERSITY OF WARWICK.	
LOW TEMPERATURE IRDA-RED CELL	
FOR USE WITH PE.621 SPECTROPHOTOMETER	
COOLANT : 1st LIQUID HELIUM 2nd LIQUID NITROGEN	
SCALE : ½ FULL SIZE	
DRAWN BY :	MR. C.J. TOPPING
GLASSWARE :	MR. K. HOLDEN
ENGINEERING :	MR. C.W. WOOLLAMS

nitrogen dewar, which supported the weight of the liquid helium dewar at the flanged joint, had a vacuum jacket on the outside. The liquid helium dewar had a Kovar-pyrex seal which was connected to a copper block containing a sample of the compound under investigation. The copper rod extended six inches into the liquid helium dewar. A metal baffle was situated about six inches above the liquid helium level. At the top of the dewar a brass plate was piceined onto the glass so that the helium was not exposed to the atmosphere except for two holes in the plate, which were used in the transfer operation. The liquid nitrogen dewar encased the whole of the bottom part of the system except for a pair of CsI plates which were piceined onto the portholes in the glass.

2(b) Method of Operation

The liquid Helium cell rested on a tripod in the sample area of a Perkin Elmer 621 spectrometer. The tripod had adjustable legs so that the cell could be aligned in the beam and adjusted for maximum optical transparency. A polythene sheet was wrapped round the bottom of the cell and the enclosure was purged with dry air. The system was evacuated through a B.19 joint on the side of the cell. This operation had to be performed very slowly at first in order to minimise the risk of implosion. Thirty minutes pumping on the rotary oil pump was sufficient for the mercury diffusion pump to take over. This pumping was continued for about two hours, in which time a room temperature spectrum was recorded. The helium section of the dewar was also evacuated to keep the compartment dry.

Liquid nitrogen was then poured into the cell at the side of the dewar shown in the diagram. The dewar was filled up to the top with nitrogen and the level could be seen through an unsilvered strip of glass which extended along the length of the dewar. A source of light was put on the opposite side of the dewar to illuminate the level of the nitrogen. Once the level of nitrogen remained steady, the tap connected to the B.19 joint was closed and

the cell was isolated from the pumping system. The copper block was consequently cooled by radiation from the liquid nitrogen which surrounded it. The system was then left for about two hours. The level of the nitrogen remained essentially unchanged during this period of time, and could be left overnight if necessary. A liquid nitrogen spectrum was recorded during this time, followed by further pumping of the system.

2(c) Transfer of Liquid Helium

The transfer of liquid helium could not be performed by one person and so Mr. K. Holden and Mr. C. Worland assisted in the operations. The vacuum inside the liquid helium compartment was released by allowing a flow of gaseous helium to be sucked in from a helium cylinder. A long piece of rubber tubing was used so that the lower part of the cell near the copper rod was under a helium atmosphere. A rapid flow of helium was necessary to expel all traces of air and was continued until just before the transfer operation. This operation was important as any nitrogen or water vapour present would be frozen down on the copper rod once liquid helium was in the dewar. This would result in poor thermal conductivity between the copper rod and the liquid helium and also in a rapid boil off of the helium.

The transfer tube is shown diagramatically in fig. 2,8 and was made of stainless steel. A vacuum jacket served to reduce heat losses during the transfer operation. The system was rigid except for an extension tube on one limb which was connected by means of a small piece of rubber tubing. This extension was necessary so that the liquid helium could be poured directly onto the copper rod in the liquid helium cell. Immediately before the transfer operation, the transfer tube was flushed with warm helium.

The dewar containing the liquid helium was accurately placed three feet from the helium cell so that the necks of each were at about the same height. The transfer tube was then quickly inserted into the two necks (fig. 2,8.) This operation required speed as any air inside the transfer tube would

Figure 2,8

Transfer Tube.

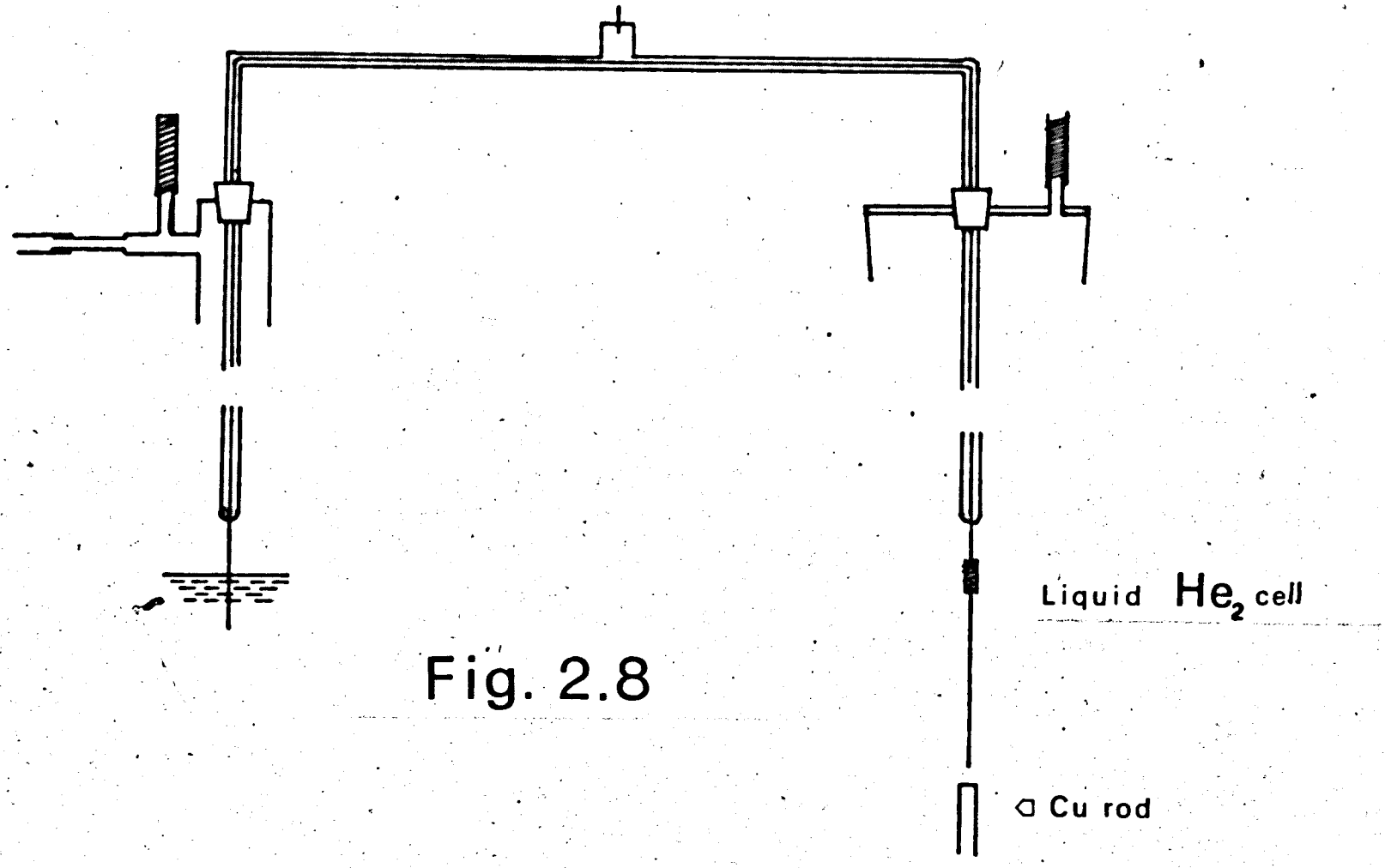

Fig. 2.8

solidify once it was exposed to cold gaseous helium. As soon as the tube was in position, the flow of helium from the cylinder was stopped and the transfer tube was fixed tightly in position by means of rubber bungs. As the pressure built up inside the liquid helium dewar, as a result of contact with the stainless steel tubing, the rubber bladder inflated. The transfer of helium was then assisted by squeezing the bladder. Initially the helium was gaseous because of heat conduction by the transfer tube, and it provided a means of expelling the last traces of air in the cell and also for gradually cooling the glass. During the transfer operation, the outlet tube which extended from the top of the helium cell to a window was checked to see if helium was coming out. If it was not, then a solid air blockage was suspected. When this occurred the system was dismantled and the whole transfer operation was started again. At any stage during the operation, if the bladder became too large, then the pressure in the system was reduced by means of a valve near the neck of the helium dewar.

After about fifteen minutes, liquid helium began to syphon over into the liquid helium cell. The helium level rose very quickly and the level could be seen through the unsilvered strip of glass. The transfer of the helium was stopped once the level reached a two litre mark shown on the side of the cell. Additional heat losses by conduction were prevented by removing the transfer tube after the operation. This again required speed and was followed by stoppering the hole where the transfer tube had been. The long piece of tubing from the outlet was replaced by a pressure valve. Greased taps could not be used near the top of the dewar as the rubber tubing by this stage, was very hard. Also in the removal operation, the extension on the transfer tube had to be cut at the rubber connection for speed in the removal operation.

Liquid helium remained in the system overnight so heat losses were at a minimum. Also, if the copper rod had been coated with solid air or ice, a considerable increase in boil off would have resulted. Spectra were

recorded once the level of the helium remained steady.

The system was left for about two days before it was certain that all the helium was gone. This was necessary as if any air was trapped in the liquid helium, then this could result in an explosion caused by contriction of the helium.

2, 6. Spectrometers.

(a) Infrared Spectra

Perkin Elmer models 137, 237, 337 and 457 were used for routine work and the 621 model was employed for the greater part of the work. The range of each model is shown below:

621	4000 - 200cm^{-1}
337	4000 - 400cm^{-1}
237	4000 - 625cm^{-1}
137	4000 - 650cm^{-1}
457	4000 - 250cm^{-1}

All the spectrometers had the same dimensions in the sample area and so low temperature spectra could be recorded on each instrument.

Far infrared spectra were recorded with a RIIC-720 far infrared interferometer at Leicester University which was kindly made available by Dr. D. M. Adams.

(b) Raman Spectra

Raman Spectra were recorded with a Cary 81 Spectrometer at Imperial College, with the kind help of Dr. D. Evans.

(c) Inelastic Neutron Scattering

Inelastic Neutron Scattering work was performed on a Dido G.H. cold neutron time-of-flight spectrometer at Harwell with the kind help of Dr. G. C. Stirling.

(d) Nuclear Magnetic Resonance Spectrometer

A Perkin Elmer R10 spectrometer was employed for proton magnetic

resonance experiments, working at a constant frequency of 60 Mc/s. All spectra were recorded at 33°C, the thermostat temperature between the pole pieces of the permanent magnet.

(e) Pure Nuclear Quadrupolar Resonance Spectrometer

A super regenerative oscillator provided the frequency scan in the spectrometer employed. The resonance condition was detected by a phase sensitive detector and Zeeman modulation together with side band suppression. The range of the spectrometer was 5 - 60 Mc/s, and ^{35}Cl resonance in the powder samples were observed in the range 30 - 40 Mc/s. The spectrometer is now marketed by Decca Ltd. Facilities were provided by Dr. J. A. S. Smith and spectra were recorded by Mr. R. Lynch

CHAPTER THREE

ASYMMETRIC HYDROGEN BONDED ANIONS.

Chapter Three

Asymmetric Hydrogen Bonded Anions

Introduction

Asymmetric H-bonded anions, XHY^-, are defined as those cases where the proton is situated between two chemically different anions, X^- and Y^-. This definition serves to relate the anions discussed in this chapter with type B hydrogen dicarboxylate anions where the asymmetry arises from the crystallographic nonequivalence of the two carboxylate groups. Type B salts will, however, be discussed in detail in chapter four. In the definition, no mention was made to the proton position in relation to the groups bonded to it. The latter will be discussed in terms of the shape of the potential energy wells shown in chapter 1.

Fuller pointed out that the chemical nature of the donor and acceptor groups determines the shape of the potential energy well in H-bonded species (31). Ubbelohde and Gallagher developed the idea of acid-base equilibria (101), which has been emphasised more recently by Hadži (75). The acid-base idea can be explained qualitately by considering any H-bonded species, AH-B, in terms of the pK_a values of the acids AH and BH^+. A H-bond with the proton situated in a symmetric single minimum potential energy well mid-way between A^- and B is possible when the pK_a values of BH^+ and AH are identical and providing the overal H-bond length is short (75, 101). Deviations from the latter, as a result of the ground state levels of the proton (proton levels) not coinciding, will give rise to an asymmetric potential well of the type discussed in Chapter 1. Since the probability of identical pK_a values is small, the difference in the proton levels will be the dominating factor in determining the shape of the well (69, 75). Crystal packing and H-bond length are, therefore, secondary factors in the systems discussed in this chapter (69, 75).

Since pK_a values cannot be measured in the solid phase, recourse must be made to solution data (101). This, however, is only a guide to the shape

of the potential well since a common standard is necessary. Hadži overcame some of these difficulties by comparing the acceptor strength of different bases in methanol, using the shift of νOH from pure methanol as a measure of the basic strength, (69). H-bond strength was defined as the extent to which proton donor-proton acceptor interaction occurs, as measured by the shift of νOH from the non-H-bonded state, and was not used strictly in a thermodynamic sense (74). A study of a wide range of liquid and crystalline H-bonded adducts suggested that the H-bond strength is dependent on the acid and base strengths (69, 73, 74).

Hadži studied H-bonded adducts of bases such as phosphine oxide and pyridine-N-oxide with acids such as HNO_3 and Cl_3CCO_2H (73, 74). Crystalline adducts were obtained in many cases (73). The adducts were divided into two groups (69). The first group were characterised by a trio of bands between 1800cm^{-1} and 3000cm^{-1} as exemplified by the three chloroacetic acids with bases such as sulphoxides and phosphine oxides. The second group constituted stronger bases such as triphenylarsine oxide with Cl_3CCO_2H. The latter group gave spectra with broad absorption below 2000cm^{-1} which resembled spectra obtained from type A hydrogen dicarboxylate salts. The origin of the trio bands in group one adducts was discussed and the conclusion reached was that one of the bands represented νOH while the other two were probably overtones of the two bending vibrations, enhanced in intensity by Fermi resonance with νCH (69, 74). By varying the acid and base strengths, and consequently the difference between the proton levels, the spectral features remained the same except for changes in the relative intensities of the trio of bands. The latter was attributed to the gradual shift of νOH to lower frequency as the H-bond strength increased, thus altering the extent of Fermi resonance The possibility of formation of a symmetric potential well is reached when the proton levels are close, hence the broad absorption below 2000cm^{-1} (69). The latter was observed in adducts of Cl_3CCO_2H with strong bases and will be discussed in more detail in a subsequent chapter (74).

Assignments of the IR spectrum of adducts of HBr and HCl with pyridine oxide indicated that νBrH was higher in frequency than νClH (73). Hadži suggested that proton transfer to the pyridine oxide occurs in both adducts. This emphasises that if proton transfer occurs in a H-bonded adduct then vibrational frequencies of the latter will differ considerably from that expected from analogous vibrations in the original acid and base. This is exemplified, also by the adduct of HNO_3 with phosphine oxide where bands were found at frequencies similar to that of HNO_3. Proton transfer, on the other hand, would have resulted in bands characteristic of NO_3^- (73).

Since an understanding of the spectra of H-bonded species have been obtained from a knowledge of acid-base strengths, the work recorded in this chapter will be discussed on a similar basis. However, before the new work is presented, the work leading to the study of the new H-bonded anions is outlined.

In 1964 Salthouse and Waddington reported $HClBr^-$ and $HClI^-$ as the first examples of asymmetric H-bonded anions (15). Assignments (table 3,1) were based on a linear triatomic model giving rise to the four IR active vibrations shown below:

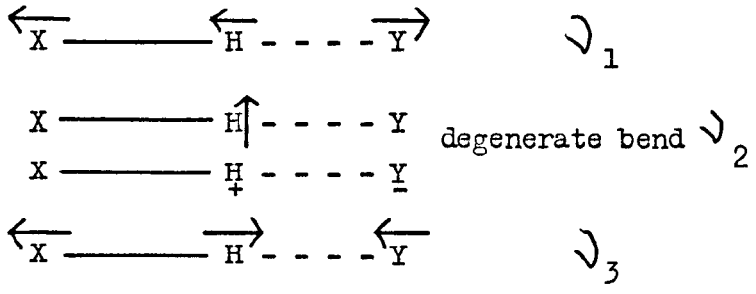

Evans and Lo, in 1966, studied the IR and Raman spectrum of $HClBr^-$ with different cations (102). Although the precise band positions were difficult to locate exactly, they suggested that the cation influenced the H-bond strength, and in all cases the proton was residing in an asymmetric potential well (see table 3,1.)

Nibler and Pimental, in 1967, suggested that the band assigned to ν_2

TABLE 3. 1

Waddington and Salthouse (15)

Anion (-)	Cation (+)	ν_3	IS(*)	ν_2	IS	ν_1
HClBr	Bu_4N	1700	1.31	1100	1.34	-
DClBr	Bu_4N	1300				-
HClI	Bu_4N	2000-2050	1.35	990	1.36	-
DClI	Bu_4N	1500		730		-

Evans and Lo (14, 102)

HFCl	Et_4N	2710		843		275
HFBr	Et_4N	2900		740		220
HFI	Et_4N	3145		635		180
HClBr	Me_4N	1890		1036		145
HClBr	Et_4N	1570	1.21	1165	1.37	170
DClBr	Et_4N	1300		848		165
HClBr	Pr_4N	1550	1.24	1145	1.37	172
DClBr	Pr_4N	1250		838		165
HClBr	Bu_4N	1730	1.28	1100	1.38	-
DClBr	Bu_4N	1350		800		-
HClBr	Pt_4N	1650	1.22	1148	1.38	165
DClBr	Pt_4N	1350		830		-
HClBr	$(Me)_3C_{16}H_{33}N$	1880		1070		155

Nibler and Pimentel (9)

HClI	Cs	2200	1.34	485	1.39	
DClI	Cs	1640		350		

* I.S. = isotopic shift

in CsClHI on Waddington's assignment was $2\nu_2$, and that it was enhanced in intensity because it had the same symmetry species as ν_3 (9, 10). This situation, they suggest, will arise in all the hydrogen dihalide anions where the symmetry is lower than $D_{\infty h}$ and C_{2v} (9).

The remaining work on halide systems was completed by Evans and Lo by the preparation of FHY^- systems (see table 3,1). Assignments were based on previous systems since their paper appeared before the work of Nibler and Pimentel (14). This series emphasises some of the important points discussed in chapter one.

(a) decrease of ν_3 as H-bond strength increases

(b) increase of ν_2 as H-bond strength increases

(c) increase of ν_1 as H-bond strength increases.

Another important point is reflected in the frequency of ν_3 in $FHBr^-$ and FHI^-. In both cases ν_3 is higher in frequency than in HBr and HI but lower than in HF (see table 3.2), therefore, suggesting that the proton is associated more closely with F^- than either Br^- or I^-. The proton must, therefore, be residing in an asymmetric potential energy well. A similar conclusion can be deduced by comparing the pK_a values of the three acids where HF is by far the weakest acid. The IR spectrum of other hydrogen dihalide anions, such as $ClHBr^-$ are, however, ambiguous since ν_3 is lower than in either of the free acids. The pK_a values, however, suggest that the proton will be closer to the weaker acid.

Salthouse and Waddington prepared an asymmetric H-bonded anion which contains a group other than a halide ion, $ClHNO_3^-$(15). Its IR spectrum was assigned on the basis of a planar anion (table 3,3). In $ClHNO_3^-$ the two bending vibrations were divided into the in-plane and out-of-plane bends. In 1966 analogous systems were prepared with carboxylic acids (table 3,4) (16). However, since deuterium samples were not prepared, a complete assignment was not possible. The remaining system which has been examined is $NCHX^-$ (22).

The assignments are shown in table 3,5 and are based on a linear arrangement of the atoms in the anion. Fermi resonance of νCH with νCN was invoked to explain the shift of νCN to lower frequency on deuteration. Both these vibrations have the same symmetry species and the isotopic shift was calculated using the product rule (22).

In this chapter, the spectra previously recorded by O'Shea have been re-examined (16). IR spectra have been recorded at liquid nitrogen temperature for most of the hydrogen and deuterium samples. The approach adopted is based on the assignment of each monomeric carboxylic acid and the changes which occur when it is H-bonded to a halide ion. New H-bonded species have also been prepared which involve F^- and I^- together with preliminary work on trifluoroacetic and dichloroacetic acid systems.

TABLE, 3, 2.

Monomeric Acid	ν(XH)cm^{-1}	ref.	pK_a	ref.
HF	3962	(110)	3.17	(105)
HCl	2886	(110	-7.30	(105)
HBr	2559	(110)	-9.0	(105)
HI	2230	(110)	-9.5	(105)
HOAc	3583	(103)	4.76	(106)
HOFm	3570	(99)	3.75	(106)
HOTF	3587	(104)	0.23	(106)
HODC			1.25	(106)
$HONO_2$	3560	(115)	-0.95	(105)
HCN	3311	(110)	9.40	(105)

TABLE 3. 3.

Band Assignments of Vibrational Spectrum of $HClNO_3^-$ (15).

Approx. description	$CHlNO_3^-(cm^{-1})$	$DClNO_3^-(cm^{-1})$
ν HCl.(H(D)-Cl stretch)	2250	1800
	1900	
δ HCl.(O-H(D)-Cl in-plane bend)	1700	1240
NO_2' asymm. stretch	1625	1600
NO_2' symm. stretch	1280	1280
NO stretch	1020	1035
γ HCl.(O-H(D)-Cl, out-of-plane bend)	870	620
NO_2' non-planar rock	782	782
NO_2' bending	687	680
NO_2' planar rock	634	634
H(D)-O stretch (overtone)?	393	n.o.

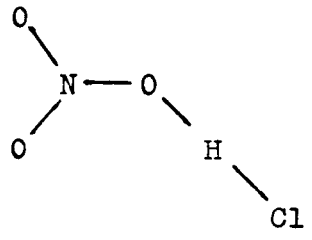

Isotopic Shifts

$\frac{\nu HCl}{\nu DCl}$	$\frac{\delta HCl}{\delta DCl}$	$\frac{\gamma HCl}{\gamma DCl}$
1.25	1.37	1.40

TABLE 3, 4.

Band Assignments for mixed carboxylate-halide systems (16)

Approx. description	$ClH(OAc)^-$ cm^{-1}	$BrH(OAc)^-$ cm^{-1}	$ClH(OFm)^-$ cm^{-1}	$BrH(OFm)^-$ cm^{-1}
νCH_3 and νOH	ca 3000	ca 3000		
νOH			2650	2650
$\nu C=O$	1720	1720	1720	1720
δOH, in-plane bend	1700	1640	1600	1650
$\nu C-O$	1210	1200	1170	1170
γOH, out-of-plane bend	830	835	900	840

Assignments were based on $HClNO_3^-$ system.

TABLE 3. 5.

Assignment of vibrational spectra of $XHCN^-$ systems (22)

Assignment	Symmetry Species	$BrHCN^-$	$BrDCN^-$	$ClHCN^-$	$ClDCN^-$
ν CN	Σ	2055	1795	2040	1760
ν CH	Σ	2920	2440 (1.37)	2850	2413 (1.37)
ν (CH X)	Σ	-	-	-	-
HCN bend	Π	850) 785)	656) 570)	870) 800)	680) 570)
XHC bend	Π	1010) 1000)	800) 783)	1010) 1000)	805) 785)
Additional bands					
13_{CN}		2025	n.o.	2010	n.o.
		1665=2x850	1280= 2x656	1715=2x870	1340= 2x680

Fermi resonance between νCN and νCH invoked to explain shift of ν CN on deuteration. Isotopic shift (shown in brackets) calculated by the product rule:

$$\frac{\nu CH . \nu CN}{\nu CD . \nu CN}$$

1. Nomenclature and Abbreviations

Bu_4N^+	Tetra-n-butylammonium.
Et_4N^+	Tetraethylammonium.
Me_4N^+	Tetramethylammonium.
HOAc	Acetic Acid.
HOFm	Formic Acid.
HOTF	Trifluoroacetic Acid.
HODC	Dichloroacetic Acid.
$XH(OAc)^-$	H-bonded anion between HOAc and X^-, where X^- can be F^-, Cl^-, Br^-, I^-.
ν	Stretching.
δ	Deformation, in-plane-bend.
γ	Torsional, out-of-plane-bend
π	Out-of-plane deformation.
ρ	Rocking
as	Asymmetric
s	Symmetric

2. Acetic Acid System, $XH(OAc)^-$

Results and Discussion

The normal modes of vibration are shown in Table 3.6 and are based on those for HOAc and a C_s point group for the H-bonded anion. On this point group classification, where the CH_3 group is treated as a point mass, the twelve normal modes of vibration can be divided into 9A' and 3A" (107). The low symmetry places no restriction on the IR activities of the fundamentals, overtones and combination bands, therefore, any departure from C_s to lower symmetric cannot be detected with any certainty from IR data. A case with higher symmetry, such as C_{2v}, will have vibrational frequencies which are no longer similar to HOAc. The H-bonded anions have been classified according to their IR spectrum, where $ClH(OAc)^-$, $BrH(OAc)^-$ and $IH(OAc)^-$ constitutes the first group and $FH(OAc)^-$ the second. Spectra were recorded at room and liquid nitrogen temperatures for all samples except the iodide case, but very little difference was found in the intensities or breadth of the bands in the spectra at the two temperatures. The strong cation absorptions, in the regions shown below, masked many of the bands associated with anion vibrations, particularly those shown. Low temperature spectra did not reduce the complexity of the cation absorption, therefore, attempts were made to prepare the anions with smaller cations, e.g. Me_4N^+ and Et_4N^+. These, however, proved too small to stabilise the anion.

region (cm^{-1})	Anion absorption in regions indicated
3000 - 2700	νCH_3 modes, νOH
1500 - 1350	δCH_3 modes
1100 - 1,000	ρCH_3 modes, δOD
890	$\nu C\text{-}C$, γOH
750	

TABLE 3. 6.

Normal modes of vibration of $XH(O_2CR)^-$ systems (103,107)

Vibration - type A' symmetry species	Approx. Description	HOAc cm^{-1}	DOAc cm^{-1}
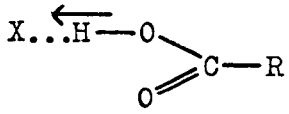	ν OH	3583	2642
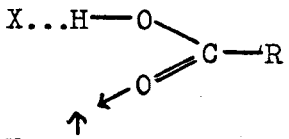	ν C=O	1788	1775
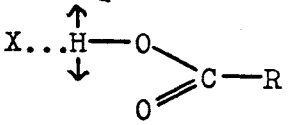	δ OH	1264	955
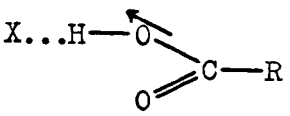	ν C-O	1182	1270
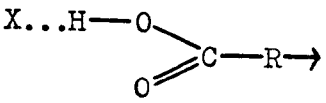	ν C-R	847	840
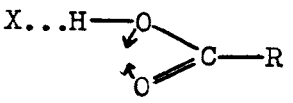	δ COO	642	603
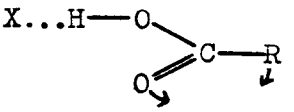	δ RCO	581	543
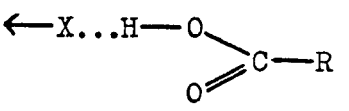	ν (X...HO)		
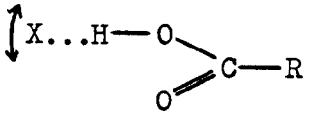	δ (X...HO)		
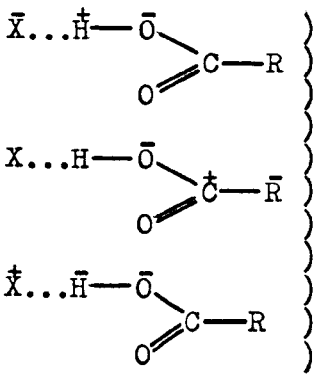 A"	γ OH	534	415
	π RCO	642	603
	γ (X...HO)		

TABLE 3, 7.

Character Tables and Selection rules (107)

Character Tables

C_1	I
A	+1

C_s	I	σ (xy)	
A'	+1	+1	T_x, T_y, R_z
A"	+1	-1	T_z, R_x, R_y

C_{2v}	I	$C_2(z)$	$\sigma_v(xz)$	$\sigma_v(yz)$	
A_1	+1	+1	+1	+1	T_z
A_2	+1	+1	-1	-1	R_z
B_1	+1	-1	+1	-1	T_x, R_y
B_2	+1	-1	-1	+1	T_y, R_x

Selection Rules

Component of Dipole Moment	C_1	C_s	C_{2v}
M_x	A	A'	B_1
M_y	A	A'	B_2
M_z	A	A"	A_1

C_1 - all fundamentals, overtone and combination bands are IR active and have the same symmetry species (A)

C_s - all fundamental, overtones and combination bands are IR active with symmetry species shown below:

	Symmetry Species	IR Activity
Fundamentals	A', A''	Active
Overtones ($A' \cdot A'$)	A'	Active
($A'' \cdot A''$)	A'	
Possible Combinations ($A' \cdot A''$)	A''	Active

C_{2v} - Fundamentals, Overtones, and Combination bands of symmetry species B_1, B_2 and A_1 are IR active.

	Symmetry Species	IR Activity
Fundamentals	B_1, B_2, A_1, A_2	all active except A_2
Overtones possible ($B_1 \cdot B_1$)	A_1	active
($B_2 \cdot B_2$)	A_1	"
($A_1 \cdot A_1$)	A_1	"
($A_2 \cdot A_2$)	A_1	"
Combinations possible ($B_1 \cdot B_2$)	A_2	inactive
($B_1 \cdot A_1$)	B_1	active
($B_1 \cdot A_2$)	B_2	"
($B_2 \cdot A_1$)	B_1	"
($B_2 \cdot A_2$)	B_1	"
($A_1 \cdot A_2$)	A_2	inactive

(a) Group 1, $ClH(OAc)^-$, $BrH(OAc)^-$, $IH(OAc)^-$.

Each anion, prepared as the Bu_4N^+ salt, has the hydrogen atom situated between a very weak acid (HOAc) and a very weak base (Halide ion). The difference in pK_a values will progressively increase in going down group 7 and so, on acid-base strengths, the H-bond in $IH(OAc)^-$ will be the weakest. In all cases, however, the H-bond will be weak. The assignments shown in table 3,8 can be compared with that for HOAc, which is shown in table 3,6.

Region 4,000cm^{-1} to 2,000cm^{-1}

The spectra showed a very broad and strong absorption in the region of 3000cm^{-1}. In all cases the band centre could not be located with certainty because of the very strong cation bands in this region. Cooling to liquid nitrogen temperature did not alter appreciably the intensity or breadth of the bands in this region. Broad bands appeared on the low frequency side of the approximate band centre at 2950cm^{-1} which resembled the spectrum of the liquid acid (42). The presence of free acid was unlikely as the solid compounds appeared dry or mulling and because bands were not observed at 1300cm^{-1} and 934cm^{-1} which are associated with liquid acetic acid (109).

On deuteration a new band appeared at 2245cm^{-1} in $BrD(OAc)^-$ and 2200cm^{-1} in $ClD(OAc)^-$, along with the disappearance of the broad band at 2950cm^{-1}. The strong band at about 2200cm^{-1} can, therefore, be assigned to νOD, and the broad band at 2950cm^{-1} to νOH. The shift of νOH is about 600cm^{-1} from HOAc and is, therefore, indicative of H-bond formation. Two important points arise from the frequencies of νOH and νOD. In all cases, the strong absorption is higher in frequency than the stretch in HCl, HBr and HI (see table 3,2). The hydrogen atom, therefore, is more associated with the carboxylate group than the halide ion, and consequently will be

TABLE 3. 8

Assignments for $XH(OAc)^-$ systems

Approx. description	$BrH(OAc)^-$	$BrD(OAc)^-$	$ClH(OAc)^-$	$ClD(OAc)^-$	$IH(OAc)^-$
A' Symmetry species	cm^{-1}	cm^{-1}	cm^{-1}	cm^{-1}	cm^{-1}
ν OH(D)	ca 2950	2245	ca 2950	2200	ca 3000
ν C=O	1716	1723	1712	1724	1785
δ OH(D)	1328	990	1350	1010	1320?
ν C-O	1197	1294	1224	1295	1190
$\rho_s CH_3$	998	982	1001	995	-
ν C-C	ca 870	818	ca 880	831	ca 870
δ COO	598	599	609	610	600
δ CCO	446	445	449	450	530
2x γ OH(D)	1640	1270	1755	-	
2x ν C-C	1740	-	1735	-	
2x δ COO	1203	-	-	-	
A" Symmetry species					
$\rho_a CH_3$	ca 1040	ca 1041	-	ca 1050	
γ OH(D)	828	638	ca 880	635	810
π CCO	ca 585	ca 599	609	610	600

Isotopic Shifts

Anion	$\frac{\nu OH}{\nu OD}$	$\frac{\delta OH}{\delta OD}$	$\frac{\gamma OH}{\gamma OD}$
$BrHOAc^-$	ca1.31	1.34	1.31
$ClHOAc^-$	ca 1.34	1.34	1.34

TABLE 3, 9

Acetic acid-base systems (108)

HOAc	Acetonitrile	Dioxane	Tetrahydro-furan	N,N-Dimenthyl-acetamide	Dimethyl sulphoxide
ν OH	3720	3125			2932
δ OH					1377
$\delta_s CH_3$					1361
ν C-O	1218	1239	1243	1255	1258
ν C-C	870			875	877
δ COO	601		608		613
δ CCO	444	450	446	452	452
DOAc					
ν OD	2432	2340	2300	2240	2210
δ OD				1059	
$\delta_s CH_3$		1374	1375	1374	1375
ν C-O	1288		1289	1297	1298
ν C-C	825	831	833	835	836
γ OD	633	650	665	675	690
δ COO	569	578	580		585
δ CCO	443	449	442	448	449

residing in an asymmetric potential well of the type shown in case 1 in chapter 1. The second important point is the slightly lower frequency of νOD in ClD(OAc)$^-$ as compared with νOD in BrD(OAc)$^-$ which suggests that the H-bond is slightly stronger in the former. This point has already been predicted on acid-base strengths.

The explanation of the breadth of νOH and νOD in carboxylic acids rests upon Fermi resonance of νOH and νOD with overtones and combination bands together with anharmonic coupling between νOH and ν(OH-O) (42). The same mechanism is probably operating in the XH(OAc)$^-$ systems. Haurie and Novak analysed the IR spectra of 1:1 H-bonded species of HOAc with various bases in a similar manner (108). Band assignments for these 1:1 H-bonded species are shown in table 3,9. The origin of the satellite bands will, however, be discussed in a subsequent section.

Region 2000cm^{-1} to 1500cm^{-1}

In HOAc only one fundamental vibration appears in this region of the spectrum and was assigned to νC=O. The spectra of XH(OAc)$^-$, on the other hand, are more complicated owing to the presence of several distinct bands, shown in table 3,10. The complex band structure cannot be due to different anions in the unit cell as a single band appears after deuteration. Haurie and Novak observed a similar feature with 1:1 adducts of HOAc with different bases, shown in table 3,11. Haurie and Novak attributed the doublet structure to Fermi resonance of νC=O with 2νC-C. Deuteration, in the methyl position shifts νC-C to lower frequency and, therefore, reduces the possibility of Fermi resonance. A similar situation was observed when the acid was deuterated in the hydroxyl position, (108).

In previous work on BrH(OAc)$^-$ and ClH(OAc)$^-$ the in-plane bend of the proton was assigned to a band in the region of 1650cm^{-1} (16). It is now believed that this band is an overtone of the out-of-plane bend. In ClH(OAc)$^-$ 2γOH adds to the complexity of νC=O as a result of Fermi resonance

TABLE 3,10

$ClH(OAc)^-$	1755, 1735, 1712	$ClD(OAc)^-$	1724
$BrH(OAc)^-$	1740, 1716	$BrD(OAc)^-$	1723
$IH(OAc)^-$	1785		

TABLE 3, 11 (108)

Solvent	CH_3CO_2H		CD_3CO_2H	
	IR	Raman	IR	Raman
Nitroethane	1723,1756	1727,1759	-	-
Ether	1728,1755	1725,1755	1742	-
Acetonitrile	1726,1754	1723,1755	1740	1739
Dioxane	1727, 1754	1727,1754	1735	1732
Tetrahydrofuran	1728,1754	- -	-	-
N,N-dimethylacetamide	1722,1750	- -	-	-
Dimethylsulphoxide	1715,1750	1717,1755	1718	-

interactions between νC=O, 2νC-C and 2γOH.

The remaining feature of this region is that no band was found which could be assigned to ν_{as}COO, which generally occurs below 1600cm^{-1} (110). This is good evidence against proton transfer to the halide ion and confirms earlier predictions.

Region 1500cm^{-1} to 950cm^{-1}

By analogy with HOAc, seven fundamental vibrations occur in this region of the spectrum. Five of these are associated with the CH_3 group and the remaining two are νC-O and δOH. In carboxylic acids the fundamental vibrations associated with νC-O and δOH cannot be treated as independent vibrations since they are strongly coupled together (109). On deuteration, νC-O shifts to an intermediate frequency, and δOH shifts to near 1000cm^{-1}. In HOAc a similar behaviour was observed (103). Hadži observed the same feature in liquid adducts of halogenated acetic acids with weak bases (69). Hadži pointed out that δOH and δOD were of low intensity and the presence of the former was suggested only by the effect of deuteration on νC-O (69). Haurie and Novak found νC-O in all cases, but failed to detect δOH and δOD in all but one case, (see table 3,9).

The spectra of ClH(OAc)$^-$, BrH(OAc)$^-$ and IH(OAc)$^-$ each had a strong band in the region of 1200cm^{-1} (table 3,12). Spectra recorded at -196° showed no appreciable change from the room temperature spectrum in the cases studied, viz. ClH(OAc)$^-$, BrH(OAc)$^-$. In ClD(OAc)$^-$ and BrD(OAc)$^-$, this band disappeared and a new strong band appeared in the region of 1290cm^{-1}. Again, no appreciable change was observed in the low temperature spectrum. By analogy with previous work, this band can be assigned to νC-O (103, 108). The search for δOH did not reveal an obvious candidate except possibly a weak band at 1328cm^{-1} in BrH(OAc)$^-$ and at about 1350cm^{-1} in ClH(OAc)$^-$. On deuteration, intensity changes occurred in the regions of 1330cm^{-1} and

1020cm^{-1}. However, both these regions are masked by a strong cation absorption in addition to CH_3 vibrational modes of the acetate group in the lower range. In HOAc, δOH and γOD appear at 1264cm^{-1} and 955cm^{-1} respectively, (103). The frequencies of these vibrations will be increased on H-bond formation, as was observed in a acetic acid and N,N - dimethylacetamide mixture where δOD was found at 1059cm^{-1} (see table 3,9). The assignment of δOD at 990cm^{-1} in BrD(OAc)$^-$ and at 1010cm^{-1} in ClD(OAc)$^-$ may account for the shift of $\rho_s CH_3$ from 998cm^{-1} to 982cm on deuteration of BrH(OAc)$^-$ and from 1001cm^{-1} to 995cm^{-1} on deuteration of ClH(OAc)$^-$. Both these modes of vibration have the same symmetry species and so the possibility of Fermi resonance exists.

The remaining point of interest in this region concerns the frequency of νC-O in relation to HOAc (table 3,12). A comparison of νC-O in the proton... species shows a gradual approach to the value in HOAc. This is a measure of the perturbing effect of the halide ion on HOAc and of the decreasing H-bond strength on going down group 7. In the deuterated samples, however, νC-O is found at approximately the same frequency. This indicates that it is the proximity of δOH which affects the frequency of νC-O. This point can be readily seen from data shown in table 3,12 and 3,9.

Table 3,12

	ν C-O(cm^{-1})		ν(C-O)cm^{-1}
HOAc	1182	DOAc	1270
ClH(OAc)$^-$	1224	ClD(OAc)	1295
BrH(OAc)$^-$	1197	BrD(OAc)	1294
IH(OAc)$^-$	1190		

Region 950cm^{-1} to 200cm^{-1}

Six normal modes of vibration are expected in this region and by analogy with HOAc one of these bands is the out-of-plane bend of the proton, γOH. In BrH(OAc)$^-$ a medium strength band was observed at 828cm^{-1} which shifted to 638cm^{-1} on deuteration. In the spectrum of ClD(OAc)$^-$ a band appeared at 655cm^{-1} which may be the deuterium analogue of the broad absorption at 880cm^{-1}. In IH(OAc)$^-$ a band was observed at 800cm^{-1} which was not present in the spectrum of Bu_4NI. A comparison with the data in table 3,9 shows that these bands are likely candidates for γOH and γOD.

It has already been pointed out that the complex band structure in the carbonyl region is due to the first overtone of νC-C (108). In the spectrum of ClH(OAc)$^-$ and BrH(OAc)$^-$ no clear band was found for νC-C as it is masked by a strong cation band at 880cm^{-1}. However, on deuteration a weak band appeared at 818cm^{-1} and 831cm^{-1} in BrD(OAc)$^-$ and ClD(OAc)$^-$, respecively, which can be compared with νC-C in Table 3,9. Evidence for the existence of a band at about 870cm^{-1} in BrH(OAc)$^-$ is suggested by the doublet structure of νC=O at 1720cm^{-1}. Since γOH has been assigned at 828cm^{-1}, its overtone will be at about 1650cm^{-1} which is close to a weak band found at 1640cm^{-1} which disappeared on deuteration. Similarly the doublet structure of νC=O was lost on deuteration as a result of νC-C shifting from about 870cm^{-1} to 818cm^{-1}. A low temperature spectrum on the cation band at 880cm^{-1} in BrH(OAc)$^-$ did not reveal with certainty a likely candidate for νC-C. In ClH(OAc)$^-$ a broad band appeared at 880cm^{-1} which was reduced in complexity on deuteration. In ClH(OAc)$^-$, therefore, both γOH and νC-C are at about 880cm^{-1} which accounts for the complex structure of the carbonyl region. A low temperature spectrum of ClH(OAc)$^-$ did not reveal any additional structure. The conclusions for ClH(OAc)$^-$ were confirmed by the absence of any band at 1640cm^{-1} and between 860 and 800cm^{-1}. Further confirmation of these results

was obtained from the spectrum of $IH(OAc)^-$ where $\nu C{=}O$ is a singlet at $1780cm^{-1}$ and γOH and $\nu C\text{-}C$ are at $810cm^{-1}$, and possibly $870cm^{-1}$, respectively.

The remaining bands in the spectrum are associated with COO skeletal vibrations and can be assigned by analogy with HOAc and the work of Haurie and Novak (108). The spectra were recorded down to $200cm^{-1}$ and no evidence was found for any band associated with the H-bond stretch.

Satellite Bands

The satellite bands in H-bonded adducts of HOAc are shown in table 3,13. The extreme breadth of this region in group 1 anions renders assignments difficult, therefore, only analogous bands to those in 3,13 have been located. Those which have been located are, however, the more intense bands in the region, particularly the first overtone of $\nu C\text{-}O$. The assignment of the strong band at $2510cm^{-1}$ to $\nu C\text{-}O + \delta OH$ in $BrH(OAc)^-$ seems to confirm the assignment of δOH at $1,328cm^{-1}$

TABLE 3. 13.

Satellite Bands (108)

Assignment	DMSO/HOAc	$BrH(OAc)^-$	$ClH(OAc)^-$	$IH(OAc)^-$	Assignment	DMSO/HOAc	$BrD(OAc)^-$	$ClD(OAc)^-$
ν OH	3000 2932	ca 2950	ca 2950	ca 2950			2370 2330	2240
2xδ OH	2735	2650	2670		ν OD	2210	2245 2065	2200 2140
ν C-O+ δ_s CH_3	2635	2590	2600		2xδ OD	2098		
ν C-O+ δ OH	2585	2510	2545	2500	$\rho_s CH_3$+δ OD	2036	2008	2020
2xν C-O	2510	2385	2445	2390		1900		

(b) Group 2. $FH(OAc)^-$

This anion was prepared with Me_4N^+ as the cation which reflects its stability over group one members where Bu_4N^+ was necessary. Extreme care was necessary to prevent hydrolysis resulting in the formation of HF_2^-. Spectra were recorded on BaF_2 plates since exchange occurred when alkali halide plates were used. The region below $750cm^{-1}$ was examined by coating CsI plates with paraffin wax. The assignment is shown in Table 3,14.

The most notable feature of the spectrum of $FH(OAc)^-$ was the absence of any strong band above $2000cm^{-1}$. The spectrum was extremely broad in the region between $2000cm^{-1}$ and $1200cm^{-1}$ and was similar to that observed for an adduct of Cl_3CCO_2H with phosphine oxide, where νOH was assigned to a broad band at 2250cm (74). Hadži pointed out that vibrations such as $\nu C{=}O$ and $\nu C{-}O$ retained their identity but are broad. A complete assignment was not, however, reported.

Diagnostically, the most useful fingerprint of acetic acid systems is $\nu C{=}O$ which is found in the region of $1700cm^{-1}$. In $FH(OAc)^-$ $\nu C{=}O$ appeared as a broad band at $1665cm^{-1}$ which shifted to $1575cm^{-1}$ on deuteration. A similar situation was observed in $ClHCN^-$ where $\nu C{\equiv}N$ shifted to lower frequency on deuteration (table 3,5). The assignment of νOH at $1900cm^{-1}$ in $FH(OAc)^-$ and at $1640cm^{-1}$ in $FD(OAc)^-$ accounts, therefore, for the shift of $\nu C{=}O$ and also for the increased breadth and complexity of the $1600cm^{-1}$ region on deuteration. Both these modes of vibration have the same symmetry species and can, therefore, interact by Fermi resonance. A low temperature spectrum revealed a complex doublet structure for νOH, but no appreciable narrowing of the bands in the region were observed. The comparitively low frequency of νOH at $1930cm^{-1}$ as compared with $2950cm^{-1}$ in group one members is indicative of a strong H-bond in $FH(OAc)^-$. This was also predicted from the fact that HF is

TABLE 3, 14.

Assignments for $FH(OAc)^-$ system.

Vibration	$FH(OAc)^-$	$FD(OAc)^-$
A' Modes	cm^{-1}	cm^{-1}
ν OH(D)	1930	1640
ν C=O	1665	1575
ν C-O	ca 1350	ca 1360
δ OH(D)	1250	ca 950
ρCH_3	1040	-
ν C-C	ca 920	ca 900
δ COO	608	605
ν (F-HO)	550	545
A" Modes		
γ OH(D)	960	ca 740
2xδ OH(A')	2480	-
2xγ OH(A')	1870	-

Isotopic Shifts

Anion	$\frac{\nu OH}{\nu OD}$ x $\frac{\nu C=O}{\nu C=O}$	$\frac{\delta OH}{\delta OD}$	$\frac{\gamma OH}{\gamma OD}$
$FH(OAc)^-$	1.24	1.32	1.30

TABLE 3. 15

IR bands for crystalline adducts with $Cl_3C.CO_2H$(73)

Assignment	Ph_3PO(I)	Ph_3PO(II)
ν OH	2250	2250
2xγ OH (see text)	1850	1850
ν C=O	1760	1680
	(1745)	(1670)
ν C-O	1270	1270
	(1312)	(1310)
ν P=O	1136	1160

Two modifications of this adduct were obtained, I and II.

OH deformation modes were not observed.

( ) signifies deuterium analogue.

the weakest acid in Group 7 hydrogen halides. Proton transfer can, however, be ruled out as the band at 1665cm^{-1} is too high to correspond to ν_{as}COO, which is found at 1556cm^{-1} in NaOAc (110).

The region below 1500cm^{-1} was complicated by strong cation absorption. However, strong bands associated with the anion were found at 1350cm^{-1}, 1250cm^{-1} and 960cm^{-1} which were not altered appreciably on cooling to -196°C. On deuteration the strong band at 1250cm^{-1} disappeared and the region near to the strong cation absorption at 950cm^{-1} became very broad. The bands at 1250cm^{-1} and 1350cm^{-1} seem, therefore, likely candidates for νC-O and δOH respectively. However, the serious drawback to this assignment is that no band of intermediate frequency appeared on deuteration (see table 3,12). Also, in the Ph_3PO systems, shown in table 3,15, the δOH deformations were too weak to be observed. In FH(OAc)$^-$ the vibrations associated with νC-O and δOH cannot be treated independently as there will be considerable mixing in the nature of the vibrations (109). Therefore, the possibility that the 1250cm^{-1} band is predominantly δOH cannot be ruled out. The assignment of νC-O at 1350cm^{-1} as compared with 1414cm^{-1} in NaOAc, is also compatible with the low frequency of νC=O in FH(OAc)$^-$. The intermediate frequencies of νC=O and νC-O reflect the gradual change of character of the OAc group as the strength of the H-bond is increased.

The deuterium analogue of the 1250cm^{-1} band was found in the region of 950cm^{-1}. The precise position could not be located with certainty because of the strong cation absorption and also because the residual FH(OAc)$^-$ in FD(OAc)$^-$ absorbs in this region. In FH(OAc)$^-$ two bands associated with νC-C and γOH are expected in the region of 950cm^{-1}. The broad band at 950cm^{-1} in FH(OAc)$^-$ seems a likely candidate for γOH. This assignment may account for the doublet structure of νOH found in the region of 1900cm^{-1}. Since the overtone of γOH at 1900cm^{-1} will have the

same symmetry species as νOH and can, therefore, interact with νOH by Fermi resonance. This can be compared with the data in Table 3,15, where a band was observed at 1850cm^{-1}. This band was not specifically assigned in the paper, but from data on the trio of bands observed in the adducts discussed by Hadži, the 1850cm^{-1} band can be assigned to γOH (69). Its enhancement in intensity can be accounted for by Fermi resonance interaction with νOH (69).

The location of νC-C is, however, not so clear even at -196°C. The region below 900cm^{-1} is transparent except for a cation band at 850cm^{-1}, therefore, νC-C must be above 900cm^{-1} and hidden by the broad absorption in this region. This assignment is not unreasonable as can be seen from the trend below. ~~(table 3,16)~~:

~~Table 3,16~~

	νOH(cm^{-1})	νC-C(cm^{-1})	ref.
HOAc Monomer	3583	847	(103)
HOAc Liquid	3029	886	(111)
HOAc Crystalline	2875	908	(112)
FH(OAc)$^-$ Crystalline	1940	908	
NaOAc Crystalline	-	924	(110)

The region below 800cm^{-1} was studied by coating the CsI plates with paraffin wax, which introduced a strong band at 745cm^{-1}. The deuterium analogue of γOH was difficult to locate because it may be hidden by the band at 745cm^{-1}. However, this region was more complex in the deuterium sample than in the protonium case. The assignment of γOD in the region 700 - 750cm^{-1} gives rise to an isotopic shift in the range 1.27 - 1.36.

A strong broad band appeared at 550cm^{-1} in FH(OAc)$^-$ which did not shift on deuteration. This band cannot be due to attack of the plates or the wax as the same spectrum was observed when the wax was replaced by a

polythene sheet. Impurities such as HF_2^- and $H_2F_3^-$ can be ruled out as this band does not appear in either (50, 113). The only possible origin may be its assignment to the symmetric stretch of the H-bond. This vibration represents the motion of F^- in the anion and can be compared with the value of $600cm^{-1}$ in the Raman spectrum of $NaHF_2$ (52). This assignment may also account for the breadth of the spectrum of $FH(OAc)^-$ and $FD(OAc)^-$ in the region 1100 to $1000cm^{-1}$ where only weak CH_3 modes are expected. A band associated with the anion was observed at $608cm^{-1}$ in $FH(OAc)^-$ and $605cm^{-1}$ in $FD(OAc)^-$ which can be assigned to a COO skeletal vibration. The remaining COO vibrations could not be found.

The assignment of νOH at $1930cm^{-1}$ suggests that $FH(OAc)^-$ is an example of a strong H-bond. However, since νOH is lower than in either of the free acids, no definite conclusions can be made with regard to the potential surface within which the proton is residing. The only indication seems to be the assignment of νC=O at $1650cm^{-1}$ which is comparable to that in crystalline acetic acid ($1638cm^{-1}$) and, therefore, suggests that the proton is associated more closely with the acetic group. A similar conclusion can be reached from a comparison of the pK_a values of HOAc and HF where the former is the weaker acid.

3. Formic Acid System ($XHOFm^-$)

Results and Discussion

The twelve normal modes of vibration are shown in Table 3,6 and assignments for HOFm are shown in Table 3,16. The symmetry of the anions are analogous to the acetic system and further details can be found in tables 3,6 and 3,7. The H-bonded anions are expected to be weak with the possible exception of $FH(OFm)^-$. However, acid-base strengths suggest that they will be stronger than their acetic acid analogues (see table 3,2). The anions were divided into two groups by analogy with the acetate system. Attempts to prepare group one anions with cations smaller than Bu_4N^+ failed. Low temperature spectra were recorded on all except the iodide case, which decomposed very easily, and a comparison of the spectra recorded at the two temperatures showed very little change.

(a) Group 1, $ClH(OFm)^-$, $BrH(OFm)^-$, $IH(OFm)^-$

The assignment for these species are shown in table 3,17. Many of the problems encountered in the corresponding acetate system were also found in this system and so some of the normal modes of vibrations could not be located with certainty. Assignments were, however, assisted by the spectral similarities between the formate and acetate systems.

Deuteration of $ClH(OFm)^-$ and $BrH(OFm)^-$ showed that the broad absorption in the region of 2900cm^{-1} was due to νOH. In $BrD(OFm)^-$ a strong broad band appeared at 2140cm^{-1} along with a sharp satellite band at 2218cm^{-1}. In $ClD(OFm)^-$ a broad band appeared at about 2170cm^{-1} whose band centre was masked by the presence of strong satellite bands at 2050cm^{-1} and 2250cm^{-1}. In previous work on $ClH(OFm)^-$ and $BrH(OFm)^-$ a strong band was observed at 2650cm^{-1} which was assigned to νOH, however, it is now believed that this is an overtone band. The increase in intensity of the satellite bands relative to those in the acetate system

TABLE 3, 16

Assignment for monomeric Formic Acid (99)

Assignment		HOFm	DOFm
ν OH	A'	3570	2632
ν CH	"	2943	2948
ν C=O	"	1770	1772
δ CH	"	1387	1360
δ OH	"	1229	990
ν C-O	"	1105	1178
δ OCO	"	636	543
ρ CH	A"	1033	ca 1000
γ OH	"	636	512

Isotopic Shifts

$\frac{\nu \text{ OH}}{\nu \text{ OD}}$	$\frac{\delta \text{ OH}}{\delta \text{ OD}}$	$\frac{\gamma \text{ OH}}{\gamma \text{ OD}}$
1.36	1.24	1.24

TABLE 3. 17

Assignments for $XH(OFm)^-$ system

Assignment	$BrH(OFm)^-$	$BrD(OFm)^-$	$ClH(OFm)^-$	$ClD(OFm)^-$	$IH(OFm)^-$
ν OH(D) A'	ca 2900	2140	ca 2900	2170	ca 3000
ν C=O "	1740	1735	1710	1715	1730
δ OH "	1360	ca 1000	1360	ca 1020	-
ν C-O "	1162	1220	1162	1215	1160
δ COO "	664	600	662	ca 600	660
ρ CH A"	1020	-	1030	1020	-
γ OH(D) "	ca 850	ca 605	878	650	ca 800
2x δ OH A'	2650		2640		
ν C-O+δOD A'		2218		2250	
2x δ OD A'		1940		2050	
2x γ OH A'	1720		1730		1570

Isotopic Shifts

Anion	$\frac{\nu\ OH}{\nu\ OD}$	$\frac{\delta\ OH}{\delta\ OD}$	$\frac{\gamma\ OH}{\gamma\ OD}$
$BrH(OFm)^-$	ca 1.36	1.36	1.37
$ClH(OFm)^-$	ca 1.36	1.33	1.35

is attributed to the lower frequency of νOH. This was confirmed by νOD in BrD(OFm)$^-$ and ClD(OFm)$^-$ which is lower than in the corresponding acetate system. This also serves to illustrate the increased H-bond strength in the formate system compared with the acetate system. Also, by analogy with the acetate system and also from the data in table 3,2, the proton must be associated more closely with the formate group and is, therefore, residing in an asymmetric potential well of the type shown in Case 1 (see chapter 1).

The spectra below 2000cm^{-1} were similar and analogous to the acetate system. The 1700cm^{-1} region shows similar features to that observed in the acetate system (table 3,10). The complex structure is attributed to the overtone of γOH which will absorb in the region of 1700cm^{-1} (table 3,18).

Table 3,18

Anion	νC=O	2γOH	γOH	Anion	νC=O	γOD
ClH(OFm)$^-$	1710	1730	880	ClD(OFm)$^-$	1715	660
BrH(OFm)$^-$	1740	1720	850	BrD(OFm)$^-$	1735	605
IH(OFm)$^-$	1730	1570	800			

In IH(OFm)$^-$ a weak band was observed at 1570cm^{-1} which can be assigned to 2γOH by analogy with BrH(OAc)$^-$ and IH(OAc)$^-$.

The region between 1500cm^{-1} and 950cm^{-1} is analogous to the acetate system and can be compared with assignments for HOFm. Strong bands were observed at approximately 1160cm^{-1} in all systems and can be assigned to νC-O. On deuteration νC-O shifts to higher frequencies as shown in Table 3,19:

Table 3,19

Anion	νC-O(cm^{-1})	Anion	νC-O(cm^{-1})
HOFm	1105	DOFm	1178
IH(OFm)$^-$	1160		
BrH(OFm)$^-$	1162	BrD(OFm)$^-$	1220
ClH(OFm)$^-$	1162	ClD(OFm)$^-$	1215

The in-plane bend was difficult to locate with certainty. However, a broad absorption was observed at 1350cm^{-1} in ClH(OFm)$^-$ and BrH(OFm)$^-$, which disappeared on deuteration. The deuterium analogues seem to be at 1012cm^{-1} and 1020cm^{-1} in BrD(OFm) and ClD(OFm)$^-$ respectively, but this is not certain because of the strong cation absorption in this region. In IH(OFm)$^-$ no obvious candidate could be found for δOH.

The region below 950cm^{-1} has two bands in all cases which are associated with anion vibrations. The band at 668cm^{-1} can be safely assigned to δCOO and the region above 800cm^{-1} is associated with γOH by analogy with the acetate system. Details of γOH can be seen in table 3,18 where they are tabulated with reference to the complex band structure of νC=O. On deuteration of ClH(OFm)$^-$ two new broad bands of medium intensity appeared at 660cm^{-1} and 620cm^{-1}. By analogy with ClD(OAc)$^-$ these bands can be assigned to γOD and δCOO, respectively. In BrD(OFm)$^-$ the situation is not so clear since only one strong band was observed at 605cm^{-1} which was considerably stronger than either of the bands in ClD(OFm)$^-$. This anomaly may be accounted for if the plane of symmetry is lost in ClH(OFm)$^-$ but still present in BrH(OFm)$^-$. This would account for γOD and δCOO being broad in ClD(OFm)$^-$ because they could interact by Fermi resonance since they will have the same symmetry species, (see tables 3, 6 and 3,7). In BrD(OFm)$^-$ γOD and δCOO will have different symmetry species and so γOD may be hidden by δCOO, thus giving rise to a strong absorption at 605cm^{-1}.

(b) Group 2, $FH(OFm)^-$

From Table 3,2, it can be seen that the pK_a values of HF and HOFm are sufficiently close to suggest that the proton may be situated midway between F^- and OFm^-. This feature was evident from its IR spectrum where a simple assignment based on HOFm was not possible. Also, during the preparation of $FH(OFm)^-$, parts of the line were etched owing to liberation of HF. Both $FH(OFm)^-$ and $FD(OFm)^-$ were ground between BaF_2 plates because agate mortars and pestils were attached and etched by HF. Assignment of the vibrational spectrum is shown in table 3,20.

The spectrum of $FH(OFm)^-$ had extreme breadth and complex structure in the region $2000cm^{-1}$ - $1000cm^{-1}$. The absence of any strong band above $2000cm^{-1}$ was a clear indication of the absence of free formic acid. By analogy with $FD(OAc)^-$ the breadth in the region of $1700cm^{-1}$ may be associated with Fermi resonance interaction of the asymmetric stretch of the proton with the carboxyl mode and combination bands falling in this region. A low temperature spectrum revealed complex structures in this region, but no appreciable contraction of band breadth was observed. This region of the spectrum is similar to the liquid adduct between tetramethylene sulphoxide and CCl_3CO_2H where a band associated with $\nu C=O$ could not be found because of the extreme breadth of the region around $1700cm^{-1}$ (74). On deuteration of $FH(OFm)^-$ a strong, broad band remained at $1590cm^{-1}$. The presence of the simple formate was suggested by a sharp band at $740cm^{-1}$, therefore, the band at 1590 in $FD(OFm)^-$ must be due, in part, to $\nu_{as}COO$ from the simple formate ion. However, the extreme breadth of the band in $FD(OFm)^-$ over that in the formate ion is a clear indication that several bands appear in this region. The adduct involving CCl_3CO_2H mentioned above, showed a similar behaviour on deuteration, where the $\nu C=O$ was found in its normal place after deuteration. Unfortunately, the only spectroscopic data published on this adduct was the appearance of a strong and broad

TABLE 3, 20

Assignments for $FH(OFm)^-$ System

Assignment	$FH(OFm)^-$	$FD(OFm)^-$
ν F-H	Associated with absorption in region 2000 - 1500cm^{-1}	masked by strong cation absorption in the region 1500 - 1350
ν_{as} COO		1595
ν_{s} COO	ca 1330	ca 1335
δ F-H	1200	ca 980
γ F-H	1125	ca 900
ρ CH	1065	1070
δ COO	775	760
ν (FH—OFm)	420	430

Isotopic Shifts

$\frac{\delta FH}{\delta FD}$	$\frac{\gamma FH}{\gamma FD}$
1.22	1.26

absorption in the region of 1600cm^{-1} which shifted on deuteration, and the presence of a broad νC-O at 1250cm^{-1} in the protonium case (74). The effect of deuteration of FH(OFm)$^-$ is analogous, therefore, in the region of 1600cm^{-1}, but owing to the strong cation absorption in the region between 1500 - 1350cm^{-1}, the deuterium analogue of the broad absorption at 1600cm^{-1} could not be found with certainty.

The region below 1500cm^{-1} showed a very broad absorption at approximately 1150cm^{-1}. Its low temperature spectrum revealed that this band was composed of several bands with approximate band centres at 1200cm^{-1}, 1125cm^{-1} and 1065cm^{-1}. The band at 1065cm^{-1} is assigned to ρCH and its breadth and intensity suggests that it is in Fermi resonance with the more complex region above 1100cm^{-1}. The region between 1050cm^{-1} and 850cm^{-1} had no bands which were associated with FH(OFm)$^-$. This is different to the situation in FH(OAc)$^-$ where a broad band at 950cm^{-1} was assigned to γOH. The failure to find a band in the region of 950cm in FH(OFm)$^-$ leads to the possibility that the two bands centred at 1200cm^{-1} and 1125cm^{-1} are associated with the two bending vibrations of the proton. This was confirmed in FD(OFm)$^-$ where two strong bands were observed at 980cm^{-1} and 890cm^{-1}. An analogous situation was observed in KHF_2 where the degeneracy of the bends was split by 30cm^{-1} because of a low site symmetry (50). In FH(OFm)$^-$ the degeneracy is losted because of the plane of symmetry of the OFm group. The departure from the spectrum of HOFm may be associated with the fact that proton transfer has taken place in FH(OFm)$^-$. This would account for the strong intensity of the bands associated with the proton motion, in particular, the bending vibrations. This feature was also apparent in FH(OAc)$^-$ but it is more pronounced in FH(OFm)$^-$.

The region below 800cm^{-1} had two bands which were associated with the anion. In FH(OFm)$^-$ these bands appeared at 782cm^{-1} and 420cm^{-1}. The band at 782cm^{-1} can be assigned to δCOO and is higher in frequency than

observed in the simple formate ($745cm^{-1}$). In $FD(OFm)^-$ δCOO is a shoulder at $755cm^{-1}$ on the side of a strong paraffin wax absorption. The band at $420cm^{-1}$ was observed in both anions but was of weaker intensity in $FD(OFm)^-$. A band of similar frequency was observed in $FH(OAc)^-$, ($550cm^{-1}$), which was assigned to the symmetric stretch. The band in $FH(OFm)^-$ must, therefore, have a similar origin.

The question of whether or not $FH(OFm)^-$ is an example of a bifurcated H-bond is difficult to answer from IR data alone. The evidence in favour of a bifurcated case is the assignment of δCOO at a frequency higher than in the simple salt. The anion, however, cannot have C_{2v} symmetry since the asymmetric stretch of the proton and $\nu_{as}COO$ would have different symmetry species and consequently cannot interact by Fermi resonance. If the H-bond is bent, and, as shown below, the distinction between bends and stretch of the proton will become blurred. This may account for the close proximity of the two bends and the stretch. A similar situation has been reported in $(Rhpy_4Br_2)NO_3HNO_3$ where all vibrations of the proton were degenerate as a result of the proton being at the centre of a distorted tetrahedron of oxygen (114).

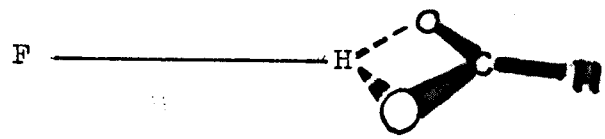

4. Trifluoroacetic Acid System (HOTF)

Results and Discussion

Preliminary work was done on the trifluoroacetate system and assignments are based on HOTF (Table 3,21). Bands associated with CF_3 modes of vibration will not be discussed as they well be similar to those observed for HOTF. The maximum symmetry expected is C_s, therefore, the symmetry species and selection rules are as shown in tables 3,6 and 3,7.

The spectrum above 1500cm^{-1} for BrH(OTF)$^-$ and ClH(OTF)$^-$ is similar in many ways to group one members of the acetate and formate systems. The broad absorptions at 2250cm^{-1} in ClH(OTF)$^-$ and at 2350cm^{-1} in BrH(OTF)$^-$ can be assigned to νOH. The lower frequency of νOH in ClH(OTF)$^-$ is consistent with it being a stronger H-bond than in BrH(OTF)$^-$. The complex structure of νOH in BrH(OTF)$^-$ may arise from Fermi resonance of νOH with overtones and combination bands falling in this region.

The carbonyl region shows features which were observed in both the acetate and formate systems. In BrH(OTF)$^-$ a very clear doublet can be seen which is similar to that observed in BrH(OAc)$^-$. In BrH(OAc)$^-$ this was attributed to the first overtone of νC-C at about 1740cm^{-1}, being enhanced in intensity as a result of Fermi resonance with νC=O. In trifluoroacetic acid systems νC-C has been assigned at 823cm^{-1} in the liquid acid and at 850cm^{-1} in sodium trifluoroacetate (116, 117, 118). In BrH(OTF)$^-$ and ClH(OTF)$^-$ several broad bands appeared in the region of 800cm^{-1}, the highest of which was at 812cm^{-1} and is, therefore, assigned to νC-C. From work on previous systems it was observed that γOH moved to higher frequency as the strength of the H-bond increased and γOH was found in the region of 880cm^{-1} in ClH(OAc)$^-$ and ClH(OFm)$^-$. In BrH(OTF)$^-$ the cation band at 890cm^{-1} is extremely broad and in ClH(OTF)$^-$ a broad shoulder was present on the strong cation absorption at about 900cm^{-1}. It is also noticeable that the weaker band in the doublet structure is at 1750cm^{-1} in BrH(OTF)$^-$ and at 1820cm^{-1}

in $ClH(OTF)^-$. This would be consistent with γOH at 900cm^{-1} in $ClH(OTF)^-$ and at less than 900cm^{-1} in $BrH(OTF)^-$.

The bands associated with νC-O and δOH were difficult to detect in both systems because of strong cation absorption and vibrations associated with CF_3 modes (1200cm^{-1} region). In $BrH(OTF)^-$ a weak band was observed at 1430cm^{-1} which was not due to the cation and can be compared with νC-O in HOTF (see table 3,21). The in-plane bend, δOH, has been assigned at 1297cm^{-1} and 1122cm^{-1} in liquid and monomeric trifluoroacetic acid, respectively (117). In $ClH(OTF)^-$ a broad band was observed at 1275cm^{-1} which may be due to δOH. The corresponding band in $BrH(OTF)^-$ could not be detected because of the strong absorption from CF_3 modes.

An attempt was made to prepare $Me_4N\ NO_3H(OTF)$. However, the resulting spectrum of the wet 1:1 mixture showed a broad absorption in the region of 3000cm^{-1} and so it was concluded that H-bond formation had not occurred. On further pumping, the excess acid was removed very easily and the spectrum of the solid residue was identical with $Me_4N.NO_3$. Since a nitrate salt with a larger cation was not available further work on this system was abandoned.

TABLE 3, 21

Assignments for $XH(OTF)^-$ system

Assignment	$ClH(OTF)^-$	$BrH(OTF)^-$	HOTF(104)
ν OH	2250	2350	3587
ν C=O	1730	1780	1830
ν C-O	-	1430	1415
δ OH	1270	-	1122
γ OH	ca 900	ca 880	661
ν C-C	812	812	781
2x γ OH	1820	1750	

5. Dichloroacetic Acid System (HODC)

Results and Discussion

Weight analysis on $Bu_4NBrH(ODC)$ indicated the presence of excess acid. The IR spectrum of the brownish oil showed a strong absorption extending from $3000cm^{-1}$ to $2300cm^{-1}$ with several band centres. In liquid dichloroacetic acid νOH can be assigned to a broad band centred at $3100cm^{-1}$ and so clearly very little free acid is present in the oil. The structure of the bands observed were similar to the previous systems though a detailed account would be fruitless in view of the presence of different H-bonded species. However, the band centre of the overal band was at $2600cm^{-1}$ which is intermediate between the corresponding formate and trifluoroacetate analogues. This serves to illustrate its intermediate H-bond strength which is expected from its intermediate pK_a value, as shown below (table 3,22)

Table 3,22

	pK_a	$BrH(O_2C.R)^-$
formic acid	3.75	$2,900cm^{-1}$
dichloroacetic acid	1.30	$2,600cm^{-1}$
trifluoroacetic acid	0.23	$2,350cm^{-1}$

The lower frequency region showed a strong broad band at $1760cm^{-1}$ which can be safely assigned to $\nu C=O$. Analysis of the region below $1700cm^{-1}$ was not undertaken because of the presence of excess acid.

Table 3,23

	$BrH(ODC)^-$, cm^{-1}
ν OH	Ca.2,600
ν C=O	1,760

6. Solution Spectra

An IR spectrum of $BrH(OAc)^-$ in methylene dibromide showed strong absorption in the region above $3000cm^{-1}$, which was indicative of the presence of free acetic acid. The presence of $BrH(OAc)^-$ was suspected from the broad absorption just below $3000cm^{-1}$ which was more intense than that observed from the same concentration of acetic acid in CH_2Br_2.

A PMR spectrum of a $BrH(OAc)^-$ solution indicated the presence of a low field signal at 0.43τ. Since rapid exchange between the free acid and $BrH(OAc)^-$ is most likely the chemical shift will be a weighted average of the chemical shifts of the species in equilibrium. Other samples of different H-bonded species were also examined and all showed low field signals, as shown below:

Table 3,24

	Chemical Shift, τ.	Solvent	Ref.
$Bu_4NBrH(OTF)$	-2.25	CH_2Br_2	Cyclohexane
$Bu_4NBrH(OFm)$	+1.80	CH_2Br_2	"
$Bu_4NClH(OFm)$	+1.59	$CHCl_3$	"
$Bu_4NBrH(OAc)$	+0.43	CH_2Br_2	"

No further conclusions can be drawn from the numerical values of the chemical shifts since detailed concentration studies were not undertaken. The fluoride systems could not be examined because of the low solubility in the solvents shown above.

7. Experimental

(i) Reagents

AnalaR grade acetic acid was obtained from Hopkin and Williams and was stored over molecular sieve to remove the last traces of water. Formic acid, a 98% solution in water, was obtained from Fisons and was stored over anhydrous copper sulphate. Trifluoroacetic acid was obtained from British Drug Houses and Dichloroacetic acid was obtained from Fisons. Both these acids were stored over Molecular sieve. All the tetraalkylammonium halides except the fluoride were obtained from British Drug Houses and were not purified further. A sample of Me_4NF was supplied by Prof. T. C. Waddington and Me_4NNO_3 was supplied by Dr. J. A. Salthouse. The IR spectra which were recorded are shown at the end of this section.

(ii) Preparation of Hydrogen Bonded Anions

(a) $n\text{-}Bu_4NBrH(OAc)$

A known amount of dry $n\text{-}Bu_4NBr$ was weighed in a reaction cell of known weight. The reaction cell was then evacuated and reweighed. The reaction cell was connected to the vacuum line and after the pump end of the line had been closed, the bromide was exposed to dry acetic acid vapour which was contained in a trap. The acid was condensed onto the bromide by means of liquid nitrogen until all the bromide was dissolved at room temperature. The excess acid was pumped away and a weight analysis was carried out. With about 38% by weight of acid the loss of weight became much slower. Finally the pumping was stopped when the stoichiometric quantity of acetic acid was present. The experimental percentage increase in weight was 18.96% as compared with a theoretical value of 18.45%. The corresponding deuterium sample was prepared in the same manner. The final results of analysis are shown below:

Compound	Weight Analysis		HOAc		Bu_4N^+		Br^-	
	Exp.	Calc.	Exp.	Calc.	Exp.	Calc.	Exp.	Calc.
n-Bu_4NBrH(OAc)	18.96	18.45	18.62	16.37	65.67	62.9	-	20.73
n-Bu_4NBrD(OAc)	18.00	18.76	16.66		62.95		20.21	

(b) n-Bu_4NClH(OAc)

A sample of n-Bu_4NCl was prepared by the method outlined in chapter two and the H-bonded species were prepared as outlined in 2(a). The last traces of excess acid were very difficult to remove which is reflected in the analytical data for the protonium compound:

Compound	Weight Analysis		HOAc		Bu_4N^+		Cl^-	
	Exp.	Calc.	Exp.	Calc.	Exp.	Calc.	Exp.	Calc.
n-Bu_4NClH(OAc)	26.00	21.64	20.1	17.7	69.8	71.85	9.80	10.50
n-Bu_4NClD(OAc)	22.84	22.00						

(c) n-Bu_4NIH(OAc)

This compound was prepared as the n-Bu_4N^+ salt by the procedure outlined in 2(a). Owing to the rapid decomposition of the anion the pumping was terminated before the correct stoichiometric amount of acid was present. The weight analysis figures for $IH(OAc)^-$ and $ID(OAc)^-$ were 18.00% and 19.87% as compared with the theoretical values of 16.24% and 16.50% respectively. Further analysis was not undertaken because the compounds turned brown within an hour.

(d) n-Bu_4NBrH(OFm)

This anion was prepared as the n-Bu_4N^+ salt by the method outlined in 2(a).

The results of the analysis are shown below:

Compound	Weight Analysis		HOFm		Bu_4N^+		Br^-	
	Exp.	Calc.	Exp.	Calc.	Exp.	Calc.	Exp.	Calc.
n-Bu_4NBrH(OFm)	14.60	14.14	10.33	13.28	66.85	65.28	22.13	21.51
n-Bu_4NBrD(OFm)	12.14	14.45	-	-	-	-	-	-

(e) n-Bu_4NClH(OFm)

The anion was prepared as the n-Bu_4N^+ salt by the method outlined in 2(a).

Compound	Weight Analysis		HOFm		Bu_4N^+		Cl^-	
	Exp.	Calc.	Exp.	Calc.	Exp.	Calc.	Exp.	Calc.
n-Bu_4NClH(OFm)	16.16	16.58						
n-Bu_4NClD(OFm)	15.63	16.94	13.26	14.09	75.61	74.95	11.13	10.96

(f) n-Bu_4NlH(OFm)

The same procedure was adopted as in 2(a) using n-Bu_4N^+ as the cation. The results of a weight analysis gave a 12.64% increase in weight as compared with a theoretical value of 11.64%. Chemical analysis was not undertaken for the same reasons as in the acetate analogue.

(g) n-Bu_4NBrH(OTF)

This anion was prepared as the n-Bu_4N^+ salt by the method described in 2(a). A weight analysis showed 35.30% by weight of acid compared with the theoretical value of 35.04%

(h) Me_4NClH(OTF)

Dry Me_4NCl was weighed out in a reaction cell which was then evacuated on

the vacuum line. The stoichiometric amount of trifluoroacetic acid was then allowed to evaporate into a ten litre flask which had been evacuated beforehand. About 10mm pressure was sufficient to provide 0.6698 gms of gaseous acid. The pump end of the line was then closed and the Me_4NCl was exposed to small quantities of the vapour. On exposure the compound became visibly wet and the pressure in the system dropped slowly to zero as the vapour was absorbed onto the solid. When zero pressure was registered by the mercury manometer, the compound was allowed to stand for about an hour while the gas-solid phase equilibrium had settled. Finally the solid was pumped dry using only the rotary oil pump to remove any traces of acid vapour and any localised excess of acid. A final weight analysis indicated 91.34% increase in weight as compared with a theoretical value of 104.03%. Although the stoichiometric quantity of acid was not present it minimises the concentration of any local excess of acid which would result in H-bonded species with more than one molecule of acid.

(i) $Me_4N.NO_3H(OTF)$

An attempt was made to prepare the Me_4N^+ salt of this anion by the method outlined in 2(a). The pumping was stopped when 72.55% by weight of acid was present. The theoretical value was 83.72% and so clearly the anion was easily decomposed. An IR spectrum of the wet solid could not be distinguished from a spectrum of trifluoroacetic acid and $Me_4N.NO_3$. On further pumping the 72.55% by weight of acid was removed very quickly and so it was concluded that the cation was too small to stabilise the anion.

(j) $n\text{-}Bu_4NBrH(ODC)$

This anion was prepared using the $n\text{-}Bu_4N^+$ cation by the method outlined in 2(a). Heating was necessary to speed up the removal of the excess acid. The solution, however, turned brown indicating decomposition of the acid and liberation of free bromine. A weight analysis on the brownish oil obtained

indicated the presence of 61.00% by weight of acid as compared with a theoretical value of 39.63%.

(k) $Me_4NFH(OAc)$

This anion was prepared as the Me_4N^+ salt using the method adopted in 2(h). A transparent polythene tube was fitted inside the reaction cell to eliminate contamination resulting from any reaction with the pyrex glass. A deuterium sample was prepared by the same method:

Compound	Weight Analysis		HOAc		Me_4N^+	
	Exp.	Calc.	Exp.	Calc.	Exp.	Calc.
$Me_4NFH(OAc)$	64.06	64.46	37.7	39.19	49.32	48.40
$Me_4NFD(OAc)$	65.52	65.53	-	-	-	-

(l) $Me_4NFH(OFm)$

This anion was prepared as the Me_4N^+ salt by the method outlined in 2(k). During the preparation, no visible traces of liquid were present in the reaction cell. Considerable heat was generated and hydrogen fluoride was liberated during the reaction. Since HOFm is the weaker acid in the $FH(OFm)^-$ system, its concentration was determined by simple acid-base titration with standard sodium hydroxyde.

Compound	Weight Analysis		Me_4N^+		HOFm	
	exp.	Calc.	Exp.	Calc.	Exp.	Calc.
$Me_4NFH(OFm)$	45.27	49.41	51.4	53.3	31.80	33.1
$Me_4NFD(OFm)$	40.02	50.48				

S P E C T R A

CONTENTS

All spectra have been recorded in Nujol unless otherwise stated.

All spectra have been recorded at -196°C unless specifically stated to the contrary.

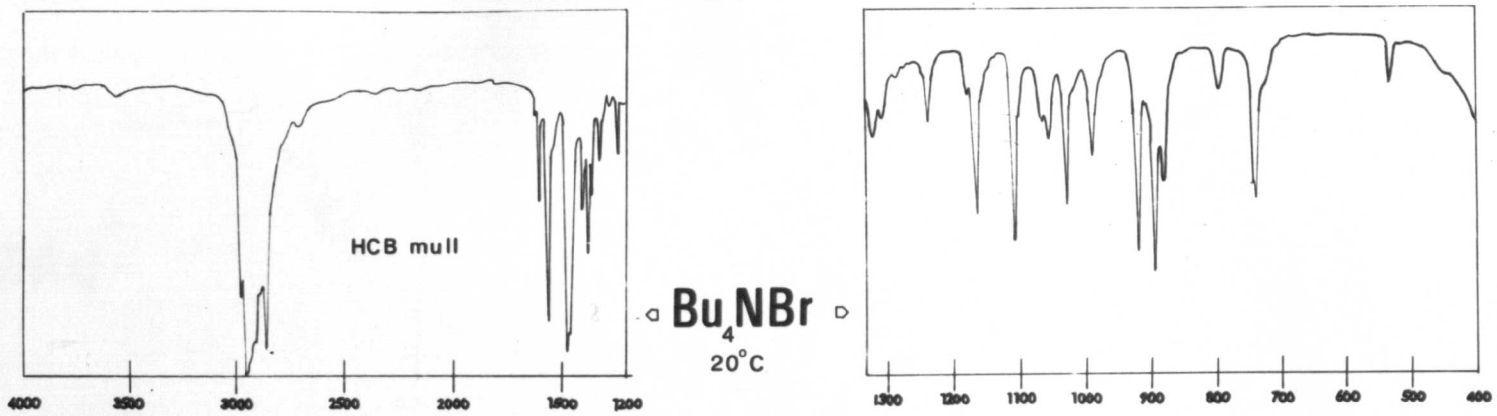
HCB mull
Bu4NBr
20°C
4000
3500
3000
2500
2000
1800
1200
1300
1200
1100
1000
900
800
700
600
500
400

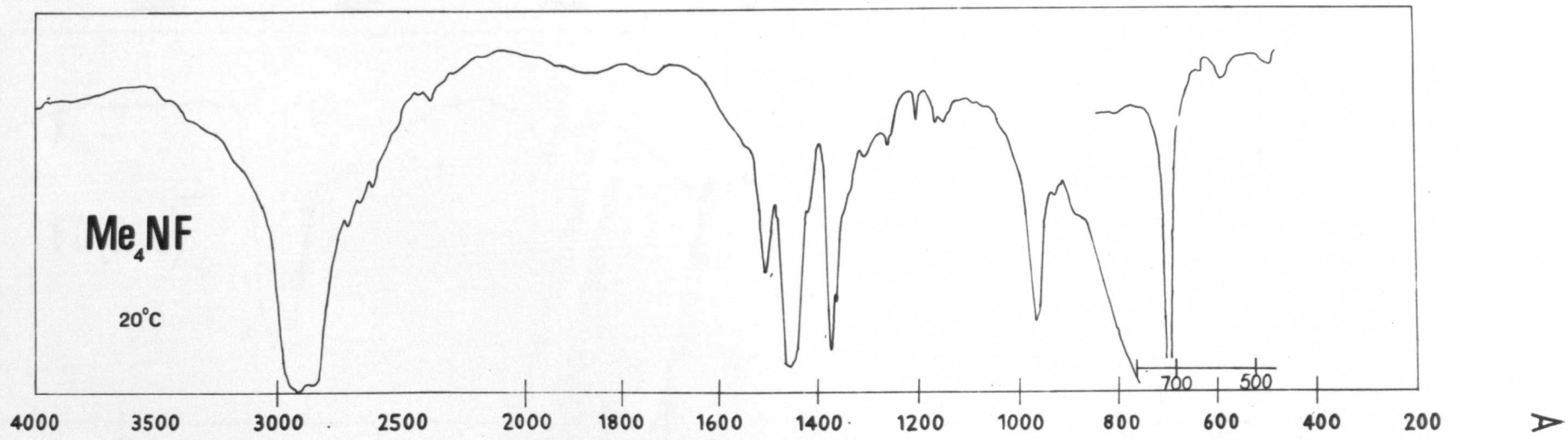
Me4NF
20°C
700
500
4000
3500
3000
2500
2000
1800
1600
1400
1200
1000
800
600
400
200
A

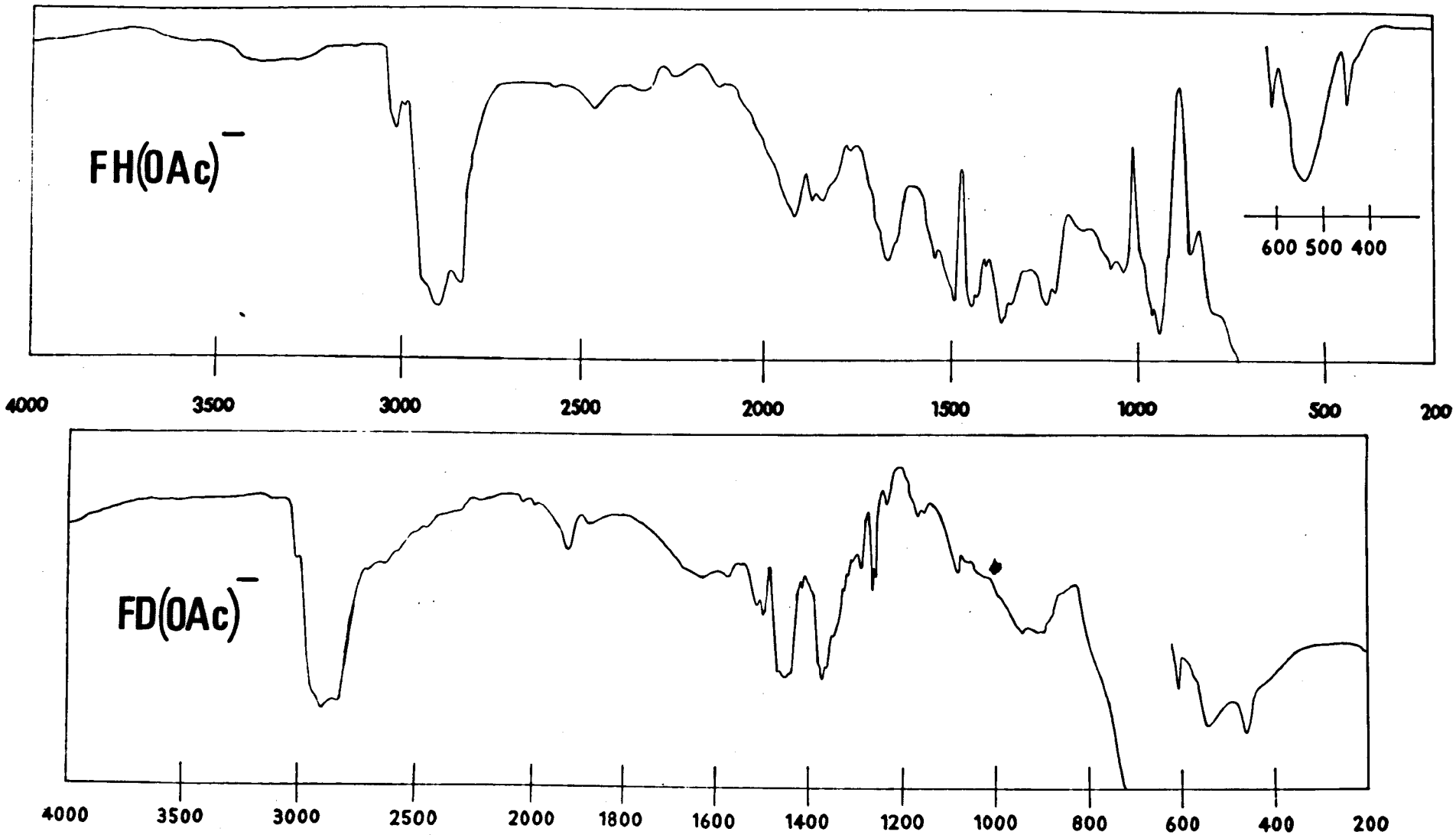
FH(OAc)⁻
600 500 400
4000
3500
3000
2500
2000
1500
1000
500
200
FD(OAc)⁻
4000
3500
3000
2500
2000
1800
1600
1400
1200
1000
800
600
400
200

B

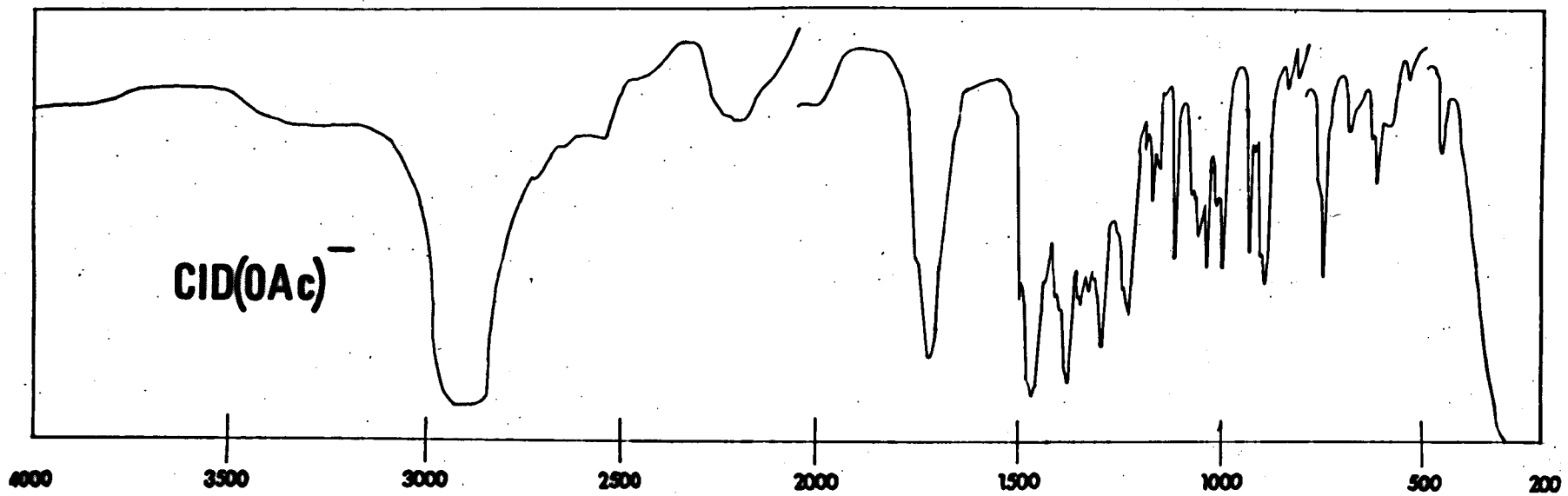
ClD(OAc)⁻
4000
3500
3000
2500
2000
1500
1000
500
200

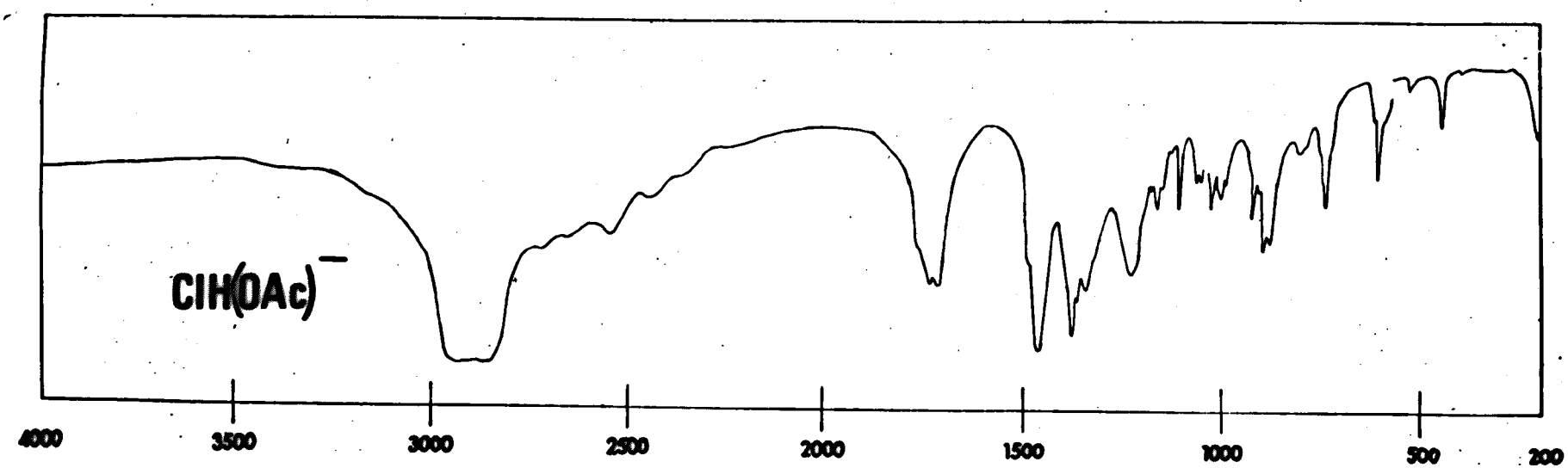
ClH(OAc)⁻
4000
3500
3000
2500
2000
1500
1000
500
200

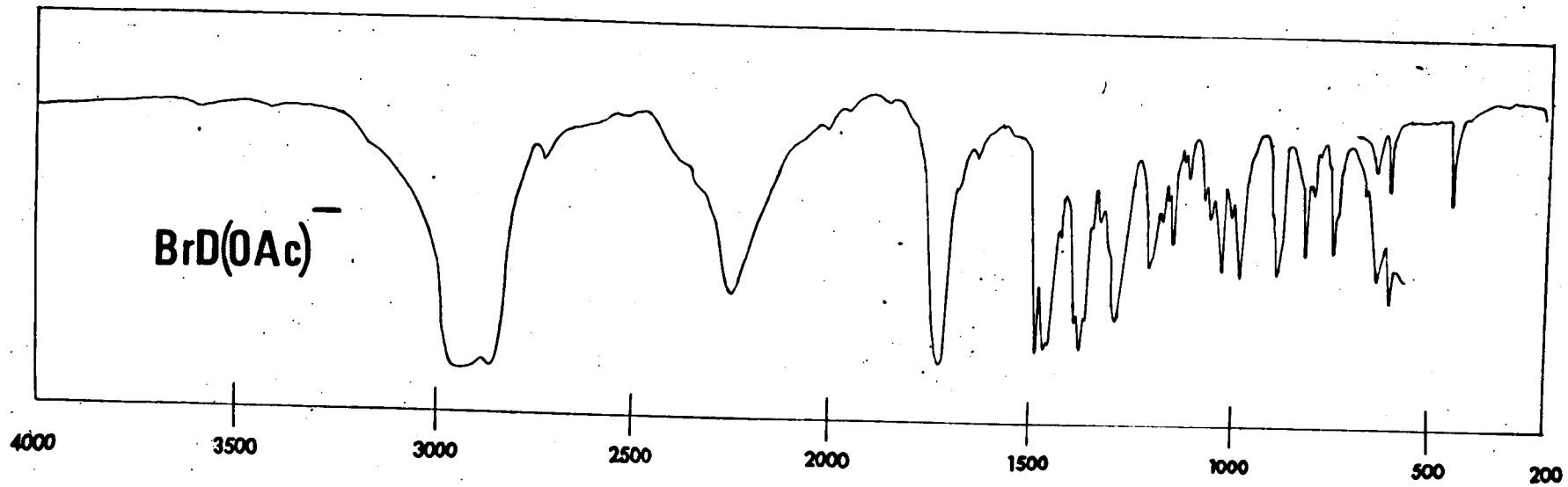
BrD(OAc)⁻
4000
3500
3000
2500
2000
1500
1000
500
200

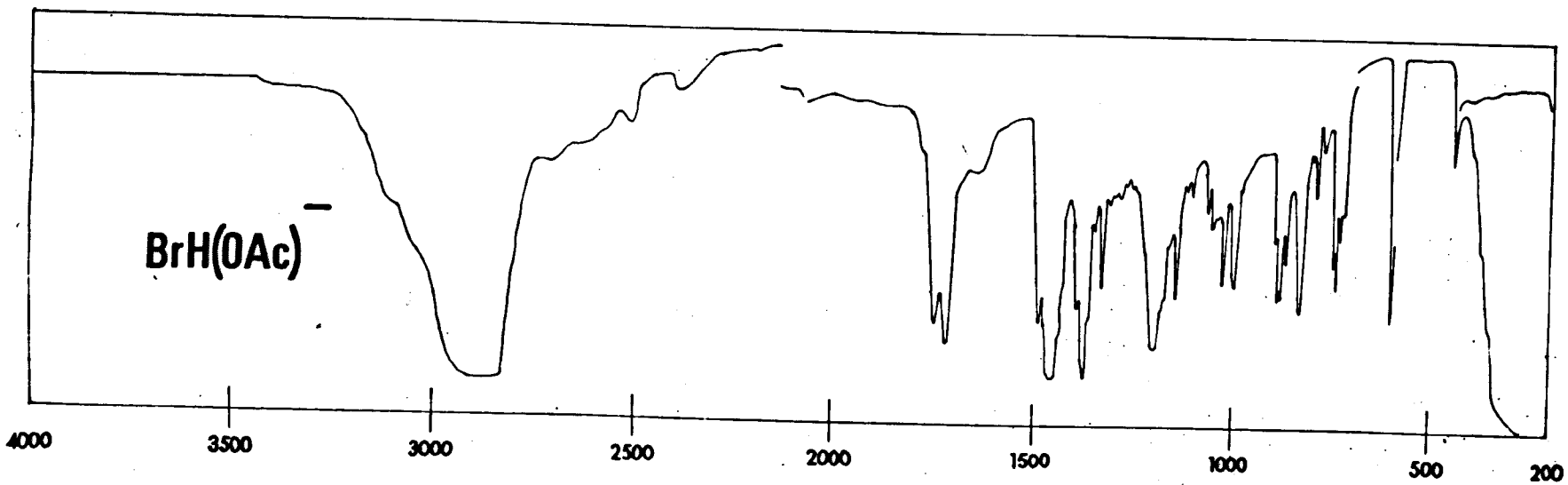
BrH(OAc)⁻
4000
3500
3000
2500
2000
1500
1000
500
200

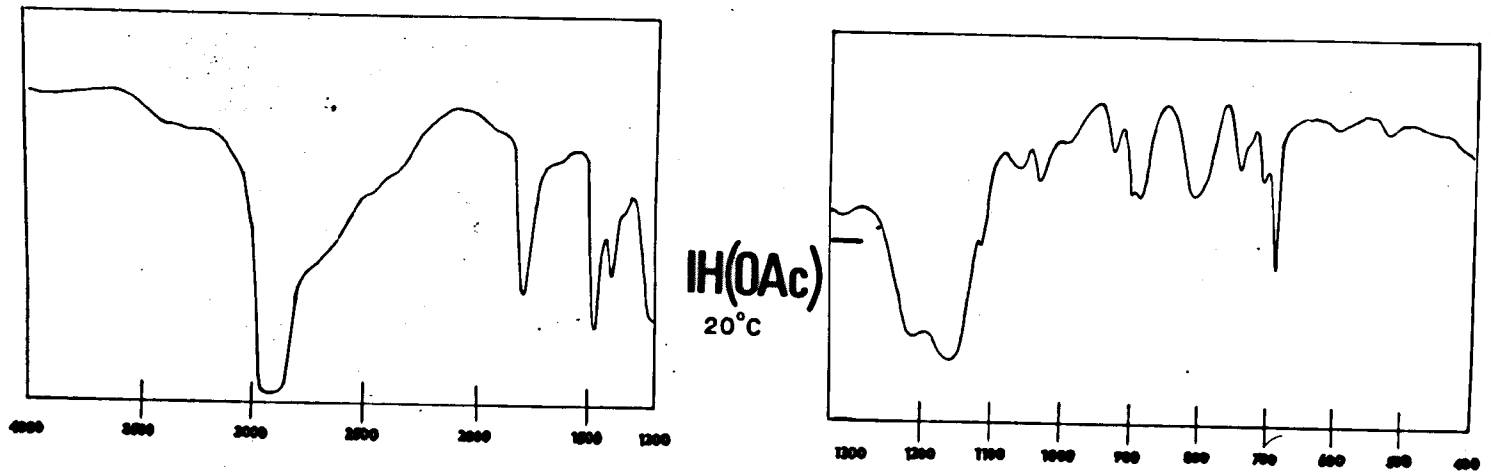
IH(OAc)
20°C

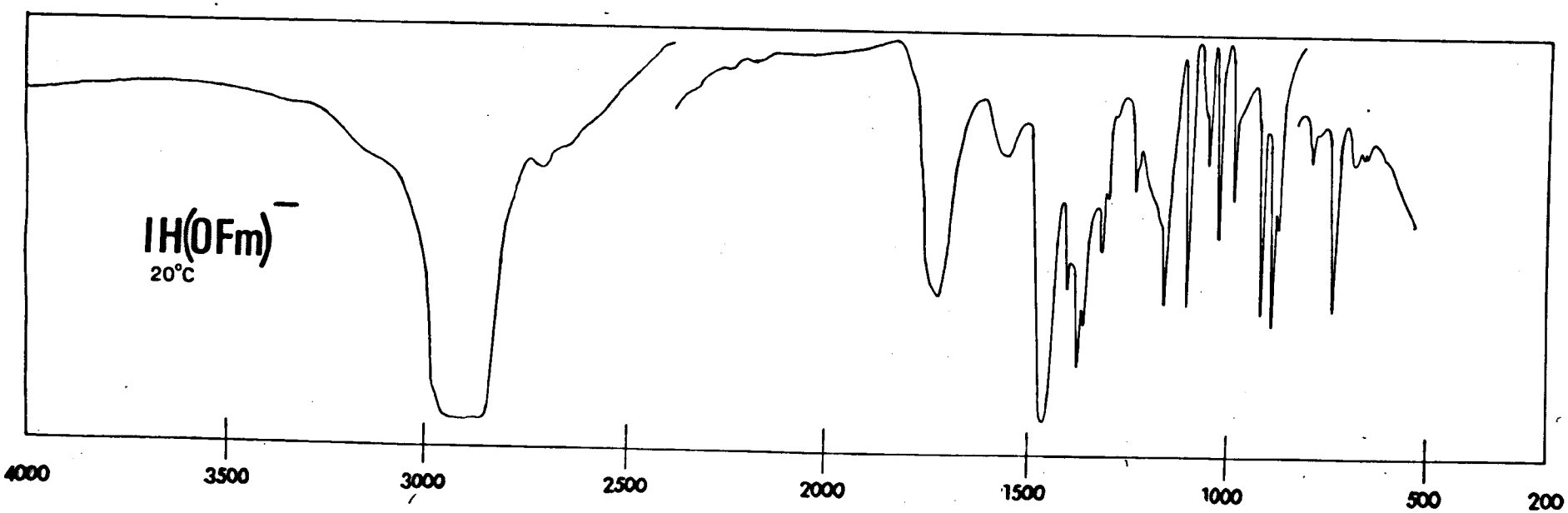
IH(OFm)⁻
20°C
4000
3500
3000
2500
2000
1500
1000
500
200

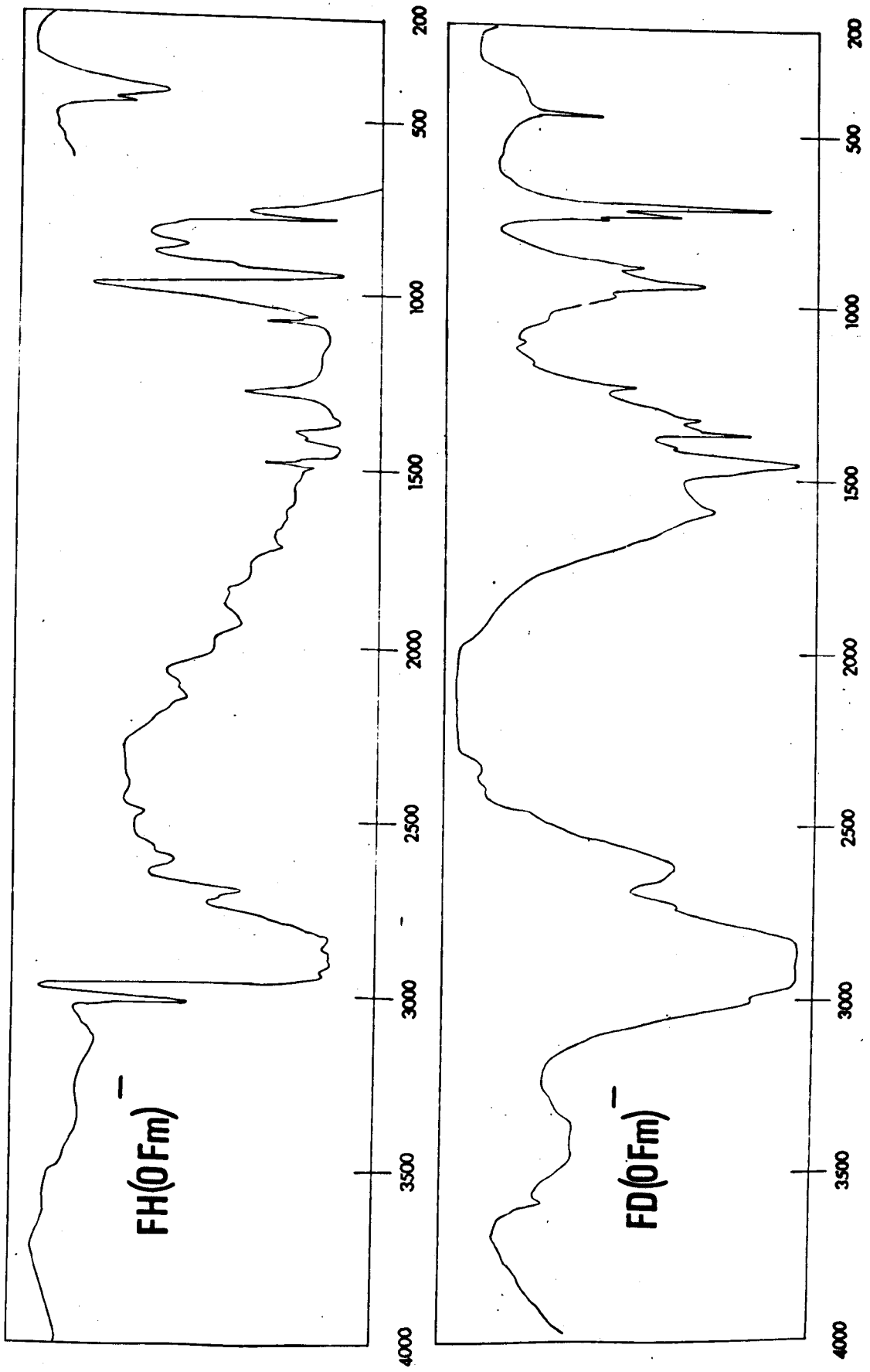
FH(OFm)⁻
FD(OFm)⁻
200
500
1000
1500
2000
2500
3000
3500
4000

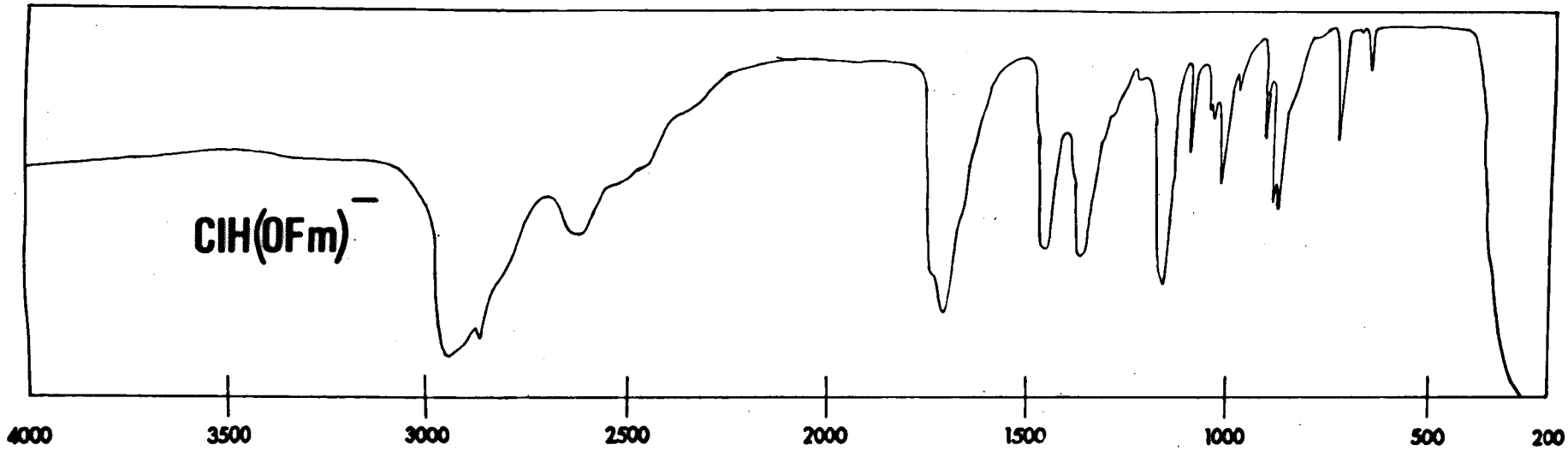
ClH(OFm)⁻
4000
3500
3000
2500
2000
1500
1000
500
200

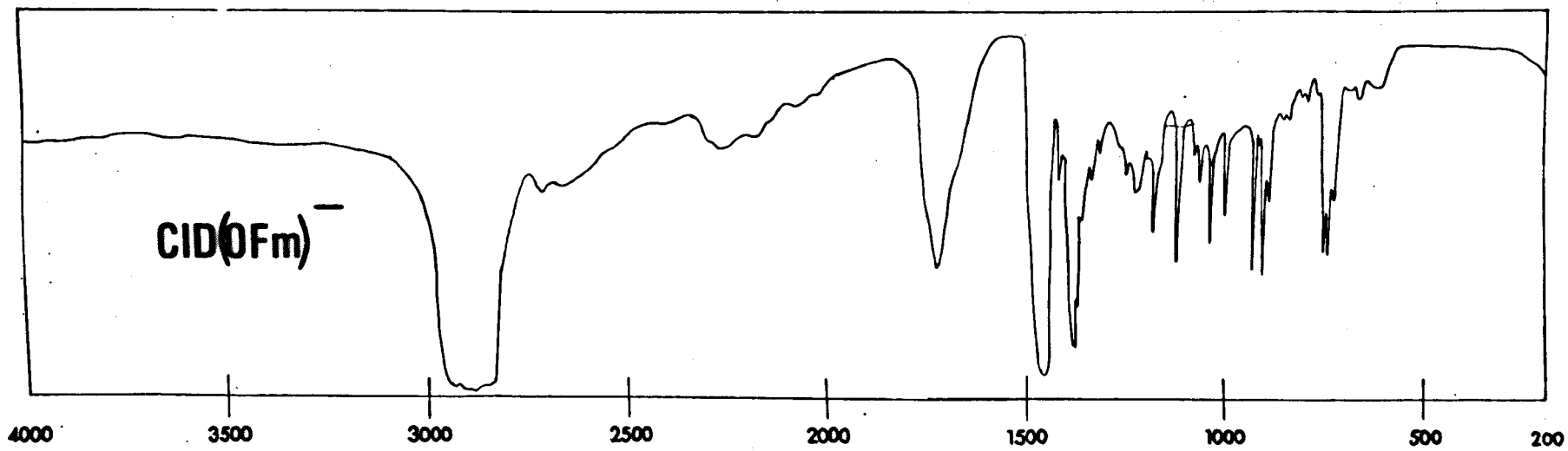
ClD(OFm)⁻
4000
3500
3000
2500
2000
1500
1000
500
200

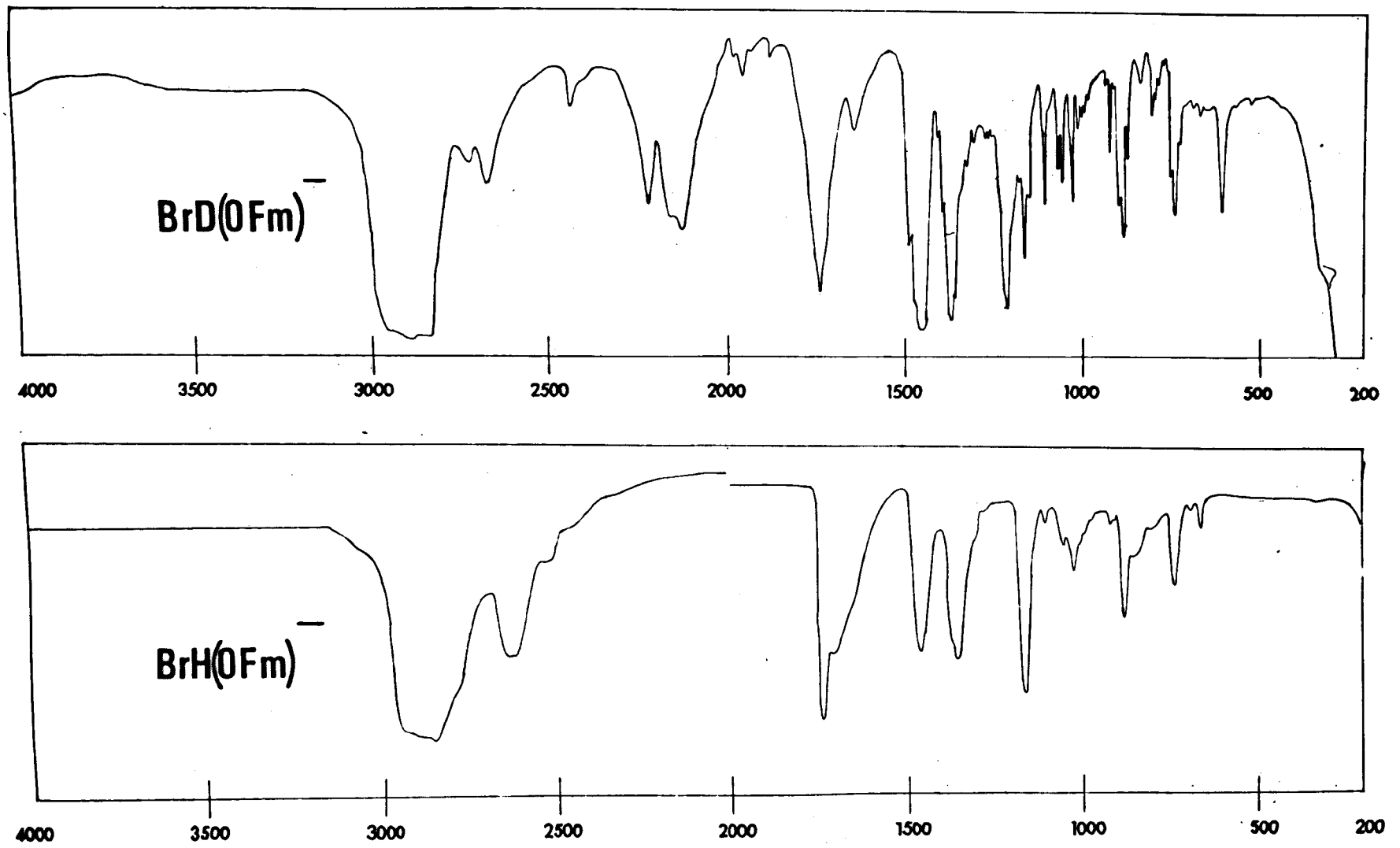
BrD(OFm)⁻
4000
3500
3000
2500
2000
1500
1000
500
200
BrH(OFm)⁻
4000
3500
3000
2500
2000
1500
1000
500
200

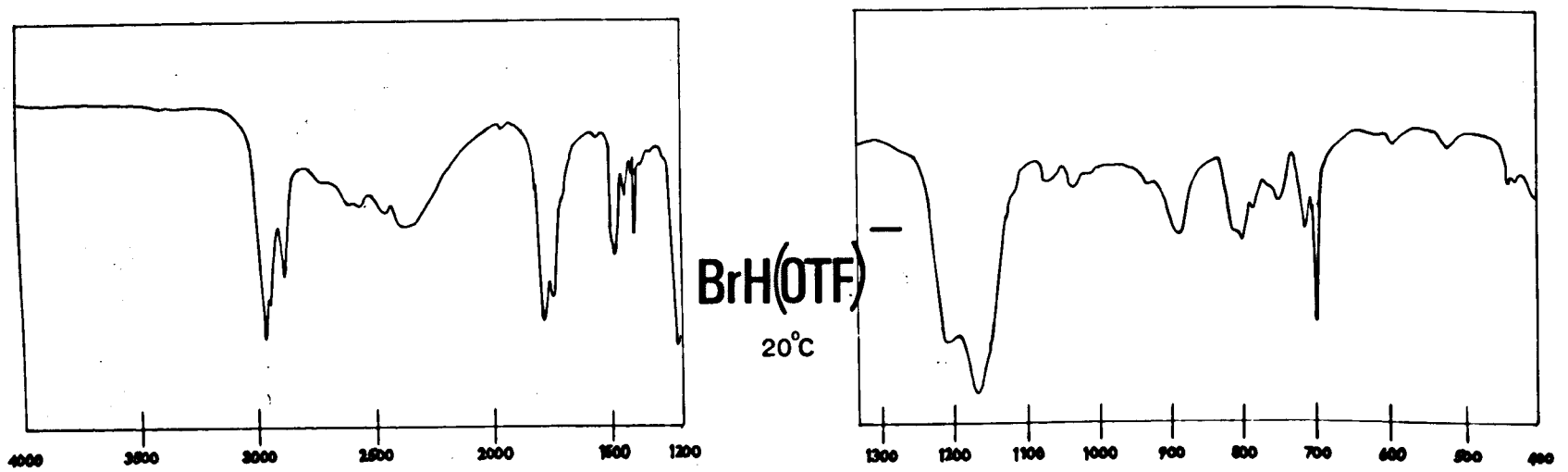
BrH(OTF)
20°C
4000
3500
3000
2500
2000
1500
1200
1300
1200
1100
1000
900
800
700
600
500
400

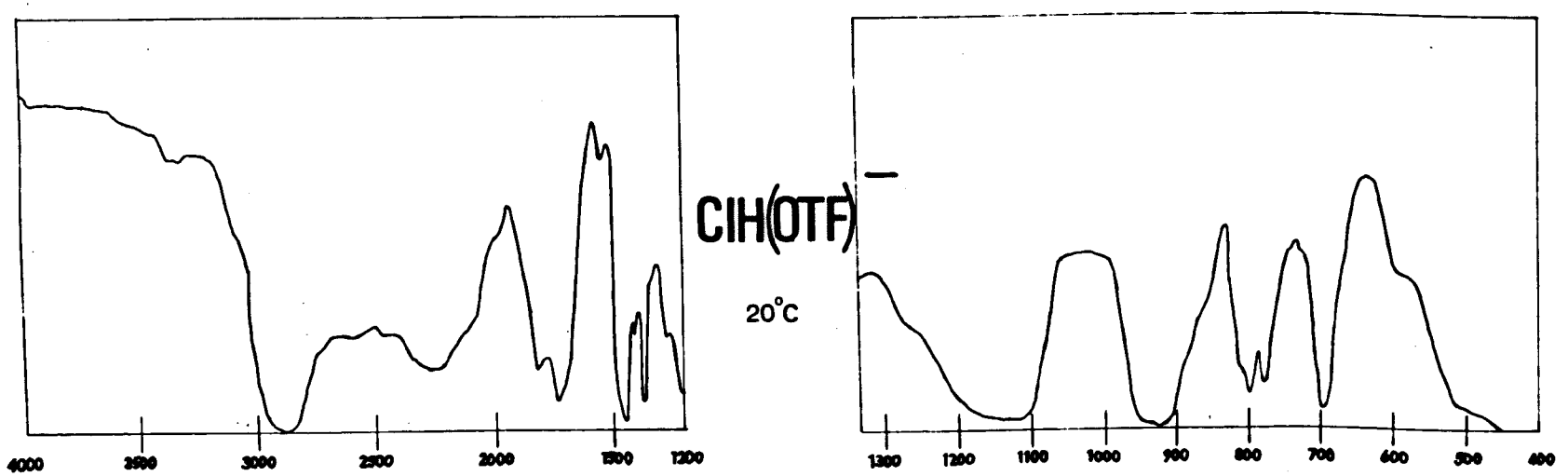
ClH(OTF)
20°C
4000
3500
3000
2500
2000
1500
1200
1300
1200
1100
1000
900
800
700
600
500
400

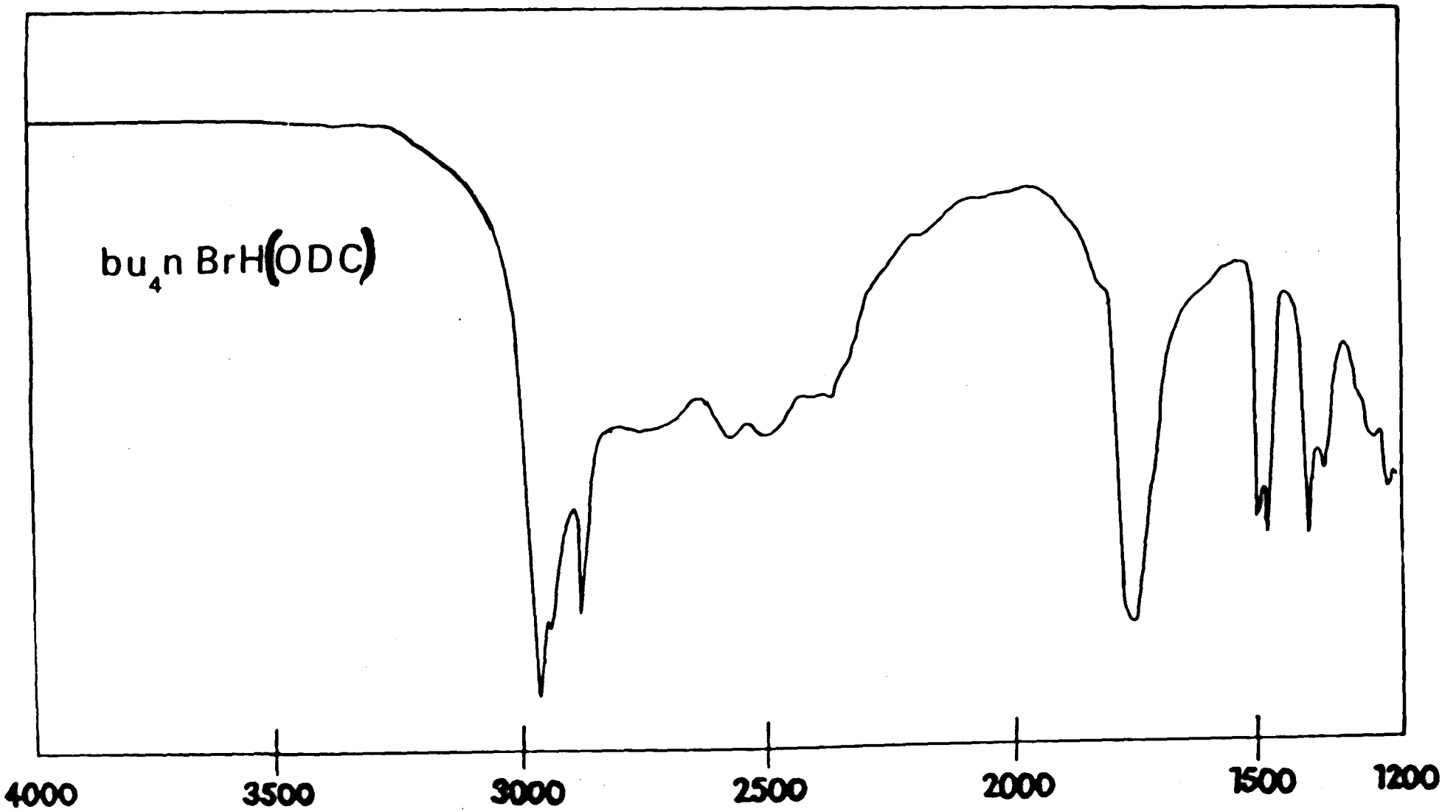
bu4n BrH(ODC)
4000
3500
3000
2500
2000
1500
1200

CHAPTER FOUR

Type B Hydrogen Dicarboxylate Salts.

Chapter Four.

Type B Hydrogen Dicarboxylate Anions.

1. Introduction.

In Chapter Three H-bonded anions were discussed where asymmetry in the proton potential energy surface arose primarily because of the noncoincidence of the proton levels in the acid and base. In Type B hydrogen dicarboxylate anions the proton levels of the acid and base are identical in the liquid phase but the crystallographic nonequivalence of the two carboxylate groups in the solid phase renders a coincidence of the proton levels unlikely. Similarly, the separation of adjacent energy levels in each well is different. The potential energy surface in which the proton is residing is likely, therefore, to be asymmetric along the bond axis. An asymmetric double minimum potential energy well with a low barrier cannot, however, be ruled out.

Unfortunately, no neutron diffraction data and very little IR data has been reported for Type B hydrogen dicarboxylate salts. Potassium hydrogen di-p-nitrobenzoate, $KH(p\text{-}NB)_2$, represents a case where both IR and X-ray data is available (30, 64). Its IR spectrum shows the expected superposition of the acid and base spectrum and is confirmation of the crystallographic nonequivalence of the two carboxylate groups. The IR spectrum of $KH(p\text{-}NB)_2$, however, differs from that of the H-bonded anions discussed in this chapter. In $KH(p\text{-}NB)_2$ the band assigned to νOH is a broad doublet with band centres at $2450cm^{-1}$ and $1920cm^{-1}$ whereas the only band of comparable breadth and intensity is at about $1100cm^{-1}$ in the anions discussed in this chapter. Fortunately, some of the liquid adducts examined

by Hadži show a similar feature with a band centre between 1500cm^{-1} and 900cm^{-1} but detailed assignments were not, however, reported (69, 74). These adducts have already been discussed in chapter one but it is worth emphasising again that the low isotopic shift of the broad band assigned to νOH below 1800cm^{-1} is a clear indication of an asymmetric double minimum potential energy well with the first excited state near to the top of the barrier (74). The low isotopic shift was predicted by Hornig and Somorjai in asymmetric double minimum potential energy wells where the ground states, and first excited states are below, and close to the barrier, respectively (119). However, in their calculations several assumptions were made, viz., separation of minima was 0.74A$^{\circ}$, O-H-O length was 2.76A$^{\circ}$, and a O-H length of 1.01A$^{\circ}$ (119). Thus the first two arbitrarily chosen parameters are considerably longer than those observed in Type B salts and probably longer than in the liquid adducts.

Hornig and Somorjai also predicted that considerable mixing of the wavefunctions of the states in the left and right hand well occurs, particularly in the region near to and above the barrier (119). The relative intensity of transitions from the ground state to excited states will not, however, be as simple as in the harmonic oscillator model. A change in the IR selection rules from "even-odd" and "odd-even" to "left-left" and "right-right" was predicted once a slight asymmetry is introduced into the original symmetric double minimum. The precise selection rule operating in asymmetric double minimum wells will depend, therefore, on the barrier height, the separation of the two minima, and the asymmetry of the well. Thus with systems discussed in this chapter neither strict "left-left" nor strict "even-odd" selection rules will operate. Anomalous features as regards isotopic shifts

and relative intensities of transitions may occur as a direct result of the difference between the deuterium and proton levels in relation to the barrier. Therefore, a slight change of selection rules to more "left-left" may occur in going from proton to deuterium H-bonded species (119). The latter point by itself is a sufficient condition for low isotopic shifts to occur and was proposed as an alternative explanation of the low isotopic shift in $HCrO_2$ (see chapter one)(120).

Hornig and Somorjai emphasised that in order to obtain an accurate potential energy surface for any H-bonded system a complete study of the intensities of fundamentals and overtones is necessary (119). Since the results recorded in this chapter are concerned only with the fundamental region, which can by themselves give only an indication of whether or not the well is symmetric, an accurate potential well cannot be constructed. However, in order to make clear the arguments expressed in this chapter, intuitively reasonable wells have been constructed which are consistent throughout the range of compounds examined in chapters four and five, but must, for the reasons already outlined, be regarded as approximate models.

The Type B hydrogen dicarboxylate salts examined in this chapter represent, in the author's opinion, cases where asymmetry exists in the potential energy well along the O-O band axis. The gaps in each acid series, which will become apparent in the text, represent the symmetric Type A salts and are discussed in chapter five.

2. Normal Modes of Vibration

The absence of any elements of symmetry in Type B salts renders no restrictions on the IR activities of the normal modes of vibration. The thirty nine modes are made up from eighteen associated with the

acid moiety, fifteen associated with the base moiety, and six low frequency modes of the H-bond. Anharmonicity renders overtones and combination bands IR active and is particularly important for vibrations involving the proton. Assignments have been made, as far as possible, by a comparison with published results on the respective acid and base concerned.

3. Nomenclature and Abbreviations

$H(OAc)_2^-$	Hydrogen Diacetate
$H(O_2C.CD_3)_2^-$	Hydrogen D_3-Diacetate
$H(OMC)_2^-$	Hydrogen Di-monochloroacetate
$H(ODC)_2^-$	Hydrogen Di-dichloroacetate
$H(OFm)_2^-$	Hydrogen Diformate
$H(ODFC)_2$	Hydrogen Di-chlorodifluoroacetate

The key to other abbreviations and symbols used in this chapter can be found in chapter three.

4. Hydrogen Diacetate Anion, $H(OAc)_2^-$

Assignments of the vibrational spectrum of salts containing this anion are shown in tables4.1, 4.2, and 4.3. Spectra are reproduced at the end of this chapter. The spectra of $KH(OAc)_2$ and $KD(OAc)_2$ are identical with those reported earlier where an assignment was not reported (16). A comparison with assignments for HOAc (table 3.6) and OAc^- ion (116, 130) assisted in the assignment of $H(OAc)_2^-$ systems.

Carboxylate Group Vibrations.

The assignment of bands associated with the carboxylate group in $KH(OAc)_2$ systems was made on the basis of a superposition of the acid and base spectrum. This is clearly emphasised in the regions of 1700cm^{-1} and below 700cm^{-1}. Deuteration in the hydroxyl position resulted in a slight shift of the bands to lower frequency, a feature also noted in HOAc (103). In general, the frequencies are intermediate between analogous vibrations in HOAc and OAc^-. The modes of vibration associated with the CH_3 group were found at their usual frequencies, but a distinction between the two sets for each mode was not possible because of their close proximity. The sharp band at 1318cm^{-1} in $KD(OAc)_2$ is of particular interest since its absence in $KD(O_2C.CD_3)$ suggests that it must be associated with a CH_3 mode. A band of similar frequency (1333cm^{-1}) and origin was found in the IR spectrum of NaOAc but was of low intensity since it is allowed only because of a low site symmetry (116, 130). The appearance of the 1318cm^{-1} band is, therefore, consistent with the low symmetry of $KD(OAc)_2$.

The Raman and IR spectrum of $KH(OAc)_2$ are similar to each other but the low point group of the anion places no restrictions on the activities of vibrations in either technique. The assignment of the

TABLE, 4, 1.

Assignment of Vibrational Spectrum of $KH(OAc)_2$, (cm^{-1}).

Approx. description	$KH(OAc)_2$			$KD(OAc)_2$	
	25°C	-196°C	Raman	25°C	-196°C
νCH_3	3010	-	-	3010	-
νCH_3	2990	-	-	2990	-
νCH_3	2935	-	-	2935	-
overtone	2430,1950	2400,2000			
$\nu C{=}O$	1710	1710	1690	1685	1687
$\nu_{as} COO$	1608	1616	1628	1598	1602
δCH_3	1420	1425	1420	1420	1417
δCH_3	1410	1412	1408	1410	
δCH_3	1330	1320	1328	1318	1318
$\nu_s COO$	1380	1370)	1380	1390	1390
νCO	1370	1360)		1370	1370
$\delta OH(D)$	1260	1280	(very broad band in region 1000 - 2000	850	850
$\nu OH(D)$	1155	1100		1100	1100
ρCH_3	1046	1040		1045	1045
ρCH_3	1016	1020		1020	1020
$\gamma OH(D)$	ca 990	1000		690	675?
νCC	917	917	928	930	932
νCC	890	890	906	830	830
δCOO	680	682	682	672	675
δCOO	625	628	628	617	615
δCCO	470	471	456	470	470
δCCO	450	449	460	440	440
πCCO	615	612	624	610	605
πCCO	608	606	608	610	605
$\nu(OO)$	260	270		250	250

Isotopic Shifts at -196°C	$\nu OH/\nu OD$	$\delta OH/\delta OD$	$\gamma OH/\gamma OD$
	1.00	1.51	1.47

TABLE 4. 2 .

Assignment of Vibrational Spectrum of $KH(O_2CCD_3)_2$, (cm^{-1})

Approx. description	$KH(O_2CCD_3)_2$		$KD(O_2CCD_3)_2$	
	25°C	-196°C	25°C	-196°C
ν CD_3	2260	2260	2260	2260
ν CD_3	2230	2225	2230	2235
ν CD_3				
overtone	2430, 1900	2400, 1900		
ν C=O	ca 1665	ca 1660	1670	1665
ν_{as} COO	1585	1580	1580	1575
δ CD_3				
δ CD_3		1100-1000		1100-1000
δ CD_3				
ν_s COO	1395	1398	1390	1395
ν CO	1365	1360	1350	1360
δ OH(D)		1220		835
ν OH(D)	1100	1020	1050	ca 1000
ρ CH_3	928	925	926	925
ρ CH_3	820	815	820	825
γ OH(D)		980		ca 700
ν CC	850	852	855	853
ν CC	820	815	800	800
δ COO	645	645	637	640
δ COO	575	565	560	560
δ CCO	425	427	420	422
δ CCO	403	405	398	395
π CCO	595	598	560	560
π CCO	525	520	520	520
ν OO	250	245	230	230

Isotopic Shifts at -196°C	ν OH/ν OD	δ OH/δ OD	γ OH/γ OD
	1.02	1.46	1.40

TABLE 4, 3.

Assignment of Vibrational Spectrum of $RbH(OAc)_2$, (cm^{-1})

Approx. description	$RbH(OAc)_2$		$RbD(OAc)_2$	
	25°C	-196°C	25°C	-196°C
νCH_3	3005	-	-	-
νCH_3	2985	-	-	-
νCH_3	2932	-	-	-
overtone	2430	2400	-	-
$\nu C{=}O$	1720	1715	1670	1670
$\nu_{as} COO$			1600	1605
δCH_3	1425	1425	-	-
δCH_3	-	-	-	-
δCH_3	1340	1340	1325	1330
$\nu_s COO$	1375	1370	1370	1370
νCO				
$\delta OH(D)$	1225	1252	950	950
0-2 transtn.	1050	1050	1000	1050
0-1 transtn.	760	700	490	495
ρCH_3	1040	1055, 1045	1050, 1040	1052, 1042
ρCH_3	1017	1022, 1010	1015	1018
$\gamma OH(D)$	965	965	-	720
νCC	880	915	880	882
νCC		875	830	830
δCOO	670	670	650	650
δCCO	-	-	-	-
πCCO	630	630	-	630
πCCO	610	610	615	615
δCCO	495	500	490	ca. 490
δCCO	440	435	420	255
$\nu (O-O)$		275	-	

Isotopic Shifts at -196°C	$\nu OH/\nu OD$	$\delta OH/\delta OD$	$\gamma OH/\gamma OD$
	1.00(1.41)	1.32	1.34

Figure in brackets refers to 0-1 transition.

Raman spectrum of $KH(OAc)_2$ is included in table 4.1.

The IR spectra at -196°C showed only small changes in breadth and intensity of carboxylate group vibrations. These results can be explained on the basis of a reduction in the number of hot bands.

The IR spectrum of $RbH(OAc)_2$ is similar to that for $NaH(OAc)_2$ and different from $KH(OAc)_2$ in the region of 1700cm^{-1}. The converse is true for the region below 700cm^{-1}. The complete IR spectrum of $RbD(OAc)_2$, on the other hand, is similar to $KD(OAc)_2$ only. An explanation of these results is not easy to find without knowledge of its crystal structure, but it may in some way be connected with the difference in the rate of proton and deuterium tunneling. The reasons for this will become more apparent from data on the monochloroacetic acid system.

The O-H-O Vibrations.

The broad band centred at approximately 1100cm^{-1} in all systems is similar to that observed in the liquid adducts of CCl_3CO_2H with strong bases such as diphenylselenium oxide, triphenylarsine oxide and pyridine oxide (69). The remarkable feature of this band is the insensitivity towards deuteration. Except for a reduction of intensity, no obvious shift occurs. Spectra recorded at -196°C were slightly narrower in band breadth but retain the features of the room temperature spectrum. The transmission window observed in all spectra, associated with Fermi resonance interactions of νC-C with the broad absorption, is more pronounced, however, at -196°C. As pointed out in the introduction, spectra of this type can be accounted for if an asymmetric potential energy well is assumed.

The series of closely related H-bonded anions included in chapters four and five suggests that a series of related potential

energy surfaces exists for the proton motion. The changes in the potential energy wells which occur from one salt to the next must be associated with the change of cation and R group. These seemingly slight changes in physical and chemical characteristics, however, have, at first sight, a dramatic effect on the IR spectrum. Thus, the potential energy well chosen must incorporate as far as possible the changes in the spectral features. Many asymmetric wells can be constructed which are intuitively reasonable but for reasons already outlined and for consistency the model shown in figure 4.4. is the most satisfactory. The assignments which have been made for proton stretching vibrations are not unambiguous since there is no guarantee that the same transition is being compared in the hydrogen and deuterium samples. However, the important point to note is that anomalies such as low isotopic shifts are consistent with asymmetric double minima.

Support for the existence of such a well was obtained from the IR spectra of Na, K and Rb salts of $H(OAc)_2^-$. In $KH(OAc)_2$ only one strong bands at $1100cm^{-1}$ was observed which is likely to be γOH, and is represented by the 0-2 transition. The insensitivity towards deuteration can be accounted for on the basis of reported work (119, 120). Alternative explanations of this band based on crystal effects and bending vibrations can be eliminated since similar features were observed in liquid adducts, and that the bending vibrations were found at their expected frequencies, respectively (74).

Other remarks concerning the spectral consequences of the shape of the well are listed below, and their importance will become apparent on further reading.

(i) The proton is essentially localised in the left hand well with only a slight probability of penetrating the barrier

(ii) Deuteration will reduce further the extent of tunneling.

(iii) The transition 0-1, which occurs as a direct result of (i) and (ii), will be of low intensity in the IR spectrum.

(iv) The potential minimum at each side of the barrier cannot be regarded as being in equivalent positions in relation to the O-O bond.

The Raman spectrum of $KH(OAc)_2$ at room temperature was not studied in detail but it was clear that there was a very broad absorption extending from 1000 - 2000cm^{-1}, the higher frequency being the limit to which the spectrum was recorded. This is comparable with the IR spectrum, and thus an explanation of both spectra based on a symmetric double minimum can be eliminated (the selection rules for the latter case are given in chapter one, fig. 1.6)(33).

The IR spectrum of $RbH(OAc)_2$ is of interest since two strong bands were observed at both room temperature and -196°C. The lower frequency band represents a likely candidate for the 0-1 transition. Assignments other than this can be eliminated by the following arguments:

(i) Candidates for δOH and γOH were found at their expected frequencies.

(ii) Both δOH and γOH are not expected to deviate markedly from a harmonic case in linear H-bonded systems.

(iii) Few overtones and combination bands are expected in the region near 760cm^{-1} in $RbH(OAc)_2$

Figure 4, 4.

Model of Potential Energy Well.

Fig. 4.4

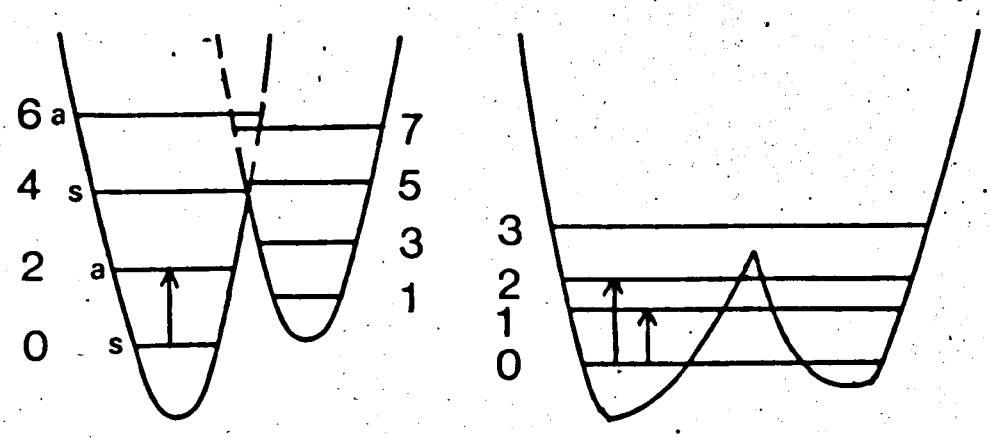

(A) Superposition of two harmonic P.E. wells.

(B) H Bonded system.

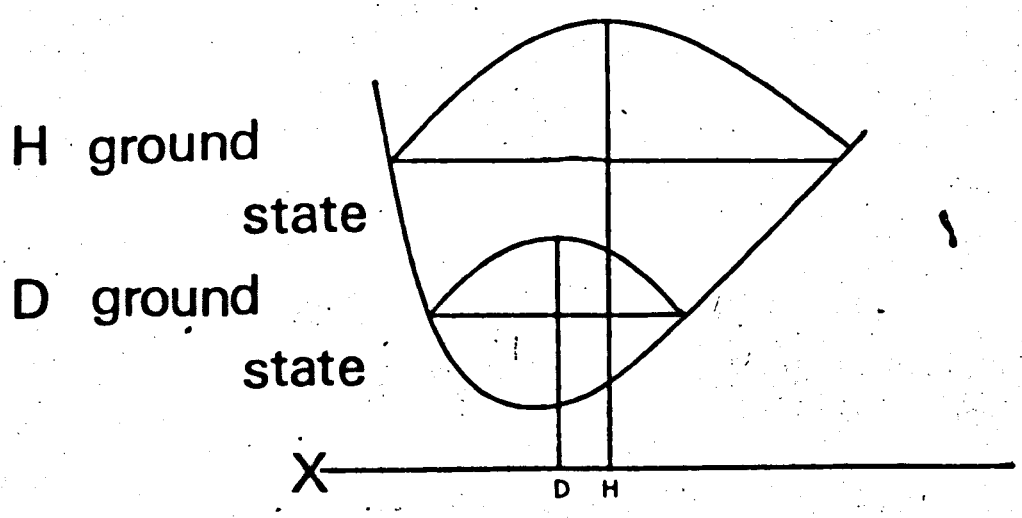

(C) Probability distribution of H and D in ground state.

The IR spectrum of $RbD(OAc)_2$ gave further confirmation of the assignment in table 4.3.

(i) The deuterium analogue of the 760cm^{-1} band is of much weaker intensity.

(ii) The 0-1 transition in $RbH(OAc)_2$ and $RbD(OAc)_2$ was found at similar frequencies in $NaH(OAc)_2$ and $NaD(OAc)_2$, respectively, where the same transition is allowed on rigourous selection rules.

(iii) The 0-2 transition shows the same low isotopic shift as in $KH(OAc)_2$ systems, and is of greater intensity than the 0-1 transition (consistent with greater degree of "left-left" selection rules in $RbD(OAc)_2$).

The failure to find any band corresponding to the 0-1 transition in $KH(OAc)_2$ may simply be indicative of its low intensity. Inelastic neutron scattering (I.N.S.) of cold neutrons by $KH(O_2CCD_3)_2$ indicated a band at 463cm^{-1} which may correspond to the 0-1 transition. The intensity of bands in the latter technique is govered by the extent of proton motion and scattering cross section, and not by the transition moment as in an IR spectrum. However, the energy gain experiment is subject to the Boltzmann distribution law and at room temperature KT is about 200cm^{-1}. It must be emphasised at this stage that the I.N.S. results reported here and elsewhere in chapters four and five are preliminary results and cannot, as yet, be treated as complete. A comparison, however, can be made with data already in the literature. The results of an I.N.S. experiment on KH_2PO_4 indicated a band at 450cm^{-1} which was assigned to the 0-1 transition (figure 4.4) (80). A knowledge of this low frequency band prompted a re-investigation of the IR spectrum in this region (80). The evidence from the IR spectrum was not conclusive in itself, but clearly indicated the

presence of a band in this region other than bands due to the PO_4 modes. The latter was based on the unexpected breadth of the bands associated with PO_4 modes, which were sharper in KD_2PO_4 and also in the nonferroelectric phase of KH_2PO_4. Theoretical calculations by the same workers showed a close approach of theory and experiment when a model similar to that shown in fig. 4.4 was assumed, where the parameters (separation of minima) were adjusted to fit neutron diffraction data (80). The low intensity of the 0-1 transition in the IR spectrum was, therefore, attributed to the small overlap of wavefunctions of the 0 and 1 levels.

The high intensity of the 0-1 transition in the IR spectrum of $RbH(OAc)_2$ can be accounted for by a closer approach of the original unperturbed states in the left and right hand wells. Thus the mean average position of the proton must be nearer to the midpoint between the two oxygen atoms than in $KH(OAc)_2$. Also, a barrier of height comparable to the 0-2 transition with rapid tunneling between two nonequivalent positions is necessary to account for the spectrum obtained. These conditions are intuitively reasonable since the spectrum of $RbH(OAc)_2$ shows features found in both $NaH(OAc)_2$ and $KH(OAc)_2$. The dramatic effect on the IR spectrum when $RbH(OAc)_2$ was deuterated can, therefore, be explained on the basis of an increased probability of finding the deuteron in the left hand well. Further results concerning the latter point will be discussed in the monochloroacetic acid system.

Hadži pointed out that the weak band found at 2400cm^{-1} in the IR spectrum of some liquid H-bonded adducts was probably an overtone of δOH (74). A band of similar frequency was found in both $KH(OAc)_2$ and $RbH(OAc)_2$ in addition to a more intense band at about 2000cm^{-1}.

The higher frequency band disappeared on deuteration but its frequency is in some doubt as it may absorb in the region of 2000cm^{-1} where the residual proton sample absorbs. The deuterium analogue of the 2000cm^{-1} band could not be found.

The explanation given by Hadži accounts for the 2400cm^{-1} band but would leave the 2000cm^{-1} band unaccounted for, unless it also represented another transition from the ground to an excited state. Alternatively, both these bands can be assigned if they are the first overtones of δOH and γOH. This was invoked to explain the trio of bands in some liquid H-bonded adducts, which have already been discussed, where bands of similar frequency were found (69). A clear answer to this question cannot be forwarded with certainty, but in view of the constancy in frequency of both bands above 2000cm^{-1} and the bending vibrations the latter explanation is favoured.

The precise frequencies of the bending vibrations δOH and γOH, in $KH(OAc)_2$ systems are in some doubt owing to the proximity of the broad band associated with νOH. The assignments made, however, are consistent for the following reasons:-

(i) The potential energy wells for the bending vibrations are not expected to differ radically in carboxylic acid systems.

(ii) A bifurcated H-bond can be eliminated since $KH(OFm)_2$ has the same features in the IR spectrum but no evidence of such a bond was found from an X-ray diffraction study (65).

(iii) The isotopic shifts of δOH and γOH are unusually high (ie. greater than 1.41).

The latter point is of interest as it resembles very closely the situation in the $HCrO_2$ system (3). In $HCrO_2$ the isotopic shift of νOH was low, whereas the in-plane-bend shift was 1.44. This was

attributed to the large decrease in the OH bond length on deuteration, which can be considered as a direct result of the asymmetry of the potential energy surface near to the zero point energy state. Details of the $HCrO_2^-$ system can be found in chapter one. Factors such as Fermi resonance interactions may contribute to the apparent isotopic shift in $KH(OAc)_2$ but the similarity with the $HCrO_2^-$ system seems too close for a coincidence. Also, if Fermi resonance interactions were the controlling factor then it is surprising that a high isotopic shift for δOH and γOH was not observed in $RbH(OAc)_2$. The latter system is similar to the $NaH(OAc)_2$ system in that it shows more normal shifts for δOH and γOH and also the 0-1 transition, discussed already, is prominent. Thus the change in the O-H-O bond length in $RbH(OAc)_2$ on deuteration may be smaller than in $KH(OAc)_2$ systems, which emphasises that the potential energy surface in the K and Rb salts are different. A discussion of the difference has already been outlined.

The IR spectrum of $KH(OAc)_2$ and $RbH(OAc)_2$ show a distinct band in the region of 250cm^{-1}. A small shift of the band to lower frequency was observed on deuteration, and, therefore, it seems a likely candidate for the symmetric stretch (table 4.5). The IR spectrum of $KH(OAc)_2$ was recorded down to about 30cm^{-1}, but the extreme breadth and complex structure of the region renders assignments very difficult. The low symmetry of the anion places no restrictions on the activities of H-bond vibrations (table 1.3) and, therefore, together with lattice modes of the potassium ion provides a qualitative explanation of the spectrum observed.

Inelastic neutron scattering experiments on $KH(O_2CCD_3)_2$

indicated the presence of broad bands at 124cm^{-1} and 53cm^{-1}. An assignment cannot be made with certainty, but the 124cm^{-1} band may be a H-bond vibration while the lower frequency band seems a likely lattice mode involving the anion (table 4.5). H-bond vibrations are, in general, motions of the two ends of the anion against each other. Therefore, for groups which do not contain hydrogen atoms, only low intensity bands will be observed in a I.N.S. spectrum. However, the large excess of deuterium atoms present may compensate for the poor scattering cross section (table 4.17). The failure to find the symmetric stretch, which occurs at 250cm^{-1} in the IR spectrum, may simply be because of its low intensity in the I.N.S. spectrum.

TABLE 4, 5.

H-bond frequencies of Acetic Acid (cm^{-1})(123)

mode	C_{2h}	Cylic dimer (Calc)	Cylic dimer (Obs) Vapour	Liq.	Soln.	Glass (-150°C)	Polymer(obs) crystal (-150°C)
ν(OH...O)	Ag	210	-	-	-	-	-
ν(OH...O)	Bu	187	188 168	184	176	186	198
γ(OH...O)	Bu	130	-	-	-	-	126
β(OH...O)	Ag	81	-	-	-	-	-
γ(OH...O)	A_u	79	-	-	-	-	-
Twist	A_u	54	50	-	-	-	82

H-bond frequencies and lattice vibrations of $KH(OAc)_2$(cm^{-1})

Approx. description	$KH(OAc)_2$	$KD(OAc)_2$	$KH(O_2CCD_3)_2$	$KD(O_2CCD_3)_2$
ν(O-H-O)	270 *	250	245	230
L(K)	176 †			
	152			
H-bond vibrations	134 ††		123.8(I.N.S.)	
	116			
CH_3 mode L(Anion)	89			
			52.9(I.N.S.)	

* recorded at -196°C

† remainder recorded at room temperature

†† very broad and complex region with approximate band centres as shown

I.N.S.= Inelastic neutron scattering data (121)

L(K) = translational motion of potassium

L(anion) = translational motion of anion.

5. Hydrogen Di-monochloroacetate Anion, $H(OMC)_2^-$

Assignments of the vibrational spectrum of K and Rb salts are shown in tables 4.6 and 4.7. The frequencies of the vibrations were located by comparison with published spectra (116, 131), and spectra are reproduced at the end of this chapter. In general, the spectra were similar to their acetic acid analogues except for differences associated with the chlorine atom substitution. Thus similar remarks can be made with regard to the insensitivity towards deuteration, the intensity of the 0-1 transition, and difficulty in locating the bending vibrations of the proton in $KH(OMC)_2$. The spectrum of $RbH(OMC)_2$ is similarly analagous to $RbH(OAc)_2$, and likewise in the effect of deuteration.

The far infrared spectrum of salts containing $H(OMC)_2^-$ and $D(OMC)_2^-$ were recorded and details are shown at the end of this chapter (table 4.16). Although insufficient data is available for a complete assignment the results, in general, parallel those expected on the basis of selection rules. For example, the spectra of $KH(OMC)_2$ and $KD(OMC)_2$ show strong bands in the region of 150 - 200 cm^{-1} which must be associated with H-bond vibrations and translational motion of the cation in the lattice. The spectrum of $CsH(OMC)_2$ and $CsD(OMC)_2$ is much simpler in the same region and is consistent with a near approach of the anion to a C_i point group and to the lower frequency of the lattice mode. The spectrum of $RbH(OMC)_2$ is similar to that of $CsH(OMC)_2$, but has bands of low intensity in this region. However, the complex structure of the 150-200 cm^{-1} region in $RbD(OMC)_2$ is consistent with a much lower symmetry for the latter as compared with $RbH(OMC)_2$. The trends, therefore, are similar to those seen in the higher frequency region.

TABLE 4, 6.

Assignment of Vibrational Spectrum of $KH(OMC)_2$, (cm^{-1}).

Approx. description	$KH(OMC)_2$		$KD(OMC)_2$	
	25°C	-196°C	25°C	-196°C
ν CH_2	3025, 2944	-	3025, 2945	-
ν CH_2	3015, 2960	-	3015, 2962	-
overtone	-	-	-	-
ν C=O	1680	1690	1645	1640
ν_{as} COO	1645	1642	1602	1603
δ CH_2	1402, 1272	1405, 1272	1400, 1272	1402, 1273
δ CH_2	1395, 1264	1394, 1264	1400, 1264	1400, 1265
ν_s COO	1355	1375	1390	1370
ν CO	1330	1337	1380	1370
CH_2 wag	1182	1184	1180	1185
CH_2 twist	-	-	1245	1248
δ OH(D)	-	-	870	880
0-2 transtn	1100	1070	ca 1000	ca 1000
0-1 transtn	585 (I.N.S.)			
γ OH(D)	-	970	675	680
CH_2 rock	910	914	-	935
ν CC	932	936	938	940
ν CC			932	935
ν CCl	770	770	768	768
ν CCl				
δ COO	730	721	720	720
δ COO	685	700	670	670
π COO	570	585	580	582
π COO		572	565	570
δ CCO	425	445	425	426
δ CCO		426		

Isotopic Shifts at -196°C	νOH/νOD	δOH/δOD	γOH/γOD
	1.07	-	1.43

TABLE 4, 7.

Assignment of Vibrational Spectrum of $RbH(OMC)_2$ (Cm^{-1})

Approx. description	$RbH(OMC)_2$		$RbD(OMC)_2$	
	25°C	-196°C	25°C	-196°C
νCH_2	-	-	3018, 2945	-
νCH_2	-	-	3008, 2955	-
overtone	-	-	-	-
$\nu C{=}O$	1730	1730	1640	1640
$\nu_{as} COO$	1730	1730	1602	1607
δCH_2	1416	1418	1400, 1268	1400, 1270
δCH_2	1408	1407	1400, 1268	1400, 1270
$\nu_s COO$	-	1370	1390	1390
νCO		1370	1375	1370
CH_2 wag	1200 region	1215, 1172	1238	1240
CH_2 twist	-	-	1257	1260
δ OH(D)	1220 region	1235	860	865
O-2 transtn	1000	1000	1050	1000
O-1 transtn	800	800	-	-
γ OH(D)	-	ca 950	675	685
CH_2 rock	920	930	930	930
ν CC	935	930	935	936
ν CC			927	928
ν CCl	787	788	761	762
ν CCl				
δ COO	730	725	715	720
δ COO	645	650	675	682
π CCO	560	555	580	580
π CCO			560	562
δ CCO	410	420	440	440
δ CCO			420	422

Isotopic Shifts at -196°C	νOH/νOD	δOH/δOD	γOH/γOD
	1.00	1.42	1.39

Inelastic neutron scattering data on $KH(OMC)_2$ indicated bands at 585, 161 and 22cm^{-1}. The high frequency band can be assigned to the 0-1 transition and remarks concerning it are analogous to those in the $KH(O_2CCD_3)_2$ system. The 161cm^{-1} band is close to the broad absorption seen in the far-IR spectrum and, therefore, seems a likely candidate for a H-bond vibration. The low frequency band cannot be assigned with certainty since secondary evidence from the far-IR spectrum was masked by absorption from the polythene discs. However, the low frequency band may be a lattice mode involving the anion.

NQR spectra were recorded for these compounds since ^{35}Cl has a quadrupole moment. The results are tabulated in table 4.8 along with a stick diagram representation. The nonequivalence of the two carboxylate groups can be readily seen, with the low frequency signal corresponding to the more ionised group and the high frequency signal to the acid group. The difference in frequency of the two signals can be attributed to several factors:

(i) A difference in charge density on each carboxylate group.

(ii) A difference in conformation of the CH_2Cl group with respect to the COO plane.

(iii) A difference in probability of finding the proton in the left and right-hand well.

Thus in $KH(OMC)_2$ and $RbH(OMC)_2$ the signal from each ^{35}Cl nuclei at each end of the anion is averaged over the two extreme positions of the proton motion. Since the ^{35}Cl nuclei in the acid and base parts of the anion are crystallographically different the average signal for each will be different. Deuteration will, however, reduce the extent of tunneling and thus the deuteron will be relatively

more localised in the left-hand well. The effect of the latter will change the frequency of the average signal for each ^{35}Cl nuclei, and thus an increased separation of the signals. Superimposed on the latter mechanism will be the increase in the O--O bond length which is a direct consequence of the asymmetry of the well near the ground state. Also the close approach of the two signals in $RbH(OMC)_2$ as compared with that in $KH(OMC)_2$ is analogous to the intermediate character of its IR spectrum. The NQR data for $CsH(OMC)_2$ and $CsD(OMC)_2$ is also tabulated and shows that, as far as NQR is concerned, the anion is symmetrical. However, since the lifetime of excited states in NQR transition is much longer than in IR spectroscopy the equivalence of the two ^{35}Cl nuclei in $CsH(OMC)_2$ and $CsD(OMC)_2$ indicates extremely rapid tunneling between two equivalent positions in both or a genuine sy metric H-bond with no tunneling. A discussion of this point is deferred until chapter five.

TABLE 4.8

^{35}Cl resonance on $H(OMC)_2^-$ systems at 77^oK

Table 4.8

^{35}Cl NQR Spectra of $H(OMC)_2^-$ Systems (Mc/s)

Compound	Frequency	34·7	35·1	35·5	35·9	36·3	36·7
NaOMC	34.794 (126)						
HOMC	36.131 36.429 (126)						
DOMC	36.152, 36.440						
$KH(OMC)_2$	34.790, 35.870						
$KD(OMC)_2$	34.623, 36.035						
$RbH(OMC)_2$	34.930, 35.720						
$RbD(OMC)_2$	34.615, 35.985						
$CsH(OMC)_2$	34.970						
$CsD(OMC)_2$	34.970						

6. Hydrogen Di-dichloroacetic Anion, $H(ODC)_2^-$

The assignments of the vibrational spectrum of the salts containing $H(ODC)_2^-$ are shown in tables 4.9 and 4.10, and are based on those published for the carboxylate ion (116). The assignments of the bands associated with carboxylate group vibrations in the K and Rb salts of $H(ODC)_2^-$ and $D(ODC)_2$ parallel those in previous systems. However, the trend observed in previous systems, viz. increase in intensity of 0-1 transition in going from $KH(OAc)_2$ to $RbH(OAc)_2$, is not evident in the $H(ODC)_2^-$ system. It may be that the 0-1 transition is extremely weak in the IR spectrum. However, inelastic neutron scattering data on $KH(ODC)_2$ indicated a band at $306cm^{-1}$ which is tempting, at first sight, to assign to the 0-1 transition. However, the band is more likely to be due to motion of the four chlorine atoms since several bands were observed at $300cm^{-1}$ in the IR spectrum. Although chlorine atoms scatter neutrons poorly, the fact that four chlorine atoms are present, and also that motion of each $CHCl_2$ group implies some motion of a hydrogen may account for the band at $306cm^{-1}$. The origin of the remaining bands seen in the I.N.S. spectrum (124, $48cm^{-1}$) is not certain. However, the similarity with previous systems suggests analogous assignments (table 4.16 and 4.17).

Results from NQR experiments are tabulated in table 4.11. Conformational effects become more important in this system since two signals arise from each carboxylate group. For an isolated carboxylate group two extreme conformations are possible:

TABLE 4. 9.

Assignment of Vibrational Spectrum of $KH(ODC)_2$, (cm^{-1})

Approx. description	$KH(ODC)_2$		$KD(ODC)_2$	
	25°C	-196°C	25°C	-196°C
ν CH	3015	3015	3017	3015
ν CH	2968	-	2968	-
overtone	2450	2450, 2000	-	-
ν C=O	1740	1738	1718	1715
ν_{as} COO	1675	1675	1662	1670
δ CH	1230	1235	1232	1228
δ CH	1190	1185, 1205	1194	1195, 1205
ν_s COO	1385	ca 1380	1385	1380
ν CO	1280	1300	1345	1347
δ OH(D)	1280	1260	-	850
ν OH(D)	1180	1150	1100	1100
ν CC	920	930	940	950
ν CC		924	920	900
γ OH(D)	-	-	710?	700?
ν CCl_2	820	830, 822	822	831, 825
ν CCl_2	795	799	793	800, 795
δ COO	728	732	710	718
δ COO	705	705	680	685
π CCO	615	615	613	611
π CCO				
δ CCO	535	537	525	528
δ CCO	489	490	480	480
δ CCl_2	325, 305	330, 308	325, 305	328, 308
δ CCl_2	280, 250	282, 250	-	278, 252
CCl_2 mode	425	430	420	430

Isotopic Shift at - 196°C	νOH/ν OD	δOH/δ OD	γOH/γ OD
	1.04	1.48	-

TABLE 4, 10.

Assignment of Vibrational Spectrum of $RbH(ODC)_2$, (cm^{-1})

Approx. description	$RbH(ODC)_2$		$RbD(ODC)_2$	
	25°C	-196°C	25°C	-196°C
ν CH	3010		3005	3010
ν CH				
overtone	2390			
ν C=O	ca 1700	1680	1655	1685, 1665
ν_{as} COO	1660	1660		1640
δ CH	1238	1240	1235, 1218	1240, 1225
δ CH	1225	1230	1190, 1185	1195, 1190
ν_s COO	1365	1380	1360	1370
ν CO	1330	1340		
δ OH(D)	1270	1280	860	870
ν OH(D)	1150	1150	1050	1050
ν CC	925	925	920	925
ν CC	918	920	880	890
γ OH(D)	970?	970?	670?	675?
ν CCl_2	822, 813	825, 815	815, 810	822, 810
ν CCl_2	770, 715	770, 720	765, 705	770, 710
δ COO	700 region	700 region	-	-
δ COO				
π CCO	640	645	635	640
π CCO	620	610	612	610
δ CCO	428	430	420	425
δ CCO	385	390	370	370
δ CCl_2	-	295		
δ CCl_2	-			

Isotopic Shift at -196°C	νOH/νOD	δOH/δOD	γOH/γOD
	1.10	1.47	1.43

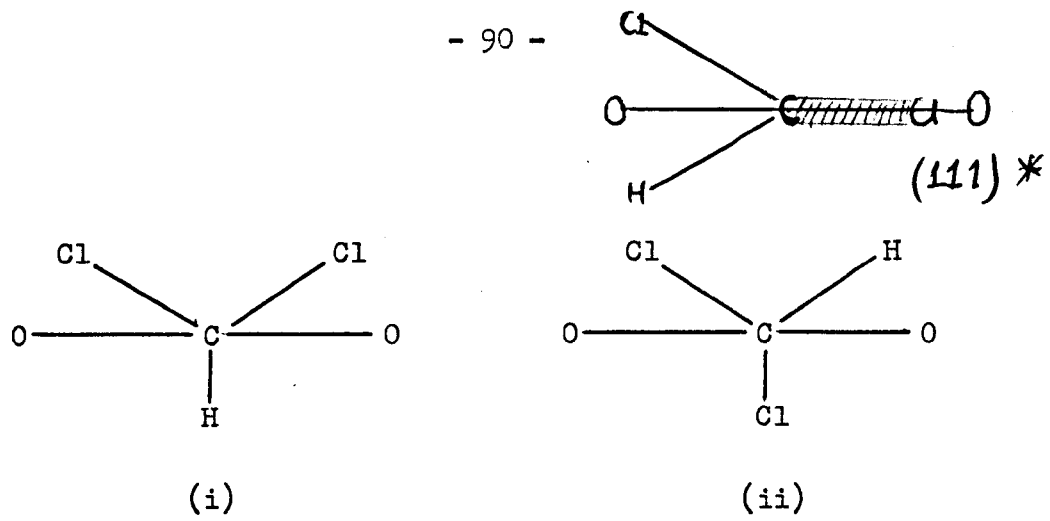

(111) *

(i) (ii)

In figure (i) each ^{35}Cl nuclei is equivalent with respect to the COO plane, since there isan equal charge density on each oxygen atom. Thus only one ^{35}Cl signal will be observed in case (i). In figure (ii), on the other hand, the different positions of the two nuclei with respect to the oxygen atoms renders a nonequivalence of the ^{35}Cl nuclei as seen by NQR. Thus two signals are possible in case (ii). An unequal charge density on each oxygen atom will also give rise to two signals. Other factors such as the arrangement of the ions in the crystal lattice will complicate the issue even further, and, therefore, without knowledge of crystal data the amount of information derived from NQR data alone is limited.

The data shown in table 4.11 emphasises some of the points already seen in the $H(OMC)_2^-$ system and also some of the uncertainties concerning the steriochemistry in the present system. Thus whether or not the two signals seen for KODC means a type (ii) structure or two different sites in the unit cell is difficult to answer from NQR data alone. Fortunately, the IR spectrum of KODC suggests type (ii) since,according to Spinner, such a conformation leads to a large splitting of the two CCl_2 modes as compared with a small splitting

*(111) Molecular Constants from Microwave Spectroscopy, Gp II, Vol IV D Starck, Springer-Verlag 1967.

in a type (i) structure (116). The large splitting of the CCl_2 modes together with the appearance of only one band associated with $\nu_{as}COO$ in the IR spectrum of KODC and also the appearance of two NQR signals seems, therefore, good evidence for a type (ii) structure in KODC.

The NQR data on $KH(ODC)_2$ seems to indicate a type (i) structure for the more carboxylate group of the anion, which is also evident from the IR spectrum where the CCl_2 modes of the carboxylate are close together. The $RbH(ODC)_2$ system shows marked differences to that of the $KH(ODC)_2$ system in both the NQR and IR spectrum. The large separation of the two low frequency signals and CCl_2 modes in the NQR and IR spectrum, respectively, indicates a structure more like type (ii) for the more ionised moiety of the anion in $RbH(ODC)_2$. The effect of the H-bond linking the two carboxylate groups will clearly influence the separation of each set of NQR signals, but whether or not the separation increases or decreases will depend on the exact conformation of the $CHCl_2$ groups. Thus the latter point is particularly important for the more acid carboxylate group, and even a comparison of IR and NQR data is not sufficient to establish the steriochemistry. However, the one thing that is clear is that both $CHCl_2$ groups in each anion are not rotating freely, since in such a situation only one signal for each $CHCl_2$ group would have been observed at a frequency lower than those in table 4.10.

The shift of the NQR signals on deuteration is not as easily explained as in the $H(OMC)_2$ system. From the IR data it is likely that the deuteron is localised more than in the proton case. The latter by itself is sufficient to alter the frequencies of the NQR signals.

TABLE 4.11

^{35}Cl resonance on $H(ODC)_2^-$ systems at 77^oK

Table 4.11

Compound	Frequency
KODC	36.40, 36.65
HODC	38.807, 37.979 (126)
$KH(ODC)_2$	36.980, 36.995, 37.500, 38.960
$KD(ODC)_2$	36.870, 36.995, 37.680, 39.080
$RbH(ODC)_2$	36.255, 37.715, 38.030, 38.72
$RbD(ODC)_2$	36.160, 37.83, 38.22, 38.63

^{35}Cl NQR Spectra of $H(ODC)_2^-$ Systems (Mc/s)

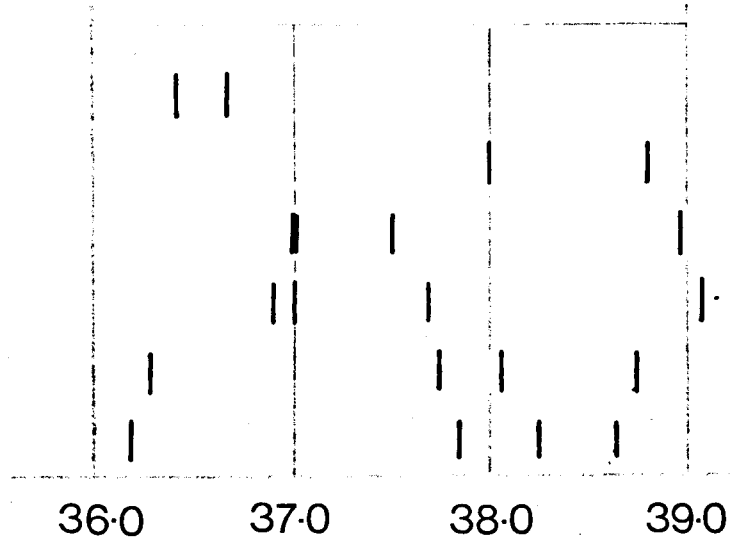

7. Hydrogen Diformate Anion, $H(OFm)_2^-$

Recent X-ray diffraction data on $KH(OFm)_2$ has shown that the salt crystallises in an orthorhombic system and space group Pbca with eight molecules in the unit cell (65). The anion was shown to contain nonequivalent formate groups and, therefore, is a member of the Type B hydrogen dicarboxylates with each carboxylate group linked by a short H-bond (2.45A°).

Although the H-bond in $KH(OFm)_2$ and $RbH(OFm)_2$ contain the simplest anion possible in hydrogen dicarboxylate systems, the same cannot be regarded of their IR spectrum (tables 4.12 and 4.13). This is primarily because the extreme breadth of all bands in the spectrum masks much of the detail even at -196°C. In general, however, the spectra were similar to previous systems, particularly with regard to the low isotopic shift of the 1100cm^{-1} band and also to the difficulty in finding δOH and γOH.

Similar remarks can be made to the origin of the 620cm^{-1} band which is very prominent at -196°C and which has a low intensity deuterium analogue (430cm^{-1}).

Inelastic neutron scattering data did not reveal with certainty a band analogous to the 620cm^{-1} band found in the IR spectrum. However, this may be due to the fact that detection of bands in this region using cold neutrons is difficult experimentally. Also, the high frequency of the band does not favour a reasonable population of the excited state and thus neutron energy gain.

The IR spectrum of $KH(OFm)_2$ below 200cm^{-1} was extremely broad and similar to that observed for $KH(OAc)_2$. However, the ill defined structure renders an assignment impossible at this stage. Inelastic

neutron scattering data indicated bands at 170cm^{-1} and 62cm^{-1} which are comparable in frequency to those in previous systems and thus may have analogous assignments. The complexity of the low frequency region as seen by an IR spectrum is, however, consistent with the low symmetry of the anion. Details of both far-infrared and neutron scattering results are shown in tables 4.16 and 4.17, respectively.

TABLE 4. 12.

Assignment of Vibrational Spectrum of $KH(OFm)_2$, (cm^{-1})

Approx. description	$KH(OFm)_2$	$KD(OFm)_2$	
	25°C	25°C	-196°C
ν CH	-	2870	-
ν CH	-	2770	-
overtone	-	-	-
ν C=O	1720, 1670. 1645	1670, 1630	1665, 1625
ν_{as} COO	ca 1550	1530	1520
δ CH	)	)	)
	)1400	) 1400	) 1400
δ CH	)	)	)
ν_s COO	1350	1360	-
ν CO	1320	1330	1320
δ OH(D)	masked	masked	masked
O-2 transition	1050	1050	1050
O-1 transition	620	-	430
ρ CH	)masked by	-	-
ρ CH	)broad absor-	-	-
γ OH(D)	)ption at 1050	-	-
δ COO	800?	795	790
δ COO	650	660	660
ν (OO)	350	350	350

Isotopic shift	O-2(H)/O-2(D)	O-1(H)/O-1(D)
	1.00	1.44

TABLE 4, 13.

Assignment of Vibrational Spectrum of $RbH(OFm)_2$, (cm^{-1})

Approx. description	$RbH(OFm)_2$		$RbD(OFm)_2$	
	25°C	-196°C	25°C	-196°C
ν CH	2860	-	-	-
ν CH	2700	-	2775	-
overtone	-	2390	-	-
ν C=O	1650	1720, 1660, 1640	1650	ca 1650
ν_{as} COO	1530	1530	1560	1560
δ CH	1400	1395		1400
δ CH				
ν_s COO	1362	1370		1355
ν CO	1310	1305		1335
δ OH(D)		1220	masked	masked
0-2 transition	very broad absorbtion with centres at 1200, 1150	1050	1060	1080
0-1 transition		600	430	430
ρ CH				
ρ CH				
γ OH(D)		900	670	675
δ COO	800?	810?		
δ COO	660	670	670	675
ν (OO)	360	380		380

Isotopic shift	0-2	0-1	γOH/γOD
	1.00	1.40	1.33

8. Hydrogen Di-difluorochloroacetate Anion, $KH(ODFC)_2^-$

The potassium salt was prepared but detailed assignments of its IR spectrum could not be made because of the strong absorption from the CF_2Cl group. However, the insensitivity of the spectrum towards temperature, and the similarity with the spectrum of $RbH(OAc)_2$ and $RbD(OAc)_2$ suggests analogous assignments. It is also of interest to note that the region below $1000cm^{-1}$ is more intense in both $KH(ODFC)_2$ and $KD(ODFC)_2$ than in previous systems. This must reflect the near symmetric nature of the H-bond in $KH(ODFC)_2$ which was also suggested by NQR data. The NQR spectrum of $KH(ODFC)_2$ showed a close doublet, and, therefore, confirms its asymmetric character. Further details of the NQR work are shown below in table 4.14:

TABLE 4.14.

KODFC	Multiple bands in the region of 36.00 Mc/s
HODFC	37.485
$KH(ODFC)_2$	36.275, 36.510

9. Experimental

(a) Reagents

Anala R Sodium and Potassium Carbonates were obtained from Hopkin and Williams

G.P.R. grade Rubidium and Caesium Carbonates were obtained from British Drug Houses

Spectroscopic Acetic acid (D_4) was obtained from Ciba.

G.P.R. grade Monochloroacetic acid was obtained from May and Baker.

G.P.R. grade Chlorodifluoroacetic acid was obtained from Aldrich

Details of the remaining materials used are recorded in chapters two and three.

(b) Preparations

The acid salts were prepared by dissolving half an equivalent of the metal carbonate in a small amount of hot water and adding one equivalent of the acid. The solutions were allowed to stand in a desciccator, during which time the acid salt slowly crystallised out of solution. The compound was then allowed to stand in a vacuum desciccator under slightly reduced pressure to assist the removal of last traces of water. The deuterium analogues were crystallised twice out of deuterium oxide.

(c) Analytical data is shown in table 4.15

TABLE 4, 15.

Analytical Data.

Compound	Acid%		Elemental							
			Cation		C		H		Haloren	
	Exp.	Theor.	Exp.	Theor.	Exp.	Theor.	Exp.	Theor.	Exp.	Theor.
$KH(OFm)_2$	33.81	35.36	-	-	18.06	18.45	2.55	2.32	-	-
$KH(OAc)_2$	35.92	37.95								
$RbH(OAc)_2$	30.75	29.35								
$KH(OMC)_2$	40.91	41.61			20.93	21.15	2.32	2.24	30.77	31.22
$RbH(OMC)_2$					19.69	17.56	2.53	1.84	29.10	25.93
$KH(ODC)_2$	42.50	43.56			15.92	16.23	1.41	1.03	47.12	47.91
$RbH(ODC)_2$			25.02	24.96	14.11	14.03	1.08	0.88	41.54	41.42
$KH(ODFC)_2$					16.40	16.06	0.17	0.33	F24.06	23.70
									25.69	25.41

TABLE 4.16

Far Infrared Data

Far Infrared Data and their Vibrational Assignments

Compounds	Bands (cm^{-1}) Observed ($300^{o}K$)	Possible Assignment (approx. description)
$KH(OAc)_2$	176	Translational motion of K
	152	H-bond Vibrations
	134	H-bond Vibrations
	116	H-bond Vibrations
	89	CH_3 mode (103)
	50	Translational motion of Anion?
$KH(OFm)_2$	Very broad absorption extending from 60 240	H-bond vibrations and lattice modes (translational)
KOMC	Very broad and complex structure from 60-240	Lattice modes, low frequency CH_2Cl modes
$KH(OMC)_2$	Distinct bands at:	
	165	H-bond vibrations and CH_2Cl modes
	155	H-bond vibrations and CH_2Cl modes
	115	H-bond vibrations and CH_2Cl modes
	95	H-bond vibrations and CH_2Cl modes
	50	Lattice mode (Anion)
$KD(OMC)_2$	182	Lattice mode (K)
	158	H-bond vibration and CH_2Cl modes
	115	H-bond vibration and CH_2Cl modes
	88	H-bond vibration and CH_2Cl modes
	50	Lattice mode Anion
	38	Lattice mode Anion
$RbH(OMC)_2$	150	H-bond vibration
	140	Lattice Mode (Rb)
	110	H-bond vibration
	92	
	40	Lattice mode (Anion)
$RbD(OMC)_2$	200 (very broad)	CH_2Cl modes, H-bond vibrations and Lattice Modes (Rb)
	137 (very broad)	CH_2Cl modes, H-bond vibrations and Lattice Modes (Rb)
	100 (very broad)	CH_2Cl modes, H-bond vibrations and Lattice Modes (Rb)
	95 (very broad)	CH_2Cl modes, H-bond vibrations and Lattice Modes (Rb)

TABLE 4.16 continued

Compound	Bands (cm^{-1}) observed ($300^{o}K$)	possible Assignment (approx. description)
$CsH(CHC)_2$	200	CH_2Cl mode
	98	Lattice mode (Cs)
	88	
	44	Lattice Mode (Anion)
	30	
$CsD(OMC)_2$	230	CH_2Cl modes
	205	
	195	Background absorption
	156 very weak	
	144 very weak	
	112	Lattice Mode (Cs)
	88	
	58	Lattice mode (Anion)
	44	
	34	

TABLE 4.17

Inelastic Neutron Scattering Data

Inelastic Neutron Scattering Data (121)

Time-of-Flight of energy gain neutrons (cold)

(Experiments conducted by Dr. F. Temme)

Sample	E (mev)	E(cm^{-1})	Approx. Description
$KH(OFm)_2$	21.06	169.9	H-bond vibration
	7.63	61.5	Lattice Mode(Anion)
$KH(O_2C.CD_3)_2$	57.36	462.9	0-1 transition in H-bond
	15.30	123.8	H-bond vibration
	6.56	52.9	Lattice Mode(Anion)
$KH(OMC)_2$	72.53	585.3	0-1 transition in H-bond
	19.94	160.9	H-bond vibration
	2.66	21.5	Lattice Mode(Anion)
$KH(ODC)_2$	37.9	305.8	$CHCl_2$ mode
	15.30	123.8	H-bond vibration
	5.92	47.8	Lattice Mode(Anion)

Neutron Scattering Data for some elements and isotopes (127)

Element	Specific Nucleus	Nuclear Spin	Neutrons b (10^{-12}cm)	$\mathcal{S}$ (barns)	σ (barns)
H	^{1}H	$\frac{1}{2}$	-0.378	1.79	81.5
	^{2}H	1	0.65	5.4	7.6
C	^{12}C	0	0.661	5.50	5.51
O	^{16}O	0	0.557	4.2	4.24
F	^{19}F	$\frac{1}{2}$	0.55	3.8	4.0
Cl	^{35}Cl	$^{3}/_{2}$	6.99	12.2	15.0
	^{37}Cl				

b Scattering amplitude in units of 10^{-12}cm

$\mathcal{S}, \sigma$ are the coherent and total scattering cross sections, respectively, in units of $10^{-24}cm^{2}$ (ie. barns)

SPECTRA

C O N T E N T S

All spectra have been recorded at -196°C unless specifically stated to the contrary. Far IR and Raman Spectra were all recorded at room temperature. Nujol mulls have been used throughout and H.C.B. was used for the regions between 3000 - 2800cm^{-1} and 1500 - 1300cm^{-1}.

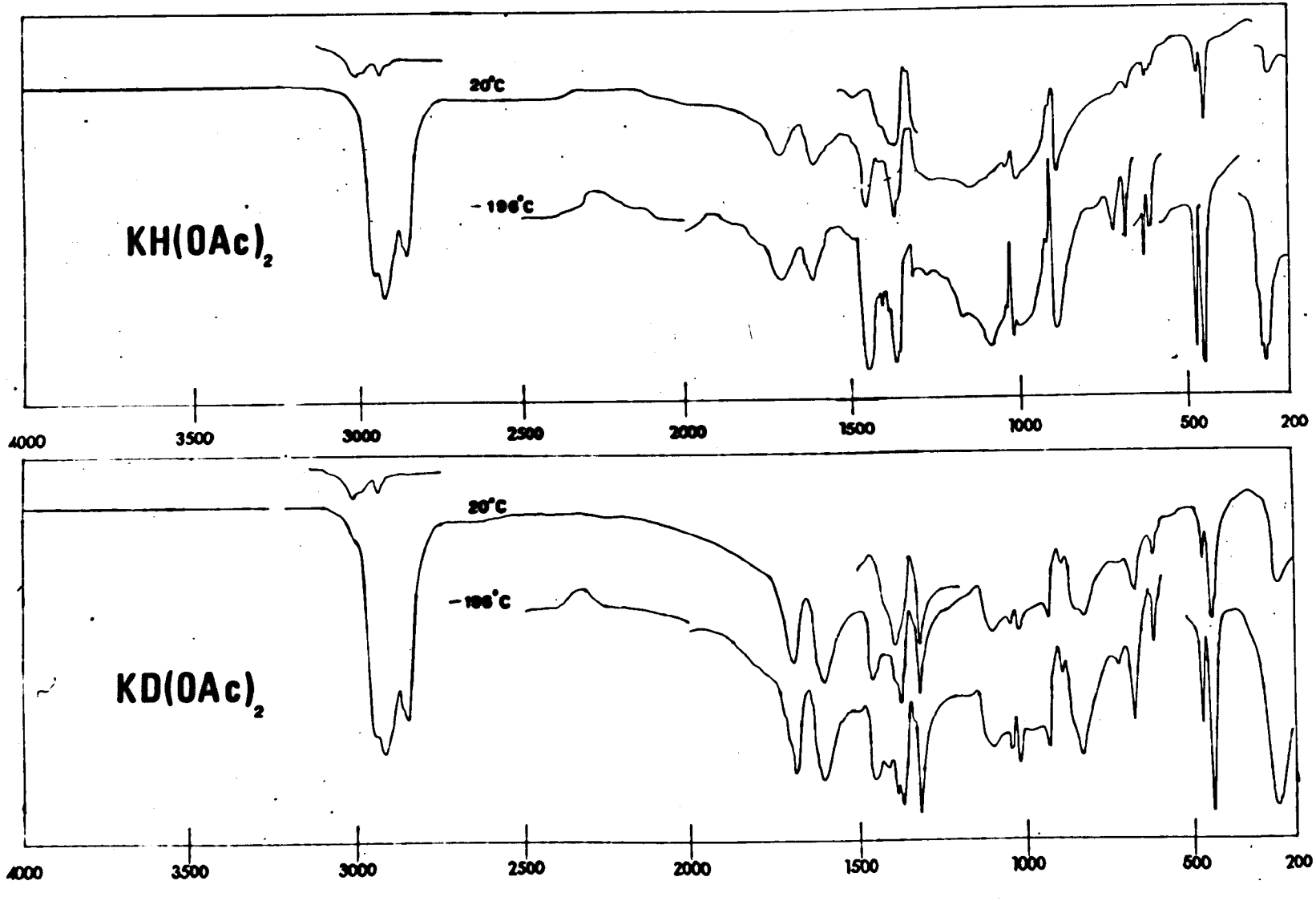
20°C
-196°C
KH(OAc)2
4000
3500
3000
2500
2000
1500
1000
500
200
20°C
-196°C
KD(OAc)2
4000
3500
3000
2500
2000
1500
1000
500
200

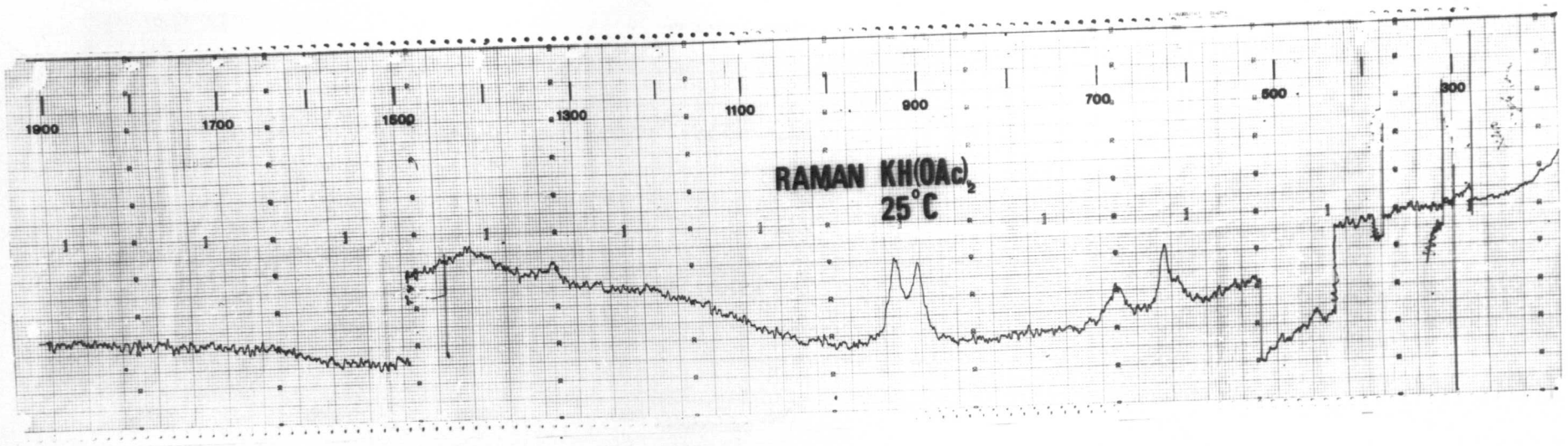
1900
1700
1500
1300
1100
900
700
500
300
RAMAN KH(OAc)2
25°C

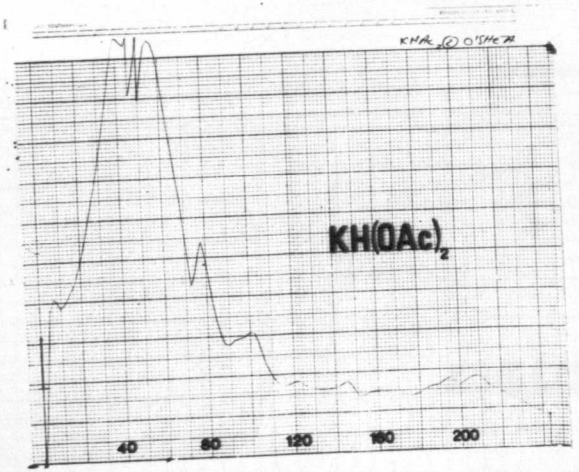
KH(OAc)2
40
60
120
160
200

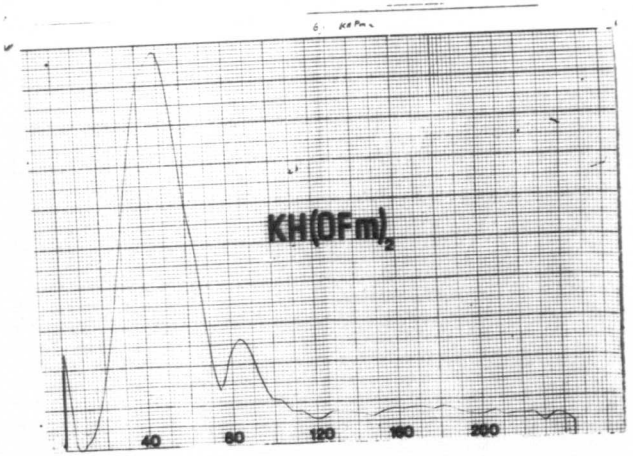
KH(OFm)2
40
60
120
160
200

B

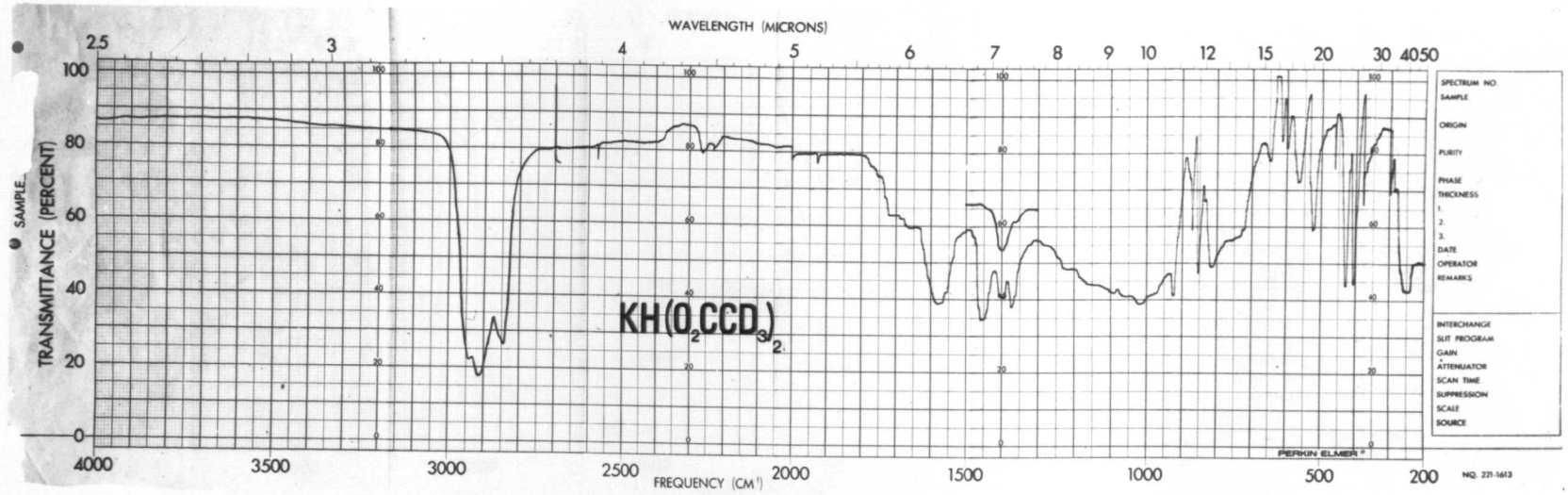
WAVELENGTH (MICRONS)
2.5
3
4
5
6
7
8
9
10
12
15
20
30
40
50
TRANSMITTANCE (PERCENT)
SAMPLE
100
80
60
40
20
0
4000
3500
3000
2500
2000
1500
1000
500
200
FREQUENCY (CM⁻¹)
KH(O2CCD3)2
PERKIN ELMER
NO. 221-1613
SPECTRUM NO.
SAMPLE
ORIGIN
PURITY
PHASE
THICKNESS
1.
2.
3.
DATE
OPERATOR
REMARKS
INTERCHANGE
SLIT PROGRAM
GAIN
ATTENUATOR
SCAN TIME
SUPPRESSION
SCALE
SOURCE

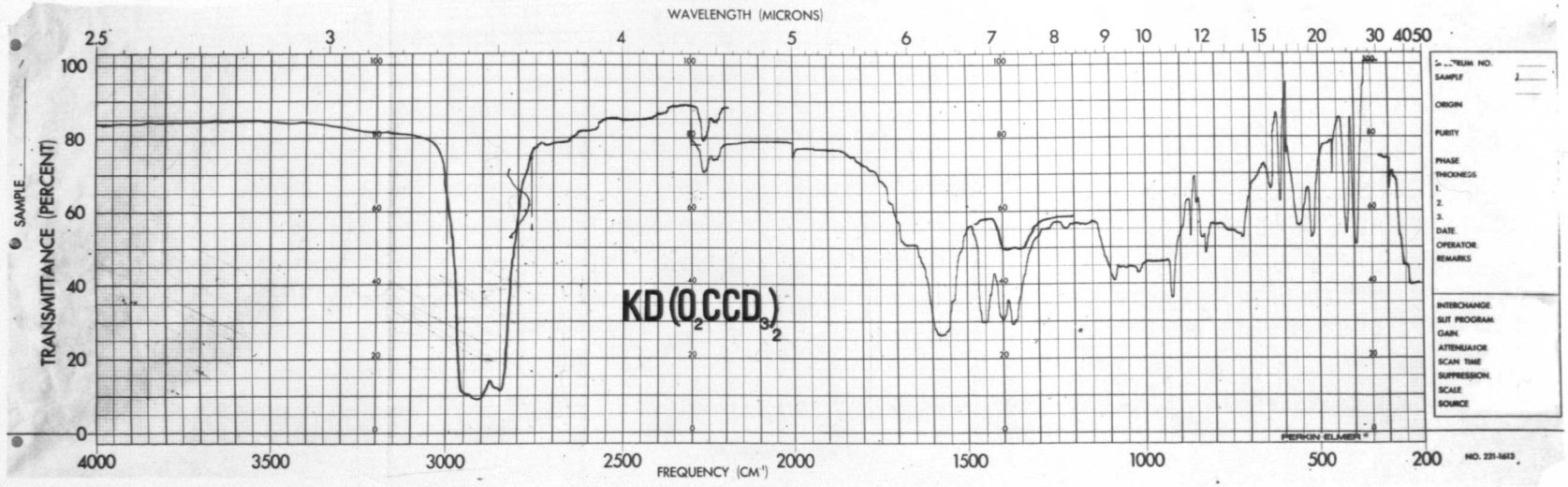
WAVELENGTH (MICRONS)
2.5
3
4
5
6
7
8
9
10
12
15
20
30
40
50
TRANSMITTANCE (PERCENT)
SAMPLE
100
80
60
40
20
0
4000
3500
3000
2500
2000
1500
1000
500
200
FREQUENCY (CM⁻¹)
KD(O2CCD3)2
PERKIN ELMER
NO. 221-1613
SPECTRUM NO.
SAMPLE
ORIGIN
PURITY
PHASE
THICKNESS
1.
2.
3.
DATE
OPERATOR
REMARKS
INTERCHANGE
SLIT PROGRAM
GAIN
ATTENUATOR
SCAN TIME
SUPPRESSION
SCALE
SOURCE

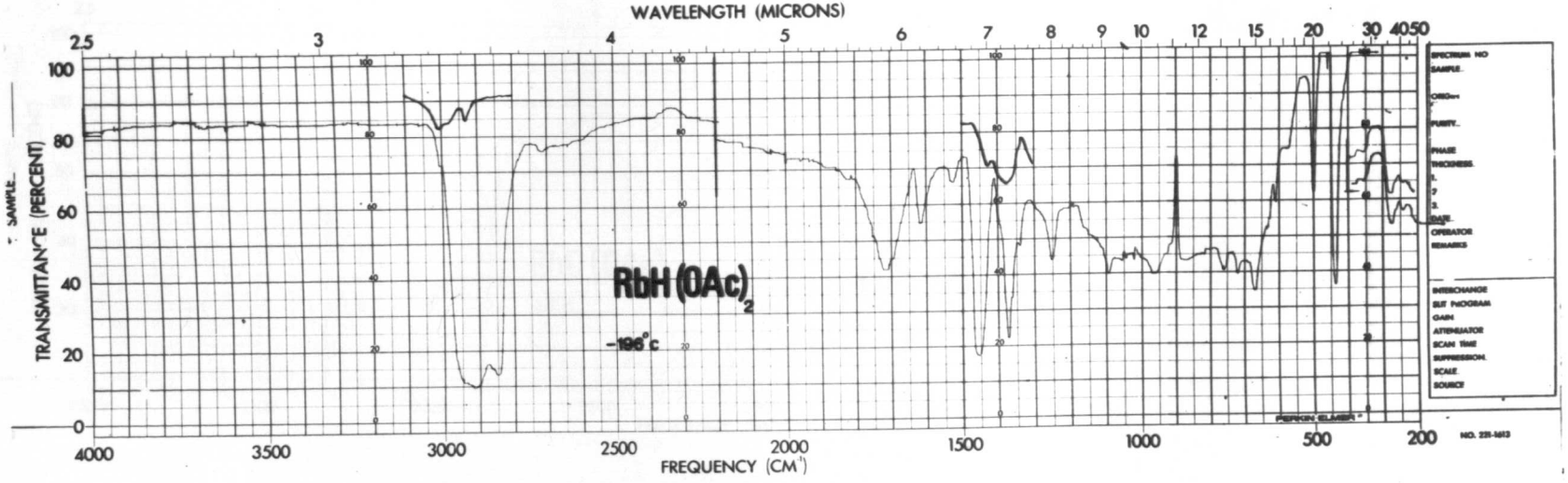
WAVELENGTH (MICRONS)
2.5
3
4
5
6
7
8
9
10
12
15
20
30
40
50
TRANSMITTANCE (PERCENT)
100
80
60
40
20
0
RbH(OAc)2
-196°C
4000
3500
3000
2500
2000
1500
1000
500
200
FREQUENCY (CM-1)

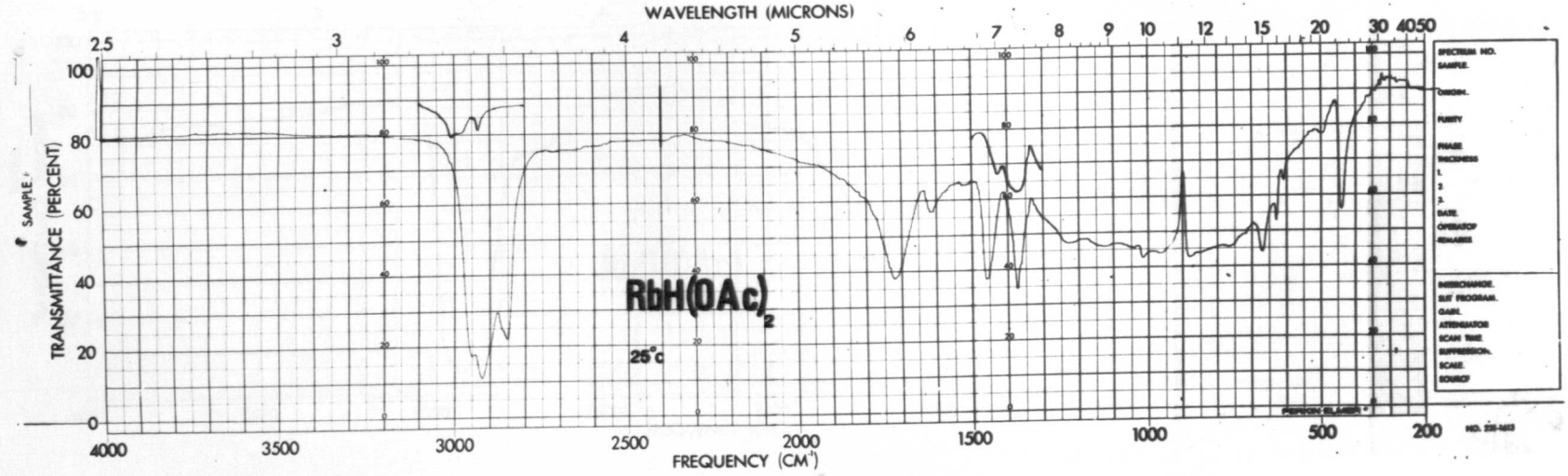
WAVELENGTH (MICRONS)
2.5
3
4
5
6
7
8
9
10
12
15
20
30
40
50
TRANSMITTANCE (PERCENT)
100
80
60
40
20
0
RbH(OAc)2
25°C
4000
3500
3000
2500
2000
1500
1000
500
200
FREQUENCY (CM-1)

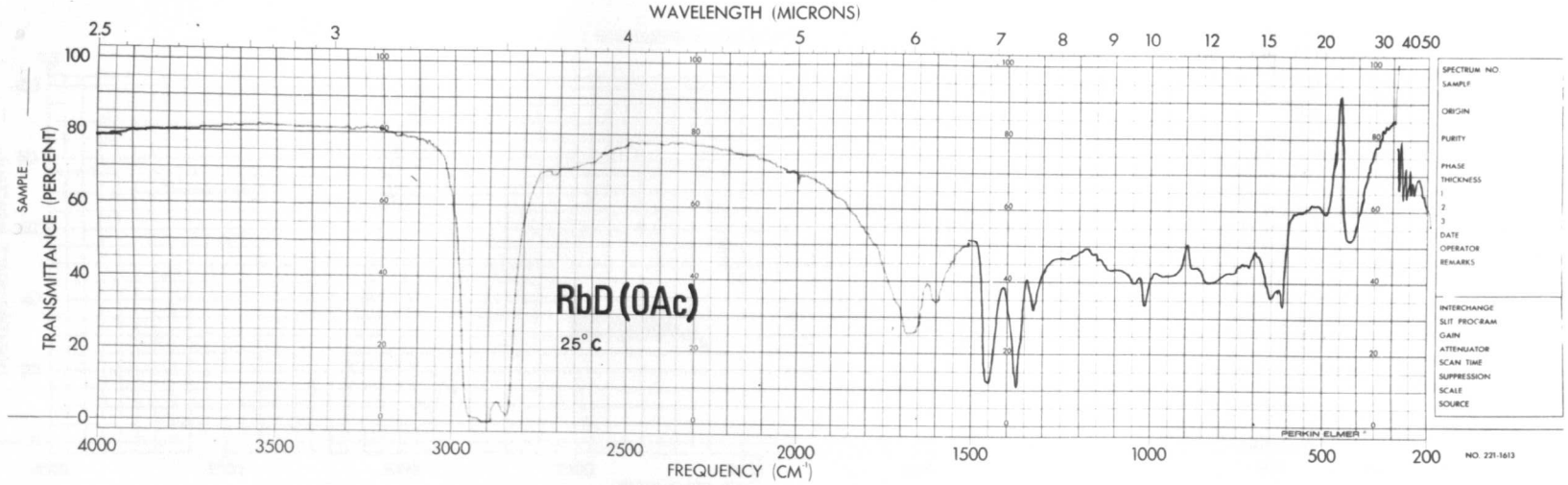
WAVELENGTH (MICRONS)
2.5
3
4
5
6
7
8
9
10
12
15
20
30
40
50
TRANSMITTANCE (PERCENT)
100
80
60
40
20
0
SAMPLE
RbD(OAc)
25°C
4000
3500
3000
2500
2000
1500
1000
500
200
FREQUENCY (CM⁻¹)
PERKIN ELMER
NO. 221-1613
SPECTRUM NO.
SAMPLE
ORIGIN
PURITY
PHASE
THICKNESS
1
2
3
DATE
OPERATOR
REMARKS
INTERCHANGE
SLIT PROGRAM
GAIN
ATTENUATOR
SCAN TIME
SUPPRESSION
SCALE
SOURCE

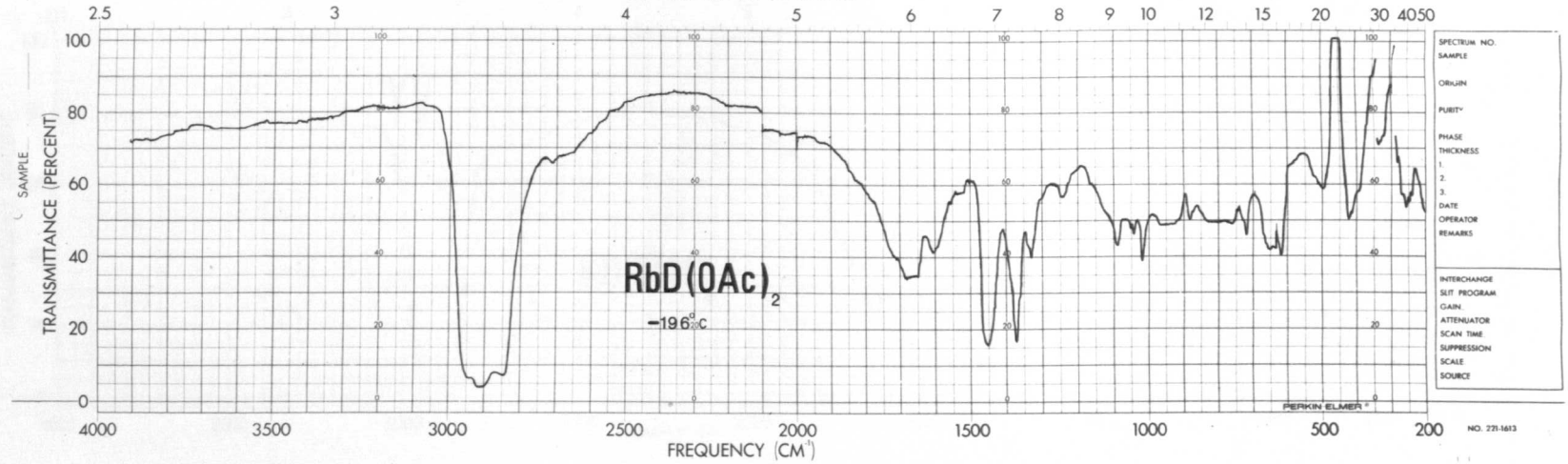
WAVELENGTH (MICRONS)
2.5
3
4
5
6
7
8
9
10
12
15
20
30
40
50
TRANSMITTANCE (PERCENT)
100
80
60
40
20
0
SAMPLE
RbD(OAc)2
-196°C
4000
3500
3000
2500
2000
1500
1000
500
200
FREQUENCY (CM⁻¹)
PERKIN ELMER
NO. 221-1613
SPECTRUM NO.
SAMPLE
ORIGIN
PURITY
PHASE
THICKNESS
1.
2.
3.
DATE
OPERATOR
REMARKS
INTERCHANGE
SLIT PROGRAM
GAIN
ATTENUATOR
SCAN TIME
SUPPRESSION
SCALE
SOURCE

E

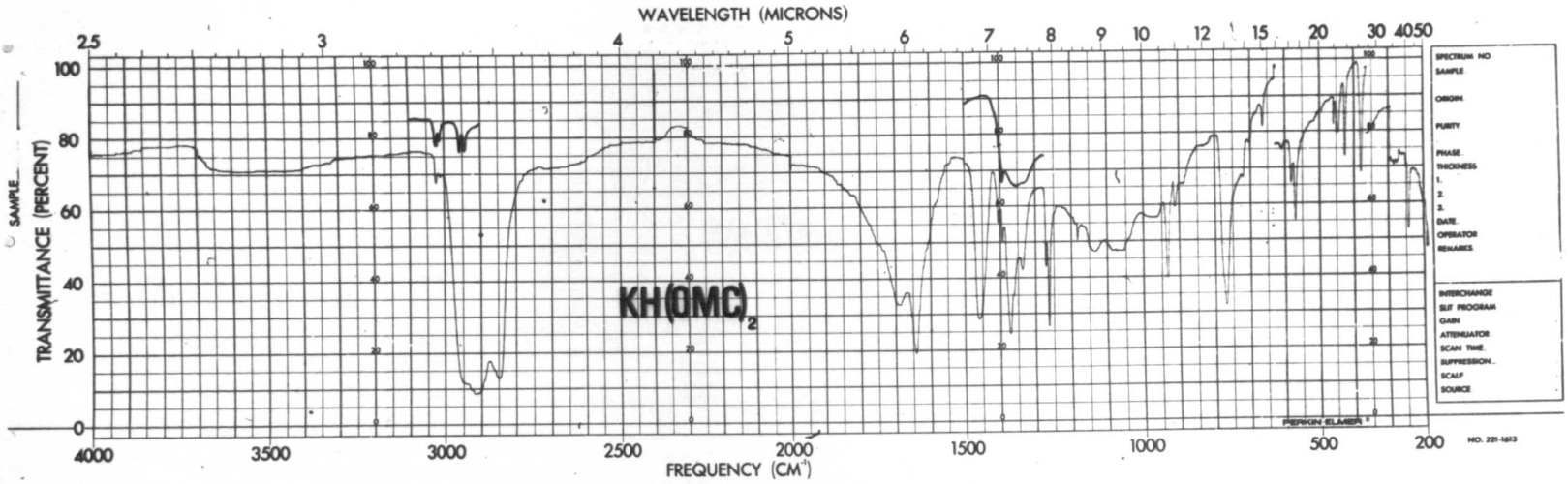
WAVELENGTH (MICRONS)
2.5
3
4
5
6
7
8
9
10
12
15
20
30
40
50
TRANSMITTANCE (PERCENT)
100
80
60
40
20
0
SAMPLE
KH(OMC)2
4000
3500
3000
2500
2000
1500
1000
500
200
FREQUENCY (CM-1)
PERKIN ELMER
NO. 221-1613
SPECTRUM NO.
SAMPLE
ORIGIN
PURITY
PHASE
THICKNESS
1.
2.
3.
DATE
OPERATOR
REMARKS
INTERCHANGE
SLIT PROGRAM
GAIN
ATTENUATOR
SCAN TIME
SUPPRESSION
SCALE
SOURCE

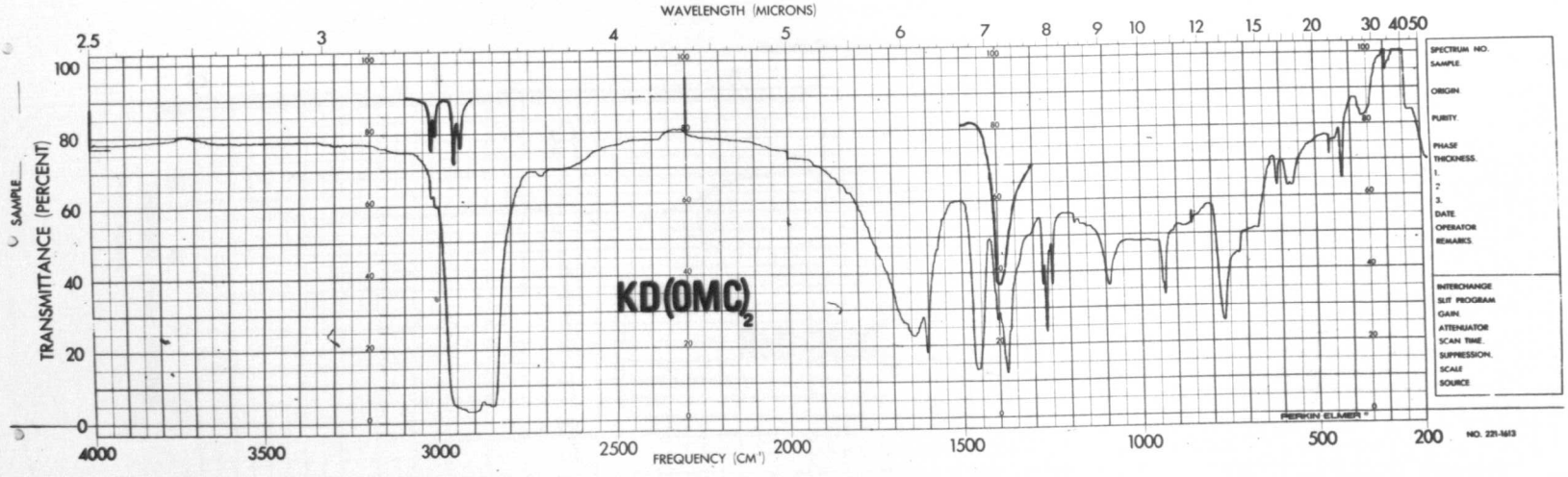
WAVELENGTH (MICRONS)
2.5
3
4
5
6
7
8
9
10
12
15
20
30
40
50
TRANSMITTANCE (PERCENT)
100
80
60
40
20
0
SAMPLE
KD(OMC)2
4000
3500
3000
2500
2000
1500
1000
500
200
FREQUENCY (CM-1)
PERKIN ELMER
NO. 221-1613
SPECTRUM NO.
SAMPLE
ORIGIN
PURITY
PHASE
THICKNESS
1.
2.
3.
DATE
OPERATOR
REMARKS
INTERCHANGE
SLIT PROGRAM
GAIN
ATTENUATOR
SCAN TIME
SUPPRESSION
SCALE
SOURCE

F

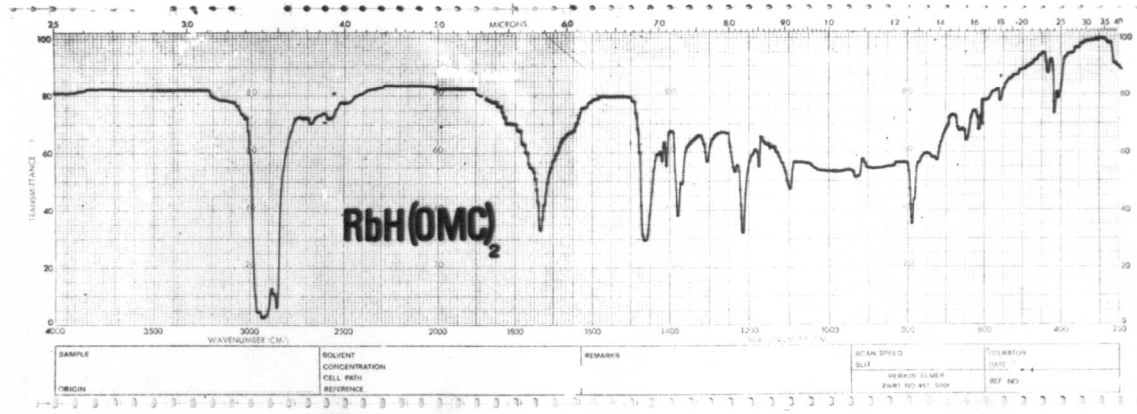
RbH(OMC)2
MICRONS
WAVENUMBER (CM-1)
TRANSMITTANCE
SAMPLE
ORIGIN
SOLVENT
CONCENTRATION
CELL PATH
REFERENCE
REMARKS
SCAN SPEED
SLIT
PERKIN ELMER
PART NO 497-5197
OPERATOR
DATE
REF NO

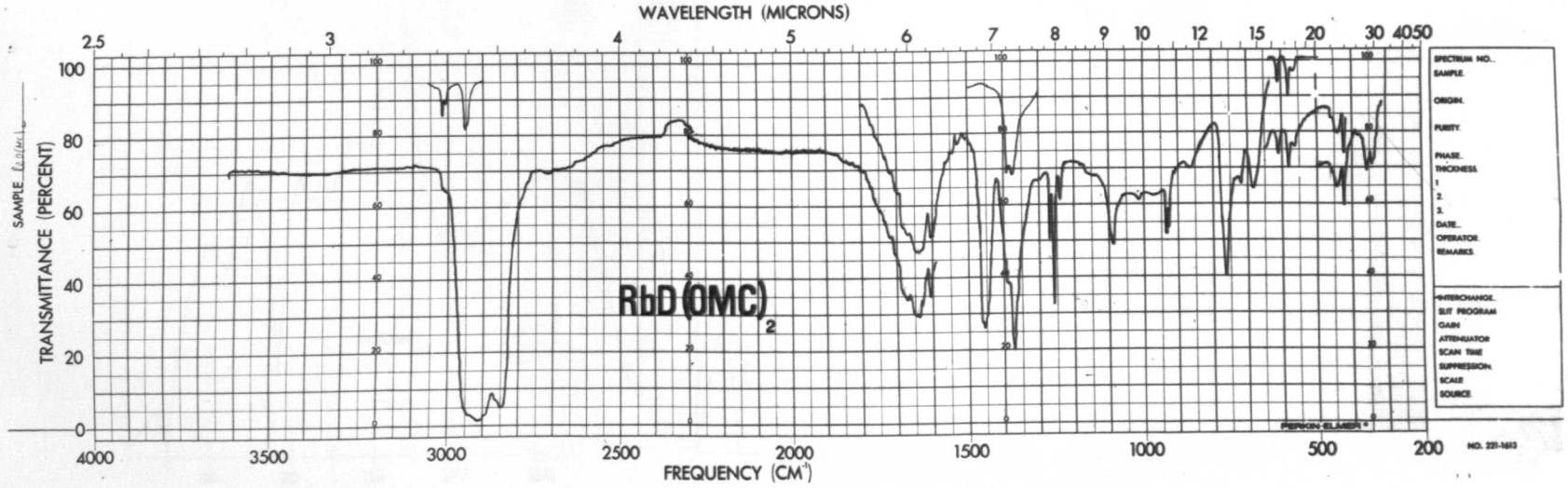
WAVELENGTH (MICRONS)
TRANSMITTANCE (PERCENT)
SAMPLE
RbD(OMC)2
FREQUENCY (CM-1)
PERKIN-ELMER
NO. 221-1613
SPECTRUM NO.
SAMPLE
ORIGIN
PURITY
PHASE
THICKNESS
1
2
3
DATE
OPERATOR
REMARKS
INTERCHANGE
SLIT PROGRAM
GAIN
ATTENUATOR
SCAN TIME
SUPPRESSION
SCALE
SOURCE

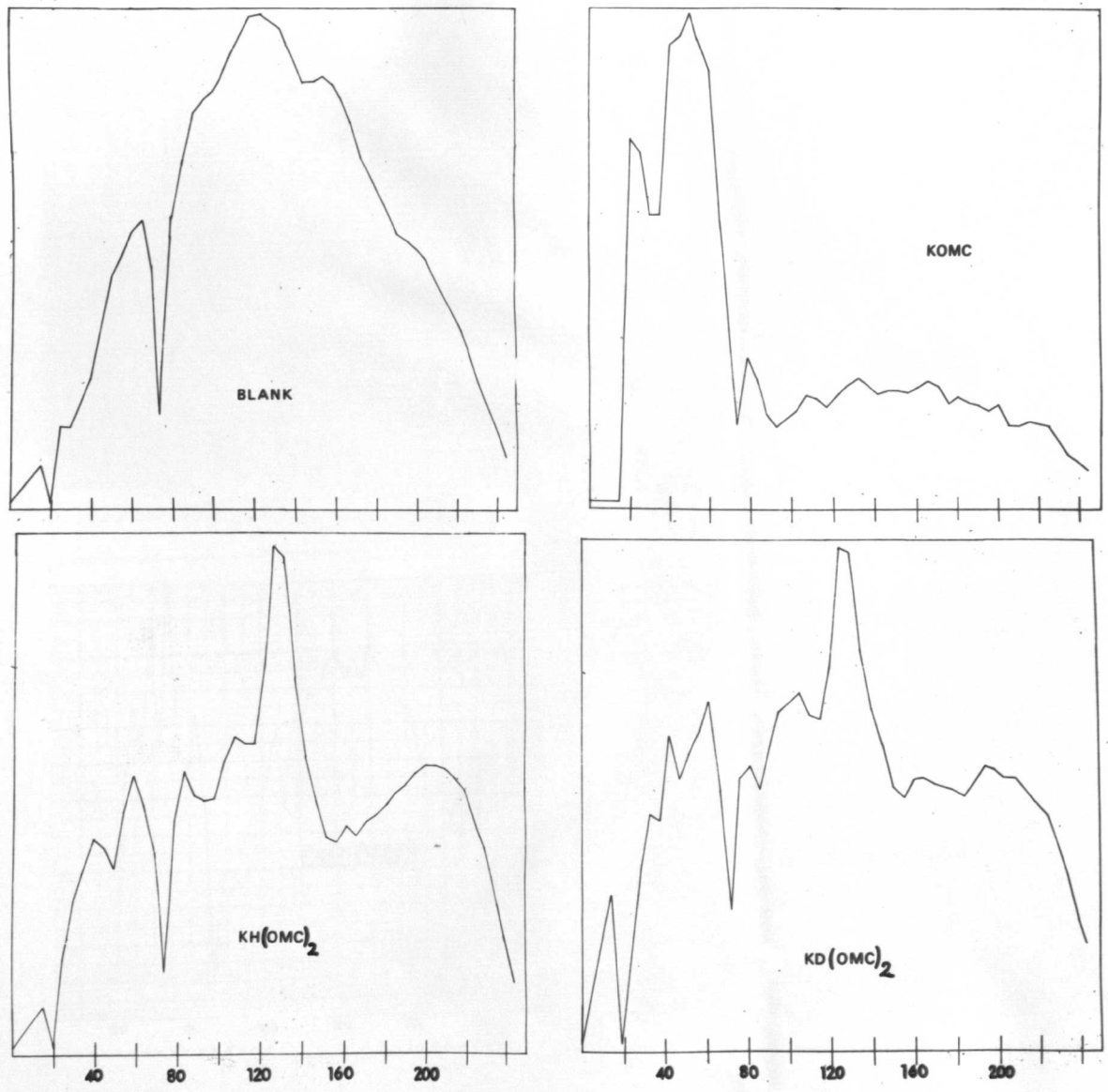
BLANK
KOMC
KH(OMC)2
KD(OMC)2
40
80
120
160
200
40
80
120
160
200

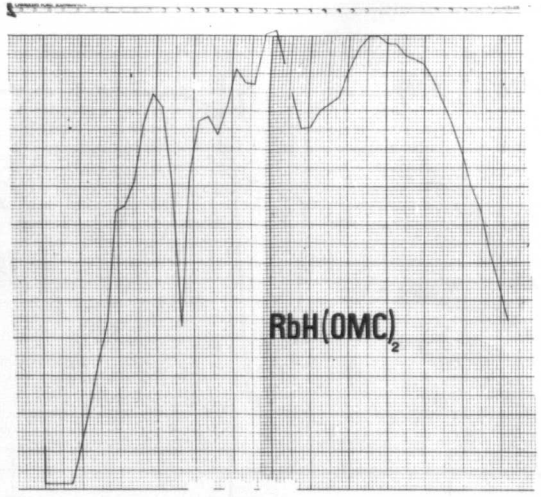
RbH(OMC)2

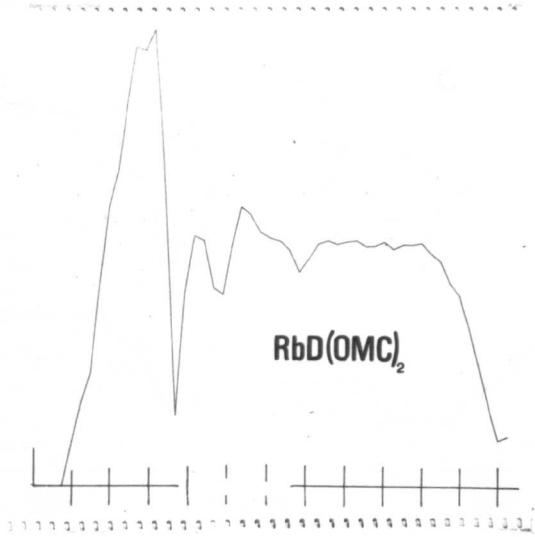
RbD(OMC)2

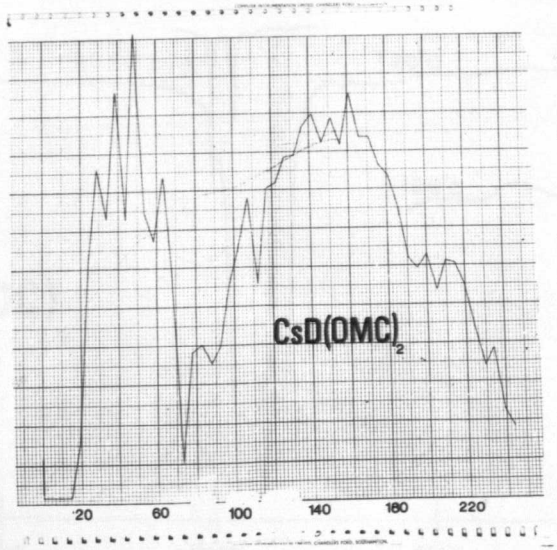
CsD(OMC)2
20
60
100
140
180
220

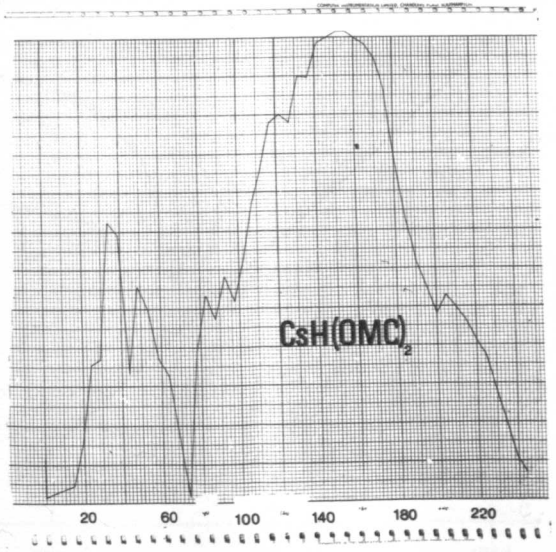
CsH(OMC)2
20
60
100
140
180
220

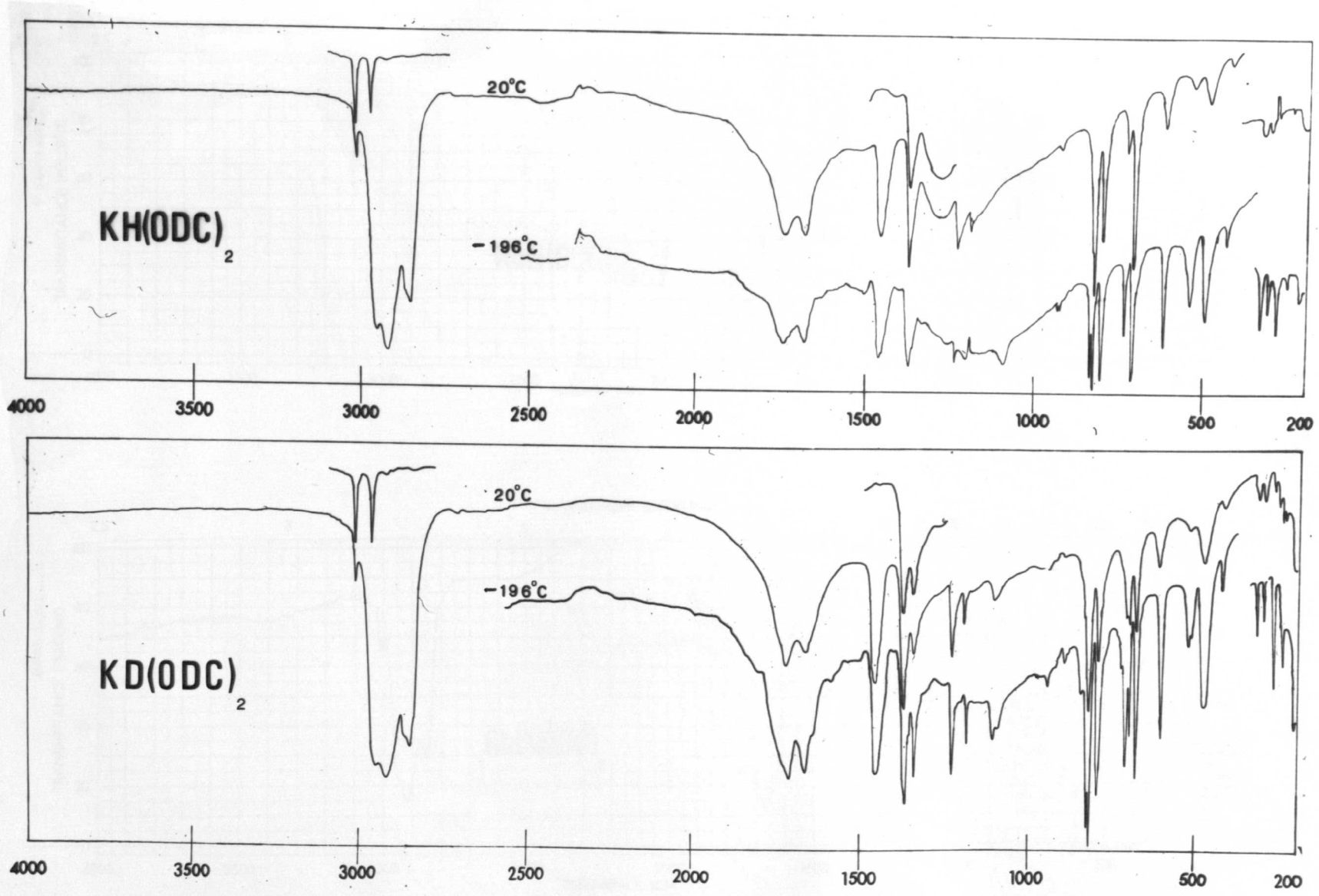
KH(ODC)2
20°C
-196°C
4000
3500
3000
2500
2000
1500
1000
500
200
KD(ODC)2
20°C
-196°C
4000
3500
3000
2500
2000
1500
1000
500
200

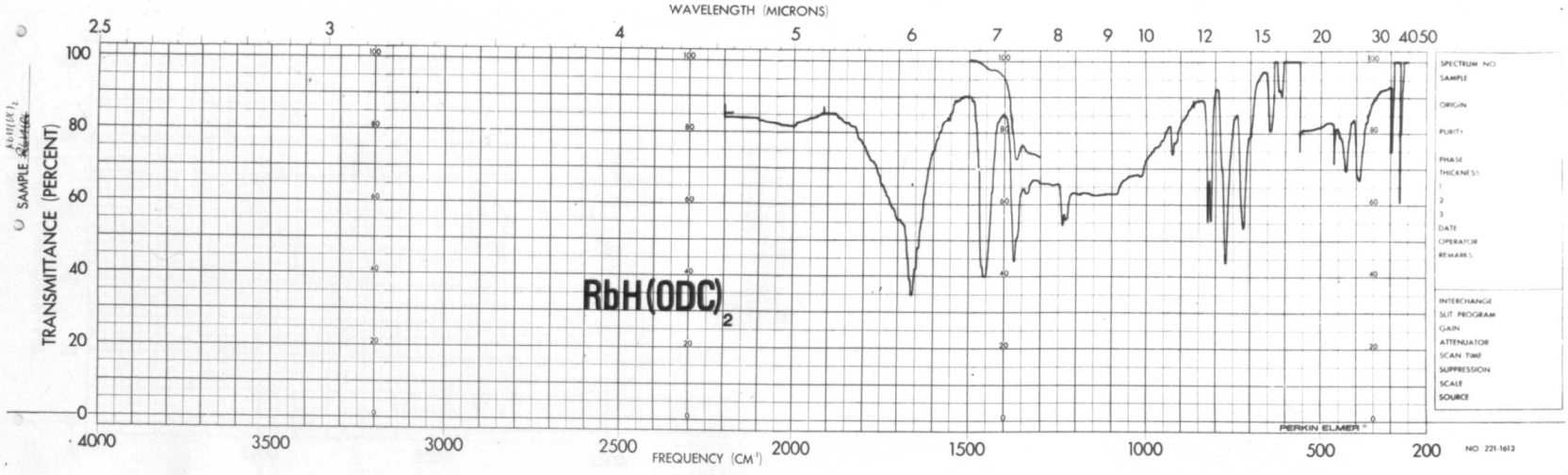
WAVELENGTH (MICRONS)
2.5
3
4
5
6
7
8
9
10
12
15
20
30
40
50
TRANSMITTANCE (PERCENT)
100
80
60
40
20
0
RbH(ODC)2
4000
3500
3000
2500
2000
1500
1000
500
200
FREQUENCY (CM-1)
PERKIN ELMER
NO. 221-1613
SPECTRUM NO.
SAMPLE
ORIGIN
PURITY
PHASE
THICKNESS
1.
2.
3.
DATE
OPERATOR
REMARKS
INTERCHANGE
SLIT PROGRAM
GAIN
ATTENUATOR
SCAN TIME
SUPPRESSION
SCALE
SOURCE

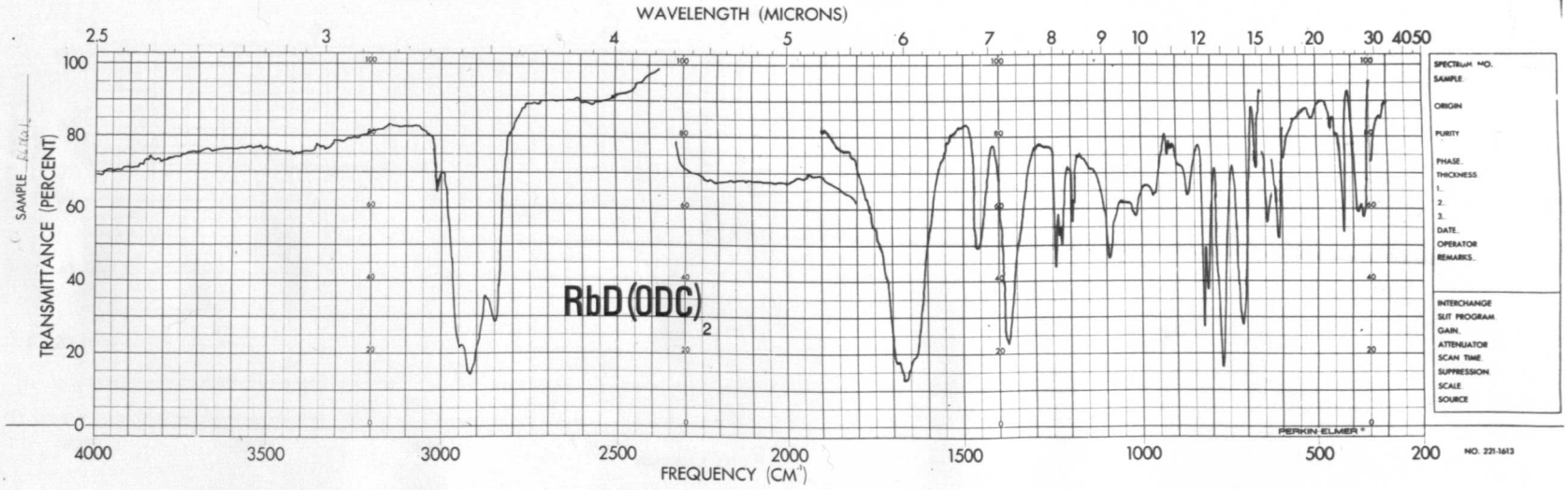
WAVELENGTH (MICRONS)
2.5
3
4
5
6
7
8
9
10
12
15
20
30
40
50
TRANSMITTANCE (PERCENT)
100
80
60
40
20
0
RbD(ODC)2
4000
3500
3000
2500
2000
1500
1000
500
200
FREQUENCY (CM-1)
PERKIN ELMER
NO. 221-1613
SPECTRUM NO.
SAMPLE
ORIGIN
PURITY
PHASE
THICKNESS
1.
2.
3.
DATE
OPERATOR
REMARKS
INTERCHANGE
SLIT PROGRAM
GAIN
ATTENUATOR
SCAN TIME
SUPPRESSION
SCALE
SOURCE

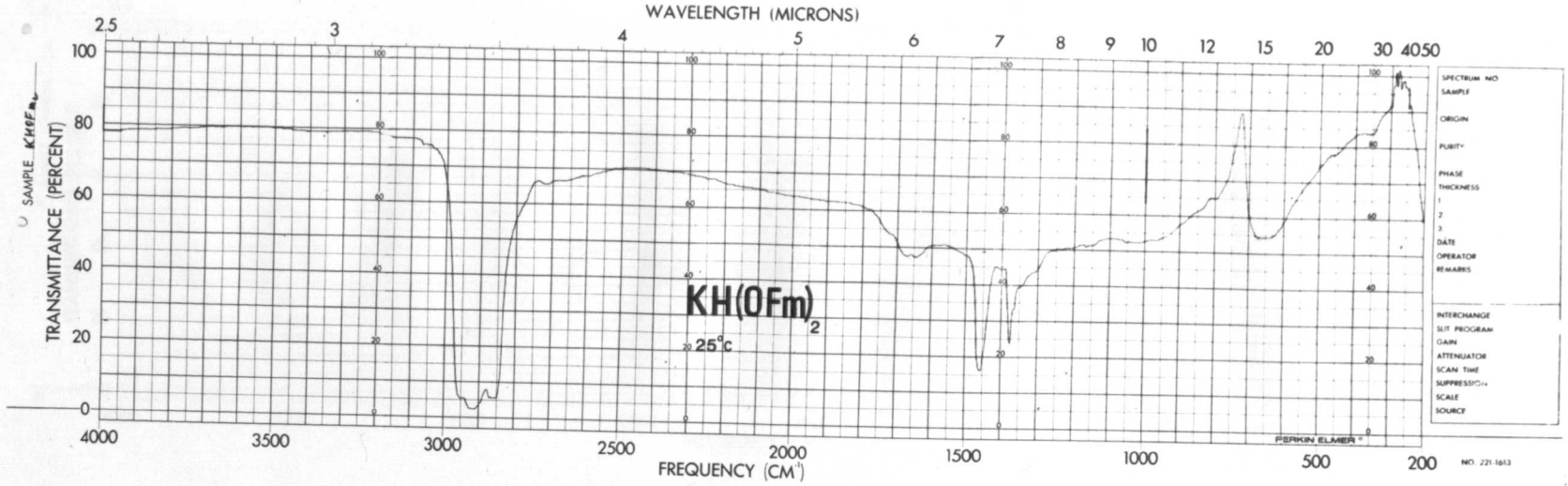
WAVELENGTH (MICRONS)
2.5
3
4
5
6
7
8
9
10
12
15
20
30
40
50
TRANSMITTANCE (PERCENT)
100
80
60
40
20
0
SAMPLE KHOFm
KH(OFm)2
25°C
4000
3500
3000
2500
2000
1500
1000
500
200
FREQUENCY (CM-1)
PERKIN ELMER
NO. 221-1613
SPECTRUM NO
SAMPLE
ORIGIN
PURITY
PHASE
THICKNESS
1
2
3
DATE
OPERATOR
REMARKS
INTERCHANGE
SLIT PROGRAM
GAIN
ATTENUATOR
SCAN TIME
SUPPRESSION
SCALE
SOURCE

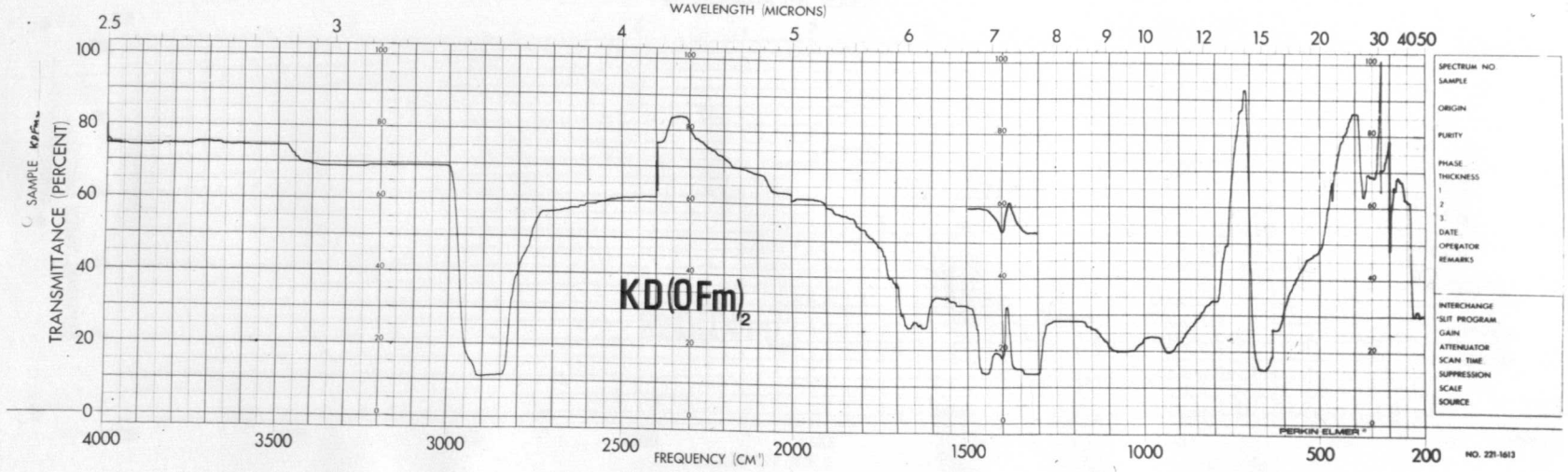
WAVELENGTH (MICRONS)
2.5
3
4
5
6
7
8
9
10
12
15
20
30
40
50
TRANSMITTANCE (PERCENT)
100
80
60
40
20
0
SAMPLE KDFm
KD(OFm)2
4000
3500
3000
2500
2000
1500
1000
500
200
FREQUENCY (CM-1)
PERKIN ELMER
NO. 221-1613
SPECTRUM NO
SAMPLE
ORIGIN
PURITY
PHASE
THICKNESS
1
2
3
DATE
OPERATOR
REMARKS
INTERCHANGE
SLIT PROGRAM
GAIN
ATTENUATOR
SCAN TIME
SUPPRESSION
SCALE
SOURCE

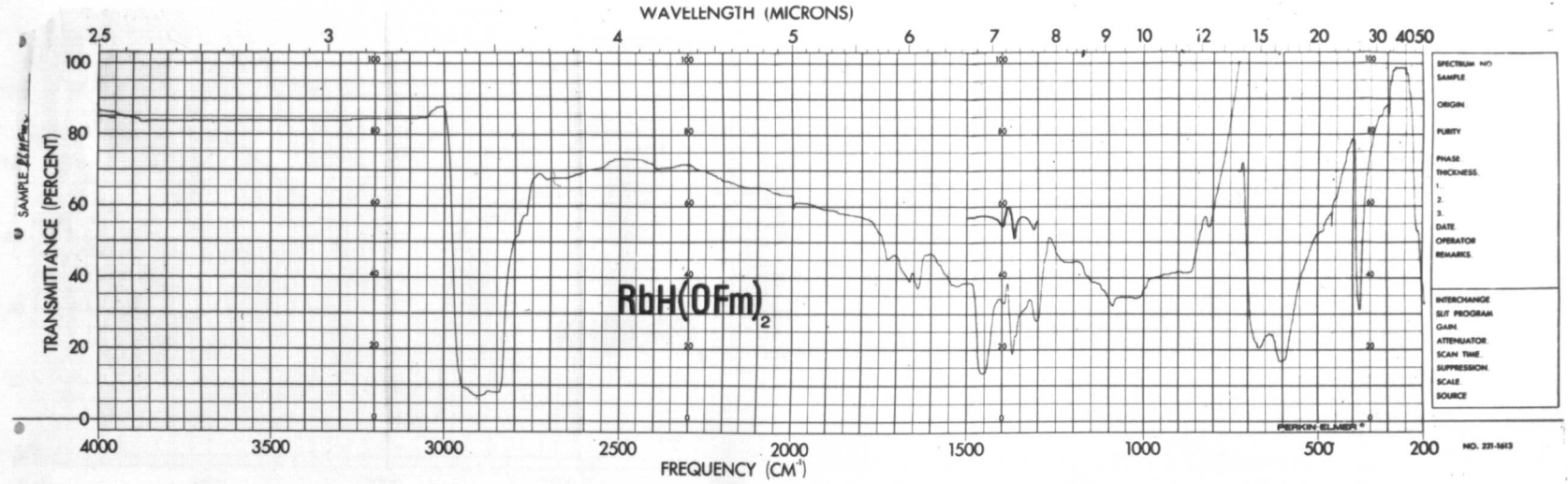
WAVELENGTH (MICRONS)
2.5
3
4
5
6
7
8
9
10
12
15
20
30
40
50
TRANSMITTANCE (PERCENT)
100
80
60
40
20
0
RbH(OFm)2
4000
3500
3000
2500
2000
1500
1000
500
200
FREQUENCY (CM-1)
PERKIN-ELMER
NO. 221-1613

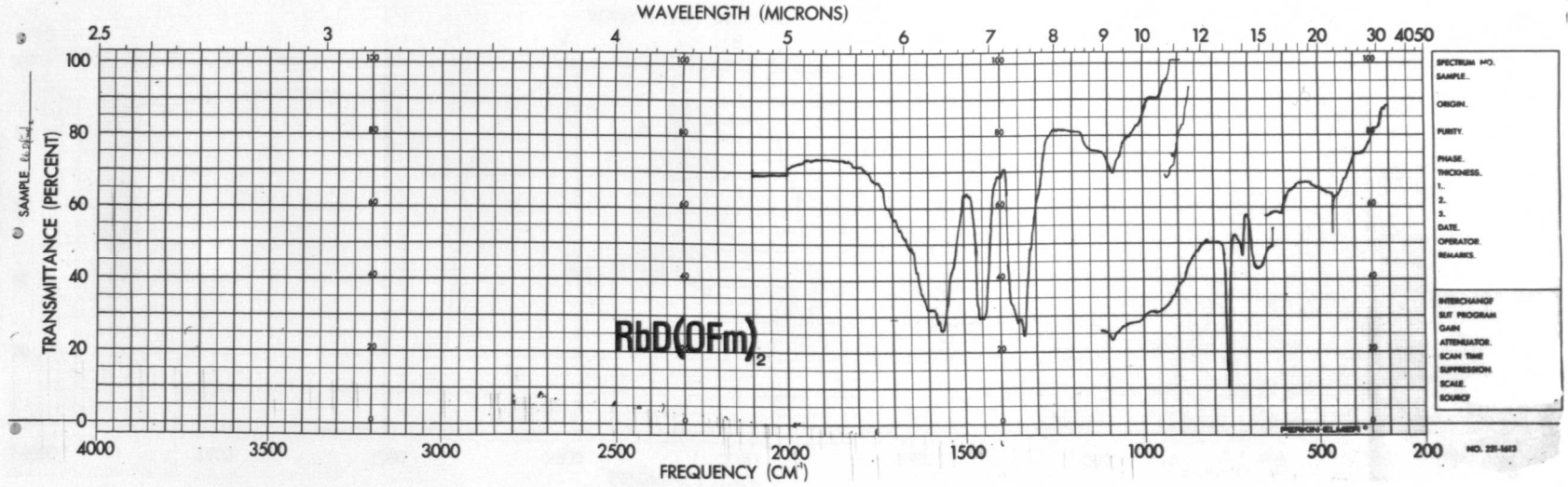
WAVELENGTH (MICRONS)
2.5
3
4
5
6
7
8
9
10
12
15
20
30
40
50
TRANSMITTANCE (PERCENT)
100
80
60
40
20
0
RbD(OFm)2
4000
3500
3000
2500
2000
1500
1000
500
200
FREQUENCY (CM-1)
PERKIN-ELMER
NO. 221-1613

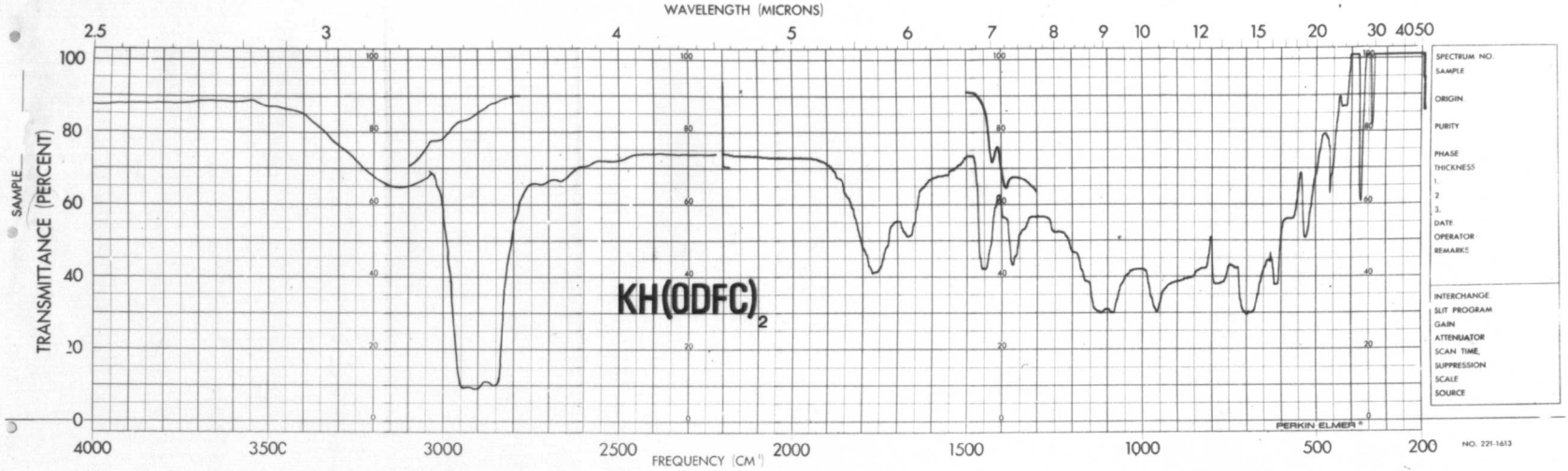
WAVELENGTH (MICRONS)
2.5 3 4 5 6 7 8 9 10 12 15 20 30 40 50
TRANSMITTANCE (PERCENT)
100 80 60 40 20 0
SAMPLE
KH(ODFC)2
4000 3500 3000 2500 2000 1500 1000 500 200
FREQUENCY (CM-1)
PERKIN ELMER
NO. 221-1613
SPECTRUM NO.
SAMPLE
ORIGIN
PURITY
PHASE
THICKNESS
1.
2
3.
DATE
OPERATOR
REMARKS
INTERCHANGE
SLIT PROGRAM
GAIN
ATTENUATOR
SCAN TIME
SUPPRESSION
SCALE
SOURCE

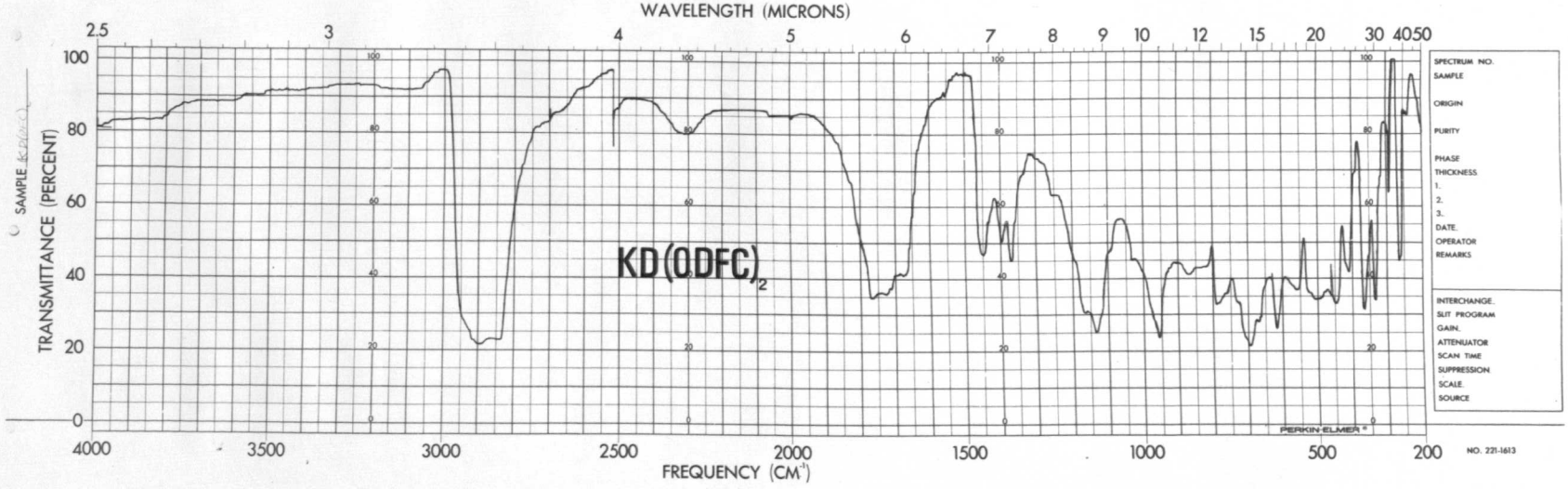
WAVELENGTH (MICRONS)
2.5 3 4 5 6 7 8 9 10 12 15 20 30 40 50
TRANSMITTANCE (PERCENT)
100 80 60 40 20 0
SAMPLE KD(ODFC)2
KD(ODFC)2
4000 3500 3000 2500 2000 1500 1000 500 200
FREQUENCY (CM-1)
PERKIN ELMER
NO. 221-1613
SPECTRUM NO.
SAMPLE
ORIGIN
PURITY
PHASE
THICKNESS
1.
2.
3.
DATE
OPERATOR
REMARKS
INTERCHANGE
SLIT PROGRAM
GAIN
ATTENUATOR
SCAN TIME
SUPPRESSION
SCALE
SOURCE

CHAPTER FIVE

Type A Hydrogen Dicarboxylate Salts.

Chapter Five.

Type A Hydrogen Dicarboxylate Anions

1. Introduction

Although a considerable number of Type A hydrogen dicarboxylate salts have been examined by spectroscopic techniques, no detailed assignment of their IR spectrum have been reported. This is primarily because of the extreme complexity of the IR spectra and secondly because of the low symmetry of the anions. The most extensive examination was undertaken by Hadži and Novak (30). The main conclusion was that the proton is residing in an odd shaped three dimensional potential energy surface with the proton essentially located midway between the two oxygen atoms (30). In more recent work Hadži has suggested that νOH may be as low as 1000cm^{-1} since, from the spectra of some liquid and crystalline H-bonded adducts the main conclusions were as follows: (69)

(a) νOH is associated with a very broad and intense band below 1700cm^{-1}.

(b) Band breadth and intensity is insensitive to change of state and concentration in an inert solvent.

(c) There is a low isotopic shift of νOH.

(d) The bending vibrations are difficult to locate with certainty.

It has already been pointed out that only the coupled use of neutron diffraction with spectroscopic techniques can determine unambiguously the symmetry of H-bonded species where the proton is likely to be symmetrically placed (3). With the latter in mind, Hamilton and co-workers calculated νOH from neutron diffraction data on potassium

hydrogen diaspirinate (70). They deduced that νOH is less than 1000cm^{-1}, with the proton residing in a very anharmonic potential energy well.

It is, therefore, the purpose of the work recorded in this chapter to analyse, as far as possible, the IR spectrum of some simple Type A hydrogen dicarboxylate salts with the view to checking the predictions outlined above, and ultimately drawing conclusions with regard to their symmetry.

The anions which have been examined are acid salts of acetic acid and its halogenated derivatives. The anions have been classified according to their IR spectrum and those discussed in this chapter all show similar features and are representative of Type A salts. The remainder, Type B, have been discussed in chapter four.

Simple acid salts of this kind were chosen because the same modes of vibration exist in all cases, the only difference being in their frequencies. Thus by increasing the weight of the R group, (CH_3, CF_3 etc.), the region above 1300cm^{-1} becomes less complicated at the expense of the lower region. Also, modes of vibration associated with the COO groups are altered in frequency as the R group is changed. Both these effects lead to a better understanding of the extent of Fermi resonance interactions with protonic vibrations. Finally the conclusions from the study have been compared with the hydrogen dihalide systems.

2. Normal Modes of Vibration

In Type A hydrogen dicarboxylate anions the two carboxylate groups are crystallographically identical and related by a centre of symmetry or a C_2 axis. Selection rules based on point group symmetry are static, therefore, any tunneling of the proton will give rise to average signals for the carboxylate group vibrations at each end of the anion. Deuteration will, however, reduce the rate of tunneling and separate signals may be observed but will clearly be limited by the intrinsic breadth of the bands and by the rate of tunneling. Thus whether or not tunneling exists cannot, therefore, be deduced unambiguously from a formal application of selection rules.

The normal modes of vibration are analogous to the monomeric acid for both ends of the anion (see chapter three) and are divided into in-phase and out-of-phase vibrations. In-phase-vibrations are those where the same vibration occurs at each end of the anion such that the symmetry of the anion is preserved. The converse situation represents the out-of-phase vibration.

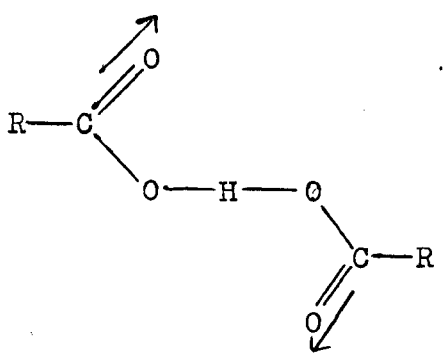

In-phase νC=O (A_g, A)

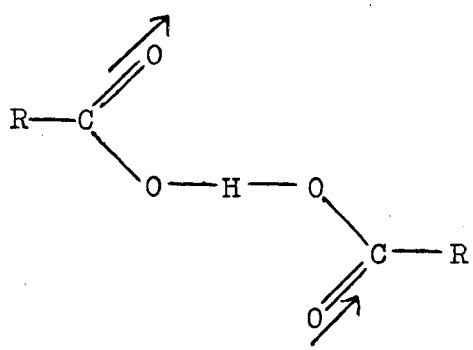

Out-of-phase νC=O (A_u, B)

There are no restrictions on the Raman or IR activities of fundamentals, overtones and combination bands for the C_2 cases. The mutual exclusion principle operates in the C_i cases. Details of these

results are tabulated in section 3.

3. Selection Rules and Character Tables (107, 132).

Twenty one normal modes of vibration are expected in the $H(O_2CR)^-$ system, where the R group is treated as a point mass.

C_2	E	C_2		
A	1	1	z, R_z	x^2, y^2, z^2, xy
B	1	-1	x, y, R_x, R_y	y_z, xz

C_i	E	i		
A_g	1	1	R_x, R_y, R_z	x^2, y^2, x^2, xy, xz, yz
A_u	1	-1	x, y, z	

Component of Dipole Moment and Polarisability	C_2	C_i
M_x	B	A_u
M_y	B	A_u
M_z	A	A_u
α_{xx}	A	A_g
α_{yy}	A	A_g
α_{zz}	A	A_g
α_{xy}	A	A_g
α_{xz}	B	A_g
α_{yz}	B	A_g

C_2	Total Symmetry Species	IR activity	Raman activity
Fundamentals	A, B	active	active
Overtones possible A.A	A	"	"
B.B	A	"	"
Combinations possible A.B	B	"	"

C_i	Total Symmetry Species	IR activity	Raman activity
Fundamentals	A_u	active	inactive
	A_g	inactive	active
Overtones possible $A_u . A_u$	A_g	"	"
$A_g . A_g$	A_g	"	"
Combinations possible $A_u . A_g$	A_u	active	inactive

4. Abbreviations

Anion (-)	
$H(OTF)_2$	hydrogen di-trifluoroacetate
$H(OTC)_2$	hydrogen di-trichloroacetate
$H(OTB)_2$	hydrogen di-tribromoacetate
$H(Op\text{-}CB)_2$	hydrogen di-p-chlorobenzoate
$H(Om\text{-}CB)_2$	hydrogen di-m-chlorobenzoate
$H(O_2DCM)$	hydrogen dichloromaleate
$H(O_2MCM)$	Hydrogen monochloromaleate

Details of other symbols and abbreviations used in this chapter can be found in chapters three and four

5. Sodium Hydrogen Diacetate.

This acid salt crystallises in the cubic system with space group Ia3, and has twenty four molecules in the unit cell (88). A short H-bond (2.444A°) links the two equivalent carboxylate groups, which are related by a C_2 axis. The dimensions of each carboxylate group are intermediate between those in ionised and non-ionised acetic acid (88).

The IR spectrum was reported by Hadži and Novak and their assignments are shown in table 5.1 (30). Several questions need to be answered if the assignments in table 5.1 are correct.

(a) Why is νC=O very broad even after coupling with OH has been removed?

(b) Why is νOD relatively sharp in comparison with all other intermolecular H-bonded species?

(c) What is the origin of the broad background absorption which contracts on cooling and shifts on deuteration?

The spectra recorded in this work are identical with those reported by Hadži and Novak. All spectra were recorded at -196°C and CD_3 samples were prepared to clarify the region above 1200cm^{-1}. Assignments are shown in tables 5.2 and 5.3 and spectra are reproduced at the end of this chapter.

4000 - 1500cm^{-1}

In this region of the spectrum only one strong band was observed and it shifted to lower frequency on deuteration in the hydroxyl position. This band is assigned to νC=O, but resolution into the A and B modes was not possible in the room temperature spectrum. Spectra recorded at -196°C and at the temperature of liquid helium showed that

TABLE 5.1

IR spectrum of $NaH(OAc)_2$

Recorded and assigned by Hadzi and Novak(30)

$NaH(OAc)_2$		$NaD(OAc)_2$	Assignment
temp.		temp.	
25°C	-196°C	25°C	
2100-1500 max. at	1900-1650 max. at	1900 - 1550 max. at	
1700(vs)	1710(vs)	-	δ OH+ νC=O
1640(m)	1638 (w)	1560(m)	combination
1540(m.b)			
		1650(vs)	ν C=O
		1330 (s)	ν OD
1500-450 max. at	1200-600 max. at	1500-600 max. at	
1440(vs)	1438(vs)	1430(vs)	$\delta_a CH_3$
1400(vs)	1405(vs)	1395(vs)	$\delta_s CH_3$
1370(sh)	1355(vs)	1370(sh)	ν CO
1250(s,b)	1290(vs)	-	δ OH
1058(m)	1060(m-s)	1052(m)	)
1025(m)	1032(m-s)	1026(m)	) CH_3
	950(b)	-	)
	720(b)		
	660(b)		
445(s)			

TABLE 5.2

Assignment of Vibrational Spectra of $NaH(OAc)_2$

Approx. Description	$NaH(OAc)_2$				$NaD(OAc)_2$	
	25°C	-196°C	-260°C	Raman (25°C)	25°C	-196°C
$\nu'_s CH_3$	3013	-	-	-	3014	-
$\nu_s CH_3$	2940	-	-	-	2939	-
$\nu_a CH_3$	2989	-	-	-	2988	-
ν C=O	1708	1707	1710	1664	1654	1658
$\delta'_s CH_3$	1428	1430	-	1444	1428	-
$\delta_s CH_3$	1360	-	-	1348	1332	1335
$\delta_a CH_3$	1400	1400	-	1408	1400	1403
ν C-O	1400	1401	1402	1408	1400	1403
δ OH(D)	1270	1283	1280	-	950	960
$\rho_s CH_3$	1024	(1033 (1026	(1030 (1025	-	1028	1030
$\rho_a CH_3$	1053	(1057 (1052	(1057 (1050	-	1055	1057
γ OH(D)	940	945	950	-	700-665	650-700
ν CC	935	925	920	928	-	889
ν OH(D)	(765 (720	720	720	756(1500)	540	530
δ COO	637	639	640	644	645	643
π CCO	609	603	610	620	629	631
δ CCO	455	449	452	425	434	420

Mode	Symm. Species
OH(D) motion	B
(O-O)	A
remainder	A,B unresolved

Mode	Isotopic Shift (-196°C)
ν OH/ν OD	Approx. 1.47
δ OH/δ OD	1.33
γ OH/γ OD	range 1.35-1.43

Frequency in brackets is an average value of the broad band extending from 1000 - 2000cm^{-1}. An accurate value is not possible since the spectrum was only recorded up to 2000cm^{-1}.

TABLE 5.3

Assignments of Vibrational Spectra of $NaH(O_2C.CD_3)_2$

Approx. Description	$NaH(O_2C.CD_3)_2$		$NaD(O_2C.CD_3)_2$	
	25°C	-196°C	25°C	-196°C
$\nu'_s CD_3$	2262	2255	2251	-
$\nu_s CD_3$	2228	-	2230	-
$\nu_a CD_3$	-	-	-	-
ν C=O	1700	1710	1645	1650
ν C-O	1388	1395	1389	1390
δ OH(D)	1260	1285	930	940
$\delta'_s CD_3$	1035	1040	1030	1035
$\delta_s CD_3$	1075	1085	1080	1082
$\delta_a CD_3$	1035	1040	1030	1035
γ OH(D)	930	930	hidden by residual $NaH(O_2C.CD_3)_2$	
ν C-C	885	885	835	840
$\rho_s CD_3$	932	930	928	930
$\rho_a CD_3$	845	845	845	850
ν OH(D)	740	720	510	505
δ COO	610	610	605	604
$\tilde{\pi}$ CCO	520	520	-	
δ CCO	405	408	394	389

Symmetry species as in table 4.3

Mode	Isotopic shift (-196°C)
ν OH/ν OD	Approx. 1.43
δ OH/δ OD	Approx. 1.36
γ OH/γ OD	-

TABLE 5.4

Assignments of Vibrational Spectra of $CsH(OAc)_2$

Approx. Description	25°C	-196°C
$\nu'_s CH_3$	3010	-
$\nu_s CH_3$	2930	-
$\nu_a CH_3$	2968	-
ν C=O	1710	1710
$\delta'_s CH_3$	ca 1420	1400
$\delta_s CH_3$	1345	1342
$\delta_a CH_3$	ca 1420	1400
ν C-O	1375	1375
δ OH	1242	1260
$\rho_s CH_3$	1015	1020
$\rho_a CH_3$	1050	1050
γ OH	940	962
ν C-C	-	915
ν OH	755	750
δ COO	-	660?
π CCO	610	608
δ CCO	432	430
ν (O-O)	330	330

the band had considerable structure, but was too complex and ill-defined to examine usefully. Several weak bands were also observed in this region which disappeared on deuteration and, therefore, seem likely candidates for overtone and combination bands (30). A Raman spectrum of $NaH(OAc)_2$ showed only one weak band at 1664cm^{-1} which can only be νC=O.

1500 - 1200cm^{-1}

The spectrum of $NaH(O_2C.CD_3)_2$ at -196°C showed the presence of two strong bands. On deuteration the band at 1285cm^{-1} disappeared while the higher frequency band remained essentially unchanged in frequency. No evidence was found for any new band appearing in this region on deuteration which suggests that the assignment of an uncoupled νOD at 1330cm^{-1} in $NaD(OAc)_2$ is erroneous. The spectrum of $NaH(OAc)_2$ and $NaD(OAc)_2$ are complicated in this region by the presence of CH_3 modes of vibration which are mixed to some degree with νC-O (103). An explanation of the new band at 1330cm^{-1} in $NaD(OAc)_2$ must, therefore, be associated with the disappearance of δOH at 1290cm^{-1} on deuteration. It is fairly clear, even at room temperature, that the shoulder at 1360cm^{-1} in $NaH(OAc)_2$ is absent in $NaD(OAc)_2$ and the only likely condidate in the latter is the 1330cm^{-1} Band. This band is, therefore, predominantly a CH_3 mode since an analogous band was not found in the spectrum of $NaD(O_2C.CD_3)_2$. This assignment is comparable with that in $KH(OAc)_2$ systems and NaOAc (see chapter four).

The νC-O band can be straightforwardly assigned to the strongest band in this region at 1390cm^{-1}. A Raman spectrum of $NaH(OAc)_2$ at room temperature indicated the presence of three clear bands whose frequencies correspond closely to the νC-O and CH_3 modes

in the IR spectrum. The failure to find any recognizable band at about 1270cm^{-1} is not inconsistent with the assignment of δOH in the IR spectrum since predominantly proton motion is expected to be of low intensity in the Raman spectrum.

1200 - 240cm^{-1}

This region marks the onset of an extremely broad and very complex band structure which contracts on cooling and shifts to lower frequency on deuteration. By analogy with the results recorded in chapter four, the bands at about 700cm^{-1} and 500cm^{-1} in $NaH(OAc)_2$ and $NaD(OAc)_2$, respectively, can be assigned to the 0-1 transition, (figs. 4.4 and 5.5). The 0-1 transition represents an "even-odd" transition resulting from a considerable splitting of the ground state levels and a very low or possible non-existent potential energy barrier. Hornig and Somorjai suggested that in symmetric double minimum wells the intensity and frequency of the 0-1 transition increases as the barrier height is lowered (119). They suggested that when the splitting was of the order of 300cm^{-1} the 0-1 transition will give rise to the most intense band associated with proton motion.

Confirmation of the assignments in table 5.2 was obtained from the Raman spectrum of $NaH(OAc)_2$ where the 0-1 transition is forbidden on strict "even-odd" selection rules. Thus in the Raman spectrum only a very weak band, barely discernible above the noise, was observed at 756cm^{-1}. Also, a very broad and intense background absorption was observed beginning at about 1000cm^{-1} and was similar to that observed in the Raman spectrum of $KH(OAc)_2$. The latter represents the 0-2 transition which is analogous to the strongest band in the Raman and IR spectrum of $KH(OAc)_2$. In $NaH(OAc)_2$ systems the strict selection

rules (shown in figure 5.5) operating for proton vibrations are in accordance with the mutual exclusion principle. However, the C_2 point group of the anion in $NaH(OAc)_2$ and the anharmonicity of proton vibrations may complex matters further, particularly with regard to the intensities of the 0-1 and 0-2 transitions.

Alternative explanations of the stong band at $720cm^{-1}$ in the IR spectrum of $NaH(OAc)_2$ which are based on a slightly asymmetric double minimum well with a low barrier cannot be eliminated entirely, since such a model will affect only the intensities of transitions from the ground state. However, an explanation based on transitions originating from levels other than the ground state can be eliminated since such bands would show a marked temperature dependence, which was not observed even in a spectrum of $NaH(OAc)_2$ at the temperature of liquid helium.

The region $800 - 400cm^{-1}$ is complicated by the presence of RCO_2 skeletal vibrations which are broadened as result of Fermi resonance with the 0-1 transition. This is particularly noticeable by comparing the intensities of the band assigned to δCCO in the proton and deuterium samples. The close approach of δCCO and 0-1 transition in $NaD(OAc)_2$ and $NaD(O_2C.CD_3)_2$ renders the δCCO considerably broader in these samples than in their protonium analogues. It is also interesting to note the lower frequency of the 0-1 transition in $NaD(O_2C.CD_3)_2$ as compared with that in $NaD(OAc)_2$. This may be due to the lower frequency of δCCO in $NaD(O_2C.CD_3)_2$ as a result of the increase in weight of the R group.

The Raman spectrum of $NaH(OAc)_2$ in this region shows weak bands for the RCO_2 modes of vibration which have analogous assignments

Figure 5.5

Potential Energy Well in Type A salts.

Fig. 5.5

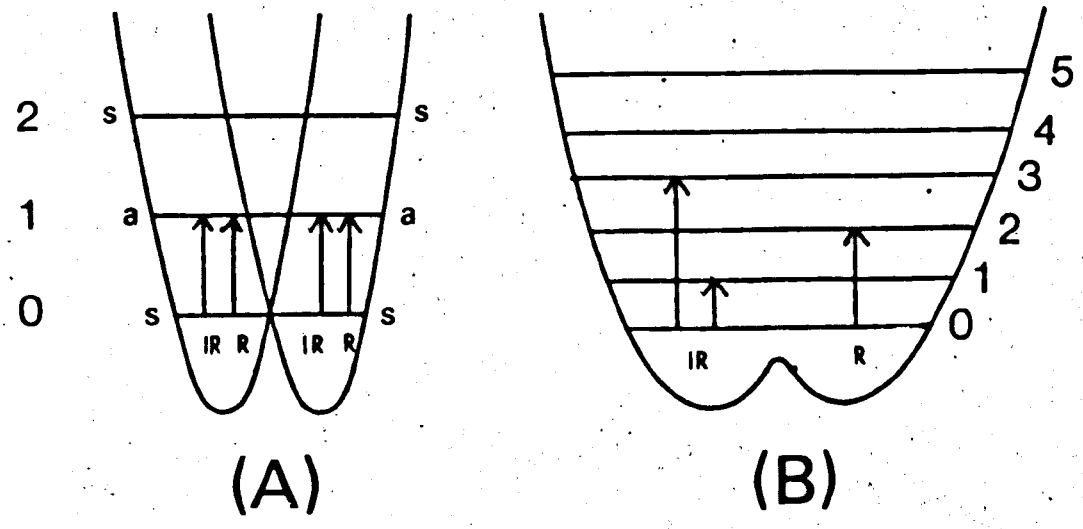

A. Two Harmonic P.E. Wells

B. Symmetric Double Minimum

to that of the IR spectrum. The only remaining band in the Raman spectrum is a very strong and sharp band at 928cm^{-1} which is the most likely candidate for νCC. In the IR spectrum νCC is close to a transmission window at 910cm^{-1} which marks the division between the 0-1 transition and the region where γOH is likely to absorb. A broad band at 945cm^{-1} seems the most likely candidate for γOH. On deuteration a relatively sharp band appears at 960cm^{-1} which is probably δOD which has shifted down from 1290cm^{-1}. The frequency of γOD is not clear since it will absorb in the region of the strong absorption near 700cm^{-1} which arises from the residual proton species. However, a strong band is present at 645cm^{-1} in NaD(OAc)$_2$ which is assigned to δCOO but whose intensity is more remarkable than its frequency. This may be due to the removal of Fermi resonance coupling with the 0-1 transition or to the proximity of γOD. The assignment of the sharp band (ie. 645cm^{-1}) to γOD, however, is unlikely since it is much sharper than expected from a comparison with γOH. The IR spectrum of the CD_3 analogues are similar to those of the CH_3 samples in this region. One very noticable difference is, however, the lower frequency of the transmission window in NaH(O$_2$C.CD$_3$)$_2$ as compared with the window in NaH(OAc)$_2$. The latter is attributed to the lower frequency of νCC in NaH(O$_2$C.CD$_3$)$_2$.

The region 1100 - 1000cm^{-1} in the IR spectrum of NaH(OAc)$_2$ and its deuterated derivatives are complicated by the presence of CH_3 and CD_3 modes of vibration. These bands can be assigned by analogy with the acid and base spectrum and show no unusual features except for the broad background absorption which contracts considerably on cooling.

A sample of CsH(OAc)$_2$ was prepared and its IR spectrum was recorded. In general, the spectrum was similar to that for NaH(OAc)$_2$

and assignments are shown in table 5.4. A band was observed at 330cm^{-1} which is prominent at -196°C and, therefore, seems the likely candidate for ν(OO). A band of similar frequency was not observed in the spectrum of $NaH(OAc)_2$, but it was found at about 250cm^{-1} in $KH(OAc)_2$ and $RbH(OAc)_2$. The increase in frequency of ν(OO) in going from $KH(OAc)_2$ to $CsH(OAc)_2$ reflects the stronger H-bond in the latter (122). The failure to find an analogous band in the spectrum of $NaH(OAc)_2$ may simply be due to its low intensity. Also, the appearance of the band in the IR spectrum of $CsH(OAc)_2$ is sufficient evidence to rule out a C_i point group for the anion. Therefore, the most likely point group of the anion in $CsH(OAc)_2$ is C_2.

The IR spectrum of $NaH(OAc)_2$ and $NaD(OAc)_2$ were recorded down to about 20cm^{-1}. Assignments of the band observed are shown below in table 5.6.

TABLE 5.6

Approx. Description	$NaH(OAc)_2$	$NaD(OAc)_2$, cm^{-1}
γCH_3	92	88
H-bond vibrations	113 127	108 127
L(Na)	205	200

The assignment of the translation lattice vibration of the cation, L(Na), is straightforward since it has been observed at a similar frequency in $NaHF_2$ (124). The point group of the anion places no restrictions on the IR activities of any H-bond vibrations. The spectrum of $NaH(OAc)_2$ in this region is much simpler than the same region for $KH(OAc)_2$, but bands of similar frequency were found in

both samples. The low intensity of the H-bond vibrations has already been commented on with reference to the failure to find $\nu(OO)$. The assignment of the band at 90cm^{-1} is straightforward since it has been calculated to be at 93cm^{-1} in HOAc and DOAc (103).

6. Hydrogen Di-trifluoroacetate Anion, $H(OTF)_2^-$.

The X-ray crystal structures of K, Rb, and Cs salts of $H(OTF)_2^-$ have been elucidated by Golic and Speakman and details are shown below in table 5.7 (91).

TABLE 5.7

Cation	Space Group	Point Group	Number of Molecules in Unit Cell	R(00)A°
K	I2/a	C_i	4	2.435
Rb	isomorphous with K salt	C_i	4	
Cs	A2/a	C_i	4	2.38

IR data has not been reported but the spectra recorded here are similar to those observed for the $NaH(OAc)_2$ systems. Assignments of their vibrational spectrum are shown in tables 5.8 and 5.9 and 5.10. The selection rules are based on the mutual exclusion principle, therefore, only out-of-phase vibrations (A_u) are IR active.

4000 - 1200cm^{-1}

Three bands were observed in the IR spectrum of each protonated species, the lower frequency band disappeared, however, on deuteration. The band at 1790cm^{-1} can be safely assigned to νC=O and is considerably sharper in $KH(OTF)_2$ and $RbH(OTF)_2$ than the same band in $NaH(OAc)_2$. However, νC=O in the spectrum of $CsH(OTF)_2$ is comparable in breadth to νC=O in $NaH(OAc)_2$. An explanation of these results may be that in the K and Rb salts of $H(OTF)_2^-$ only the A_u mode is IR active whereas

TABLE 5.8

Assignment of Vibrational Spectrum of $KH(OTF)_2$

Approx. Description	25°C	-196°C
ν C=O	1790	1790
ν C-O	1416	
δ OH	1225	1230
ν CF_3	1189	1195
ν CF_3	1125	1125
τ OH	950	948
ν OH	885	860
ν C-C	790	780
ν CF_3	789	788
δ COO	710	700
π COO	580	590
δ CF_3	580	590
δ CF_3	515	518
ρ CCF_3	432	434
δ CCO	390	392
π CCF_3	250	267

TABLE 5.9

Assignments of IR spectrum of $RbH(OTF)_2$

Approx. Description	$RbH(OTF)_2$			$RbH(OTF)_2$	
	IR A_u modes			A_u	
	25°C	-196°C	Raman A_g	25°C	-196°C
ν C=O	1788	1790	1724	1735	1730
ν C-O	1414	-	1440	1427	1432
δ OH	1220	1230	-	940	935
ν CF_3	1200	1198		1215	1200
ν CF_3	1125	1122		1125	1122
γ OH	940	938		ca 700	ca 700
ν C-C	870	857	848	860	868
ν OH	790	760	broad background in region of 1150cm^{-1}	520	525
ν CF_3	798	788	746	785	780
δ COO	708	700 675		692	695
π CCO	570	582		masked	610
δ CF_3	570	570		masked	masked
δ CF_3	512	515	484	510	515
ρ CCF_3	429	430	424	422	425
δ CCO	387	389	324	370	368
π CCF_3	262	262	254	255	256
ν (O...O)			182		

Isotopic Shifts	ν OH/ν OD	δ OH/δ OD	γ OH/γ OD
	1.45	1.32	1.34

TABLE 5.10

Assignment of Vibrational Spectrum of $CsH(OTF)_2$

Approx. Description	$CsH(OTF)_2$		$CsD(OTF)_2$ (partly decomposed)	
	A_u modes		A_u modes	
	25°C	-196°C	25°C	-196°C
ν C=O	1790	1790	1740	
ν C-O	1408	1414		
δ OH		ca 1230	900	
ν CF_3	1195	1190		
ν CF_3	1145	1140		
γ OH	930	940	700	
ν C-C	860	865		
ν OH	ca 770	750	ca 500	470
ν CF_3	787	790		795
δ COO	705	680		695
π CCO	560	570		605
δ CF_3	583	585		570
δ CF_3	510	512		
ρ CCF_3	425	427	422	420
δ CCO	386	390	370	350
π CCF_3	265, 254	268, 255	255	245
lattice mode	99			
CF_3 torsion	53			

Isotopic shifts	ν OH/ν OD	δOH/δ OD	γ OH/γ OD
	1.59	1.37	1.34

both A and B are active for $NaH(OAc)_2$. The different space group of $CsH(OTF)_2$ may in some way be connected with the breadth of $\nu C{=}O$ in the IR spectrum.

Similar remarks can be made to the insensitivity of $\nu C{=}O$ to temperature and its shift to lower frequency on deuteration as noted previously in the $NaH(OAc)_2$ system. Also, a Raman spectrum of $RbH(OTF)_2$ showed a sharp band of low intensity at $1774cm^{-1}$ which can be straightforwardly assigned to the in-phase $\nu C{=}O$.

The region between $1500cm^{-1}$ and $1200cm^{-1}$ is analogous to that in the $NaH(OAc)_2$ system and provides additional confirmation of the absence of any bands due to νOH and νOD in this region. The two bands at $1414cm^{-1}$ and $1230cm^{-1}$ in the spectrum of $RbH(OTF)_2$ can, therefore, be assigned to νCO and δOH, respectively. For $CsH(OTF)_2$ the band associated with δOH is masked by high intensity CF_3 vibrations but its presence is suspected by the reduction in complexity on deuteration.

$1200 - 200cm^{-1}$

The effect of cooling and deuteration on the IR spectrum of $H(OTF)_2$ systems in this region is similar to that observed in the $NaH(OAc)_2$ system. The contraction of the broad absorption at $-196^{\circ}C$ is more marked in $H(OTF)_2$ systems and several distinct bands can be seen. A comparison with the Raman data on $RbH(OTF)_2$ for this region shows that the strong band at $847cm^{-1}$ in the IR spectrum and the band at $857cm^{-1}$ in the Raman spectrum is associated with νCC. The region near $800cm^{-1}$ is complicated by CF_3 modes, which can be identified by their intensity and sharpness in the IR spectrum. The latter vibrations are, however, much weaker in intensity in the Raman spectrum.

The strong bands at 760cm^{-1} and 700cm^{-1} are similar in frequency and breadth to those observed in the IR spectrum of $NaH(OAc)_2$. A comparison with published results on the IR spectrum of OTF^- shows that the 700cm^{-1} band is δCOO (117). Its breadth and intensity must be associated with Fermi resonance with the 0-1 transition, at 760cm^{-1}. These assignments were confirmed on deuteration where the region above 700cm^{-1} was less complicated together with the appearance of a new band at 500cm^{-1} and an increase in breadth of δCCO at 368cm^{-1}. In the IR spectrum of $CsH(OTF)_2$ the band at 580cm^{-1} is much more intense and broader than the corresponding band in $RbH(OTF)_2$. This band is, however, a RCO_2 skeletal vibration and is, therefore, in Fermi resonance with the 0-1 transition.

The absence of any strong band in the region of 700cm^{-1} in the Raman spectrum of $RbH(OTF)_2$ is confirmation of the selection rules operating, ie. mutual exclusion principle. The 0-2 transition should, however, be Raman active and may be associated with the broad absorption in the region of 1150cm^{-1}. However, CF_3 modes of vibration occur also at 1150cm^{-1} and may add to the complexity of this region.

The remaining bending vibration, γOH, is clearly visible at 940cm^{-1} and is similar in frequency to γOH in $NaH(OAc)_2$. On deuteration changes occur in this region which are associated with the appearance of δOD, which has shifted down from 1230cm^{-1}, and the disappearance of γOD. The precise frequency of γOD is uncertain for the same reasons as outlined previously, but it must be in the region of 700cm^{-1} by analogy with $NaD(OAc)_2$.

The IR spectrum $H(OTF)_2^-$ systems below 200cm^{-1} is free from any broad absorption. The only bands appearing were also found in

RbOTF, and, therefore must be associated with CF_3 modes of vibration. Details are shown in table 5.11 and assignments have been made as far as possible. In particular the lattice translations of the cation were difficult to find. The reasons for this may be that the strong absorption from the CF_3 group masks the lattice vibrations which are probably in the region of $100cm^{-1}$, $130cm^{-1}$ in $CsH(OTF)_2$ and $RbH(OTF)_2$ respectively (117). The failure to find any absorption other than CF_3 modes is consistent with the C_i point group of the anions. The three H-bond vibrations, which originate from lost translational degrees of freedom, are all IR inactive (modes of vibration shown in fig. 1.3). The Raman spectrum indicated a band at $182cm^{-1}$ in $RbH(OTF)_2$ which seems a likely candidate for the symmetric stretch. Also, a band was found at about $170cm^{-1}$ from inelastic neutron scattering data for $KH(OTF)_2$ and, therefore, seems a likely candidate for $\nu(O...O)$. The transparency of this region in the IR spectrum which is contrary to the Raman and inelastic neutron scattering spectrum, suggests, therefore, that selection rules based on a C_i point group are fully operating. The H-bond vibrations arising from lost rotational degrees of freedom will be at a considerably lower frequency than those arising from translation and, therefore, may not be observable in the region of the interferometer.

TABLE 5.11

Far IR data on $H(OTF)_2$ Systems

	RbOTF	$RbH(OTF)_2$	$RbD(OTF)_2$	$CsH(OTF)_2$
CF_3 modes	37	40	40	52
		83	78	80
	105	108	107	100
	135	118		

TABLE 5.12

Ineleastic Neutron Scattering Data

$KH(OTF)_2$

H-bond vibration or Lattice mode	$62cm^{-1}$
ν (O-O)	$170cm^{-1}$

7. Hydrogen Di-trichloroacetate Anion, $H(OTC)_2^-$

Structural data has not been reported on this system, but IR data on the K and Rb salts suggests that they are members of Type A salts. Assignments are shown in tables 5.13 and 5.14. The region below $1000cm^{-1}$ is complicated by the presence of strong absorption from the CCl_3 groups, but they can be easily recognized by their narrow band width and by comparison with published spectra on the simple salts (116). The remaining bands are associated with proton and skeletal vibrations of the carboxylate group. The band breadth of the latter skeletal vibrations as in previous systems, is due to Fermi resonance with the 0-1 transition. The latter was confirmed on deuteration where δ CCO is very broad as a result of the proximity of the 0-1 transition at $500cm^{-1}$. The bending vibrations, δ OH and γ OH, were found at their usual frequencies and show normal isotopic shifts.

The region below $200cm^{-1}$ was examined and showed similar features to those observed in the $H(OTF)_2^-$ system, (table 5.15). The bands observed were very sharp and no evidence was found for any H-bond vibrations. The narrow band width and high intensity of the bands suggests that they are due to CCl_3 modes of vibration. As in the $H(OTF)_2^-$ system the spectra of $H(OTC)_2^-$ samples are consistent with a C_i symmetry for the anion. Inelastic neutron scattering data on $KH(OTC)_2$ showed two bands at $225cm^{-1}$ and $45cm^{-1}$. The moderate scattering cross section of ^{35}Cl (see table 4.17) and the high concentration of chlorine atoms may account for the $225cm^{-1}$ band since strong absorption is evident in the IR spectrum of $KH(OTC)_2$ and $KD(OTC)_2$ at this frequency. The assignment of the lower frequency band ($45cm^{-1}$), as in previous systems, is uncertain. However, its assignment to a lattice translation of the

TABLE 5.13.

Assignment of Vibrational Spectrum of $KH(OTC)_2$

Approx. Description	$KH(OTC)_2$		$KD(OTC)_2$	
	25°C	-196°C	25°C	-196°C
ν C=O	1768	1765	1720	1720
ν C-O	1315	1330	1332	1335
δ OH	1200	1212		870
γ OH	-	990	690	690
ν C-C	masked	masked	masked	masked
ν OH	850	860	540	540
ν CCl_3	845	830	825	825
δ CCO	780	790	-	ca 760
ν CCl_3	710	710	705	700
ν CCl_3	675	675	670	671
π CCO	-	640	-	640
δ CCl_3	435	436	420	415
δ CCO	420	420	408	408
π CCl_3	272	275	270	270
δ CCl_3	280	280	270	270
δ CCl_3	280	280	270	270
ρ CCl_3	211			
ρ CCl_3	195			

Isotopic Shifts	ν OH/ν OD	δ OH/δ OD	γ OH/γ OD
	1.60	1.40	1.43

TABLE 5.14

Assignment of Vibrational Spectrum of $RbH(OTC)_2$

Approx. Description	$RbH(OTC)_2$		$RbD(OTC)_2$	
	25°C	-196°C	25°C	-196°C
ν C=O	1750	1748	1710	1700
ν C-O	1300	1325	1340	1343
δ OH	1205	1215	870	890
γ OH	960	990	705	700
ν C-C	-	945	-	931
ν OH	850	890	520	810
ν CCl_3	840	840	836	838
δ COO	770	768	-	770
ν CCl_3	715	710	705	700
ν CCl_3	680	680	680	680
π CCO	-	625	-	630
δ CCl_3	430	430	430	400
δ CCO	420	422	410	400
π CCl_3	285	285	285	268
δ CCl_3	275	263	272	268
δ CCl_3		265	272	268
ρ CCl_3	210			
ρ CCl_3	195			

Isotopic Shifts	ν OH/ν OD	δ OH/δ OD	γ OH/γ OD
	1.66	1.37	1.41

anion cannot be ruled out without further evidence.

TABLE 5.15

Far IR Data

Approx. Description	$KH(OTC)_2$	Approx. Description	$RbH(OTC)_2$ *
L (Anion)	40		
CCl_3 modes	88 124	CCl_3 mode or L(Rb)	104
L(K)	144		
CCl_3 mode	196 212	CCl_3 mode	210

* Very thin mull

Inelastic Neutron Scattering Data

	$KH(OTC)_2$
L(Anion)	45 cm^{-1}
CCl_3 mode	225 cm^{-1}

NQR studies were also carried out on $H(OTC)_2^-$ systems and details are shown in tables 5.16, 5.17 and 5.18. Three signals were observed which seems to confirm the equivalence and intermediate character of the carboxylate groups. The origin of the three signals is associated with a fixed conformation of the CCl_3 group with respect to the COO plane.

Spectra recorded at room temperature did not indicate any marked free rotation of the CCl_3 group, since in all spectra three signals were observed (125).

The most interesting point to emerge from the NQR work is the insensitivity of the signals to isotopic substitution of the hydrogen. This can be contrasted with Type B hydrogen dicarboxylate systems, discussed in chapter four, where large isotopic shifts were observed. The explanation given in Type B salts was that each ^{35}Cl signal was averaged over two extreme cases represented by the two possible positions of the proton. The deuterium analogue, however, gave rise to a different average ^{35}Cl signal because the probability of finding the deuterium in the two wells is different to that of the proton. Thus the NQR of Type B salts can be explained on the basis of an asymmetric double minimum potential well where the asymmetry, as seen by NQR, is accentuated in the deuterium analogue. In Type A salts, however, the fact that separate signals for each end of the anion was not observed and the insensitivity towards deuteration suggests that these salts are consistent with the well shown in figure 5.5.

NQR data from a variety of systems are shown in tables 5.16 and 5.17. These salts were not studied in detail, but the NQR data

on the aromatic systems shown are consistent with them being Type A salts. Also, the NQR of chlorinated maleate systems were recorded and in the dichloro case, the insensitivity towards deuteration is clearly observed, but in each sample two signals were observed. An intermolecular H-bond can, however, be eliminated in the latter since its IR spectrum in the solid phase and in DMSO are identical (28). The NQR results on KH(DCM) are perhaps not so remarkable since a symmetric H-bond has been suggested in KH(MCM) even though the two COO groups are nonequivalent (76)

TABLES 5.16, 5.17 and 5.18

NQR Data at 77°K

TABLE 5.16

NQR (^{35}Cl) Data at $77^{o}K$

Compound	Frequency, Mc/s
KOTC	No signals observed
$KH(OTC)_2$	39.115, 39.155, 39.750
$KD(OTC)_2$	39.065, 39.120, 39.685
HOTC	40.240, 40.165, 39.967 (126)
RbOTC	No signals observed
$RbH(OTC)_2$	39.115, 39.220, 40.18
$RbD(OTC)_2$	39.120, 39.220, 40.18
KOp-CB	35.480
$KH(Op\text{-}CB)_2$	35.395
HOp-CB	34.673
KOm-CB	34.740
$KH(Om\text{-}CB)_2$	34.880
HOm-CB	35.227
K_2O_2DCM	35.485, 35.980
$KH(O_2DCM)$	36.590, 37.180
$KD(O_2DCM)$	36.580, 37.170
$H_2(O_2DCM)$	37.690, 38.140
Anhydride	37.980, 38.055
$KH(O_2MCM)$	37.72
Monochloromaleic anhydride	37.159

TABLE 5.17

Stick Diagram Representation of NQR Data

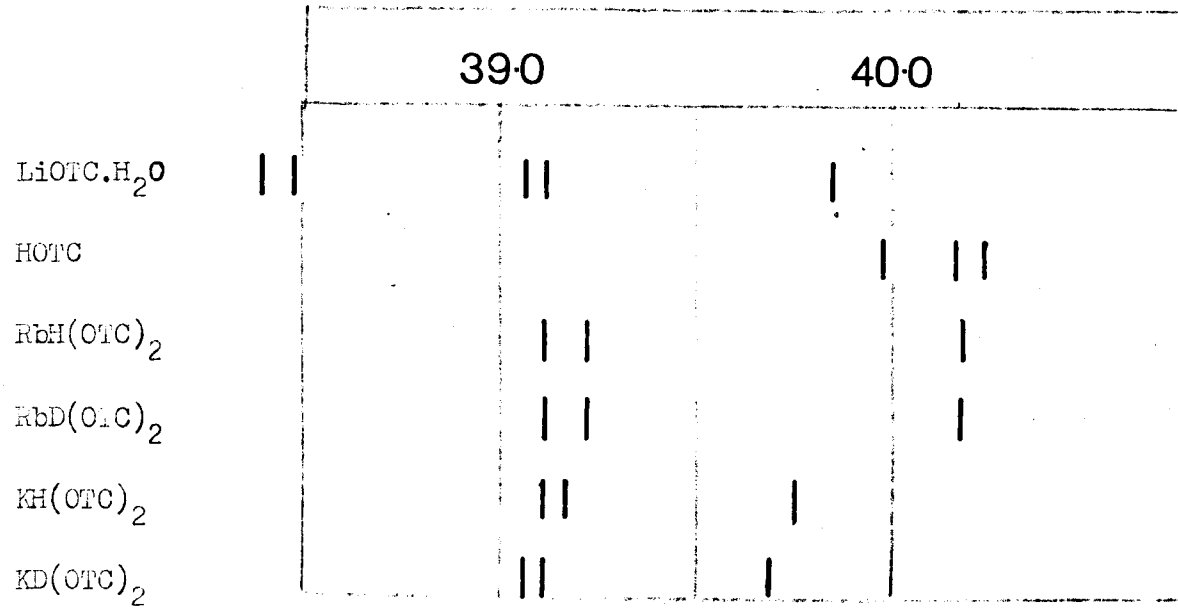

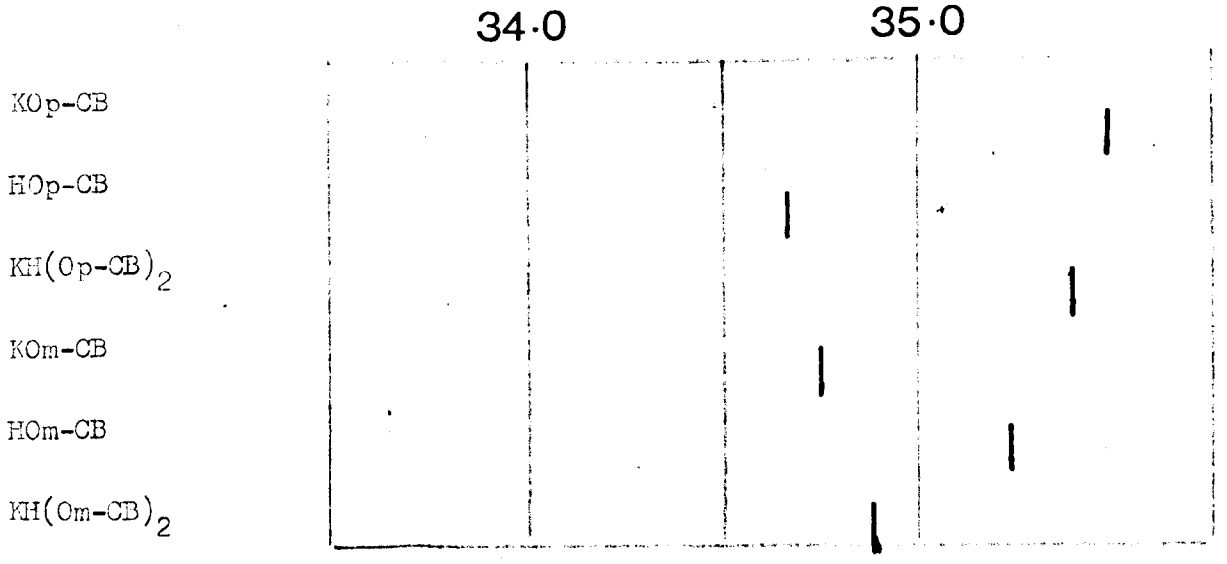

TABLE 5.18

Stick Diagram Representation of NQR Data

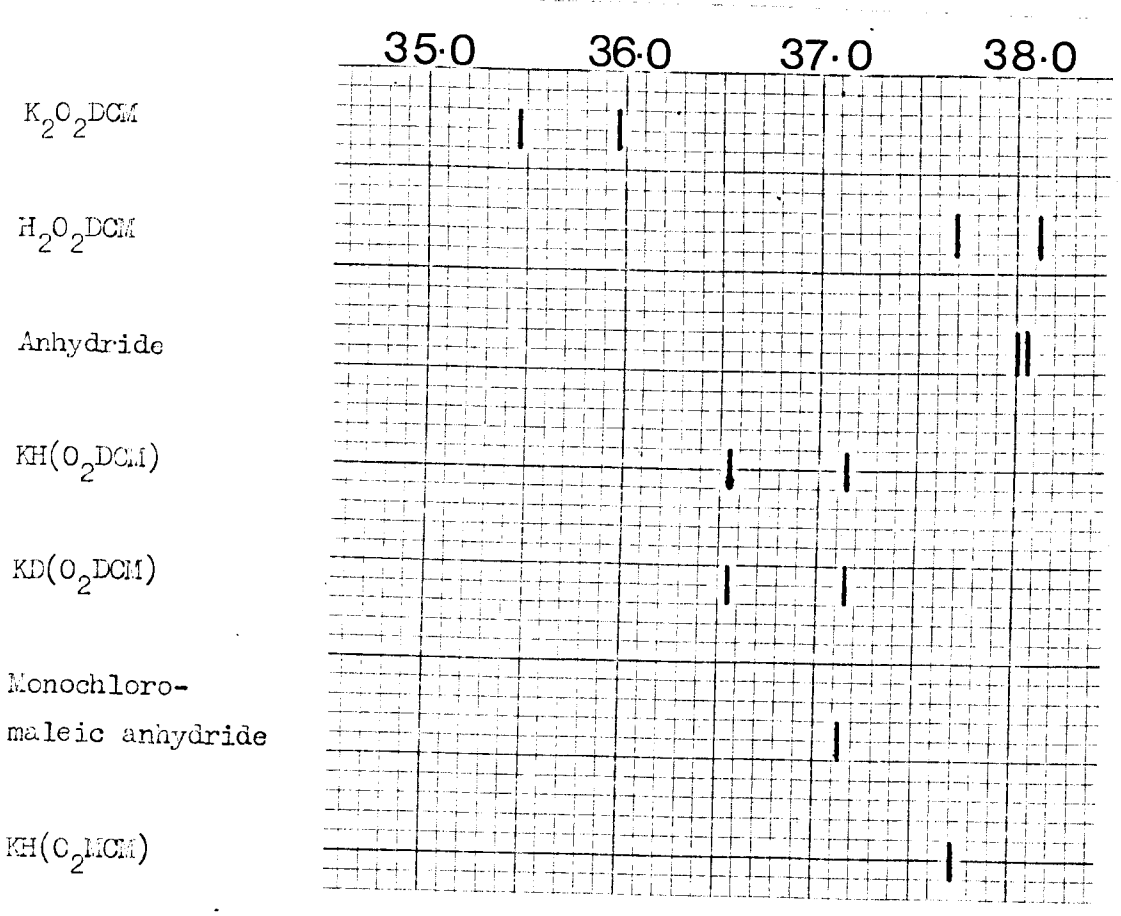

8 Hydrogen Di-tribromoacetate Anion, $H(OTB)_2^-$

Crystallographic data has not been reported for this system. Assignments of their IR spectra are shown in tables 5.20 and 5.19 and spectra are reproduced at the end of this chapter. All the features emphasised so far in this chapter are present also in this system. Also, the narrow band width of $\nu C=O$ and the similarity with the spectrum of $KH(OTC)_2$ suggests that the point group of the $H(OTB)_2$ anion is C_i.

TABLE 5.19

Assignments of Vibrational Spectra of $KH(OTB)_2$

Approx. description	$KH(OTB)_2$		$KD(OTB)_2$	
	25°C	-196°C	25°C	-196°C
ν C=O	1740	1740	1686	1680
ν C-O	1315	1323	1328	1334
δ OH	1200	1196	895	878
γ OH	930	930	670	670
ν C-C	900	905		925
ν OH	ca 800	800	500	470
δ COO	775	780	804	803
$\nu_{as}CBr_3$	760	758	770	772
$\nu_{as}CBr_3$	692	692	685	680
$\nu_{s}CBr_3$	605	606	603	608
π CCO	550	540		540
δ CCO	385	385	375	372
$\delta_{s}CBr_3$	290			288
$\delta_{as}CBr_3$	230	225	230	
ρ $CCBr_3$	185			
π $CCBr_3$	185			

Isotopic Shifts	νOH/νOD	δOH/δOD	γOH/γOD
	1.70	1.35	1.39

TABLE 5.20

Assignments of Vibrational Spectrum of $RbH(OTB)_2$

Approx. Description	$RbH(OTB)_2$	
	25°C	-196°C
ν C=O	1730	1738
ν C-O	1310	1300
δ OH	1195	1205
γ OH	925	920
ν C-C	890	910
ν OH	800	800
δ COO	-	750
$\nu_{as}CBr_3$	770	750
$\nu_{as}CBr_3$	690	685
$\nu_{s}CBr_3$	603	605
π CCO		540
δ CCO	380	382
$\delta_{s}CBr_3$		292
$\delta_{as}CBr_3$		240
ρ $CCBr_3$		
π $CCBr_3$		

9. Hydrogen Di-monochloroacetate Anion, $H(OMC)_2$

It was pointed out in Chapter four that $CsH(OMC)_2$ can be classed as a Type A salt. This is confirmed by its IR spectrum and by NQR data (table 4.8). Assignment of its IR spectrum is shown in table 5.21 and the remarks thereof are analogous to previous systems.

TABLE 5.21

Assignment of Vibrational Spectrum of $CsH(OMC)_2$-

Approx. Description	$CsH(OMC)_2$		$CsD(OMC)_2$	
	25°C	-196°C	25°C	-196°C
ν CH_2	3008	-	-	-
ν CH_2	2962	-	-	-
ν C=O	1725	1730	1685	1685
ν C-O	1410	1412	1405	1408
δ CH_2	1400	1400	1400	1400
δ CH_2	1220	1235	1232	1245
CH_2 wagging	1180	1183	1180	1182
CH_2 twist	1200	1205	1215	1220
δ OH(D)	1300	1305	950	910 - 950
ν OH(D)	ca 700	ca 700	450	460
γ OH(D)	940	950	715	715
CH_2 rock	915	916	930	930
ν C-C	932	935	890	890
ν CCl	785	785	775	780
δ COO	710	690	685	685
π COO	538	540	555	560
δ COO	395	400	360	350

Isotopic Shift (-196°C	ν OH/ν OD	δ OH/δ OD	γ OH/γ OD
	1.52	1.36	1.33

10. Conclusion

The main conclusions concerning the IR spectrum of Type A hydrogen dicarboxylate salts are summarised below:

(1) Absence of any band above 1300cm^{-1} that can be assigned to νOD or νOH.

(2) The bending vibrations, δ OH and γ OH, were found at similar frequencies in all the anions and show normal isotopic shifts.

(3) The band assigned to νOH (ie. the 0-1 transition) is lower in frequency than either δ OH or γOH and shows abnormally high isotopic shifts (ie. greater than $\sqrt{2}$).

(4) Fermi resonance coupling of ν OH and ν OD with RCOO skeletal vibrations is invoked to explain band breadth of the latter.

(5) The far infrared spectra were consistent with the point group of the anions

The most remarkable feature in the conclusions above concerns the assignment of νOH (0-1 transition) at a frequency below that of both δ OH and γ OH. Such a situation is impossible in a harmonic potential energy surface and so clearly the shape of the well along the bond axis is considerably more anharmonic than that lateral to the bond axis. Also, the high isotopic shift observed in all cases is consistent with an anharmonic well (128). The justification of the previous sentence is based on a short paper by Blinc where he questioned the proposed symmetry of HF_2^- (128). Blinc suggested that if there was any quartic character in the potential energy well of the proton, then the isotopic shift would be greater than 1.41 (128). Blinc suggested that to a first approximation the isotopic shift is given by $(m_D/m_H)^{n/n+2}$, where

the potential energy varies for small displacements, as the n^{th} power of the displacement (128). Blinc then suggested an alternative assignment of the IR spectrum of KHF_2 based on a symmetric double minimum with a very low potential energy barrier (figure 5.5). It was suggested that the strong band at $1450cm^{-1}$, which was previously assigned to νFH, represented a large splitting of the ground state and was, therefore, an IR allowed "even-odd" transition. Similarly the first overtone is an "even-even" transition and is, therefore, forbidden in the IR spectrum. These predictions fitted the spectral data up to $6000cm^{-1}$, and it was concluded that it was a matter of convenience whether to say that the H-bond in KHF_2 is a symmetric one or that it represents a limiting case of a double minimum type (128).

In view of the recent work of Ibers, which has already been discussed, the model proposed by Blinc seems doubtful in HF_2^-. However, the model shown in figure 5.5 is essentially the same as that proposed by Blinc. Therefore, in view of the work of Hornig, Sormorjai and Blinc the model chosen is capable of explaining both the high isotopic shift of νOH, and its low frequency since the transition (0-1) is essentially the splitting of the ground state as a result of a low potential energy barrier.

The HCl_2^- system, particularly those which are thought to be symmetric (see chapter one) also show a high isotopic shift for νHCl, (55). In a recent paper Pimentel and Noble prepared HCl_2 radical and suggested that νHCl was at $694cm^{-1}$ and had an isotopic shift of 1.50 (129). Thus both these cases are similar to the Type A hydrogen dicarboxylates in that they show some of the IR features summarised earlier.

Perhaps the most important piece of evidence concerning the symmetry of Type A salts comes from the neutron diffraction study of potassium hydrogen diaspirinate (70). Hamilton et al suggested, but did not give details of the calculation, that the proton was situated in an extremely anharmonic potential energy well with a barrier no greater than 200cm^{-1} in height. Such a model together with the neutron diffraction data gave rise to a frequency of less than 1000cm^{-1} for νOH (70).

The IR spectrum of potassium hydrogen diaspirinate has not been reported in recent years and is, therefore, included at the end of this chapter. It can be seen, even without detailed assignments of its complex structure, that there is a close resemblence to the much simpler Type A salts studied in detail in this chapter.

Thus the remarkable similarity of the IR spectra of the anions discussed in this chapter and potassium hydrogen diaspirinate, together with the close agreement of theory and experiment seems good evidence for suggesting that the proton and deuterium in Type A salts are symmetrically located between the oxygen atoms.

11. Experimental

(1) Reagents

G.P.R. grade Tribromoacetic acid was obtained from Ralph N. Emanual.

G.P.R. grade Trichloroacetic acid was obtained from Hopkin and Williams.

G.P.R. grade Trifluoroacetic acid was obtained from B.D.H.

Monochloro substituted benzoic acids were obtained from B.D.H.

Monochloromaleic anhydride was obtained from Columbia Organic Chemical Co., inc.

The remaining chemicals and reagents used are listed in chapters two, three and four.

(2) Preparation

Details of experimental work is recorded in chapter four.

(3) Analytical data is tabulated in table 5.22.

TABLE 5,22

Analytical Data

Compound	Acid % by Weight		Elemental % by Weight									
			Cation		Carbon		Hydrogen		Halogen		Oxygen	
	Found	Calc.	Found	Calc.	Found	Calc.	Found	Calc.	Found	Calc.	Found	Exp.
$NaH(OAc)_2$	42.27	42.26										
$CsH(OAc)_2$	24.50	23.82										
$RbH(OTF)_2$	34.35	36.48										
$CsH(OTF)_2$	31.42	31.67										
$KH(OTC)_2$	44.16	44.78			13.79	13.16	0.51	0.29	57.74	58.30		
$RbH(OTC)_2$	42.09	39.73			12.46	11.68	0.51	0.25	52.36	51.36	16.64	15.56
$KH(OTB)_2$					7.81	7.56	0.14	0.73	74.92	75.59		
$RbH(OTB)_2$			12.32	12.60	6.96	7.08	0.16	0.14	70.66	70.71		
$KH(OM\text{-}CB)_2$					48.47	47.87	2.76	2.52	19.92	20.19		
$KH(Op\text{-}CB)_2$					49.45	47.87	2.90	2.52	19.38	20.19		
KH(ODCM)					21.45	21.53	0.61	0.45	31.45	31.79		

S P E C T R A

C O N T E N T S

All spectra have been recorded at -196°C unless specifically stated to the contrary. Far IR and Raman Spectra were all recorded at room temperature. Nujol mulls have been used throughout and H.C.B. was used for the regions between 3000 - 2800cm^{-1} and 1500 - 1300cm^{-1}.

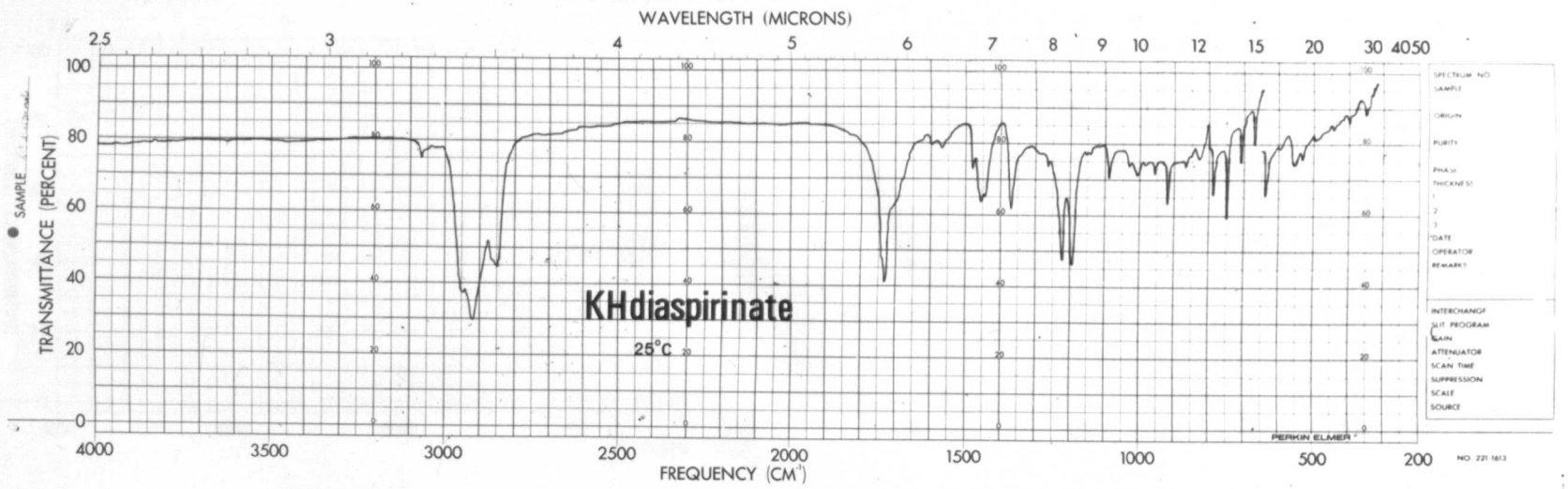
WAVELENGTH (MICRONS)
2.5
3
4
5
6
7
8
9
10
12
15
20
30
40
50
TRANSMITTANCE (PERCENT)
SAMPLE
KH diaspirinate
25°C
FREQUENCY (CM⁻¹)
4000
3500
3000
2500
2000
1500
1000
500
200
PERKIN ELMER
NO. 221-1613
SPECTRUM NO.
SAMPLE
ORIGIN
PURITY
PHASE
THICKNESS
1.
2.
3.
DATE
OPERATOR
REMARKS
INTERCHANGE
SLIT PROGRAM
GAIN
ATTENUATOR
SCAN TIME
SUPPRESSION
SCALE
SOURCE

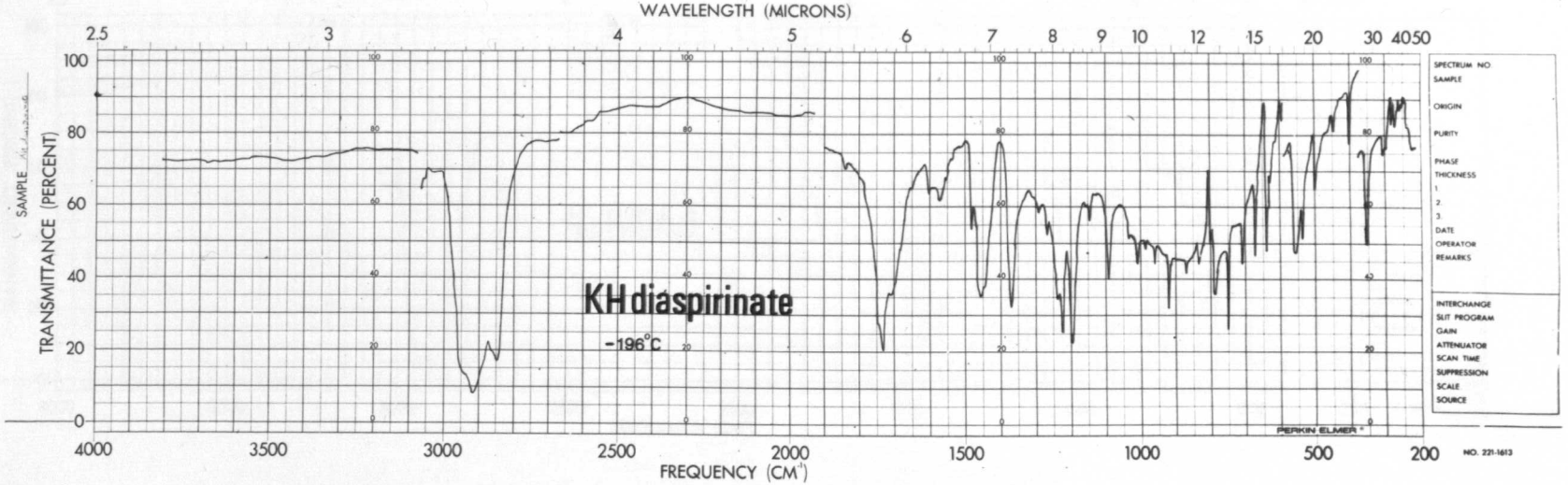
WAVELENGTH (MICRONS)
2.5
3
4
5
6
7
8
9
10
12
15
20
30
40
50
TRANSMITTANCE (PERCENT)
SAMPLE
KH diaspirinate
-196°C
FREQUENCY (CM⁻¹)
4000
3500
3000
2500
2000
1500
1000
500
200
PERKIN ELMER
NO. 221-1613
SPECTRUM NO.
SAMPLE
ORIGIN
PURITY
PHASE
THICKNESS
1.
2.
3.
DATE
OPERATOR
REMARKS
INTERCHANGE
SLIT PROGRAM
GAIN
ATTENUATOR
SCAN TIME
SUPPRESSION
SCALE
SOURCE

A

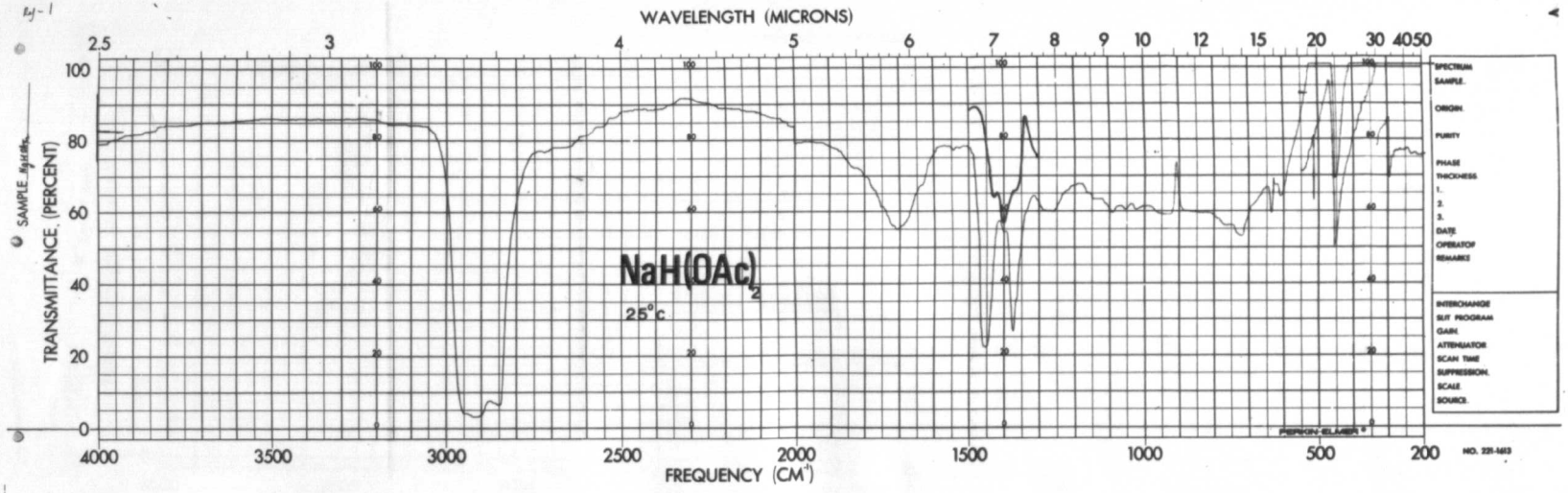
WAVELENGTH (MICRONS)
2.5
3
4
5
6
7
8
9
10
12
15
20
30
40
50
TRANSMITTANCE, (PERCENT)
100
80
60
40
20
0
NaH(OAc)2
25°c
4000
3500
3000
2500
2000
1500
1000
500
200
FREQUENCY (CM-1)

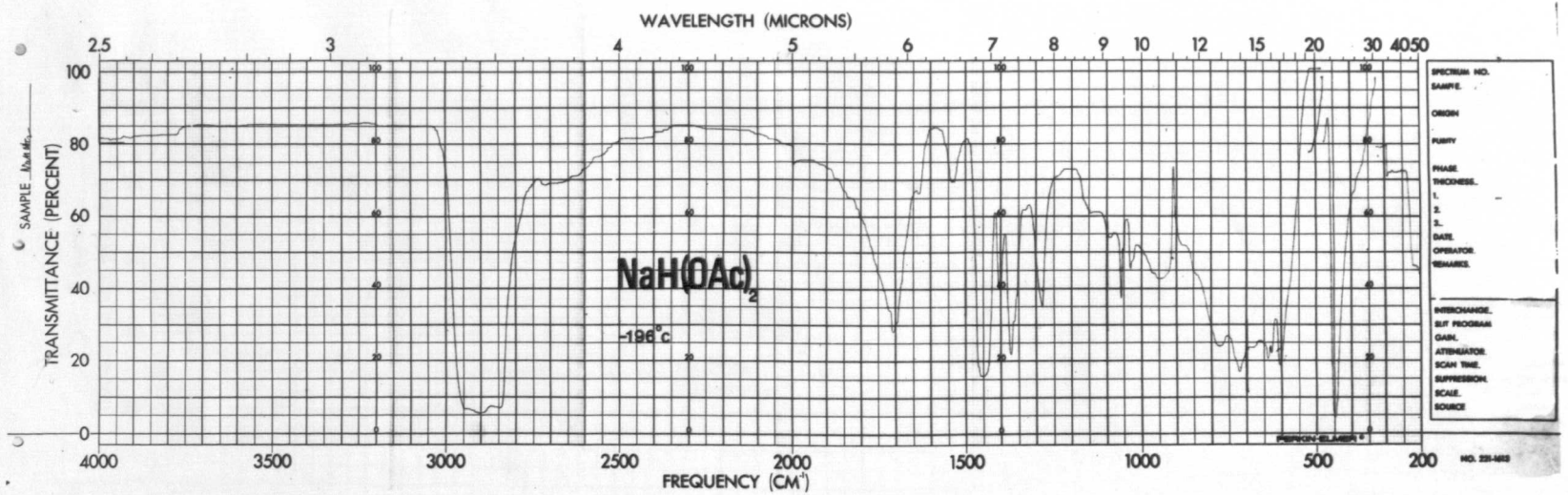
WAVELENGTH (MICRONS)
2.5
3
4
5
6
7
8
9
10
12
15
20
30
40
50
TRANSMITTANCE (PERCENT)
100
80
60
40
20
0
NaH(OAc)2
-196°c
4000
3500
3000
2500
2000
1500
1000
500
200
FREQUENCY (CM-1)

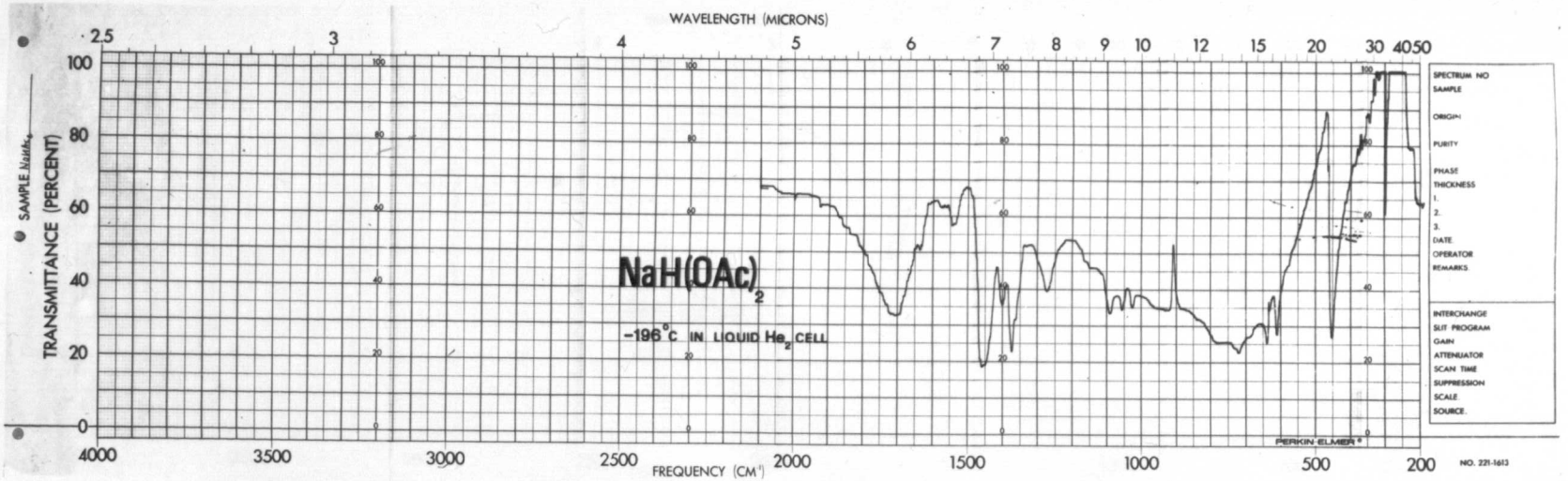
WAVELENGTH (MICRONS)
2.5
3
4
5
6
7
8
9
10
12
15
20
30
40
50
TRANSMITTANCE (PERCENT)
100
80
60
40
20
0
SAMPLE Nah(OAc)2
NaH(OAc)2
-196°C IN LIQUID He2 CELL
4000
3500
3000
2500
2000
1500
1000
500
200
FREQUENCY (CM-1)
PERKIN-ELMER
NO. 221-1613
SPECTRUM NO
SAMPLE
ORIGIN
PURITY
PHASE
THICKNESS
1.
2.
3.
DATE
OPERATOR
REMARKS
INTERCHANGE
SLIT PROGRAM
GAIN
ATTENUATOR
SCAN TIME
SUPPRESSION
SCALE
SOURCE

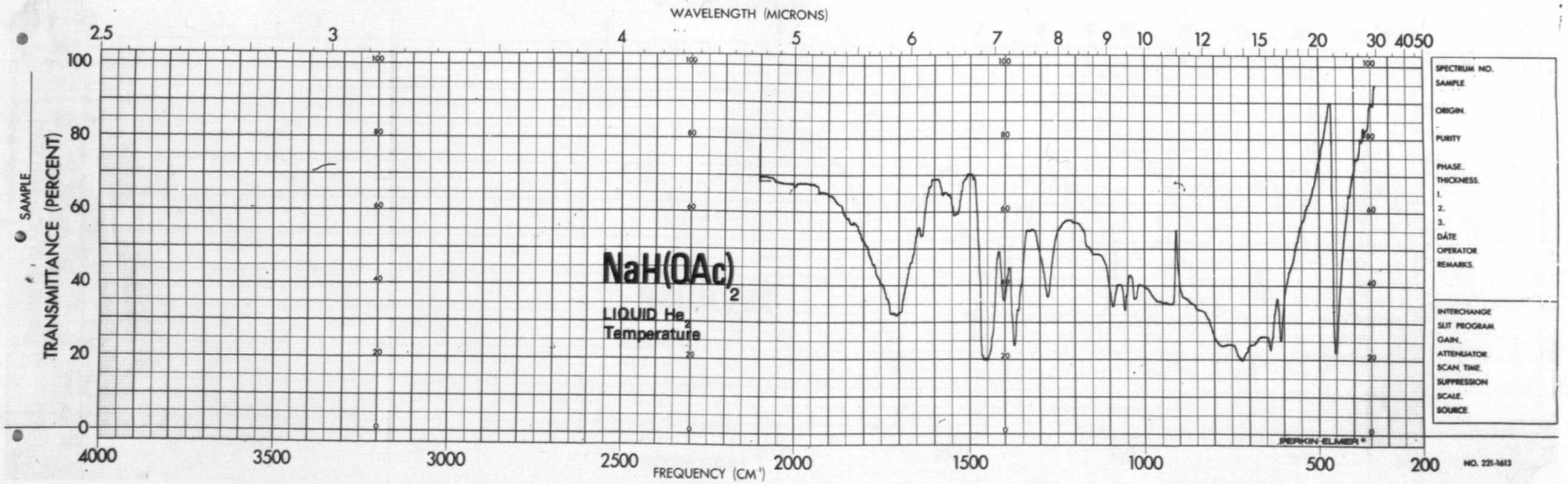
WAVELENGTH (MICRONS)
2.5
3
4
5
6
7
8
9
10
12
15
20
30
40
50
TRANSMITTANCE (PERCENT)
100
80
60
40
20
0
SAMPLE
NaH(OAc)2
LIQUID He2
Temperature
4000
3500
3000
2500
2000
1500
1000
500
200
FREQUENCY (CM-1)
PERKIN-ELMER
NO. 221-1613
SPECTRUM NO.
SAMPLE
ORIGIN
PURITY
PHASE
THICKNESS
1.
2.
3.
DATE
OPERATOR
REMARKS
INTERCHANGE
SLIT PROGRAM
GAIN
ATTENUATOR
SCAN TIME
SUPPRESSION
SCALE
SOURCE

C

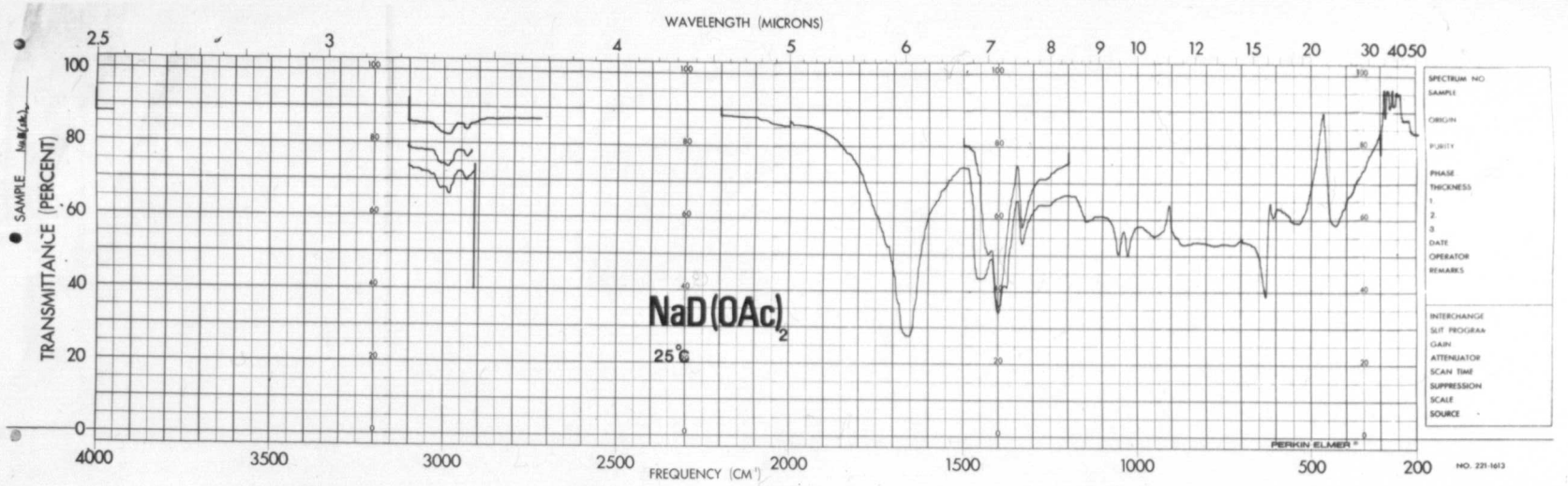
WAVELENGTH (MICRONS)
2.5
3
4
5
6
7
8
9
10
12
15
20
30
40
50
TRANSMITTANCE (PERCENT)
100
80
60
40
20
0
NaD(OAc)2
25°C
4000
3500
3000
2500
2000
1500
1000
500
200
FREQUENCY (CM-1)
PERKIN ELMER
NO. 221-1613

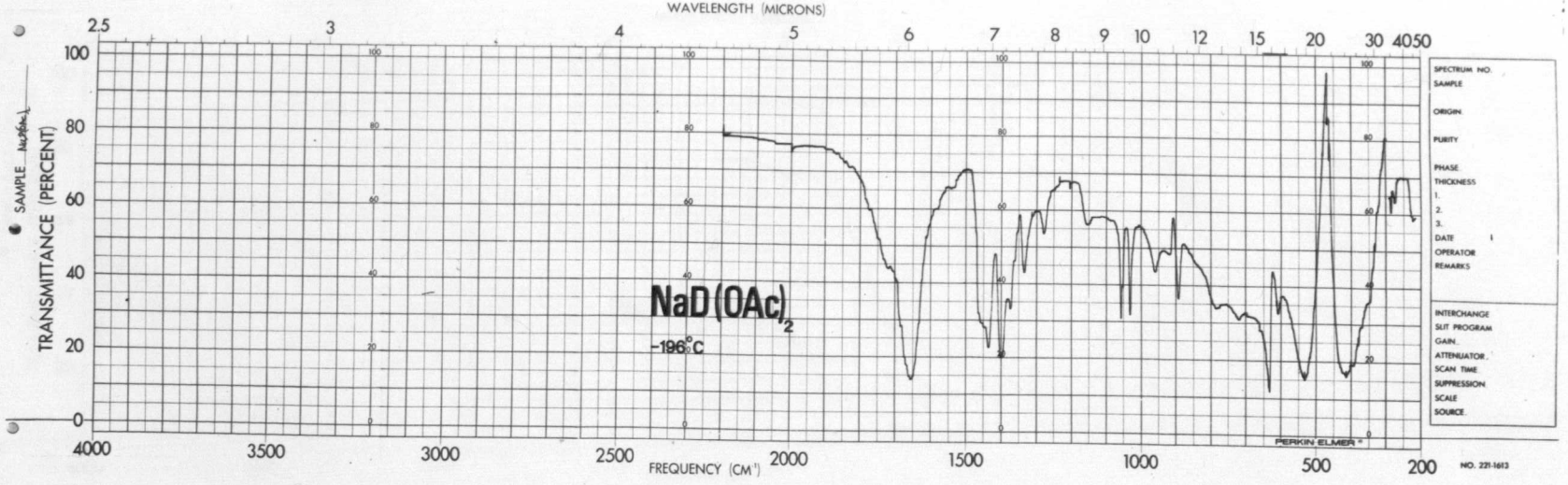
WAVELENGTH (MICRONS)
2.5
3
4
5
6
7
8
9
10
12
15
20
30
40
50
TRANSMITTANCE (PERCENT)
100
80
60
40
20
0
NaD(OAc)2
-196°C
4000
3500
3000
2500
2000
1500
1000
500
200
FREQUENCY (CM-1)
PERKIN ELMER
NO. 221-1613

D

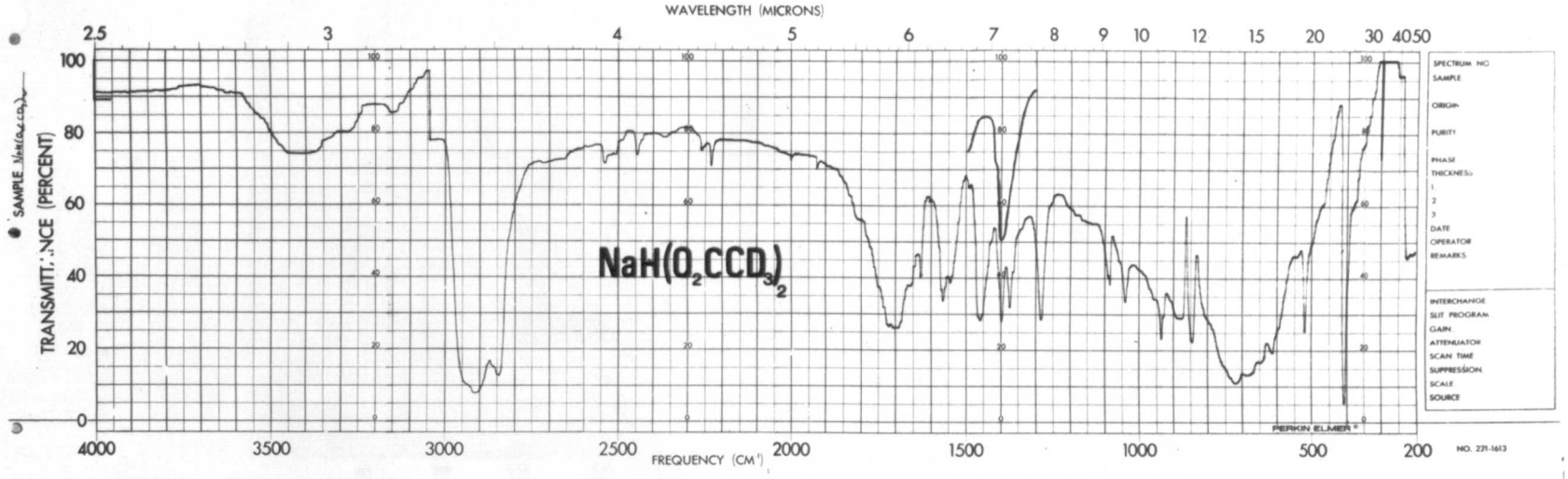
WAVELENGTH (MICRONS)
2.5
3
4
5
6
7
8
9
10
12
15
20
30
40
50
TRANSMITTANCE (PERCENT)
100
80
60
40
20
0
NaH(O2CCD3)2
4000
3500
3000
2500
2000
1500
1000
500
200
FREQUENCY (CM-1)
PERKIN ELMER
NO. 221-1613
SPECTRUM NO.
SAMPLE
ORIGIN
PURITY
PHASE
THICKNESS
1.
2
3
DATE
OPERATOR
REMARKS
INTERCHANGE
SLIT PROGRAM
GAIN
ATTENUATOR
SCAN TIME
SUPPRESSION
SCALE
SOURCE

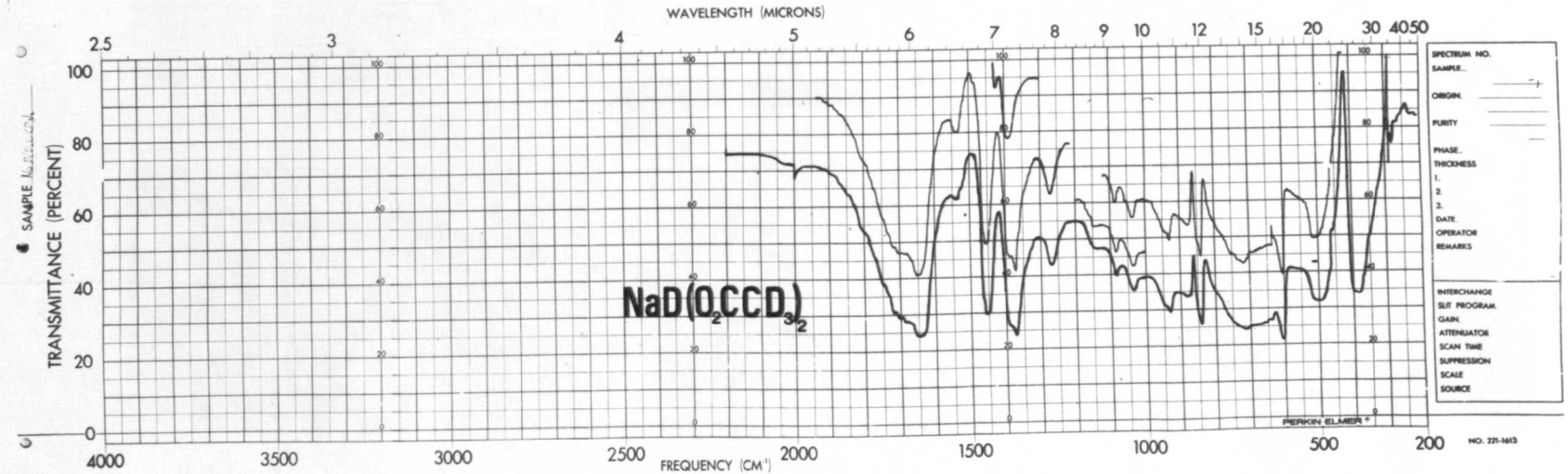
WAVELENGTH (MICRONS)
2.5
3
4
5
6
7
8
9
10
12
15
20
30
40
50
TRANSMITTANCE (PERCENT)
100
80
60
40
20
0
NaD(O2CCD3)2
4000
3500
3000
2500
2000
1500
1000
500
200
FREQUENCY (CM-1)
PERKIN ELMER
NO. 221-1613
SPECTRUM NO.
SAMPLE
ORIGIN
PURITY
PHASE
THICKNESS
1.
2.
3.
DATE
OPERATOR
REMARKS
INTERCHANGE
SLIT PROGRAM
GAIN
ATTENUATOR
SCAN TIME
SUPPRESSION
SCALE
SOURCE

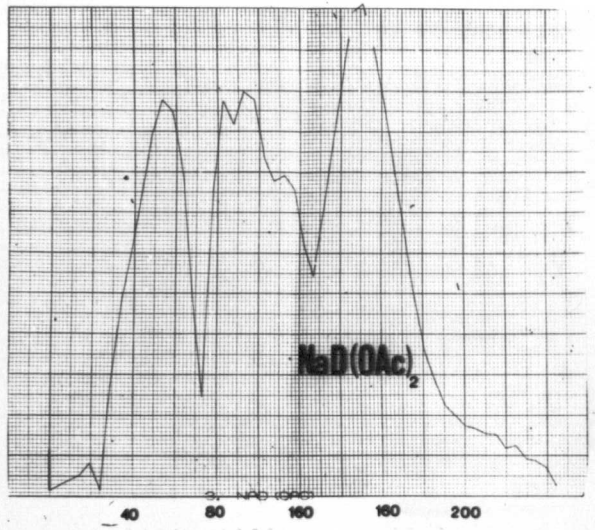
NaD(OAc)2
40
80
160
180
200

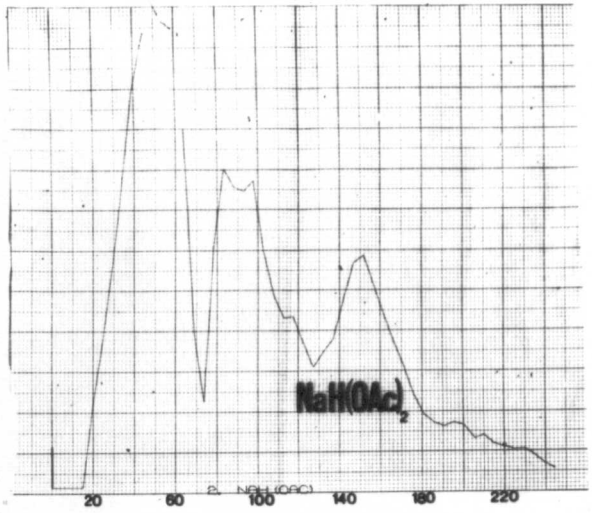
NaH(OAc)2
20
60
100
140
180
220

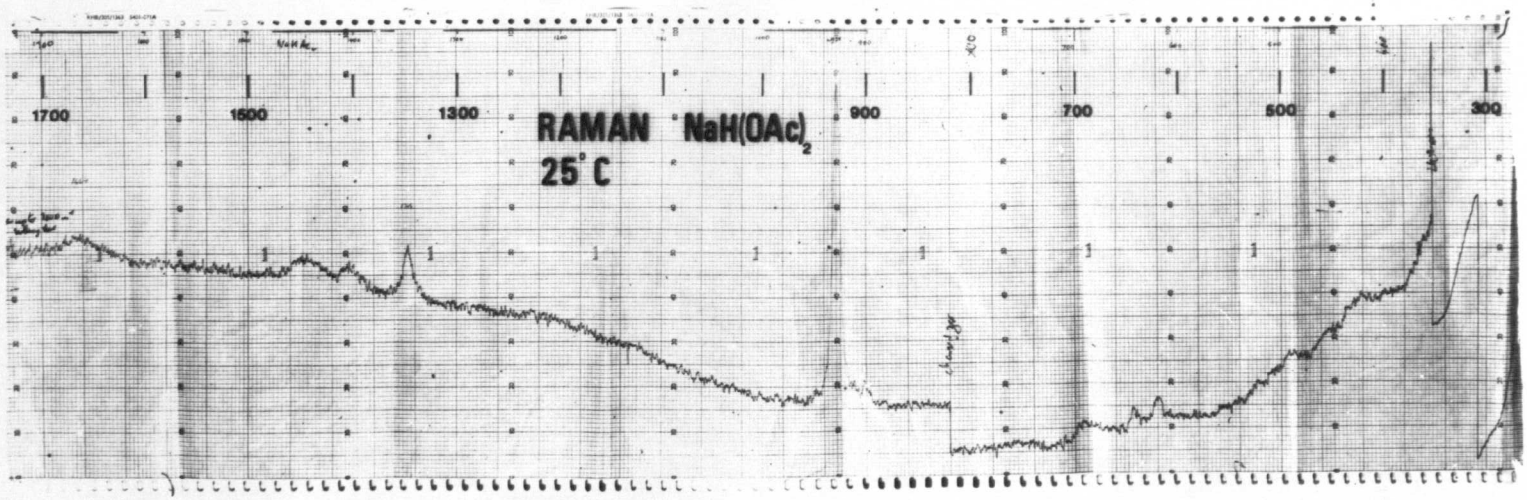
1700
1500
1300
RAMAN NaH(OAc)2
25°C
900
700
500
300

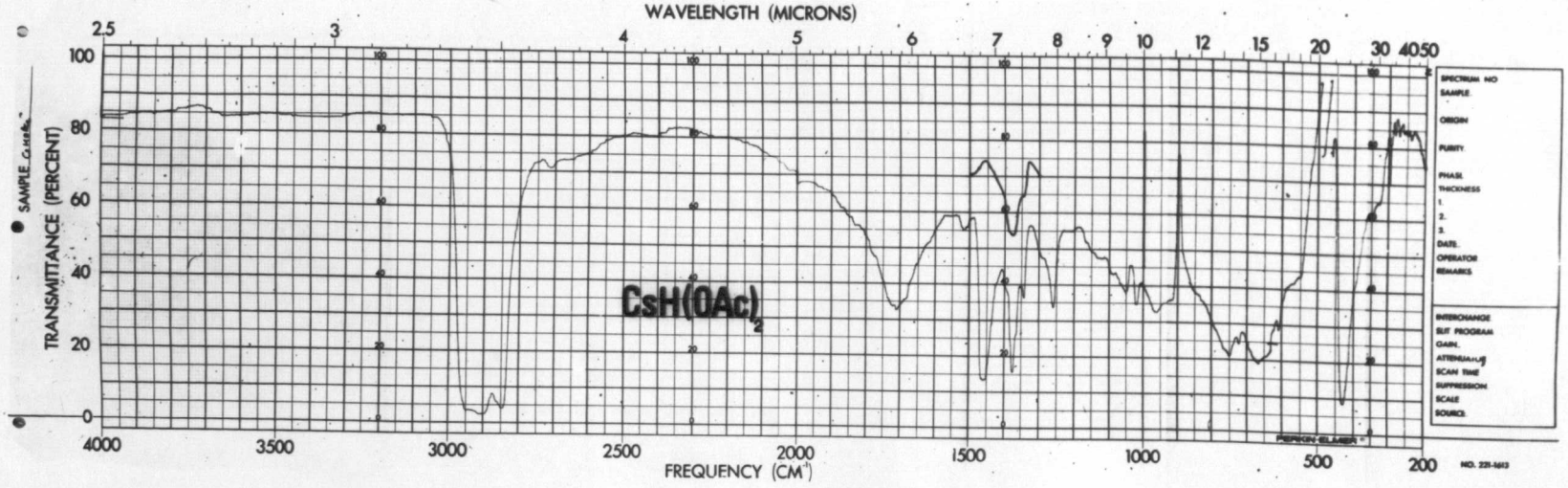
WAVELENGTH (MICRONS)
2.5
3
4
5
6
7
8
9
10
12
15
20
30
40
50
TRANSMITTANCE (PERCENT)
100
80
60
40
20
0
4000
3500
3000
2500
2000
1500
1000
500
200
FREQUENCY (CM⁻¹)
CsH(OAc)2
PERKIN-ELMER

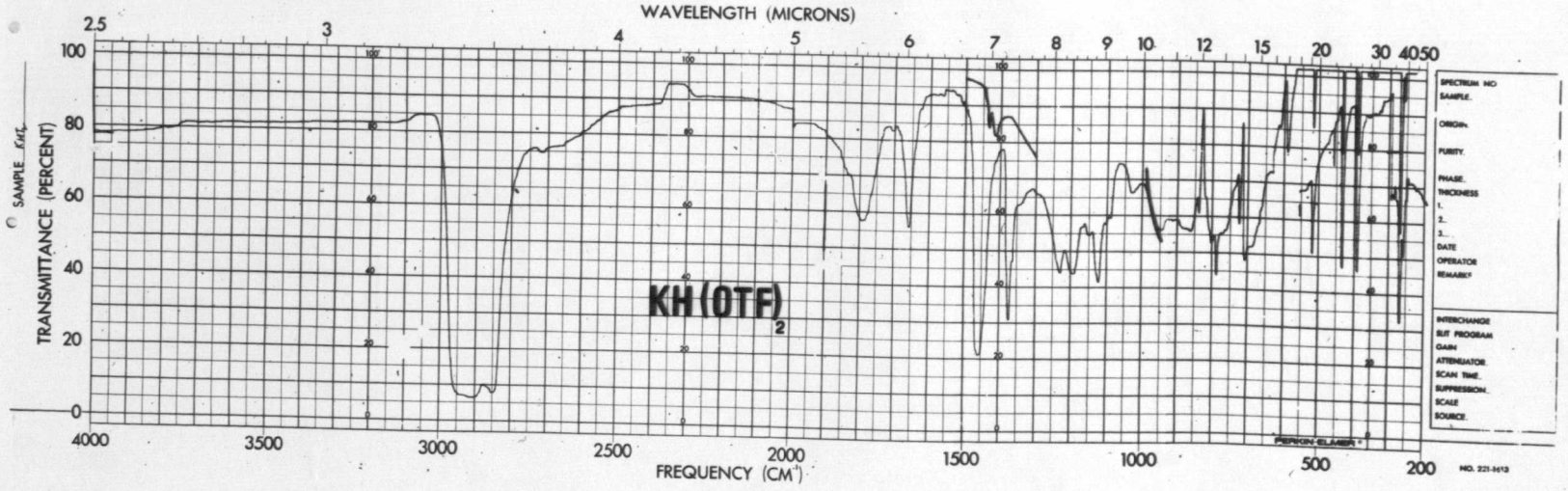
WAVELENGTH (MICRONS)
2.5
3
4
5
6
7
8
9
10
12
15
20
30
40
50
TRANSMITTANCE (PERCENT)
100
80
60
40
20
0
4000
3500
3000
2500
2000
1500
1000
500
200
FREQUENCY (CM⁻¹)
KH(OTF)2
PERKIN-ELMER

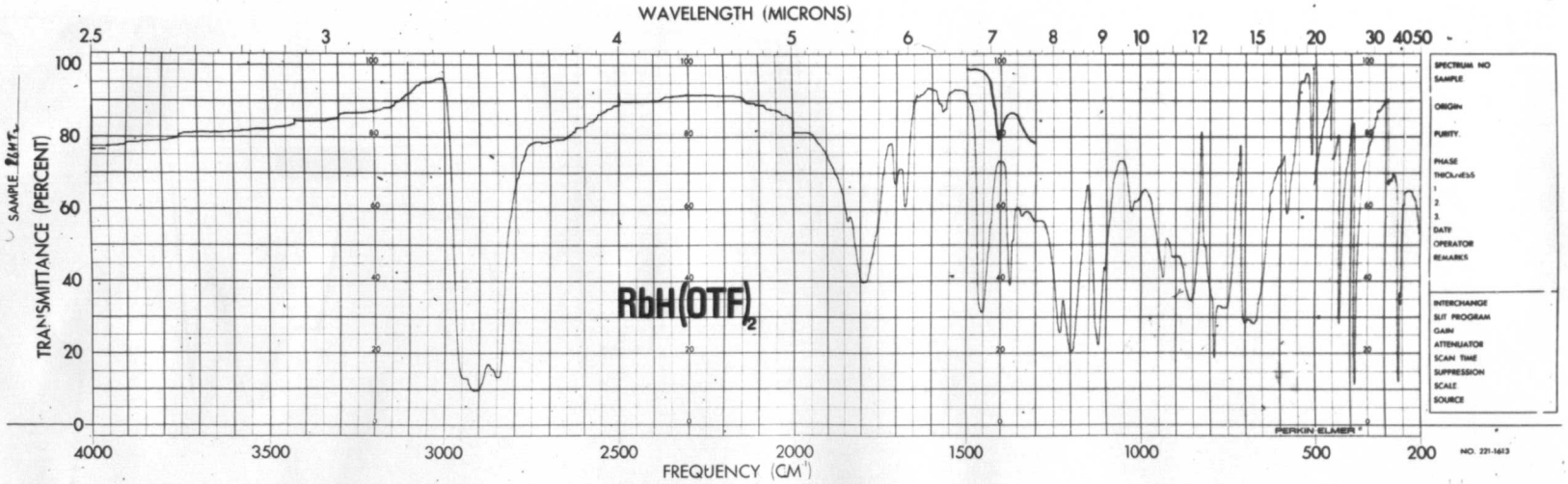
WAVELENGTH (MICRONS)
2.5 3 4 5 6 7 8 9 10 12 15 20 30 40 50
TRANSMITTANCE (PERCENT)
100 80 60 40 20 0
RbH(OTF)2
4000 3500 3000 2500 2000 1500 1000 500 200
FREQUENCY (CM-1)
PERKIN ELMER
NO. 221-1613
SPECTRUM NO
SAMPLE
ORIGIN
PURITY
PHASE
THICKNESS
1
2
3
DATE
OPERATOR
REMARKS
INTERCHANGE
SLIT PROGRAM
GAIN
ATTENUATOR
SCAN TIME
SUPPRESSION
SCALE
SOURCE

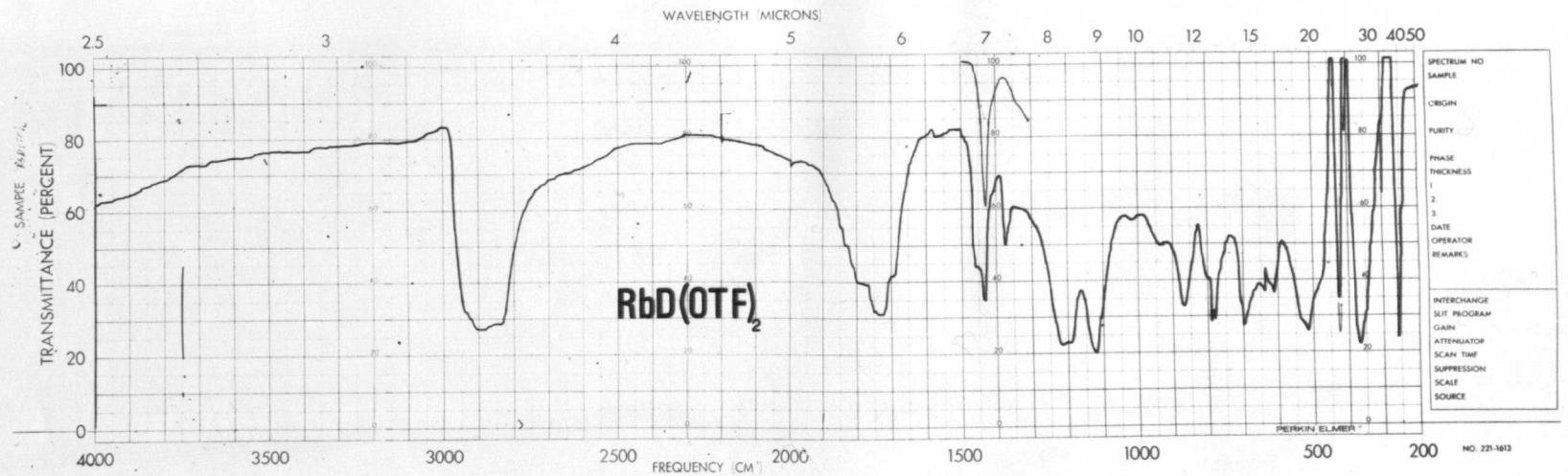
WAVELENGTH (MICRONS)
2.5 3 4 5 6 7 8 9 10 12 15 20 30 40 50
TRANSMITTANCE (PERCENT)
100 80 60 40 20 0
RbD(OTF)2
4000 3500 3000 2500 2000 1500 1000 500 200
FREQUENCY (CM-1)
PERKIN ELMER
NO. 221-1613
SPECTRUM NO
SAMPLE
ORIGIN
PURITY
PHASE
THICKNESS
1
2
3
DATE
OPERATOR
REMARKS
INTERCHANGE
SLIT PROGRAM
GAIN
ATTENUATOR
SCAN TIME
SUPPRESSION
SCALE
SOURCE

H

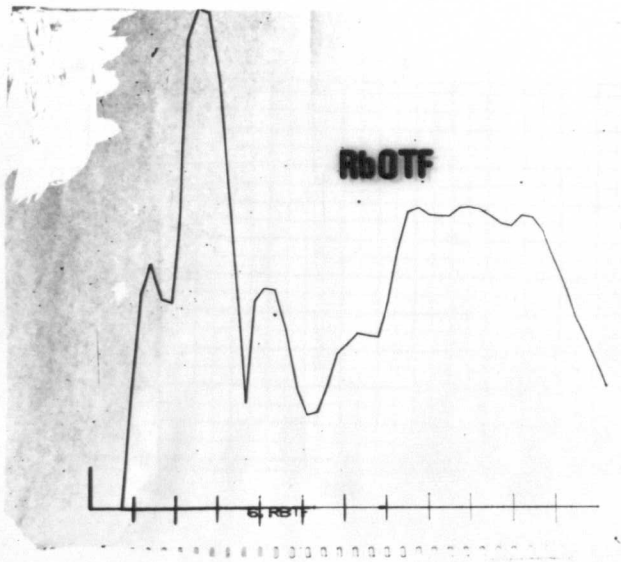
RbOTF

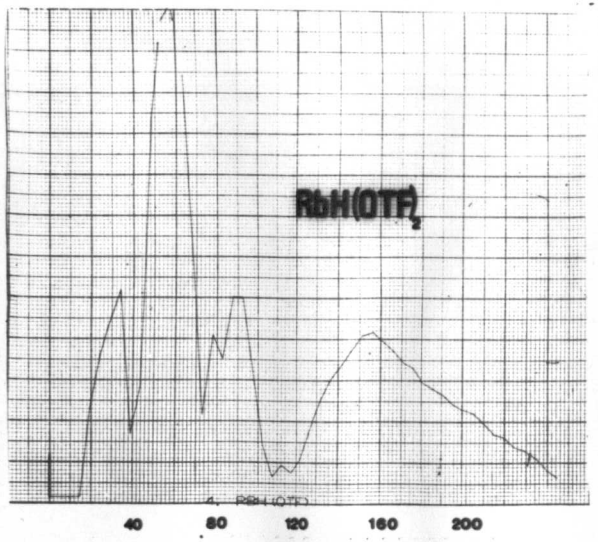
RbH(OTF)2
40
80
120
160
200

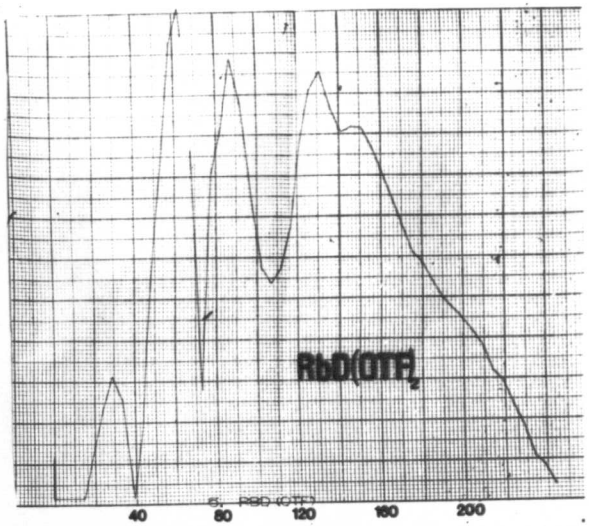
RbD(OTF)2
40
80
120
160
200

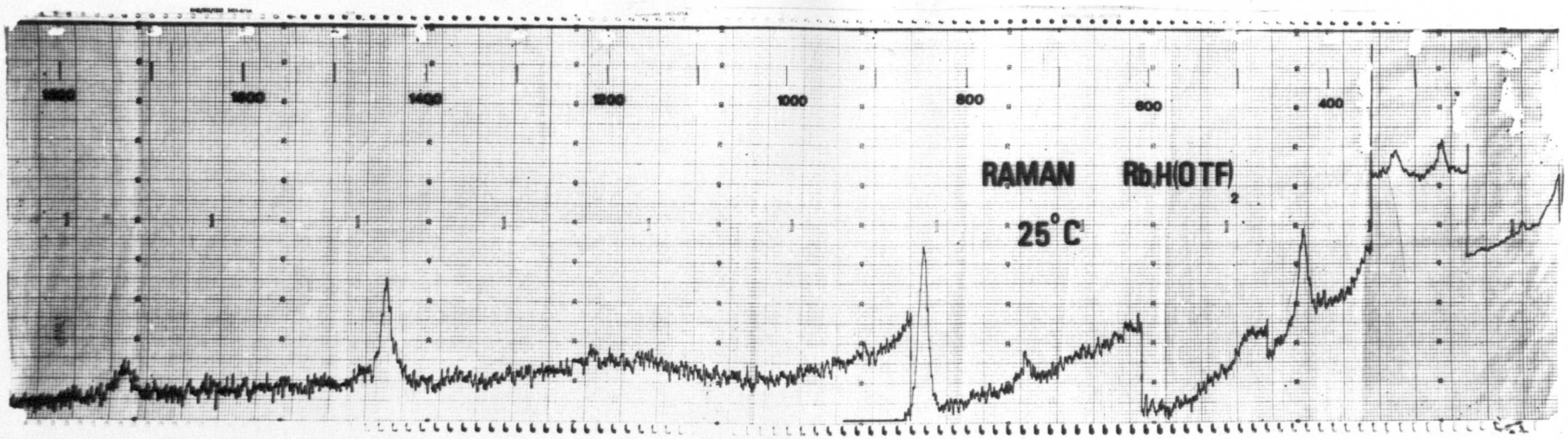
1800
1600
1400
1200
1000
800
600
400
RAMAN
RbH(OTF)2
25°C

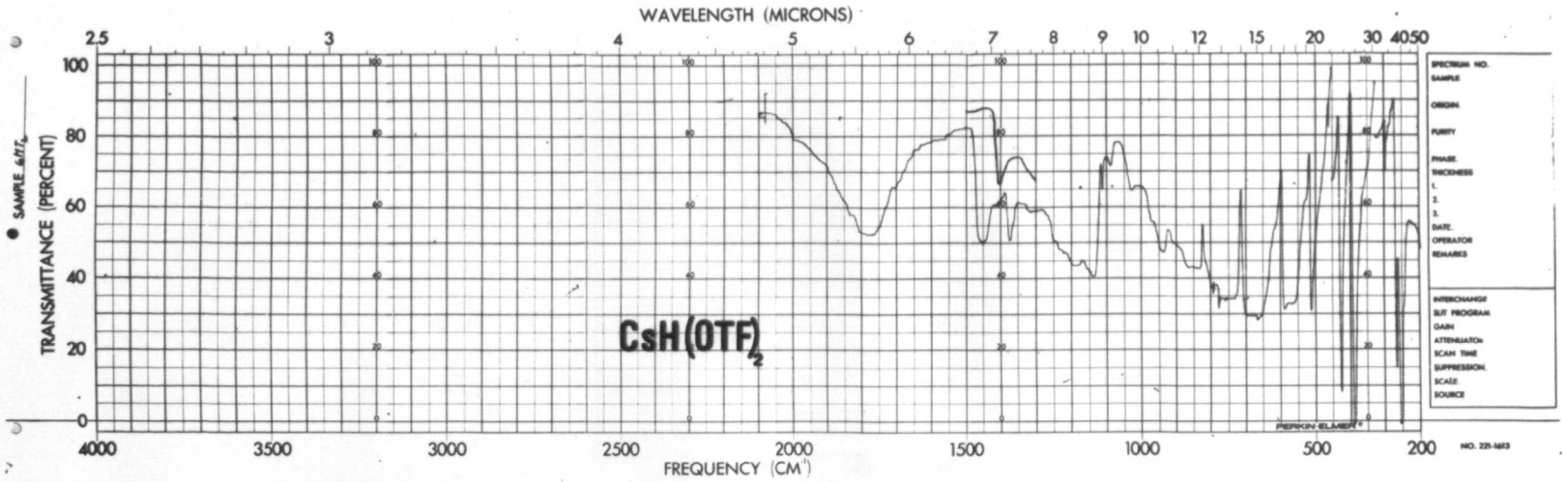
WAVELENGTH (MICRONS)
2.5
3
4
5
6
7
8
9
10
12
15
20
30
40
50
TRANSMITTANCE (PERCENT)
100
80
60
40
20
0
CsH(OTF)2
4000
3500
3000
2500
2000
1500
1000
500
200
FREQUENCY (CM-1)
PERKIN-ELMER

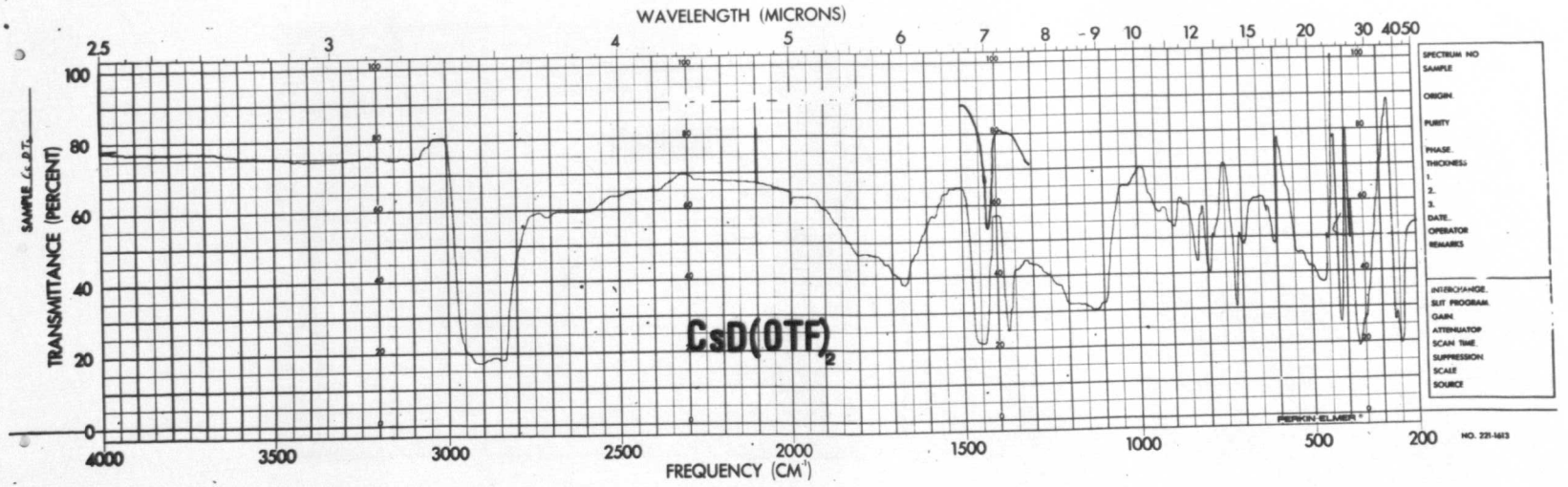
WAVELENGTH (MICRONS)
2.5
3
4
5
6
7
8
9
10
12
15
20
30
40
50
TRANSMITTANCE (PERCENT)
100
80
60
40
20
0
CsD(OTF)2
4000
3500
3000
2500
2000
1500
1000
500
200
FREQUENCY (CM-1)
PERKIN-ELMER

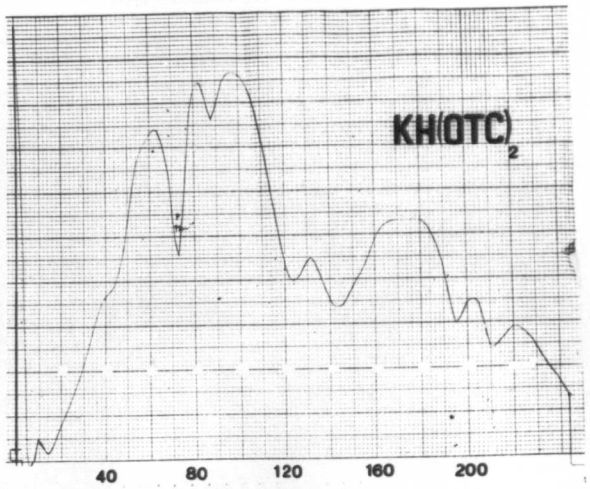

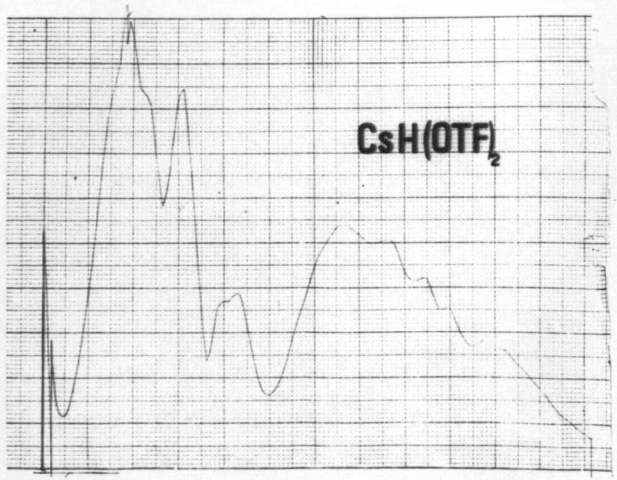

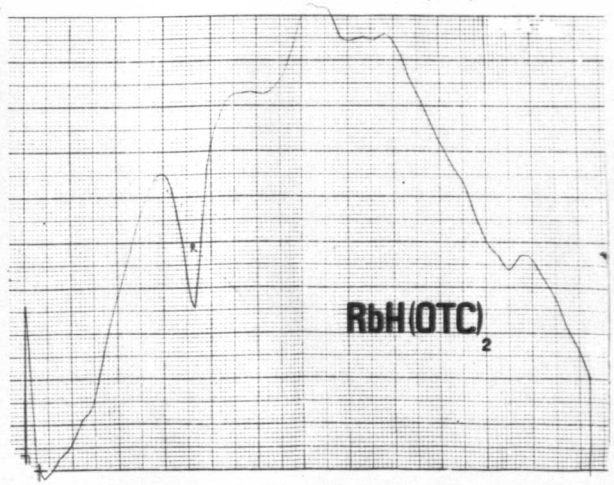

K

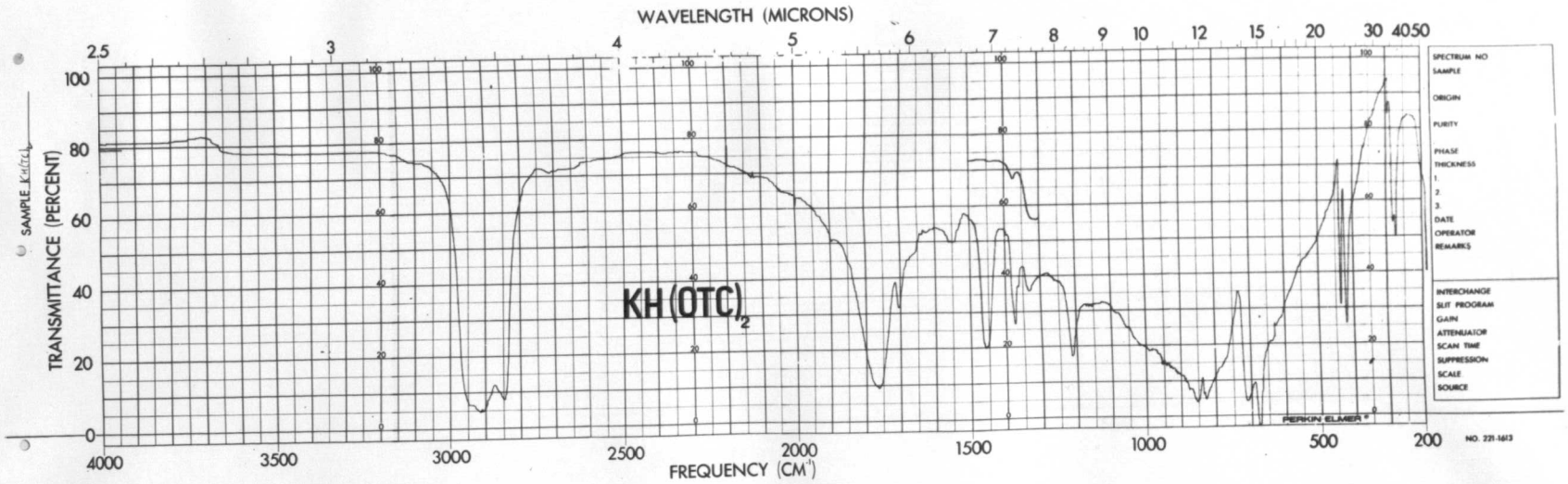
WAVELENGTH (MICRONS)
2.5
3
4
5
6
7
8
9
10
12
15
20
30
40
50
TRANSMITTANCE (PERCENT)
100
80
60
40
20
0
KH (OTC)2
4000
3500
3000
2500
2000
1500
1000
500
200
FREQUENCY (CM-1)
PERKIN ELMER
NO. 221-1613

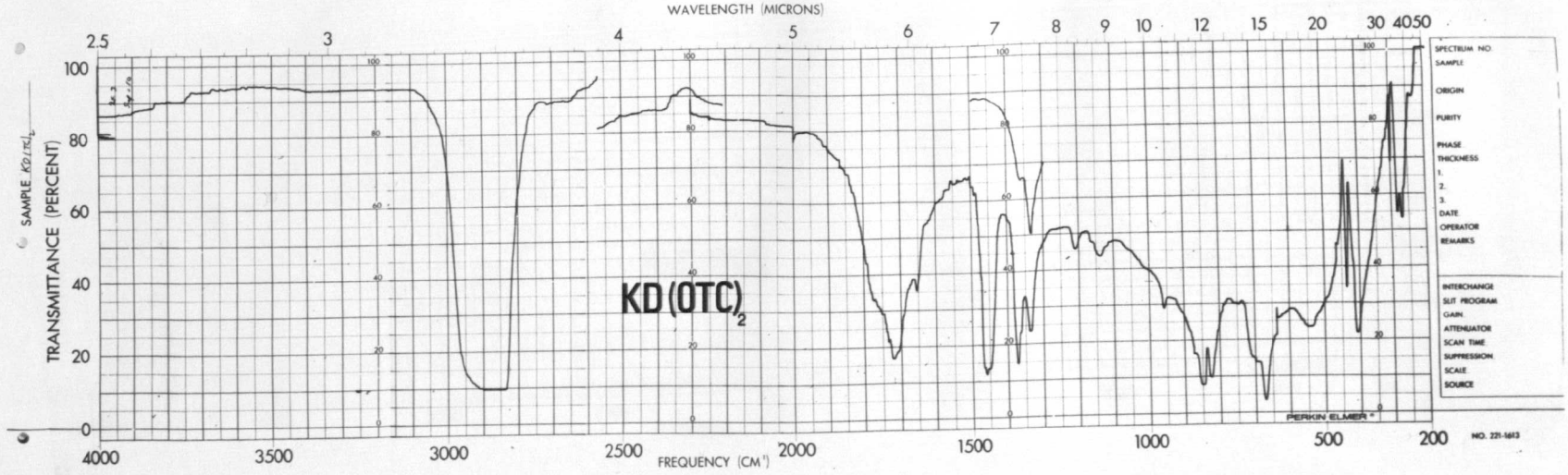
WAVELENGTH (MICRONS)
2.5
3
4
5
6
7
8
9
10
12
15
20
30
40
50
TRANSMITTANCE (PERCENT)
100
80
60
40
20
0
KD (OTC)2
4000
3500
3000
2500
2000
1500
1000
500
200
FREQUENCY (CM-1)
PERKIN ELMER
NO. 221-1613

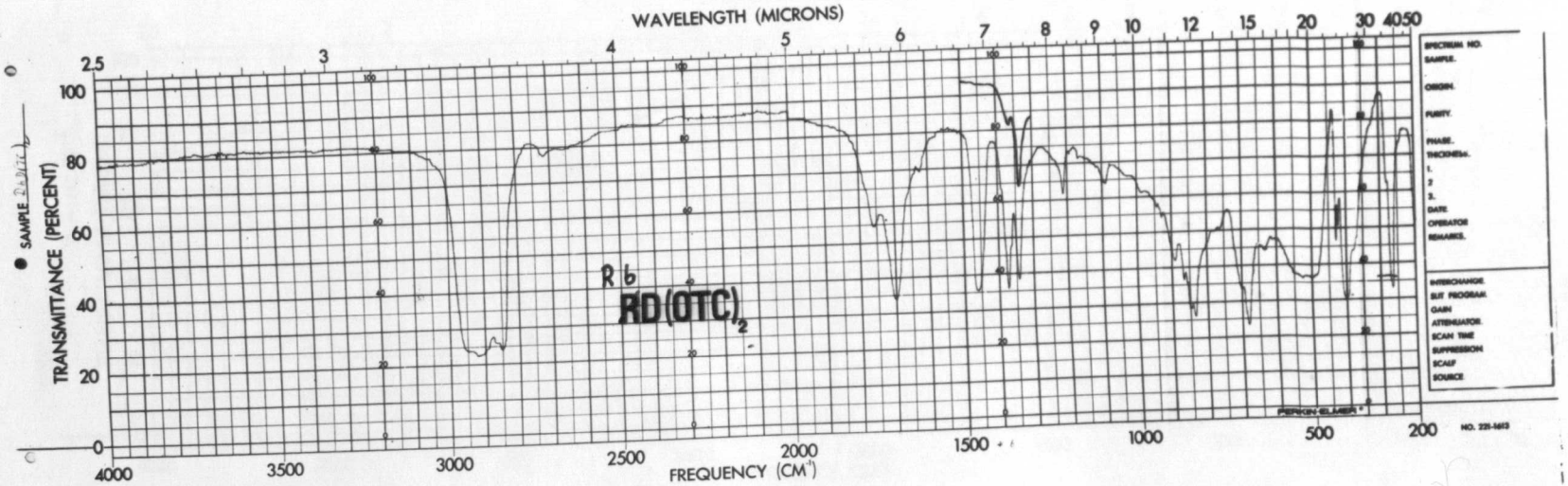
WAVELENGTH (MICRONS)
2.5
3
4
5
6
7
8
9
10
12
15
20
30
40
50
TRANSMITTANCE (PERCENT)
100
80
60
40
20
0
4000
3500
3000
2500
2000
1500
1000
500
200
FREQUENCY (CM⁻¹)
Rb
RD(OTC)2
SAMPLE
SPECTRUM NO.
SAMPLE.
ORIGIN.
PURITY.
PHASE.
THICKNESS.
1.
2.
3.
DATE.
OPERATOR.
REMARKS.
INTERCHANGE.
SLIT PROGRAM.
GAIN.
ATTENUATOR.
SCAN TIME
SUPPRESSION.
SCALE
SOURCE.
PERKIN-ELMER
NO. 221-1613

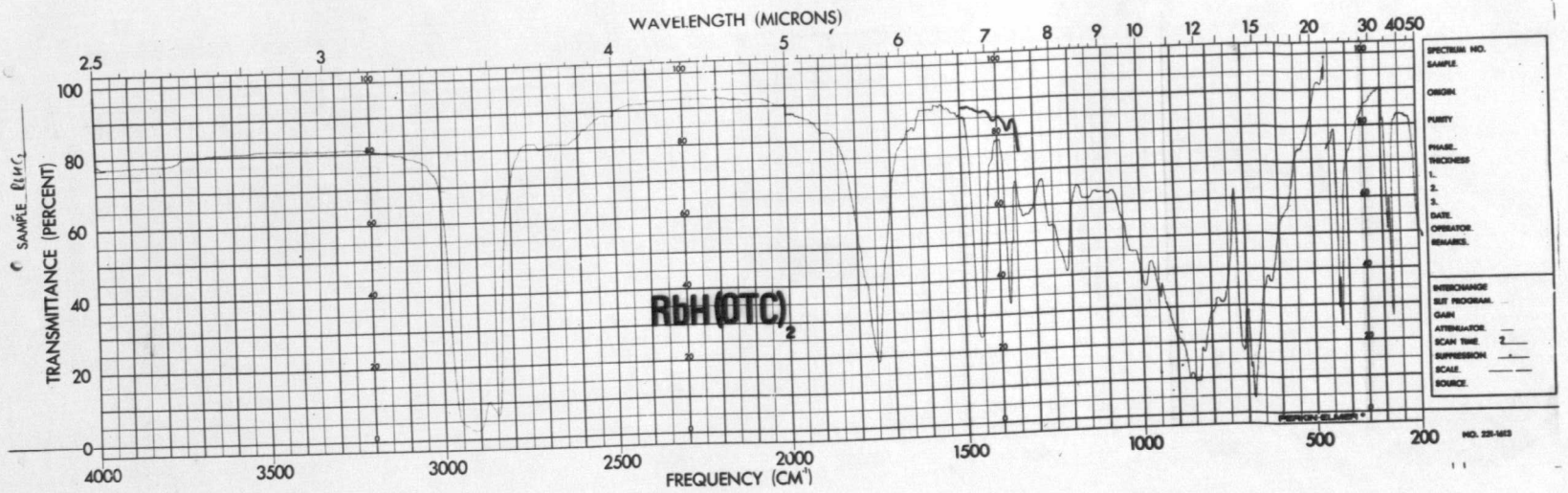
WAVELENGTH (MICRONS)
2.5
3
4
5
6
7
8
9
10
12
15
20
30
40
50
TRANSMITTANCE (PERCENT)
100
80
60
40
20
0
4000
3500
3000
2500
2000
1500
1000
500
200
FREQUENCY (CM⁻¹)
RbH(OTC)2
SAMPLE
SPECTRUM NO.
SAMPLE.
ORIGIN.
PURITY
PHASE.
THICKNESS
1.
2.
3.
DATE.
OPERATOR.
REMARKS.
INTERCHANGE
SLIT PROGRAM.
GAIN
ATTENUATOR.
SCAN TIME
SUPPRESSION.
SCALE.
SOURCE.
PERKIN-ELMER
NO. 221-1613

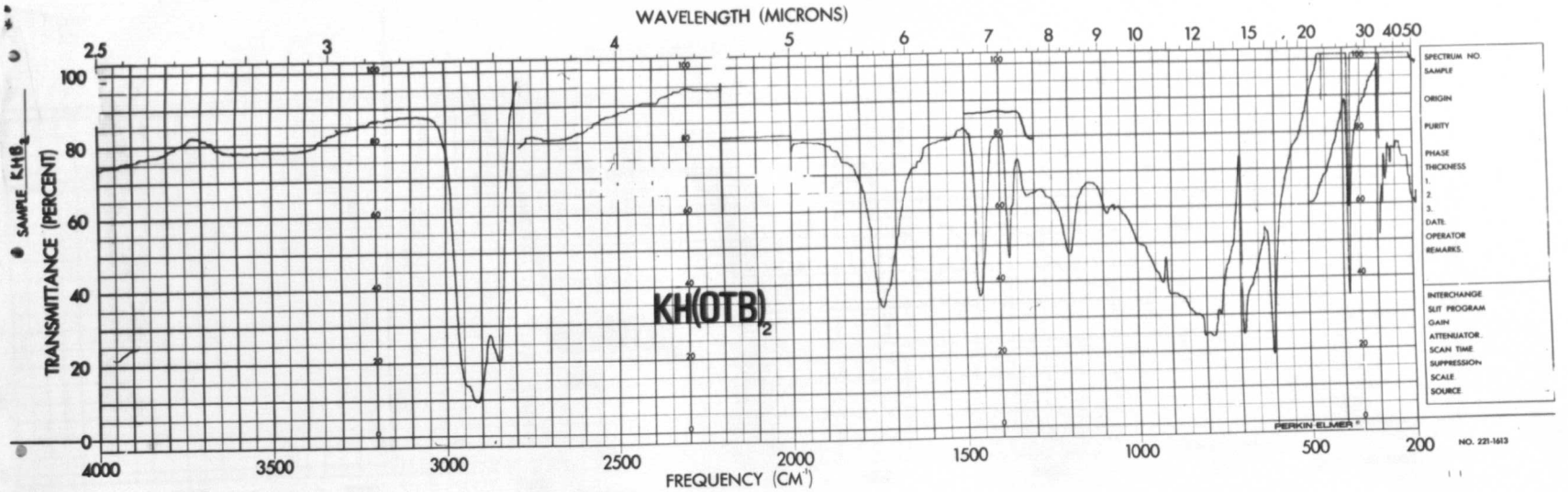
WAVELENGTH (MICRONS)
2.5
3
4
5
6
7
8
9
10
12
15
20
30
40
50
SAMPLE KHB
TRANSMITTANCE (PERCENT)
100
80
60
40
20
0
KH(OTB)2
4000
3500
3000
2500
2000
1500
1000
500
200
FREQUENCY (CM-1)
PERKIN ELMER
NO. 221-1613
SPECTRUM NO.
SAMPLE
ORIGIN
PURITY
PHASE
THICKNESS
1.
2.
3.
DATE
OPERATOR
REMARKS
INTERCHANGE
SLIT PROGRAM
GAIN
ATTENUATOR
SCAN TIME
SUPPRESSION
SCALE
SOURCE

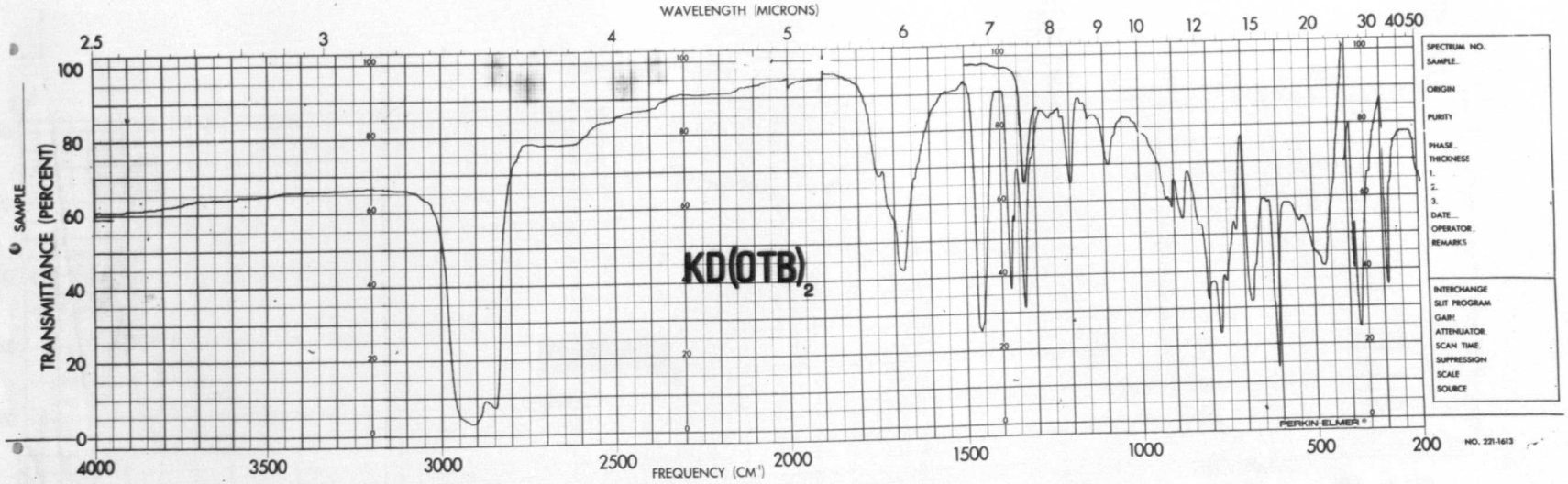
WAVELENGTH (MICRONS)
2.5
3
4
5
6
7
8
9
10
12
15
20
30
40
50
SAMPLE
TRANSMITTANCE (PERCENT)
100
80
60
40
20
0
KD(OTB)2
4000
3500
3000
2500
2000
1500
1000
500
200
FREQUENCY (CM-1)
PERKIN ELMER
NO. 221-1613
SPECTRUM NO.
SAMPLE
ORIGIN
PURITY
PHASE
THICKNESS
1.
2.
3.
DATE
OPERATOR
REMARKS
INTERCHANGE
SLIT PROGRAM
GAIN
ATTENUATOR
SCAN TIME
SUPPRESSION
SCALE
SOURCE

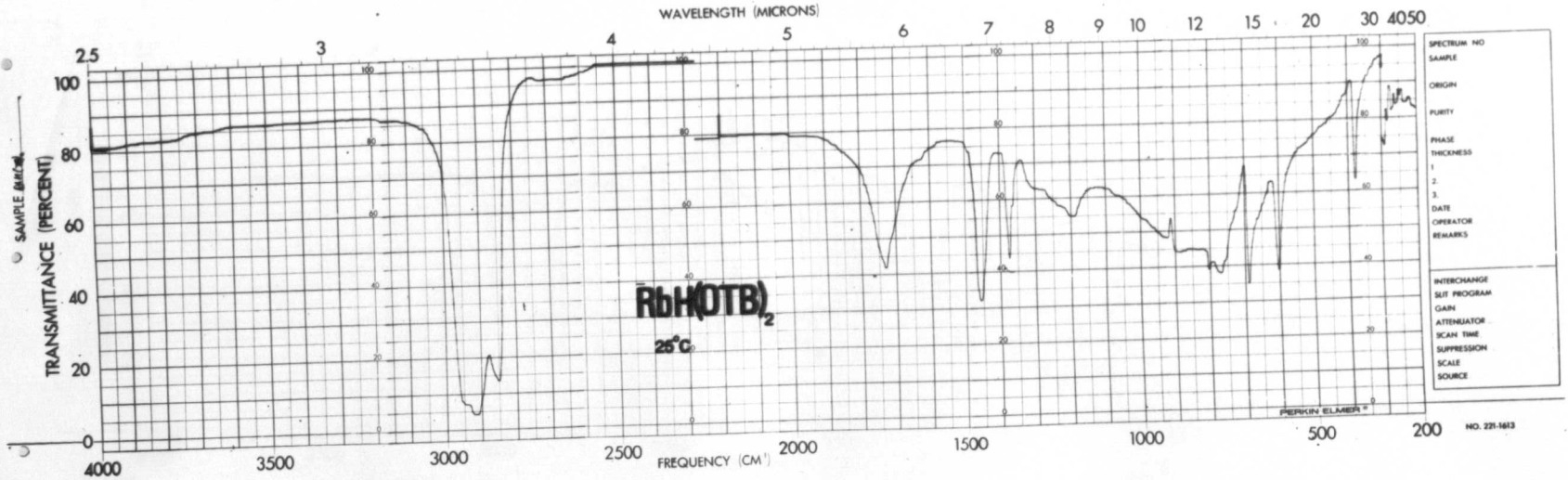
WAVELENGTH (MICRONS)
2.5
3
4
5
6
7
8
9
10
12
15
20
30
40
50
100
80
60
40
20
0
TRANSMITTANCE (PERCENT)
SAMPLE BANDS
RbH(OTB)2
25°C
4000
3500
3000
2500
2000
1500
1000
500
200
FREQUENCY (CM-1)
PERKIN ELMER
NO. 221-1613
SPECTRUM NO
SAMPLE
ORIGIN
PURITY
PHASE
THICKNESS
1
2.
3.
DATE
OPERATOR
REMARKS
INTERCHANGE
SLIT PROGRAM
GAIN
ATTENUATOR
SCAN TIME
SUPPRESSION
SCALE
SOURCE

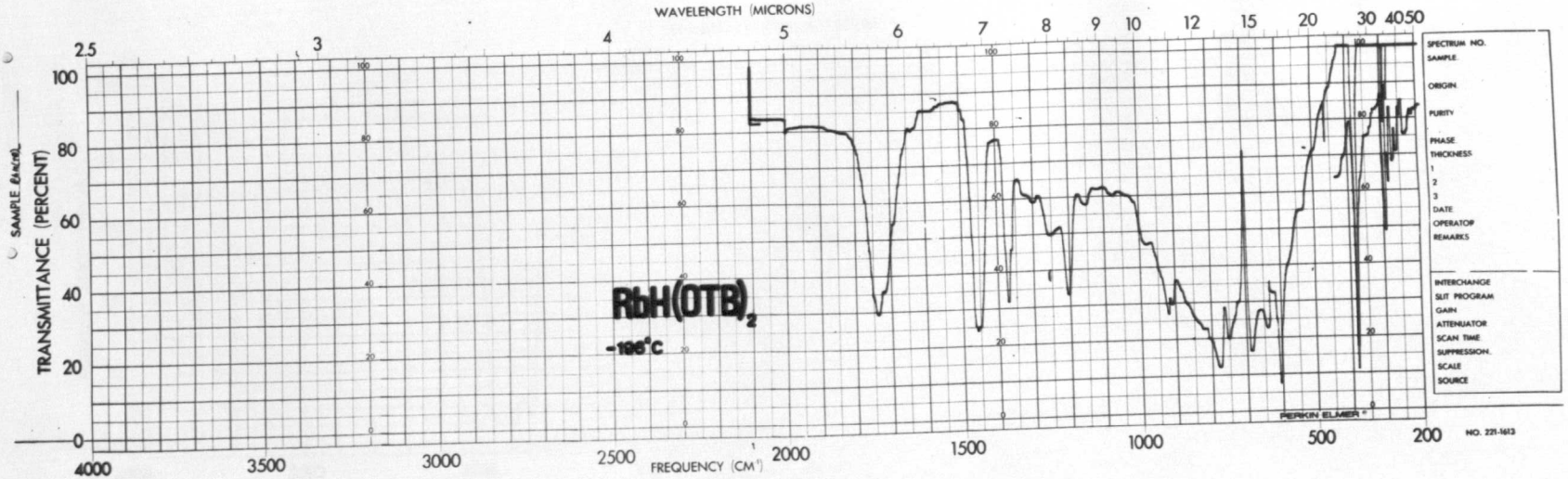
WAVELENGTH (MICRONS)
2.5
3
4
5
6
7
8
9
10
12
15
20
30
40
50
100
80
60
40
20
0
TRANSMITTANCE (PERCENT)
SAMPLE BANDS
RbH(OTB)2
-196°C
4000
3500
3000
2500
2000
1500
1000
500
200
FREQUENCY (CM-1)
PERKIN ELMER
NO. 221-1613
SPECTRUM NO.
SAMPLE
ORIGIN
PURITY
PHASE
THICKNESS
1
2
3
DATE
OPERATOR
REMARKS
INTERCHANGE
SLIT PROGRAM
GAIN
ATTENUATOR
SCAN TIME
SUPPRESSION
SCALE
SOURCE

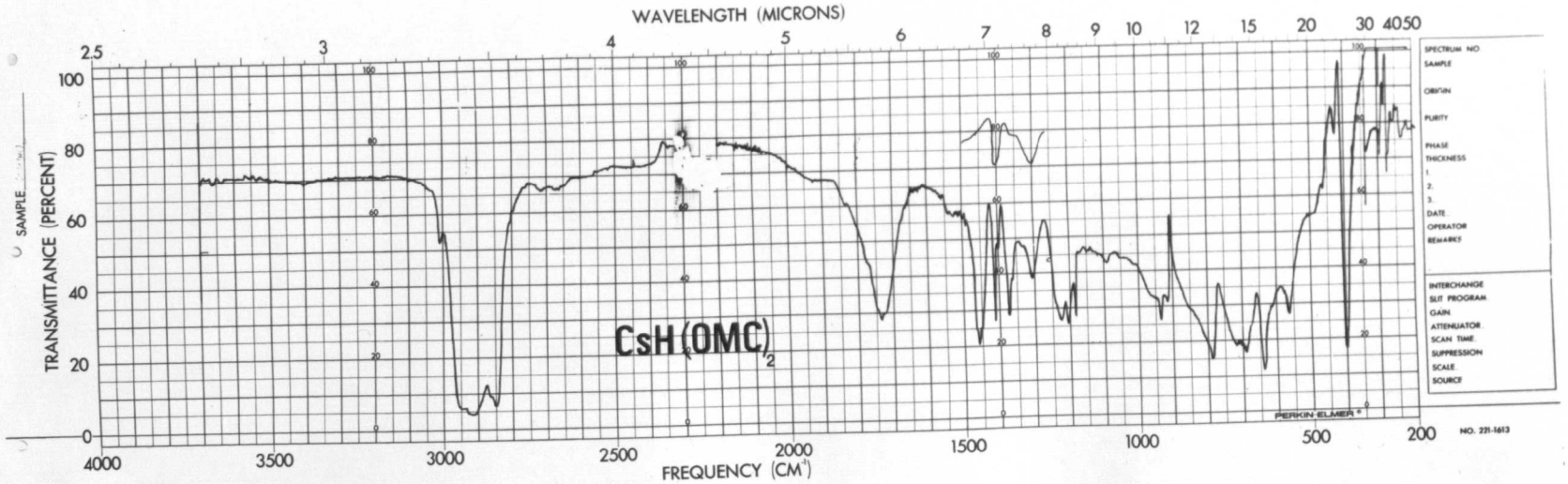
WAVELENGTH (MICRONS)
2.5
3
4
5
6
7
8
9
10
12
15
20
30
40
50
TRANSMITTANCE (PERCENT)
100
80
60
40
20
0
4000
3500
3000
2500
2000
1500
1000
500
200
FREQUENCY (CM-1)
CsH(OMC)2
SAMPLE
SPECTRUM NO
SAMPLE
ORIGIN
PURITY
PHASE
THICKNESS
1.
2.
3.
DATE
OPERATOR
REMARKS
INTERCHANGE
SLIT PROGRAM
GAIN
ATTENUATOR
SCAN TIME
SUPPRESSION
SCALE
SOURCE
PERKIN-ELMER
NO. 221-1613

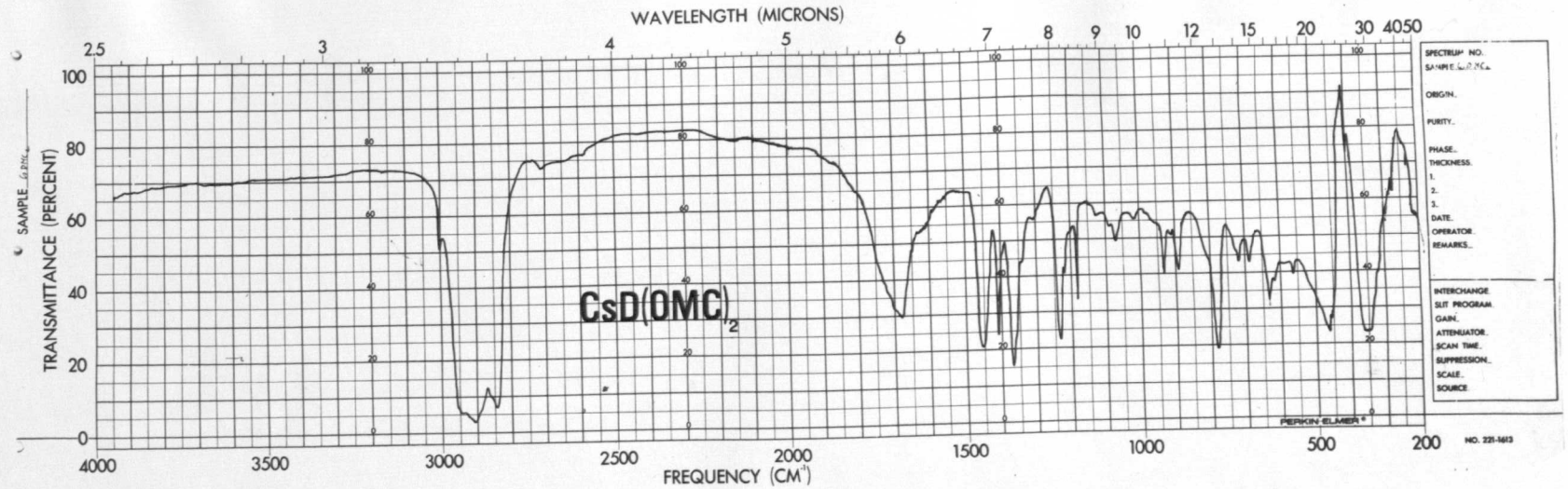
WAVELENGTH (MICRONS)
2.5
3
4
5
6
7
8
9
10
12
15
20
30
40
50
TRANSMITTANCE (PERCENT)
100
80
60
40
20
0
4000
3500
3000
2500
2000
1500
1000
500
200
FREQUENCY (CM-1)
CsD(OMC)2
SAMPLE
SPECTRUM NO.
SAMPLE
ORIGIN.
PURITY.
PHASE.
THICKNESS.
1.
2.
3.
DATE.
OPERATOR.
REMARKS.
INTERCHANGE
SLIT PROGRAM.
GAIN.
ATTENUATOR.
SCAN TIME.
SUPPRESSION.
SCALE.
SOURCE.
PERKIN-ELMER
NO. 221-1613

REFERENCES

REFERENCES

1. G. C. Pimentel and A. L. McClennan, "The Hydrogen Bond", W. H. Freeman and Co., 1960.
2. D. Hadži, ed "Hydrogen Bonding", Pergamon, 1959.
3. W. Hamilton and J. A. Ibers, "Hydrogen Bonding in Solids", W. A. Benjamin, 1968.
4. G. C. Pimentel, J. Chem. Phy., 1951, 19, 446.
5. C. G. Cannon, Spect. Acta, 1958, 10, 341.
6. A. Ocvirk, A. Ažman and D. Hadži, Theoretica Chem. Acta, 1968, 10, 187.
7. E. F. Westrum and K. S. Pitzer, J.A.C.S., 1949, 71, 1940.
8. T. C. Waddington, Trans. Faraday Soc., 1958, 54, 25.
9. J. W. Nibler and G. C. Pimentel, J. Chem. Phys., 1967, 47, 710.
10. T. C. Waddington, J. Chem. Soc., 1958, 1708.
11. D. G. Tuck and E. J. Woodhouse, Proc. Chem. Soc., 1963, 53.
12. T. C. Waddington and J. A. White, J. Chem. Soc., 1963, 2701.
13. K. M. Harmon and P. A. Gebauer, Inorg. Chem., 1963, 2, 1319.
14. J. C. Evans and G. Y-S. Lo, J. Phys. Chem., 1966, 70, 543.
15. J. A. Salthouse and T. C. Waddington, J. Chem. Soc. (A)., 1966, 28.
16. T. A. O'Shea, M.Sc Thesis, University of Warwick, 1966.
17. B. D. Faithful, R. D. Gillard, D. G. Tuck and R. Ugo, J. Chem. Soc. (A)., 1966, 1185.
18. B. D. Faithful and D. G. Tuck, Chem. and Industry, 1966, 1036.
19. M. F. A. Dove, Chem. Comm., 1965, 23.
20. C. J. Ludman, Ph.D. Thesis, Cambridge University, 1966.
21. J. A. Salthouse, Ph.D. Thesis, Cambridge University, 1965.

22. J. A. Salthouse and T. C. Waddington. To be published.

23. R. M. Dieters, W. G. Evans, and D. H. McDaniel, Inorg. Chem., 1968, 7, 1615.

24. Wyckoff, Am. J. Sci., 1922, 4, 175.

25. H. M. E. Cardwell, J. D. Dunitz and L. E. Orgel, J. Chem. Soc., 1953, 3740.

26. S. W. Peterson and H. A. Levy, J. Chem. Phys., 1958, 29, 948.

27. G. Ferguson, J. G. Sime, J. C. Speakman, and R. Young, Chem. Comm 1968, 3, 162.

28. D. Hadži and A. Novak, Spect. Acta, 1962, 18, 1059.

29. B. L. McGaw and J. A. Ibers, J. Chem. Phys., 1963, 39, 2677.

30. D. Hadži and A. Novak, "IR Spectra of, and Hydrogen Bonding in, some acid salts of carboxylic acids", Ljubljana, 1960.

31. W. Fuller, J. Phys. Chem., 1959, 63, 1705.

32. W. C. Hamilton and J. A. Ibers, Acta Cryst., 1963, 16, 1209.

33. R. Blinc and D. Hadži, J. Mol. Phys., 1958, 1, 391.

34. R. M. Hill and S. K. Ichiki, J. Chem. Phys., 1968, 48, 838.

35. J. A. Ibers, J. Chem. Phys., 1964, 40, 402.

36. N. Sheppard in ref. 2 page 85.

37. R. E. Rundle and M. Parasol, J. Chem. Phys., 1952, 20, 1487.

38. K. Nakamoto, M. Margoshes and R. E. Rundle, J.A.C.S., 1955, 77, 6480.

39. G. C. Pimentel and C. H. Sederholdm. J. Chem. Phys., 1956, 24, 639.

40. R. Blinc, D. Hadži and A. Novak, Zeit fur Elekrochemie, 1960, 64, 567.

41. H. Ratajczak and W. J. Orville-Thomas, J. Mol. Structure, 1967, 1, 449.

42. S. Bratož, D. Hadži and N. Sheppard, Spect. Acta, 1956, 8, 249.

43. Y. Marechal and A. Witkowski, J. Chem. Phys., 1968, 48, 3697.

44. C. Perchard and A. Novak, J. Chem. Phys., 1968, 48, 3079.

45. A. Novak and A. Lautie, Nature, 1967, 216, 1202.

46. J. A. Salthouse and T. C. Waddington, J. Chem. Phys.,1968, 48, 5274.

47. R. J. Jakobsen, J. W. Braschand Y. Mikawa, J. Mol. Structure, 1967, 1, 309.

48. S. Bratož and D. Hadži, J. Chem. Phys., 1957, 27, 991.

49. J. A. Ibers, J. Chem. Phys., 1964, 41, 25.

50. G. L. Cote and H. W. Thompson, Proc. Roy. Soc. A., 1951, 210, 206.

51. R. Newman and R. M. Badger, J. Chem. Phys., 1951, 19, 1207.

52. L. Couture-Mathieu and J. P. Mathieu, Comp. Rend., 1950, 230, 1054.

53. J. S. Waugh, F. B. Humphrey and D. M. Yost, J. Phys. Chem., 1953, 51, 436.

54. H. Boutin, G. J. Safford and V. Brajovic, J. Chem. Phys., 1963, 39, 3135.

55. J. C. Evans and G. Y-S. Lo, J. Phys. Chem., 1966, 70, 11.

56. J. C. Evans and G. Y-S. Lo, J. Phy. Chem., 1966, 70, 2702.

57. J. C. Evans and G. Y-S. Lo, J. Phy. Chem., 1967, 71, 3697.

58. L. Schroeder and J. A. Ibers, Inorg. Chem., 1968, 7, 594.

59. R. W. West, J.A.C.S., 1957, 79, 4568.

60. A. G. Maki and R. W. West, Inorg. Chem., 1963, 2, 657.

61. T. C. Waddington, Private Communication.

62. C. A. Coulson in ref. 2 page 339.

63. J. C. Speakman, Chem. Comm., 1967, 32.

64. H. N. Shrivastava and J. C. Speakman, J. Chem. Soc., 1961, 1151.

65. G. Larsson and I. Nahringbauer, Acta Cryst., 1968, B24, 666.

66. L. Manojlovic and J. C. Speakman, Acta Cryst., 1968, B24, 323.

67. G. E. Bacon and N. A. Curry, Acta Cryst., 1957, 10, 524.

68. G. E. Bacon and N. A. Curry, Acta Cryst., 1960, 13, 717.

69. D. Hadži, Rev. of Pure and Applied Chemistry, 1965, 11, 435.

70. A. Sequeira, C. A. Berkebile and W. C. Hamilton, J. Mol. Structure, 1967, 283.

71. R. Blinc and D. Hadži, Spect. Acta, 1960, 16, 853.

72. R. Blinc and D. Hadži, Nature, 1966, 212, 1307.

73. D. Hadži, J. Chem. Soc., 1962, 5128.

74. D. Hadži and N. Kobilorov, J. Chem. Soc., (A)., 1966, 439.

75. D. Hadži, Boll. Sci. Fac. Chim. Ind. Bologna, 1963, 21, 23.

76. R. D. Ellison and H. A. Levy, Acta Cryst., 1965, 19, 260.

77. G. E. Bacon and R. S. Pease, Proc. Roy. Soc. (London), 1953, A220, 397.

78. G. E. Bacon and R. S. Pease, Proc. Roy. Soc. (London), 1955, A230, 359.

79. D. Hadži, J. Chem. Phys., 1961, 34, 1445.

80. Y. Imry, I. Pelah, and E. Wiener, J. Chem. Phys., 1965, 43, 2332.

81. J. A. Ibers, C. H. Holm, and C. R. Adams, Phy. Rev., 1961, 121, 1620.

82. A. Benoit, Spect. Acta, 1963, 19, 2011.

83. R. G. Snyder and J. A. Ibers, J. Chem. Phys., 1962, 36, 1356.

84. J. J. Rush and J. R. Ferraro, J. Chem. Phys., 1966, 44, 2496.

85. J. M. Skinner and J. C. Speakman, J. Chem. Soc., 1951, 185.

86. L. Manojlovic, Acta Cryst., 1968, B24, 326.

87. J. M. Skinner, G. M. D. Steward and J. C. Speakman, J. Chem. Soc., 1954, 180.

88. H. H. Mills and J. C. Speakman, J. Chem. Soc., 1961, 1164.

89. R. F. Bryan, H. H. Mills and J. C. Speakman, J. Chem. Soc., 1963, 4350.

90. H. H. Mills and J. C. Speakman, J. Chem. Soc., 1963, 4355.

91. L. Golic and J. C. Speakman, J. Chem. Soc., 1965, 2530.

92. S. Grunvall and R. F. Wengelin, J. Chem. Soc (A)., 1967, 968.

93. L. Manojlovic and J. C. Speakman, J. Chem Soc., 1967, 971.

94. D. R. McGregor and J. C. Speakman, J. Chem. Soc. (A), 1968, 2106.

95. L. Golic and J. C. Speakman, J. Chem. Soc., 1963, 2521.

96. T. C. Downie and J. C. Speakman, J. Chem. Soc., 1954, 787.

97. R. E. Dodd and P. L. Robinson, "Experimental Inorganic Chemistry" Elsevier, 1954, page 56.

98. A. I. Vogel, "Quantitative Inorganic Analysis", Longmans, 1961.

99. R. C. Millikan and K. S. Pitzer, J. Chem. Phys., 1957, 27, 1305.

100. J. A. Salthouse, Private Communication.

101. A. R. Ubbelohde and K. J. Gallagher, Acta Cryst., 1955, 8, 71.

102. J. C. Evans and G. Y-S. Lo, J. Phys. Chem., 1966, 70, 20.

103. M.Haurie and A. Novak, J. Chim. Phys., 1965, 62, 146.

104. W. V. F. Brooks and C. M. Haas, J. Phys. Chem., 1967, 71, 650.

105. "Stability Constants", Special Publication No. 17, The Chemical Soc.

106. A. Albert and E. D. Serjeant, "Ionisation Constants of Acids and Bases", Methuen and Co. Ltd., 1962.

107. G. Herzberg, "IR and Raman Spectra of Polyatomic Molecules", D. Van Nostrand Company inc., 1964.

108. M. Haurie and A. Novak, J. Chim. Phys., 1967, 64, 679.

109. D. Hadži and N. Sheppard, Proc. Roy. Soc., 1953, A216, 247.

110. K. Nakamoto, "IR Spectra of Inorganic and Co-ordination Compounds", J. Wiley and Sons, inc., 1962.

111. M. Haurie and A. Novak, J. Chim. Phys., 1965, 62, 136.

112. M. Haurie and A. Novak, Spect. Acta, 1965, 21, 1217.

113. A. Ažman, A. Ocvirk, D. Hadži, P. A. Giguere and M. Schneider, Canad. J. Chem., 1967, 45, 1347.

114. G. C. Dobinson, R. Mason and D. R. Russell, Chem. Comm., 1967, 62.

115. H. Cohn, C. K. Ingold and H. G. Poole, J. Chem. Soc., 1952, 472.

116. E. Spinner, J. Chem. Soc., 1964, 4219.

117. M. J. Baillie, D. H. Brown, K. C. Moss and D. W. A. Sharp, J. Chem. Soc. (A)., 1968, 3110.

118. R. E. Kagarise, J. Chem. Phys., 1957, 27, 519.

119 D. Hornig and R. L. Somorjai, J. Chem. Phys., 1962, 36, 1980.

120 R. L. Somorjai, Ph.D. Thesis, Princeton University, 1963.

121 T. C. Waddington and F. Temme, Work in progress.

122. J. W. Brasch, R. J. Jakobsen, W. G. Fateley and N. T. McDevitt, Spect. Acta, 1968, 24A, 203.

123 R. J. Jakobsen, Y. Mikawa and J. W. Brasch, Spect. Acta, 1967, 23A, 2199.

124 T. C. Waddington, Unpublished results.

125 D. Biedenkapp and A. Weiss, Ber. der Bunsengesellschaft, 1966, 70, 788.

126 H. C. Adams, J. Phys. Chem., 1953, 57, 501.

127 G. E. Bacon, "Applications of Neutron Diffraction in Chemistry", Pergamon, 1963.

128 R. Blinc, Nature, 1958, 182, 1016.

129 P. N. Noble and G. C. Pimentel, J. Chem. Phys., 1968, 49, 3165.

130 J. D. Donaldson, J. F. Knifton and S. D. Ross, Spect. Acta, 1965, 21, 275.

131 A. V. R. Warrier and P. S. Narayanan, Spect. Acta, 1967, 23A, 1061.

132 F. A. Cotton, "Chemical Applications of Group Theory", J. Wiley and Sons, Inc., 1964.